Universitat
de Girona

BOND BEHAVIOUR BETWEEN CFRP AND CONCRETE FOR NSM SYSTEMS UNDER SUSTAINED LOADING

Javier Gómez Colom

Universitat de Girona

Escola Politècnica Superior

Doctoral Thesis

Bond behaviour between CFRP and concrete for NSM systems under sustained loading

Javier Gómez Colom

2021

Doctoral Program in Technology

Supervisor:

Dr Cristina Barris Peña

Universitat de Girona

Thesis submitted to the University of Girona for the degree of Doctor

Javier Gómez Colom

Bond behaviour between CFRP and concrete for NSM systems under sustained loading

Doctoral Thesis, 2021

Doctoral Program in Technology

Supervisors: Dr Cristina Barris Peña

University of Girona

AMADE Research Group

Escola Politècnica Superior

Department of Mechanical Engineering and Industrial Construction

Carrer Universitat de Girona, 4

17003, Girona

To my family and friends.

"The greatest teacher, failure is"

Yoda (Star Wars)

Acknowledgements

First of all, I would like to express my most sincere gratitude to Dr Cristina Barris. I will never be enough grateful for all the work that you have done for this thesis and to be so supportive in the hardest times. Thanks for encouraging me to start the PhD, which has been an amazing journey thanks to your advice and guidance.

This work could not be completed without the help of Dr Lluís Torres and Dr Marta Baena, who were always available to help me and supervise this work. With your experience and knowledge, we could achieve our objectives. I would also like to thank Pau for his hard work and help during these years. It has been essential to complete this thesis.

I am also extremely grateful to Dr José Sena Cruz to host my research stay and bringing me the opportunity to work in the ISISE Institute.

I would also like to thank all the people in AMADE. I have to say that thanks to all of you, my experience in AMADE has been extremely positive and will be unforgettable. To my colleagues in AMADE: Sergio, Aravind, Adrià, Juan José, Jordi, Edwin, Younes, Rodrigo, Said, Anni, Oriol, Ivan, Alba and Yi, I would like to thank you for all the time spent together which has helped me in many ways. Furthermore, I am very grateful to the people from the lab, Pere, Sergi and Jordi, who have always helped me during this thesis.

I want to express my most sincere thanks to my family, my father, my mother and my sister, who have always supported me and helped me all my life. Thanks to you, I have become who I am, and I will always be grateful for that. Thanks to my friends Guixe, David, Dome and Pere for your support and unconditional friendship, which undoubtedly has helped me to reach my objectives. Lastly, this journey would not have been possible without the support and love of my dear Sandra. I have accomplished this task thanks to the energy and positivism that you have transmitted to me.

Without all of you, this thesis would not have been possible.

Preface

The work performed in this thesis was conducted in the AMADE research group (Department of Mechanical Engineering and Industrial Construction, University of Girona, Spain).

List of publications

The present thesis is prepared as a compendium of journal papers, according to the requirements of the Universitat de Girona. The following papers have been generated from this thesis:

- **Gómez J.**, Torres L., Barris C. Characterization and simulation of the bond response of NSM FRP reinforcement in concrete. ***Materials***, 13 (2020), 1770. doi: 10.3390/ma13071770.

- EISSN: 1996-1944, Impact factor: 3.623 and ranked 17/80 in the category of Metallurgy & Metallurgical Engineering (1st quartile)[1].

- **Gómez J.**, Barris C., Jahani Y., Baena M., Torres L. Experimental study and numerical prediction of the bond response of NSM CFRP laminates in RC elements under sustained loading. ***Construction and Building Materials***, 288 (2021) 123082. doi: 10.1016/j.conbuildmat.2021.123082.

- ISSN: 0950-0618, Impact factor: 6.141 and ranked 7/136 in the category of Civil Engineering (1st quartile)[1].

- **Gómez J.**, Barris C., Jahani Y., Baena M., Torres L. The effect of steady and cyclic environmental conditions on the tensile behaviour of a structural adhesive under sustained loading. Submitted to ***Composite Structures*** on 24th March 2021.

- **Gómez J.**, Barris C., Baena M., Perera R., Torres L. Sustained loading bond response and post-sustained loading behaviour of NSM CFRP-concrete elements under different service temperatures. ***Applied sciences***, 11 (2021), 18. doi: 10.3390/app11188542.

- EISSN: 2076-3417, Impact factor: 2.679 and ranked 38/91 in the category of Engineering Multidisciplinary (2nd quartile)[1].

[1]According to the 2021 Journal Citation Reports

Conferences

- **Gómez J.**, Torres L., Barris C. Effect of the bond-slip law on the bond response of NSM FRP reinforced concrete elements. 5th International Conference on Mechanical Models in Structural Engineering (CMMoST). Alicante (Spain), 23-25th October 2019.

- **Gómez J.**, Barris C., Baena M., Perera R. Bond behaviour of NSM FRP strengthening systems on concrete elements under sustained load. 3rd RILEM spring convention 2020. Guimarães (Portugal), 10-14th March, 2020.

- **Gómez J.**, Barris C., Jahani Y., Baena M., Torres L. Bond behaviour of NSM strengthening systems on concrete elements under sustained load and cyclic service temperature. 23rd International Conference on Composite Structures (ICCS). Porto (Portugal), 1-4th September 2020.

- **Gómez J.**, Barris C., Jahani Y., Baena M., Torres L. Experimental study on the bond behaviour between CFRP NSM strengthening system and concrete under fatigue loading. *fib* Symposium 2021: Concrete Structures: New trends for Eco-Efficiency and Performance. Lisbon (Portugal), 14-16th June 2021.

- **Gómez J.**, Barris C., Jahani Y., Baena M., Torres L. Bond behaviour of NSM strengthening systems on concrete elements under sustained load and high ambient temperature. 10th International Conference on FRP Composites in Civil Engineering (CICE2020). Istanbul (Turkey), 8-10th December 2021.

Universitat
de Girona

To whom it might concern,

Dr Cristina Barris Peña, associate professor at the Universitat de Girona of the Department of Enginyeria Mecànica i de la Construcció Industrial,

CERTIFIES that,

The study entitled *Bond behaviour between CFRP and concrete for NSM systems under sustained loading* has been carried out under her supervision by Javier Gómez Colom and that it fulfils the requirements to aim for the International Mention,

Girona, November 2021,

Dr Cristina Barris Peña

Universitat de Girona, Spain

Table of Contents

List of Figures

List of Tables

Nomenclature

α	curing degree
A_c	cross-section area of the concrete
A_f	cross-section area of the CFRP strip/plate
A_ε	amplitude of strain caused by the thermal cycle
β_l	bonded length factor
β_w	CFRP-concrete width ratio factor
b_c	width of the concrete element
b_f	width of the CFRP plate
ε_c	strain in the concrete
ε_f	strain in the FRP
ε_{fe}	effective strain level in the FRP at the ultimate limit state
E_a	elastic modulus of the adhesive
E_c	elastic modulus of the concrete
E_f	elastic modulus of the CFRP
$E_{a,LT}$	elastic modulus of the CFRP after sustained loading
f_c	compressive strength of the concrete
f_c'	concrete cylinder compressive strength
f_{ct}	tensile strength of the concrete
f_{ctm}	mean value of the tensile strength of the concrete
f_{fe}	tensile strength of the CFRP
f_{ta}	tensile strength of the adhesive
$f_{ta,LT}$	tensile strength of the adhesive after sustained loading
$f(t)$	strength reduction coefficient
G_a	shear modulus of the adhesive
G_f	fracture energy of the bonded joint in mode II
h_g	depth of the groove
H_r	residual enthalpy of reaction
J_c	creep compliance
K_e	stiffness of the ascending branch of the bond-slip law

K_s	stiffness of the descending branch of the bond-slip law
L_b	bonded length
L_{eff}	effective bonded length
$L_{failure}$	perimeter of the failure surface
L_{per}	cross-section length of plane failure
P	load in the bonded joint
P_u	ultimate load of the bonded joint
σ_c	tensile stress on the concrete
σ_f	tensile stress on the CFRP
s	local slip
Δs	increment of slip
s_1	slip at the bond shear strength
s_f	maximum slip of the bond-slip law
τ_{avg}	average bond shear strength
τ_{max}	bond shear strength
τ_f	friction bond shear strength
T_g	glass transition temperature
t	time
t_a	thickness of the adhesive layer
t_c	thickness of the concrete layer
t_g	thickness of the groove
t_f	thickness of the CFRP strip/plate
Φ_{Ef}	creep coefficient of the elastic modulus
Φ_k	creep coefficient of K_e
x	position in the bonded length

Abstract

The rehabilitation of civil structures has been gaining importance during the last decades. Owing to their mechanical, corrosion resistance and lightweight properties, Carbon Fibre-Reinforced Polymers (CFRP) present an excellent solution to strengthen Reinforced Concrete (RC) structures, being the Near-Surface Mounted (NSM) one of the main used techniques because of a better protection of the FRP against external agents. During their service life, civil structures are submitted to cyclic temperatures due to the day and night cycles, which can affect the durability of the strengthening system. It is therefore of outmost importance to study how these actions can affect the NSM CFRP-concrete bond performance to properly design the strengthening systems and avoid premature failures.

In this thesis, the sustained-loading bond behaviour of NSM CFRP-concrete joints has been evaluated from experimental and numerical points of view. A numerical methodology based on a finite differences model has been implemented to predict the instantaneous global response of the bonded joints. To verify the numerical model, an experimental programme on the instantaneous behaviour of NSM CFRP-concrete specimens was performed through single shear tests until failure. Different values of groove thicknesses and bonded lengths were tested to study the effect of these parameters on the global response of the bonded joint in terms of failure mode and ultimate load. A parametric study was then performed to investigate the effect of the main parameters of the bond-slip law in the ultimate load and effective bonded length.

Afterwards, the effect of high service temperature and sustained loading on the creep behaviour of the bonded joint was studied through (i) single shear tests in NSM CFRP-concrete specimens, and (ii) tensile tests on epoxy adhesive specimens. Five experimental series were carried out inside a climatic chamber under different service temperatures for 1000 hours. In the sustained loading tests, the effect of the sustained load level, the groove thickness and the bonded length were studied. Results showed that the evolution of strain (in the adhesive) and slip at the loaded end (in the NSM CFRP-concrete specimen) increased with the average temperature and the sustained load level.

Thereafter, after sustained loading tests, instantaneous tests were carried out until failure for all the specimens to study the residual capacity of the specimens. An overall slight decrease

on the mechanical properties of the bonded joints (ultimate load and stiffness) and the adhesive (tensile strength and elastic modulus) were observed.

Finally, the numerical procedure developed to predict the instantaneous behaviour of the bonded joint was adapted to calculate the creep behaviour of the NSM CFRP-concrete joints by implementing the degradation of the bond-slip law with time. From this numerical methodology, the evolution of slip at the loaded end with time was obtained for each specimen configuration and was compared with the experimental results.

Resum

Durant les últimes dècades, la rehabilitació d'estructures civils ha adquirit especial importància. Els materials compostos de fibra de carboni i matriu polimèrica (en anglès, Carbon Fibre Reinforced Polymers, CFRP) s'han introduït en el sector com a solució excel·lent per al reforç estructural de formigó armat, gràcies a les seves propietats mecàniques, la seva resistència a la corrosió i la seva lleugeresa. La tècnica del reforç inserit al recobriment (en anglès, Near-Surface Mounted, NSM) ha resultat ser una de les principals metodologies emprades gràcies a la protecció de l'FRP envers als agents externs. No obstant això, la durabilitat del reforç extern es pot veure afectada durant la seva vida útil, ja que les estructures es troben sotmeses a agents externs com càrregues sostingudes i temperatures cícliques degudes al cicle dia-nit. Per tal de dissenyar correctament el sistema de reforç i evitar fallades prematures per desenganxament del CFRP, és extremadament important estudiar com aquestes accions poden afectar a l'adherència entre el formigó i el reforç NSM CFRP.

Aquesta tesi presenta un estudi del comportament de la unió adherida NSM CFRP-formigó des d'un punt de vista experimental i numèric. Inicialment, es va dissenyar una metodologia numèrica basada en un model de diferències finites per a predir la resposta global instantània de les unions adherides. Posteriorment, per a verificar el model numèric, es va realitzar una campanya d'assajos experimentals per estudiar l'adherència de la unió NSM CFRP-formigó a través d'assajos d'adherència fins a la ruptura. Es van assajar espècimens amb diferents valors d'amplada de regata i de longituds adherides per investigar l'efecte d'aquests paràmetres en la càrrega última i el mode de falla de la unió adherida. Mitjançant la metodologia numèrica, es va realitzar un estudi paramètric per investigar la influència dels principals paràmetres de la llei adherència-lliscament en la càrrega última i en la longitud d'adhesió efectiva de les unions adherides.

A continuació, es va estudiar l'efecte de diferents temperatures de servei i nivells de càrrega sostinguda en la fluència de la unió adherida a través de (i) assajos d'adherència d'espècimens NSM CFRP-formigó i (ii) assajos a tracció d'espècimens d'adhesiu epòxid. Es va realitzar un total de cinc campanyes experimentals. Els espècimens es van assajar dins d'una cambra climàtica combinant tres nivells de càrrega sostinguda i diverses temperatures durant 1000 hores. Dels resultats experimentals es va observar que l'evolució de la deformació unitària (en adhesius) i

de lliscament a l'extrem carregat (en espècimens NSM CFRP-formigó) augmentava a mesura que la temperatura mitjana de la cambra i el nivell de càrrega sostinguda augmentaven.

Tot seguit, els espècimens sotmesos a assajos en servei es van assajar fins a ruptura per tal d'estudiar-ne la capacitat residual d'aquests. D'aquests assajos es va observar un decreixement general de les propietats mecàniques de les unions adherides (en termes de càrrega última i rigidesa) i dels espècimens d'adhesiu (en termes de resistència a tracció i mòdul elàstic).

Finalment, el procediment numèric desenvolupat per a predir el comportament instantani de les unions adherides va ser adaptat per al càlcul del comportament a llarg termini de la unió NSM CFRP-formigó a partir de la implementació de la degradació de la llei adherència-lliscament amb el temps. Amb aquesta metodologia numèrica es va calcular l'evolució del lliscament a l'extrem carregat amb el temps per a cada configuració d'espècimen i es va fer la comparació amb el corresponent assaig experimental.

Resumen

A lo largo de las últimas décadas, la rehabilitación de estructuras civiles ha ganado especial importancia. Los materiales compuestos de fibra de carbono y matriz polimérica (en inglés, Fibre Reinforced Polymers, FRP) se han introducido en el sector como solución excelente para el refuerzo estructural de hormigón armado, gracias a sus propiedades mecánicas, su resistencia a la corrosión y su ligereza. La técnica del refuerzo insertado en el recubrimiento (en inglés, Near-Surface Mounted, NSM) ha resultado ser una de las principales metodologías empleadas gracias a la protección del FRP frente agentes externos. La durabilidad del refuerzo externo se ve afectada durante su vida útil, puesto que las estructuras están sometidas a agentes externos como son las cargas sostenidas y temperaturas cíclicas debidas al ciclo día-noche. Para diseñar correctamente los refuerzos con NSM CFRP y evitar fallos prematuros de adherencia, es extremadamente importante estudiar cómo estas acciones pueden afectar a la adherencia del refuerzo.

Esta tesis presenta un estudio del comportamiento de la unión adherida NSM CFRP-hormigón desde un punto de vista experimental y numérico. Inicialmente, se diseñó una metodología numérica basada en un modelo de diferencias finitas para predecir la respuesta global instantánea de las uniones adheridas. Posteriormente, se realizó una campaña de ensayos experimentales de especímenes NSM CFRP-hormigón a cortante hasta el fallo para verificar el modelo numérico. Se ensayaron especímenes con diferentes valores de anchura de regata y de longitudes adheridas para investigar el efecto de estos parámetros en la carga última y el modo de falla de la unión adherida. Mediante la metodología numérica, se realizó un estudio paramétrico para investigar la influencia de los principales parámetros de la ley adherencia-deslizamiento en la carga última y la longitud adherida efectiva de las uniones.

A continuación, se estudió el efecto de las temperaturas de servicio y la carga sostenida en la fluencia de la unión adherida a partir de (i) ensayos de adherencia en especímenes NSM CFRP-hormigón y (ii) ensayos a tracción de especímenes de adhesivo epoxi. Se realizó un total de cinco campañas experimentales dentro. Los especímenes se ensayaron dentro de una cámara climática combinando distintos niveles de carga sostenida y varias temperaturas de servicio durante 1000 horas. De los resultados experimentales se pudo observar que la evolución de la deformación unitaria (en especímenes de adhesivo)

y deslizamiento en el extremo cargado (en especímenes NSM CFRP-hormigón) aumentaba a medida que la temperatura mediana de la cámara y el nivel de carga sostenida aumentaban.

Seguidamente, los especímenes sometidos a carga mantenida se ensayaron hasta rotura para evaluar la capacidad residual de la unión. De los ensayos, se observó un decrecimiento general de las propiedades mecánicas de las uniones adheridas (carga última y rigidez) y de los especímenes de adhesivo (resistencia a tracción y módulo elástico).

Finalmente, el procedimiento numérico desarrollado para predecir el comportamiento instantáneo de las uniones adheridas fue adaptado para calcular la fluencia en la unión NSM CFRP-hormigón a partir de la implementación de la degradación de la ley adhere—ncia-deslizamiento con el tiempo. A partir de esta metodología numérica se obtuvo la evolución de deslizamiento en el extremo cargado con el tiempo para cada configuración de espécimen y se comparó con el correspondiente ensayo experimental.

PART I: Introduction

1 Introduction

1.1 Overview and motivation

Rehabilitation and strengthening of infrastructures and existing buildings represents an effective action to extend their service life and to reduce the environmental impact associated to raw materials consumption and associated procedures. Consequently, an increase in the economic efforts for rehabilitation and maintenance is expected to take place in the next years, in front of the budged addressed to new construction. For this reason, there is a need of taking advantage of the new emerging technologies to mitigate deterioration and efficiency manage maintenance efforts on civil structures. In this sense, novel materials such as Fibre Reinforced Polymers (FRP) have appeared as new reinforcing materials and for strengthening of existing structures.

FRP materials present an attractive combination of mechanical properties, ease of assembly and durability, in comparison with other traditional materials. FRP materials have several advantages compared to steel, for example, their higher tensile strength and resistance against corrosion. On the other hand, FRP materials have several disadvantages, being the cost of manufacturing and their low fire resistance.

As a result of their growing application, some code proposals and recommendations for the design of reinforced concrete (RC) structures reinforced or strengthened with FRP have already been published, and it is foreseen their introduction in the new modification of Eurocode 2 [1]. The structural behaviour of concrete elements strengthened with FRP greatly depends on the bond behaviour of the joint concrete-FRP, in which an epoxy adhesive is generally used. The bond behaviour under static loading at ambient temperature has been extensively studied in the last years. However, concrete structures are often subjected to dynamic loading and harsh environmental conditions that may affect their durability and long-term performance.

Nowadays, several applications have been developed to reinforce or strengthen structures with FRPs, using them as unique material or in combination with concrete. Along the last decades, FRP materials have been extensively studied as external reinforcement of concrete structures. Externally Bonded Reinforcement (EBR) consists of bonding a FRP sheet or laminate onto the concrete surface using an adhesive, usually an epoxy adhesive. EBR are easy to install and they can significantly increase the carrying capacity of an existing structure. But on the other

hand, EBR are more affected to environmental conditions. Another well-known strengthening technique is the Near-Surface Mounted (NSM), in which a groove is cut in the concrete structure and afterwards, it is filled with an adhesive and the FRP is inserted. This strengthening method, in comparison with the EBR, provides a better anchorage capacity and a better protection of the FRP strip against external agents such as environment conditions or vandalism.

1.2 Objectives of the PhD

The main objective of this PhD thesis is to study, from an experimental and numerical point of view, the effects of different environmental and loading conditions on the bond behaviour of NSM FRP-concrete joints to provide analytical expressions that can evaluate the effectiveness of the given strengthening system.

This main goal is divided into six sub-objectives that will be addressed along with the thesis:

1. The study of the effect of the specimen configuration in terms of bonded length and groove thickness on the global behaviour of the bonded joint.
2. The investigation of the influence of the shape and the main parameters of the bond-slip law on the global behaviour of the bonded joint.
3. Develop a numerical model to predict the instantaneous response of the NSM CFRP-concrete joints.
4. The study of the creep behaviour and the residual tensile strength of an epoxy adhesive under the combination of sustained loading and different service temperatures (steady and cyclic).
5. The study of the creep behaviour and the residual bond capacity of NSM CFRP-concrete joints under the combination of sustained loading and service temperatures.
6. The proposal of a numerical procedure to predict the bonded joint response with time under sustained loading and room conditions.

1.3 Thesis layout

This thesis is written as a compendium of articles, each of them being presented in a chapter. Initially, the state-of-the-art is presented in Chapter 2 where a detailed study of the current state of the art is carried out.

In Chapter 3, the methodology followed in the experimental campaigns carried out in this thesis is presented. In this section, the characterization of the materials, the instantaneous and

sustained loading tests of NSM CFRP-concrete specimens are described. Furthermore, the numerical models developed to predict the instantaneous and the time-dependent response are presented in this chapter.

Chapter 4 presents the first article of the thesis, where the instantaneous behaviour of NSM CFRP-concrete specimens is studied and a numerical methodology is developed to predict the monotonic bonded joint response. The second paper of the thesis is presented in Chapter 5 where the experimental performance of NSM CFRP-concrete joints under sustained loading is presented and a numerical methodology is adapted to predict the time-dependent behaviour of the bonded joints. Chapter 6 provides the third paper, where the behaviour of an epoxy adhesive under different service conditions is studied through sustained tensile tests. In Chapter 7 the fourth article of this thesis is shown. This paper aims to study the bond behaviour of NSM CFRP-concrete specimens under the combination of sustained loading and high service temperatures.

The discussion and the concluding remarks of this thesis are presented in Chapters 8 and 9, respectively. Finally, Chapter 10 provides the possible future works derived from the research line followed in this thesis.

PART II: Literature review and methodology

2   Literature review

2.1   Introduction

Thanks to the excellent resistance against temperature and corrosion, high durability and low cost, concrete is widely used as a construction material in civil engineering. Even though civil structures are designed for a long service life, external agents, such as environmental conditions, seismic activities or changes on the load requirements can lead to rehabilitation and strengthening [2,3].

2.2   Fibre Reinforced Polymers (FRP) in civil engineering

Owing to their excellent properties, nowadays Fibre Reinforced Polymers (FRP) are used in an wide range of sectors, such as aerospace and aircraft, wind, construction, marine and medical, among others [4]. FRP materials present excellent mechanical properties, which allow enhancing the carrying capacity of the structure. Furthermore, they are corrosion resistant, and in terms of installation, FRP materials are easier to install due to their low weight, leading to a reduction of assembling time.

In this subsection, a summary of FRP components, mechanical properties and typical applications of FRP materials in civil engineering is shown.

2.2.1   FRP components

FRP materials are composed by: fibres, which provide the strength to the composite, and the matrix, which acts as the bonding agent among fibres [5].

Fibres

The fibres provide strength and toughness to the FRP. Typically, four fibre types can be found in FRPs: carbon, glass, aramid and basalt.

Carbon fibres are manufactured from heating fibres without the presence of oxygen. This process removes the non-carbon atoms and obtains a long inter-locked chain of carbon atoms. FRPs made of carbon fibres (CFRP) are widely used for strengthening concrete structures, due to their stiffness and tensile strength. Furthermore, they present high resistance against corrosion. The main disadvantages of carbon fibres may be that they are electrically conductive, hence, in case of contact with steel, they may create galvanic corrosion [6].

Glass fibres are made of filaments of glass, obtained from melting and moulding processes. Their use is very extended in the FRP materials, mainly because of their low production cost, high tensile strength, and good chemical resistance. On the other hand, this type of fibres presents lower fatigue resistance and stiffness, and higher brittleness than CFRP [7].

Aramid fibres are organic fibres formed by a long chain of synthetic polyamide and are created from a solution of PPTA (p-phenylene terephthalamides) polymer and sulfuric acid [8]. This type of fibre is characterized by its heat-resistance and lightness, compared with carbon and glass fibres. Regarding their mechanical properties, they present relatively higher tensile strength but lower elastic modulus in comparison with carbon fibres and steel. Compared with the other types of FRP, AFRP exhibit lower compressive and shear strengths [7,9].

Basalt fibres are obtained from crushed basalt, that is heated until melting. This fibre type has better mechanical properties than glass fibres and is cheaper than the carbon fibre [7]. The main disadvantages of the BFRP are the difficulty of the heating process and the quality control of the fibres [10].

Matrix

The matrix acts as bonding agent among fibres. Usually, the matrix is made of a thermoset, a polymer that is hardened by a curing process. The thermosetting polymers have high thermal stability at service temperature, and have better chemical resistance, compared to the thermoplastics. The most used types of thermoset adhesives are polyester, vinylester and epoxy. Polyester and vinylester have similar performing characteristics, although vinylester provides higher tensile strength and resistance to corrosion. On the other hand, epoxy adhesive is the most expensive option, but it has excellent bond properties, low shrinkage during curing time and good chemical resistance. The main disadvantage of thermoset adhesives is that their properties are highly affected at temperatures above their glass transition temperature (T_g) [7,9].

2.2.2   Mechanical properties of FRP materials

The constitutive stress-strain relationship of the most typical FRP types and steel according to *fib* Bulletin 90 [11] is shown in Figure 2.1.
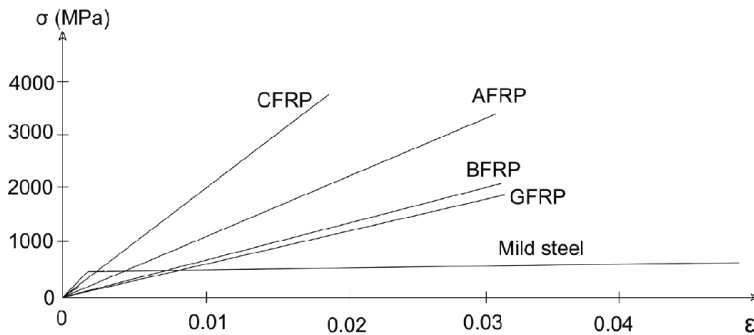
Figure 2.1: Uniaxial tensile stress-strain diagrams of FRP materials compared to steel [11].

As observed, FRP materials present a higher tensile strength and generally a lower elastic modulus in comparison to steel. Furthermore, their stress-strain behaviour is linear until failure [12], leading to a brittle rupture, instead of the ductile failure of steel.

2.2.3   Applications of FRP materials in civil engineering

Due to FRPs' excellent mechanical properties, their use in civil structures has been widely extended during the last years. Three main applications are distinguished: as core materials to build a complete structure, as strengthening system of an existing element (Figure 2.2a) or as internal reinforcement of concrete elements (i.e. as substitute of traditional steel, Figure 2.2b).

Figure 2.2: Examples of the use of FRP materials as (a) strengthening method and (b) reinforcing method [5].

2.3 FRP for strengthening concrete structures

Strengthening systems allow enhancing the carrying capacity of the concrete structure during its service life, becoming an optimal solution for rehabilitation and repair of buildings and civil infrastructure. In this section, the two main strengthening methods used in civil engineering (Externally Bonded Reinforcement, EBR, and Near-Surface Mounted, NSM) are presented.

2.3.1 Externally Bonded Reinforcement (EBR)

The EBR technique consists of bonding FRP strips or sheets onto the tensile concrete surface, previously roughened to improve the bond performance, with a structural adhesive, usually being an epoxy resin. The most commonly used FRP material used in the EBR application is the CFRP, being GFRP and AFRP only used in specific situations.

The EBR can be applied either by wet lay-up (FRP laminate cured in-situ onto the concrete surface) or prefabricated (precured FRP bonded onto concrete). The wet lay-up system is typically used to strengthen concrete elements in one or more directions, such as in columns or beams. The prefabricated system consists of bonding a unidirectional laminate or strip of FRP, previously manufactured and cured, with an adhesive to a flat surface.

The main advantage of the EBR technique is the simplicity of installation and the adaptability of the technique. It can be applied in many circumstances, for example, for wrapping a column to enhance its confinement level or for strengthening a beam or slab to enhance its flexural or shear behaviour, as can be seen in Figure 2.3.
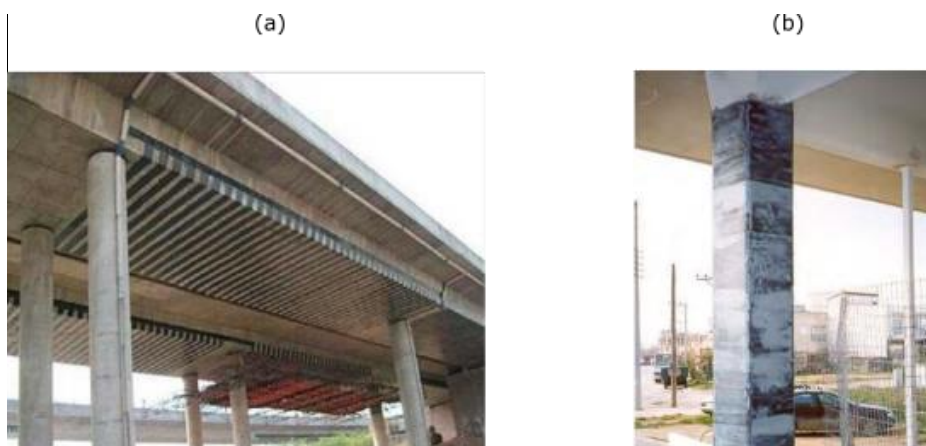
Figure 2.3: Examples of EBR installation [13,14].

Although EBR is a common strengthening technique used in civil engineering, the main failure mode of concrete flexural elements strengthened with EBR FRP is the debonding of the FRP, providing a very brittle failure, and besides, not recommendable in terms of safety. Because the failure is debonding of the strengthening element, the FRP does not reach its ultimate capacity [15] and further anchorage mechanisms need to be developed.

On the other hand, one of the main disadvantages of this technique is that the FRP is exposed to the environmental conditions and external agents. In particular, the exposition of the adhesive to ambient temperatures can decrease its bond properties. Other bonding agents, such as cementitious adhesives, may provide higher resistance to high temperatures although it is not recommended to use them under cyclic loading due to the lower shear strength and brittleness [16].

2.3.2   Near Surface Mounted (NSM)

The Near Surface Mounted (NSM) technique started to be used during the 40s, however, the NSM application with FRP materials has only been studied during the last two decades. The NSM consists of cutting a groove along the concrete surface, filling it with adhesive and introducing the FRP reinforcement so that the FRP reinforcement is completely coated by the adhesive. Figure 2.4 shows an example of application of a NSM FRP reinforcement on a two-way RC slab: in Figure 2.4a the adhesive is inserted into the groove, and Figure 2.4b shows the installation of the CFRP bar into the groove.

(a)   (b)

Figure 2.4: Examples of NSM installation: (a) installation of the epoxy adhesive and (b) installation of CFRP bar [17].

The shape of the NSM FRP reinforcement that can be used with this technique can be either rectangular/square strips or round bars. Sharaky *et al.* [18,19] performed an investigation on the effect of the shape and material of the FRP reinforcement on the instantaneous behaviour of the bonded joint. The study concluded that GFRPs can be used in most of the applications of the NSM, although their lower tensile strength and stiffness than CFRP implies the use of higher cross-sectional areas and grooves. Furthermore, it was observed that bars with a textured surface increased the ultimate load around 34% compared to bars with a smoother surface. A typical cross-section of the grooves and FRP materials of the NSM technique is shown in Figure 2.5.
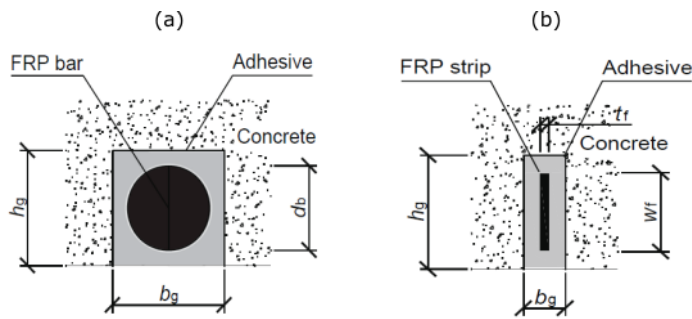
Figure 2.5: Cross-section of NSM systems using: (a) using a bar and (b) using a strip [20].

De Lorenzis *et al.* [21], and Sena *et al.* [22] extensively studied the NSM technique, concluding that NSM has several advantages over EBR technique. Although the laminates used in the NSM have smaller dimensions than those used in the EBR, the bonded perimeter/area of the reinforcement ratio is higher than in the EBR, improving the efficiency of the FRP material (Seracino *et al.* [23]) because the confinement provided by surrounding concrete makes the FRP less prone to debond [22,24]. FRP laminate also is less affected by unfavourable environmental conditions. Besides, no surface conditioning is needed, except for the cutting of the groove, and can be easily pre-stressed, making it more attractive for its application in the construction industry.

2.4   Instantaneous bond behaviour of FRP-concrete joints

The instantaneous bond behaviour of the FRP-concrete joint is typically characterized by a mechanical test from which the most relevant properties of the joint can be obtained. In this sub-chapter, the most typical test set-ups, together with a summary of the bond failure modes are explained. Then, the ultimate load and effective bonded length are defined, and the most

relevant models are presented. The local and global bond behaviour of the FRP-concrete joint are next explained, and some of the most used bond-slip models available in the literature for EBR and NSM SYSTEMS are shown. Finally, the concept of fracture energy is introduced and some of the most well-known analytical models are presented.

2.4.1 Test set-up

Nowadays, the bond capacity of the FRP-concrete interface can be evaluated by using different test setups, being the most accepted ones the single-shear test [25,26], the double-shear test [27], and the beam test [28].

The pull-out single-shear test consists of bonding an FRP laminate on the lateral surfaces of the concrete block, then pulling the FRP while the movement of the concrete block is restricted, or vice versa. This type of test has been adopted by many researchers due to its simplicity [15,22,26], however, in this methodology, the load is usually applied eccentrically with respect to the centroid of the specimen, causing an attempt of rotation of the concrete block. Some researchers [19,29] proposed more complex geometries for the concrete block to avoid these eccentricities, but the resultant block was not that operable.

The double shear test was proposed to solve the eccentricity problem [27,30]. In this test, two FRPs are bonded on opposite surfaces of the concrete element, creating a symmetry of loading. However, this test is much more difficult to control because the imperfections of both surfaces can cause unavoidable asymmetries.

Finally, in the beam test [15,31], two prismatic blocks are connected by a hinge in the compression flange and the FRP laminate is bonded on the tensile surface of the concrete specimens. The shortest bonded length side is used to register the slip and strain during the test, while the longest side works as an anchorage.

Figure 2.6 presents the classification of tests set-up proposed by Yao *et al.* [15].
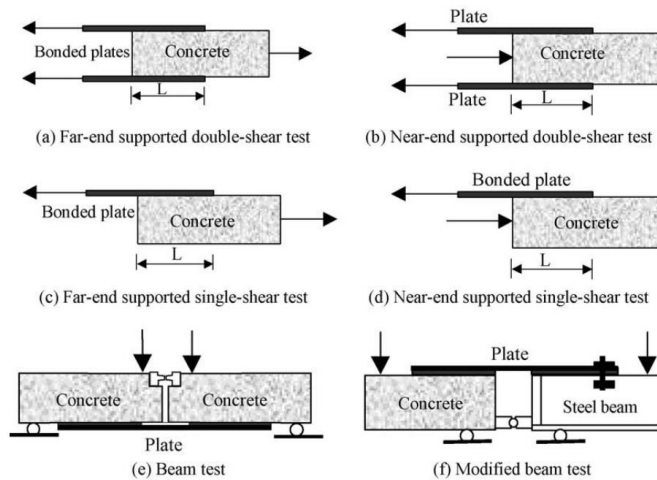
Figure 2.6: Classification of bond tests according to Yao *et al.* [15].

2.4.2 Bond failure modes of the bonded joint

The control of the failure modes of the bonded joint is crucial for an adequate structural design. The main bond failure modes of the FRP-concrete joint [21,32,33] are shown in Figure 2.7 and briefly explained below.
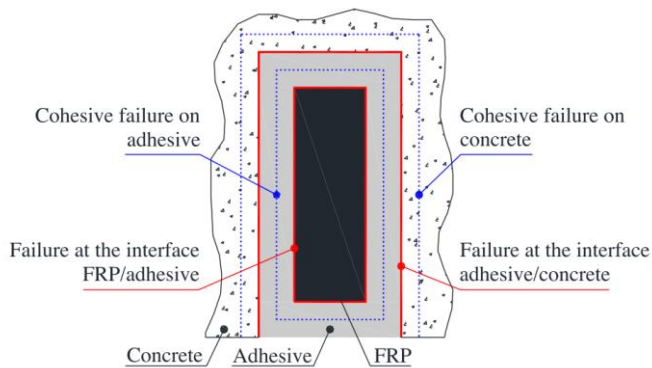
Figure 2.7: Failure modes for the NSM reinforcement [32].

- Interfacial bond failure between the FRP and the adhesive: The interfacial bond failure between the FRP and the adhesive is mainly due to the lack of adhesion between these two surfaces, which can be caused by the smoothness of the laminate's surface or an inappropriate spread of the adhesive through the laminate [34,35].

- Interfacial bond failure between the adhesive and the concrete: This failure mode also derives from a lack of adhesion between these two elements. In this case, the surface treatment of the concrete may be the main responsible. Having a high level of roughness in the concrete implies better contact with the adhesive layer [35–37].
- Cohesive failure in the adhesive: This failure is achieved when the shear stress applied to the specimen surpasses the shear strength of the adhesive. This failure mode has only been observed NSM strengthening systems using strips with a roughened surface [38,39].
- Cracking of the concrete element: In this failure mode, the splitting of concrete is attained when the concrete element cannot withstand the tensile and shear stresses transferred from the FRP strengthening system [40].
- Rupture of the FRP: When the FRP reaches its tensile stress before debonding takes place. This type of failure is more common when strips are used, rather than laminates or bars, because they have less cross-sectional area and higher perimeter/area ratio. In this failure mode, despite being brittle, it is desired because the FRP attains its tensile strength [35,41,42].

2.4.3   Ultimate load and effective bonded length models

The ultimate load of the FRP-concrete joint is of outmost interest for calculating the withstanding capacity of the bonded joints. In the last decades, much research has been focused to obtain analytical expressions to easily calculate the ultimate load. Moreover, the concept of effective bonded length, proposed by Maeda *et al.* [43] and defined as the minimum length to develop the maximum load of the bonded joint, has attracted the attention of the scientific community to predict the maximum shear strength of the FRP-concrete joint.

In the following two sub-sections, the main existing models in the literature for the ultimate load and effective bonded length of the FRP-concrete joint are introduced.

Ultimate load empirical models

A pragmatic and reliable method for calculating the bond strength of the joint is needed. In this sense, many research can be found, being analytical expressions usually adjusted to given experimental results [23,25,43–47]. From these empirical formulation, standards are proposed to establish a common procedure to design this type of joints, being nowadays the most used standards the ACI 440.2R [48], the CNR-DT 200 R1 [49] and the *fib* [50].

A summary of the most important bond strength models is presented in Table 2.1 for EBR and in Table 2.2 for NSM bonded joints. These equations provide the maximum shear strength (or ultimate load) of the bonded joint, considering that the load is applied in pure shear mode, hence, no bending moments are considered.

Effective bonded length empirical models

The effective bond length is the minimum bonded length needed for reaching the ultimate load. In other words, it is the length needed for having the complete strain profile along the bonded length of the FRP, as further explained in chapter 4. Having a longer bonded length does not imply an increase of strength, but a shifting of the strain profile along the bonded FRP, causing an increase of slip between the FRP and the concrete. On the other hand, a shorter bonded length implies that the joint will not reach its maximum bond load, and that the strain profile will not be completely developed.

As for the case of the ultimate load, several authors have defined analytical expressions adjusted from their experimental results. Standards such as the *fib* Bulletin 90 [50], CNR-DT 200 R1 [51], ACI 440.2R [48] and the SA [52] have proposed analytical expressions to calculate the effective bonded lengths of EBR and NSM systems. The most important expressions are summarised in Table 2.1 for EBR and in Table 2.2 for NSM.

Table 2.1: Bond strength models for EBR systems.

Model	Ultimate load (P_u)	Effective length (L_{eff})	Parameters
Neubauer et al. [47]	$P_u = \begin{cases} 0.64\beta_w b_f \sqrt{E_f t_f f_t}, & L_b \geq L_{eff} \\ 0.64\beta_w b_f \sqrt{E_f t_f f_t}\dfrac{L_b}{L_{eff}}\left(2 - \dfrac{L_b}{L_{eff}}\right), & L_b < L_{eff} \end{cases}$	$L_{eff} = \sqrt{\dfrac{E_f t_f}{2 f_t}}$	$\beta_w = \sqrt{1.125\dfrac{2 - b_f/b_c}{1 + b_f/400}}$
Maeda et al. [43]	$P_u = 110.2 \times 10^{-6} E_f t_f b_f L_{eff}$	$L_{eff} = e^{6.13 - 0.58 \ln\ln E_f t_f}$	-
Chen and Teng [25]	$P_u = 0.427 b_f \beta_L \sqrt{f_c} b_f L_{eff}$	$L_{eff} = \sqrt{\dfrac{E_f t_f}{\sqrt{f_c}}}$	$\beta_l = \begin{cases} 1, & L_b \geq L_{eff} \\ L_e \sin\dfrac{\pi L_b}{2 L_{eff}}, & L_b < L_{eff} \end{cases}$ $b_f = \sqrt{\dfrac{2 - b_f/b_c}{1 + b_f b_c}}$
Lu et al. [44]	$P_u = b_f \beta_w \sqrt{2 E_f t_f G_f}$	$L_{eff} = a + \dfrac{1}{2\lambda_1}\ln\dfrac{\lambda_1 + \lambda_2 \tan(\lambda_2 a)}{\lambda_1 - \lambda_2 \tan(\lambda_2 a)}$	G_f and β_w defined in Table 2.5 $a = \dfrac{1}{a}\arcsin[0.99\sqrt{\dfrac{s_f - s_1}{s_f}}]$ $\lambda_1 = \sqrt{\dfrac{\tau_{max}}{s_1 E_f t_f}}$ $\lambda_2 = \sqrt{\dfrac{\tau_{max}}{(s_f - s_1) E_f t_f}}$

			$\tau_{max} = 1.5\beta_w f_t$
Dai et al. [53]	$P_u = \dfrac{b_f \tau_{max}}{\sqrt{\dfrac{\tau_{max}^2}{2G_f}\left(\dfrac{1}{E_f t_f} + \dfrac{b_f}{E_c t_c b_c}\right)}}$	-	G_f defined in Table 2.5
Camli and Binici [45]	$P_u = \sqrt{\tau_{max} s_f}\sqrt{E_f t_f}\, b_f\, tanh\left(\dfrac{\theta L_b}{L_{eff}}\right)$	$L_{eff} = \sqrt{\dfrac{E_f t_f}{\sqrt{f_c}}}$	$\theta = \sqrt{\dfrac{\tau_{max}}{s_f\sqrt{f_c}}}$ $\tau_{max} = 3.5 f_c^{0.19}$ $s_f = f_c^{-0.4}\left(\dfrac{L_b}{L_{eff}}\right)^{0.8}\left(\dfrac{b_f}{b_c}\right)^{0.4}$
Iso [54]	$P_u = b_f L_{eff} 0.93 f_c^{0.44}$	$L_{eff} = 1.89\left(E_f t_f\right)^{0.4}$	-
Sato [54]	$P_u = (b_f + 7.4)L_{eff} 2.68 f_c^{0.2} E_f t_f \times 10^{-5}$	$L_{eff} = 0.125\left(E_f t_f\right)^{0.57}$	-
fib Bulletin 90 [50]	$P_u = \alpha c_1 k_c \beta_w b\sqrt{E_f t_f f_t}$	$L_{eff} = \sqrt{\dfrac{E_f t_f}{2 f_t}}$	$\beta_w = 1.06\sqrt{\dfrac{2 - b_f/b_c}{1 + b_f/400}} \geq 1$ $c_1 = 0.64$

*CNR-DT
200 R1
[51]*

\-

$$L_{eff} = min\left(\frac{1}{\gamma_{Rd}\tau_{max}}\frac{\pi E_f t_f}{G_f}, 200\right)$$

$$\beta_w = 1.06\sqrt{\frac{2 - b_f/b_c}{1 + b_f/400}} \geq 1$$

G_f defined in Table 2.5

$$\tau_{max} = \frac{2G_f}{s_f}$$

$$s_f = 0.25\ mm$$

$$\gamma_{Rd} = 1.25$$

Table 2.2: Bond-strength models for NSM strengthening systems.

Model	Ultimate load (P_u)	Effective length (L_e)	Parameters
Zhang *et al.* [46]	$P_u = \begin{cases} \sqrt{2G_f E_f A_f C_{failure}}, & L_b \geq L_{eff} \\ \beta_l \sqrt{2G_f E_f A_f C_{failure}}, & L_b < L_{eff} \end{cases}$	$L_{eff} = \dfrac{1.66}{\eta}$	$C_{failure} = 2b_f + t_f$ $\eta = \dfrac{\tau_{max}^2 C_{failure}}{2G_f E_f A_f}$ $\beta_l = \dfrac{L_b}{L_{eff}}(2.08 - 1.08\dfrac{L_b}{L_{eff}})$
Seracino *et al.* [23]	$P_u = \alpha_p 0.85 \beta_e \beta_{L,s} \gamma_s^{0.25} f_c^{0.33} \sqrt{E_f A_f L_{failure}\left(\dfrac{b_f + L_{per}}{L_{per}}\right)^{1.2}}$	$L_{eff} = \dfrac{\pi}{2(0.802 + 0.078)}\sqrt{\dfrac{0.976\gamma_s^{0.526} E_f A_f}{f_c^{0.6} L_{crit}}}$	$\alpha_p = 1$ $\beta_e = 0.283\dfrac{a_e}{b_f} + 0.196$ ≤ 1 $\beta_{L,s} = \dfrac{L_b}{L_{eff}} \leq 1$ $L_{crit} = 2b_f + t_f + 4$
Bilota *et al.* [35,55]	$P_u = kb_f\sqrt{2E_f t_f \beta_w f_c^{0.6}}$	-	$\beta_w = \sqrt{\dfrac{2 - b_f/b_c}{1 + b_f/b_c}}$ $k = 0.255$

Oehlers et al. [40]	$P_u = \sqrt{\tau_{max}s_f L_{per}}\sqrt{n(E_f A_f) + k_{EAC}E_c A_c}$	-	$k_{EAC} = 0.2$ $n =$ number of plates
SA [52]	$P_u = \begin{cases} \dfrac{\sqrt{\tau_{max}s_f}\sqrt{L_{per}E_f A_f}}{1000}, & L_b \geq L_e \\ \dfrac{\sqrt{\tau_{max}s_f}\sqrt{L_{per}E_f A_f}}{1000}\dfrac{L_b}{L_{eff}}, & L_b < L_e \end{cases}$	$L_{eff} = \dfrac{\pi}{2\sqrt{\dfrac{\tau_{max}L_{per}}{s_f E_f A_f}}}$	$L_{per} = 2t_f + 2b_f$
ACI 440.2R [56]	$P_u = \dfrac{f_{fe}b_f t_f}{1000}$	$L_{eff} = \dfrac{23300}{\left(\dfrac{E_f}{E_c}t_f E_f\right)^{0.58}}$	$f_{fe} = E_f \varepsilon_{fe}$ $\epsilon_{fe} = 0.41\sqrt{\dfrac{f_c'}{E_f t_f}}$

2.4.4 Local bond behaviour of the bonded joint

The bond law, often referred as the bond-slip law or interface law, is the relationship between the bond shear stress of the joint and the relative displacement between the FRP and the concrete. A commonly accepted approximation of the bond behaviour for a NSM strengthening system is a bilinear law, consisting of three main stages: elastic, softening and debonding [25,57], as it is shown in Figure 2.8.
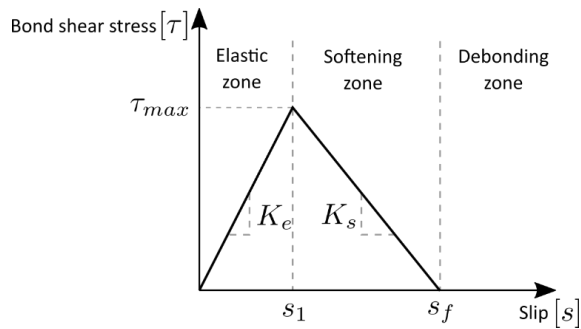
Figure 2.8: Bilinear bond-slip law [58].

In the elastic zone, the bond shear stress increases linearly with the slip until reaching the bond shear strength. At this point, the joint starts to damage, entering in the softening stage, where the bond shear stress decreases linearly with the slip. Finally, when the bond shear stress becomes null, the section of the bonded joint is in the debonding stage.

Yuan *et al.* [59] considered that a more representative bond-slip law would have an additional stage in between the elastic and the softening ones, called hardening (Figure 2.9). This stage represents a decrease in the ascending stiffness of the curve before reaching the shear strength.
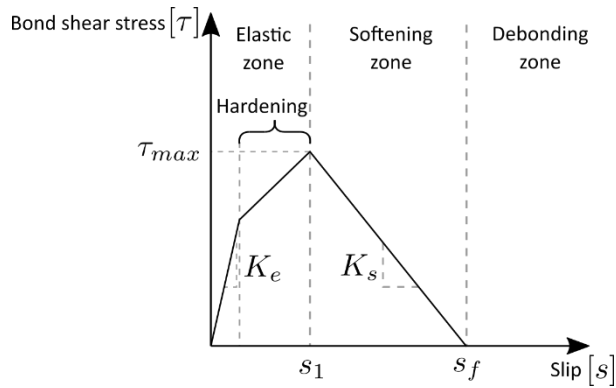
Figure 2.9: Bond-slip law including a hardening stage [59].

Borchert *et al.* [60], in turn, proposed a bond-slip law where the debonding branch considers friction between CFRP and concrete through a residual bond shear strength (τ_f), a non-linear ascending branch and a plateau of the bond shear stress when the slip is between s_1 and s_2. Figure 2.10 presents the bond-slip proposed in [60].
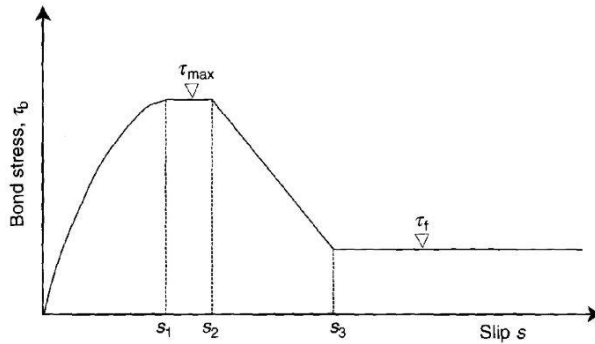
Figure 2.10: Bond-slip law proposed in Borchert *et al.* [60].

Depending on the considered bond-slip law, the prediction of the joint's strength will be somehow different. The most common methodology to represent the bond-slip law is to use a piecewise function, where the stages of the bond-slip can be calculated through their own equation. A list of the most used bond-slip models for EBR and NSM is presented in Table 2.3 and Table 2.4, respectively.

Table 2.3: Bond-slip models for EBR systems in the literature.

Model	Ascending branch	Descending branch	Parameters
Brosens and Van Gemert [61]	$\tau = \tau_{max}\left(\dfrac{s}{s_1}\right)$	$\tau = \tau_{max}\left(\dfrac{s_f - s}{s_f - s_1}\right)$	$\tau_{max} = 1.8\beta_w f_{ct}$ $s_1 = 2{,}5\tau_{max}\left(\dfrac{t_a}{E_a} + \dfrac{50}{E_c}\right)$ $s_f = \dfrac{2G_f}{\tau_{max}}$ $\beta_w = \sqrt{1.5\dfrac{2 - b_f/b_c}{1 + b_f/100}}$
Neubauer et $al.$ [47]	$\tau = \tau_{max}\left(\dfrac{s}{s_1}\right)$	0	$\tau_{max} = 1.8\beta_w f_{ct}$ $s_1 = 0.202\beta_w$ $\beta_w = \sqrt{1.125\dfrac{2 - b_f/b_c}{1 + b_f/400}}$
Brosens [62]	$\tau = \tau_{max}\left(\dfrac{s}{s_1}\right)$	$\tau = \tau_{max}\left(\dfrac{s_f - s}{s_f - s_1}\right)$	$\tau_{max} = \beta_w\beta_c\dfrac{f_t f_c}{f_t + f_c}$ $s_1 = \tau_{max}\left(2.4\dfrac{t_c}{E_c} + 2.5\dfrac{t_f}{E_f} + n\dfrac{t_a}{E_a}\right)$ $s_f = \dfrac{2G_f}{\tau_{max}}$

			$\beta_w = \sqrt{k\dfrac{2 - b_f/b_c}{1 + \dfrac{b_f}{b_c}}}$
Monti *et al.* [63]	$\tau = \tau_{max}\left(\dfrac{s}{s_1}\right)$	$\tau = \tau_{max}\left(\dfrac{s_f - s}{s_f - s_1}\right)$	$\tau_{max} = 1.8\beta_w f_{ct}$ $s_1 = 2{,}5\tau_{max}\left(\dfrac{t_a}{E_a} + \dfrac{50}{E_c}\right)$ $s_f = 0.33\beta_w$ $\beta_w = \sqrt{1.5\dfrac{2 - b_f/b_c}{1 + b_f/100}}$
Nakaba *et al.* [64]	$\tau = \tau_{max}\left(\dfrac{s}{s_1}\right)\left[\dfrac{3}{\left(2 + \left(\dfrac{s}{s_1}\right)^3\right)}\right]$		$\tau_{max} = 3.5(f_c)^{0.19}$ $s_1 = 0.065$ mm
Savioia *et al.* [65]	$\tau = \tau_{max}\left(\dfrac{s}{s_1}\right)\left[\dfrac{2.86}{\left(1.86 + \left(\dfrac{s}{s_1}\right)^{2.86}\right)}\right]$		$\tau_{max} = 3.5(f_c)^{0.19}$ $s_1 = 0.065$ mm
Dai *et al.* [53]	$\tau = 2BG_f(e^{-Bs} - e^{-2Bs})$		$\tau_{max} = 0.5BG_f$ $s_f = 0.693B$ $B = 6.846(E_f t_f)^{0.108}\left(\dfrac{G_a}{t_a}\right)^{0.833}$

Lu (precise) [44]	$\tau = \tau_{max}\sqrt{\dfrac{s}{s_1 A} + B^2} - B$	$\tau = \tau_{max}e^{\left(-\alpha\left(\frac{s}{s_1}-1\right)\right)}$	$A = \dfrac{s_1 - s_e}{s_1} \qquad B = \dfrac{s_e}{2(s_1 - s_e)}$
			$K_0 = \dfrac{K_a K_c}{K_a + K_c} \quad K_a = \dfrac{G_a}{t_a} \quad K_c = \dfrac{G_c}{t_c}$
			$\alpha = \dfrac{\tau_{max} s_1}{G_f - G_a}$
			$\alpha_1 = 1.5 \qquad \alpha_2 = 0.0195 \qquad \alpha_3 = 0.308$
			$G`_a = \tau_{max} s_1 \dfrac{2A}{3}\left(\dfrac{1 + B^2 A}{A}\right)^{3/2} - B - \dfrac{2}{3}B^3 A$
			$\beta_w = \sqrt{\dfrac{2.25 - b_f/b_c}{1.25 + b_f/b_c}}$
			G_f is defined in Table 2.5
Lu (simplified) [44]	$\tau = \tau_{max}\sqrt{\dfrac{s}{s_1}}$	$\tau = \tau_{max}e^{\left(-\alpha\left(\frac{s}{s_1}-1\right)\right)}$	$\tau_{max} = 1.5\beta_w f_{ct}$
			$s_1 = 0.0195\beta_w f_{ct}$
			$\alpha = \dfrac{1}{\dfrac{G_f}{\tau_{max}} - \dfrac{2}{3}}$
			G_f is defined in Table 2.5

| Lu (bilinear) [44] | $\tau = \tau_{max} \left(\dfrac{s}{s_1} \right)$ | $\tau = \tau_{max} \left(\dfrac{s_f - s}{s_f - s_1} \right)$ | $\tau_{max} = 1.5\beta_w f_{ct}$
 $s_1 = 0.0195\beta_w f_{ct}$
 $s_f = \dfrac{2G_f}{\tau_{max}}$
 G_f is defined in Table 2.5 |

Note: parameters of each bond-slip law are defined in their respective references.

Table 2.4: Bond-slip models for NSM systems in the literature.

Model	Ascending branch	Descending branch	Parameters
Seracino *et al.* [57]	$\tau = \tau_{max}\left(\dfrac{s}{s_1}\right)$	$\tau = \tau_{max}\left(\dfrac{s_f - s}{s_f - s_1}\right)$	$\tau_{max} = 0.54\sqrt{f_c}\,b_f{}^{0.4}t_f{}^{0.3}$ $s_1 = 0.2$ mm $s_f = 0.78\dfrac{f_c{}^{0.27}}{t_g{}^{0.3}}$ $t_g = t_f + 1$
Sena *et al.* [66]	$\tau = \tau_{max}\left(\dfrac{s}{s_1}\right)^{\alpha}$	$\tau = \tau_{max}\left(\dfrac{s}{s_1}\right)^{\alpha'}$	$\tau_{max} = 23.2$ MPa $s_1 = 0.0042L_b$ $\alpha = 0.18 \quad \alpha' = -0.18$
Borchert *et al.* [60]	$\tau = \begin{cases} \tau_{max}\left(\dfrac{s}{s_1}\right)^{\alpha}, & 0 \le s \le s_1 \\ \tau_{max}, & s_1 < s \le s_2 \end{cases}$	$\tau = \begin{cases} \tau_{max} - (\tau_{max} - \tau_f)\left(\dfrac{s - s_2}{s_3 - s_2}\right), & s_2 < s \le s_3 \\ \tau_f, & s > s_3 \end{cases}$	$\tau_{max} = 0.54\sqrt{f_c}\,b_f{}^{0.4}t_f{}^{0.3}$ $s_1 = 0.8s_2 \quad s_2 = \dfrac{2\tau_{max}t_a\eta_{ar}}{G\,\eta_{s2}}$ $s_3 = s_2 + \dfrac{(\tau_{max}-\tau_f)t_a}{G\,\eta_{s23}}$ $G = \dfrac{E_{dyn}}{2(1+v)}$ $\tau_f = C_{\tau,f}\eta_{ar}\tau_{max}$ $\eta_{ar} = \tanh\tanh\left(\dfrac{a_r}{80}\right) \text{ if } a_r < 150\ mm$ $\alpha = C_{\alpha,1}t_\alpha + C_{\alpha,2}\alpha_{lim} = 0.31$

			$\eta_{si} = C_{si,1}t_\alpha + C_{si,2}t_\alpha$
			$C_{\tau,max} = 0.59 \quad C_{\tau,max} = 0.415$
			$C_{\alpha,1} = 0.38 \quad C_{\alpha,2} = -0.105$
			$C_{\eta2,1} = 0.076 \quad C_{\eta2,2} = -0.008$
			$C_{\eta23,1} = 0.025 \quad C_{\eta23,2} = -0.010$
Ceroni *et al.* [67]	$\tau = \begin{cases} m_{lin} \cdot s, & 0 \le s \le s_{lin} \\ \tau_{max}\left(\dfrac{s}{s_1}\right)^\alpha, & s_{lin} < s \le s_1 \end{cases}$	$\tau = \tau_{max}\left(\dfrac{s}{s_1}\right)^{\alpha'}$	$s_{lin} = 0.01 \; mm$ $m_{lin} = \tau_{lin}/s_{lin}$ $\alpha = 0.40 \quad \alpha' = -0.31$
Zhang *et al.* [68]		$\tau = A\left(\dfrac{2B-s}{B}\right)^2 \sin\left(\dfrac{\pi}{2}\dfrac{2B-s}{B}\right)$	$\tau_{max} = 1.15\gamma^{0.138}f_c^{0.613}$ $A = 0.72\gamma^{0.138}f_c^{0.613}$ $B = 0.37\gamma^{0.284}f_c^{0.006}$ $\gamma = \dfrac{h_g}{t_g}$
ACI 440.2R-17 [69]		$\tau = 6.91 \; MPa$	
fib *Bulletin 90* [11]	$\tau = \begin{cases} \tau_{max}\left(\dfrac{s_f - s}{s_f}\right)^\alpha, & 0 \le s \le s_1 \\ \tau_{max}, & s_1 < s \le s_2 \end{cases}$	$\tau = \begin{cases} \tau_{max} - (\tau_{max} - \tau_f)\left(\dfrac{s - s_2}{s_3 - s_2}\right), & s_2 < s \le s_3 \\ \tau_f, & s > s_3 \end{cases}$	$\tau_{max} = 2\sqrt{f_c}$ $\tau_f = 0.15\tau_{max}$ $s_2 = 0.6 \; mm$ $s_3 = 1 \; mm$ $\alpha = 0.4$

SA [52]	-	$\tau = \tau_{max}\left(\dfrac{s_f - s}{s_f}\right)$	$\tau_{max} = (0.078\rho + 0.8)f_c^{0.6}$
			$s_f = 0.78\dfrac{\rho^{0.5}f_c^{0.67}}{\tau_{max}}$
			$\rho = 2b_f + 2t_f$

To experimentally obtain the bond-slip law of the bonded joint, several authors have used strain gauges bonded along the FRP to register the strain profile of the reinforcement so as to calculate the average shear stress and slip between two subsequent strain gauges (Figure 2.11) [35,53,70–72].
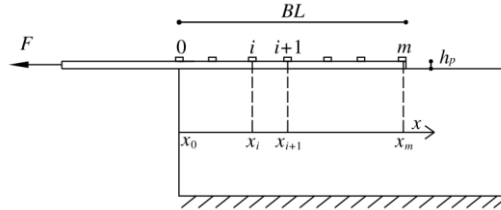
Figure 2.11: Location of the strain gauges used in Ferracuti *et al.* [70].

The shear stress between two strain gauges can be calculated using Eq. 2.1,

$$\tau_{i+1/2} = -\frac{E_f A_f (\varepsilon_{f,i+1} - \varepsilon_{f,i})}{L_{failure} (x_{f,i+1} - x_{f,i})} \tag{2.1}$$

where E_f and A_f are the elastic modulus and cross-section area of the FRP, $L_{failure}$ is the perimeter of the failure surface, ε_f is the strain measured by a strain gauge and x is the position in the bonded length. In case of EBR, $L_{failure}$ equals to the width of the laminate, b_f, while in case of NSM, it is equal to $2 * (b_f + t_a) + (t_f + t_a)$ [73], where t_a and t_f are the thicknesses of the adhesive layer and of the FRP strip, respectively.

The slip (s) along the FRP can be obtained from integration of the strain profile using Eq. 2.2.

$$s(x) = s(x_{i+1}) - \frac{(\varepsilon_{f,i+1} - \varepsilon_{f,i})}{(x_{i+1} - x_i)} \frac{(x_{i+1} - x_i)^2}{2} + \varepsilon_{f,i}(x_{i+1} - x_i) \tag{2.2}$$

Finally, the average slip between two gauges can be calculated using Eq. 2.3. As a result, the experimental bond τ -slip s law can be obtained.

$$s_{i+1/2} = -\frac{s(x_{i+1}) + s(x_i)}{2} \tag{2.3}$$

2.4.5   Global behaviour of the bonded joint

The global load-slip behaviour of the bonded joint can be experimentally obtained by simply measuring the load applied on the specimen and the relative slip between the FRP and the concrete block. Yuan *et al.* [74] and Ali *et al.* [75] proposed analytical solutions for the governing differential equation of an EBR and an NSM CFRP-concrete joint, respectively. The differential

equation governing the bonded joint is obtained from the stress equilibrium between the FRP and the concrete, and is expressed using Eq. 2.4,

$$\frac{d\sigma_f}{dx} - \frac{\tau(s) * L_{per}}{A_f} = 0, \tag{2.4}$$

where L_{per} is the perimeter of the FRP strip or laminate.

In these analytical models, no bending moments were considered and a bilinear slip law was assumed.

In the instantaneous test of the bonded joint, as the load applied increases, the bonded joint will gradually experience different stages. All the stages of the load-slip curve for a specimen with a bonded length longer than L_{eff} and a bilinear bond-slip law is shown in Figure 2.12, and the bond shear stress profile of the FRP at each stage of the load-slip curve is shown in Figure 2.13.
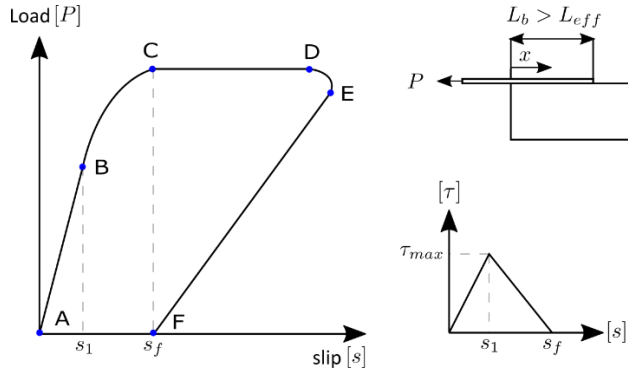
Figure 2.12: Stages of the load-slip curve of considering a bilinear local bond-slip relationship.

Stage A-B

$[\tau]$

$s < s_1$

$\tau < \tau_{max}$

$Position[x]$

- -

Point B

$[\tau]$

τ_{max}

$s <= s_1$

$Position[x]$

- -

Stage B-C

$[\tau]$

$s < s_f$ | $s <= s_1$

τ_{max}

$\tau < \tau_{max}$

$Position[x]$

- -

Point C

$[\tau]$

$s <= s_f$ | $s <= s_1$

τ_{max}

a_d

L_{eff}

$Position[x]$

- -

Stage C-D

$[\tau]$

$s > s_f$ | $s <= s_f$ | $s <= s_1$

τ_{max}

a_d

L_{eff}

$Position[x]$

- -

Stage D-E

$[\tau]$

τ_{max}

a_d

$Position[x]$

- -

Point E

$[\tau]$

τ_{max}

a_u

$Position[x]$

- -

Stage E-F

$[\tau]$

$\tau < \tau_{max}$

a_u

$Position[x]$
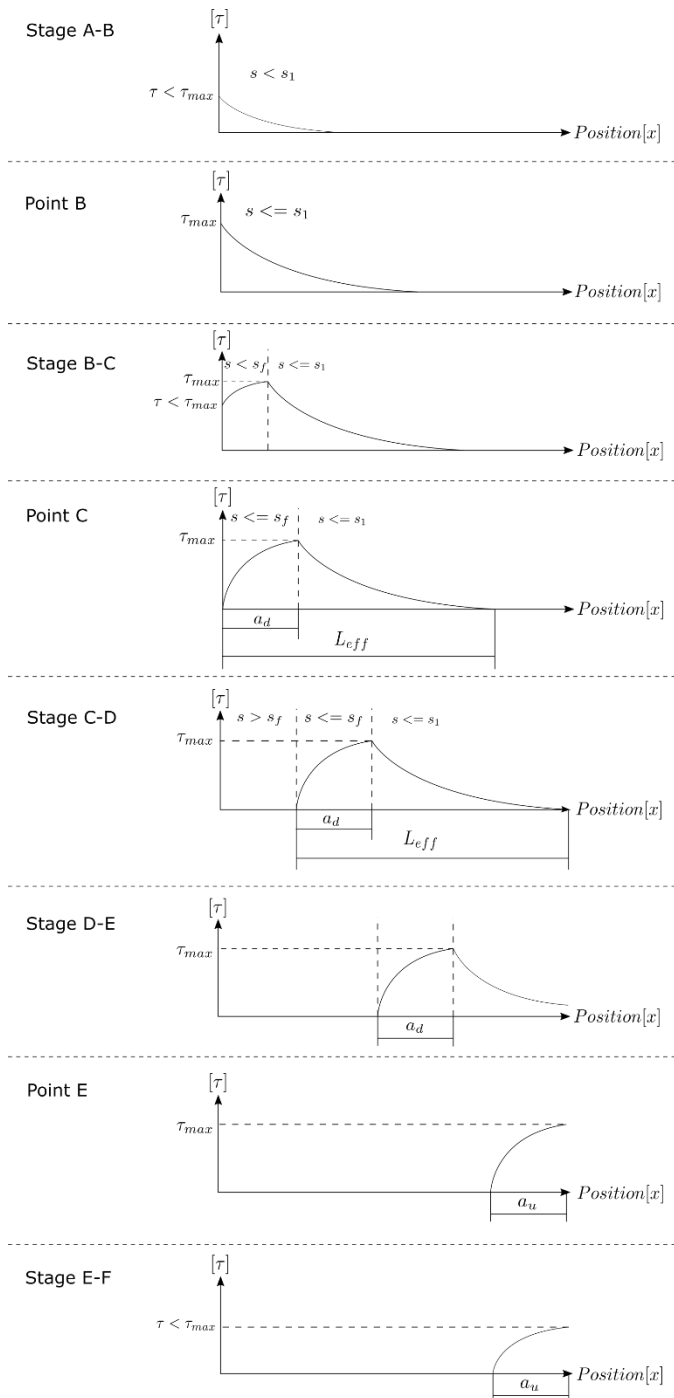
Figure 2.13: Bond shear stress distribution along the FRP for each stage in the load-slip curve.

In the following sub-sections, each stage of the global behaviour of the bonded joint will be explained.

- Elastic stage A-B: During this stage, the local behaviour of each section of the bonded length is in the ascending branch of the bond-slip law. Hence, during this stage, the load-slip stiffness is elastic and linear. The last point of the elastic stage is the point B (see Figure 2.12), where the loaded end reaches the bond shear strength (τ_{max}) of the bond-slip law.

- Elastic-softening stage B-C: Once point B is reached, the loaded end section of the joint will be in softening branch, because the slip in the loaded end (which, in turn, equals to the total slip), is higher than s_1. Then, as the applied load keeps growing, the sections near the loaded end will start damaging and entering to the softening stage. In all sections lying in the softening branch, the transferred local shear stress between FRP and concrete is lower than the bond shear strength. Consequently, the stiffness of the global load-slip curve will decrease as well. In Figure *2.13*, it can be seen that during the stage B-C, the activated length (bonded length that is transferring bond shear stress) increases until the point C is reached. Once the point C is achieved, the shear stress profile is fully developed, meaning that the joint has reached its ultimate load, hence, the activated length is equal to the effective bond length (L_{eff}). For bonded lengths shorter than L_{eff}, the point C will not be reached because not enough bonded length will be available to develop the complete strain profile.

- Softening stage C-D: At point C, the slip at the loaded end is equal to the maximum slip (s_f) meaning that the loaded end is completely damaged and cannot transfer any more stresses. The load carrying capacity of the bonded joint reaches its maximum capacity, therefore as the slip in the loaded end continues increasing, the load carried by the bonded joint does not experience any increase. The stage C-D ends when the free end starts to transfer shear stress and as a consequence, the activated length is reduced. Beyond this point, the load starts to reduce (point D).

- Debonding stage D-E-F: In this stage the activated length decreases causing a reduction on the load carried by the bonded joint until the remaining bonded sections are completely damaged (point F). This stage cannot be experimentally observed, due to the brittleness of the failure.

2.4.6 Fracture energy

The fracture energy of the bonded joint is the dissipated energy by the joint until the debonding, and is defined as the area under the local bond-slip law [25,76]. Fracture energy is calculated using Eq. 2.5.

$$G_f = \int_0^{s_f} \tau ds \qquad (2.5)$$

Considering a bilinear bond-slip law (Figure 2.14), the fracture energy can be easily obtained from Eq. 2.6.

$$G_f = \frac{1}{2}\tau_{max} s_f \qquad (2.6)$$
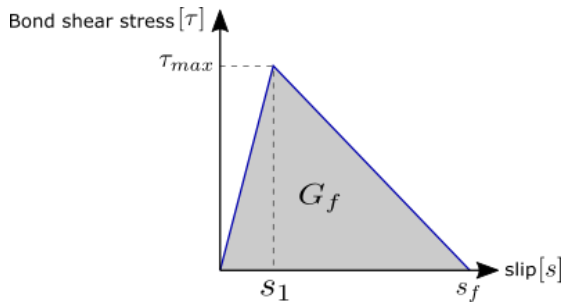
Figure 2.14: Fracture energy in a bilinear bond-slip law.

The calculation of the fracture energy has become a key parameter in the strength predictions of the joint. A summary of the most important empirical equations for calculating the fracture energy of strengthening systems is shown in Table 2.5.

Table 2.5: Existing fracture energy expressions in the literature.

Author	Fracture energy	Parameters
JSCE [77]	$G_f = \dfrac{P_u^2}{8b_f^2 E_f t_f}$	-
Lu *et al.* [44]	$G_f = 0.308\beta_w\sqrt{f_{ct}}$	$\beta_w = \sqrt{\dfrac{2.25 - b_f/b_c}{1.25 + b_f/b_c}}$
Neubauer *et al.* [47]	$G_f = c_f f_{ctm}$	$c_f = 0.204$
Savoia *et al.* [65]	$G_f = \dfrac{P_u^2}{2b_f^2 E_f t_f}$	-
Zhang *et al.* [68]	$G_f = 0.40\gamma^{0.422} f_c^{0.619}$	$\gamma = \dfrac{h_g}{t_g}$
Dai *et al.* [53]	$G_f = 0.446\left(\dfrac{G_a}{t_a}\right)^{-0.352} f_c'^{0.236}(E_f t_f)^{0.023}$	-
fib Bulletin 90 [11]	$G_f = k^2\beta_w^2 f_{cm}^{2/3}$	$\beta_w = \sqrt{\dfrac{2 - b_f/b_c}{1 + b_f/b_c}} \geq 1$ $k = 0.25 - 0.17$
CNR DR-200 R1 [51]	$G_f = \dfrac{\beta_w k_G}{FC}\sqrt{f_{cm}f_{ctm}}$	$FC = 1(safety factor)$ $k_G = 0.023/0.037$ (pre-impregnated/post impregnated laminate) $\beta_w = \sqrt{\dfrac{2 - b_f/b_c}{1 + b_f b_c}}$

2.5 Bond behaviour of FRP-concrete joints under service conditions

Civil structures are exposed to the combination of sustained loading and high service temperature. To accurately design FRP strengthening systems, the effect of these service conditions on the mechanical properties of the materials and the global behaviour of the bonded joint need to be further investigated. In the following sections, the existing studies regarding the effects of sustained loading and service temperature on the CFRP, the adhesive and the bonded joint are presented.

2.5.1 Effect of sustained loading

Effect on the CFRP

CFRP strips under sustained loading experience an increase of the tensile strain with time of the CFRP strip, which can cause a decrease of its elastic modulus with time. The ACI 440.2R [48] suggests calculating the long-term effect of the CFRP by using the concept of effective elastic modulus, which is determined by Eq. 2.7,

$$E_f(t) = \frac{E_f(t_0)}{1 + \phi_{E_f}(t)} \tag{2.7}$$

where $E_f(t)$ is the effective elastic modulus at a time t, and $E_f(t_0)$ is the elastic modulus at $t = 0$. The creep coefficient, ϕ_{E_f}, is calculated using Eq. 2.8,

$$\phi_{E_f}(t) = \frac{\epsilon_f(t) - \epsilon_f(t_0)}{\epsilon_f(t_0)} \tag{2.8}$$

where $\epsilon_f(t)$ and $\epsilon_f(t_0)$ are the strains at a certain and at the initial time, respectively.

The long-term properties of CFRP strips have been studied in [78–82]. Yamaguchi et al [81] and Malvar [82] concluded that for a 50-year period, the strength of the CFRP must be multiplied by 0.9. Furthermore, Ascione *et al.* [79] observed that CFRP strips were practically insensitive to creep deformation, being the creep strain only 2% higher than the instantaneous strain after 500 days. Using the experimental data obtained in Ascione *et al.* [79], Mazzotti *et al.* [80], calibrated Eq. 2.9 to calculate the creep coefficient (ϕ_{E_f}) of the CFRP with time.

$$\phi_{E_f}(t) = 0.02 \left(1 - exp^{\frac{-t}{130}}\right) \tag{2.9}$$

From Eq. 2.9 it can be noticed that for $t = \infty$, E_f will only decrease 2% of its initial value.

The higher the sustained load levels are, the higher the creep deformations will be. Eventually, sustained loading can lead to the tensile failure of the FRP. This type of failure is commonly known as creep rupture. Goertzen *et al.* [78] performed an experimental campaign based on tensile and flexural tests of CFRP dog-bone and rectangular specimens, respectively, where specimens were loaded until the 77% of their ultimate load, observing no creep rupture. From this study, it was concluded that CFRP under ambient conditions (30 ˚C) are highly resistant to creep failure. Standards such as the *fib* Bulletin 90 [83] and the ACI 440.2R [48] consider CFRP can withstand stress levels up to 80% of the tensile strength.

Effect on the adhesive

Structural adhesives are designed to transmit the load from the structure to the FRP strengthening system. Among the range of types of structural adhesives, epoxies are the most widely used for civil engineering applications. Epoxy adhesives present a viscoelastic behaviour, meaning that they can develop time-dependent strains under sustained loading.

Some examples of investigations on the creep behaviour of epoxy adhesives can be found in the literature. For instance, Findley *et al.* [84] observed that creep behaviour can be described in three stages, presented in Figure 2.15.
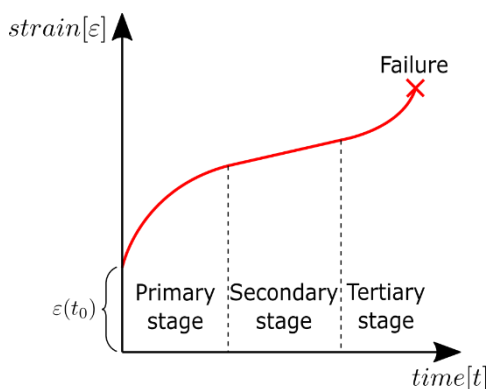
Figure 2.15: Stages of the creep behaviour [84].

As observed in Figure 2.15, the adhesive experiences an instantaneous strain $\varepsilon(t_0)$ due to loading, followed by a primary creep stage with a non-linear increase of the strain, a secondary stage, where the adhesive strain grows linear with time, and a third stage with a steep increase of strain until the failure is attained.

Majda *et al.* [85] and Meshgin *et al.* [86] performed sustained tensile and shear tests, respectively, at room conditions and under a maximum sustained load level of 65% the tensile strength (in Majda et al [85]) and a 62% the shear strength (in Meshgin *et al.* [86]). Both studies concluded that creep in the adhesive increases with the increase of the sustained load level, which can eventually lead to failure in cases with high sustained loading levels. Furthermore, these studies calibrated rheological models with the experimental results to obtain empirical expressions to predict the adhesive behaviour with time.

Emara *et al.* [87] studied the strain evolution in the adhesive under sustained loading and different environmental conditions. From the evolution of strain, the creep compliance was calculated, observing a linear viscoelastic behaviour for sustained loading levels until 60% the tensile strength; however, this limit decreased as the service temperature and humidity increased. Furthermore, a creep function was calibrated from the experimental creep coefficients.

Time-dependent behaviour of CFRP-concrete bonded joints

To study the time-dependent behaviour of CFRP-concrete bonded joints under sustained loading, several studies have performed experimental programmes using pull-out single shear tests to study the slip evolution and strain redistribution in EBR [80,88] and NSM systems [60,73] with time.

In the field of EBR strengthening systems, Gullapalli *et al.* [88] tested EBR CFRP-concrete specimens under a sustained load level of 80% the ultimate load and two different temperatures (room temperature and 40 ˚C). The authors concluded that the proposal presented by Chen *et al.* [25] is suitable for instantaneous conditions but the accuracy decreases when experimental tests are performed under sustained loading and high temperatures.

Mazzotti *et al.* [80] experimentally studied the redistribution of the bond shear stress along the CFRP, loading EBR CFRP strengthened concrete elements up to 50% their ultimate load during 930 days. Furthermore, a model to calculate the evolution of the creep coefficient (ϕ_k, Eq. 2.11) with time was adjusted and used to reduce the stiffness of the elastic branch of the bond-slip law ($K_e(t, t_0)$, Eq. 2.10),

$$K_e(t, t_0) = \frac{K_e(t_0)}{1 + \phi_k(t, t_0)} \tag{2.10}$$

$$\phi_k(t) = 1.65 \left(1 - exp^{\frac{-t}{160}} \right) \tag{2.11}$$

where t is expressed in days. The creep function was assumed to be asymptotic, thus, it was unable to predict the third branch of the creep behaviour.

Other studies such as Borchert *et al.* [60] and Emara *et al.* [73] studied the time-dependent behaviour of NSM CFRP strengthening systems under sustained loading. Borchert *et al.* [60] performed sustained loading tests with different load levels (40%, 60% and 80% the ultimate load) and curing times of the adhesive, obtaining a range of creep functions. It was observed that the creep effect increased with the load applied while decreased with the curing time.

In this study, the authors proposed an analytical model to predict the evolution of the bond-slip law under sustained loading. This analytical model was based on the decrease of the stiffness of the elastic stage, while the stiffness of the softening branch remained unaffected. Figure 2.16 presents the degradation of the bond-slip law suggested by the authors.
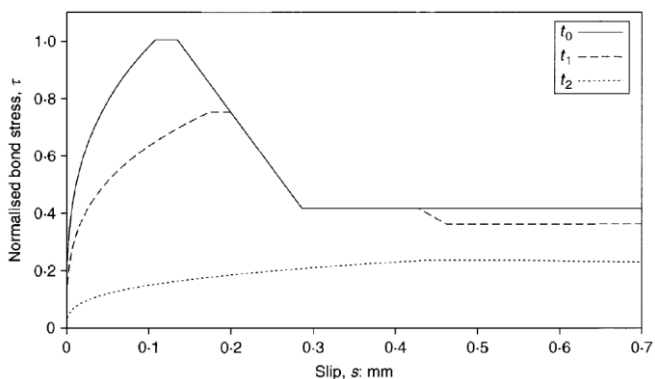
Figure 2.16: Evolution of bond-slip law proposed in Borchert *et al.* [60].

In this model, two creep coefficients need to be calibrated to damage the bond-slip law with time, one decreasing the bond shear strength (τ_{max}) and a second one increasing the slip at the maximum shear strength (s_1).

The authors specified that only the ascending branch of the bond-slip law could be simulated, otherwise, the fracture energy of the joint (G_f) would increase with time, which was physically not possible.

Emara *et al.* [73] carried out an experimental campaign on sustained loading tests of NSM CFRP-concrete pull-out single-shear specimens and tensile adhesive specimens, under sustained load levels of 25% and 50% the ultimate load during 40 days at room conditions. Figure 2.17 shows the set-up used for sustained loading tests in [73].

Figure 2.17: Experimental set-up for tests under sustained load used in Emara *et al.* [73].

In both studies a steep increase in the slip at the loaded end was observed in all the specimens, being higher as higher was the sustained load level.

Emara *et al.* [73] adopted Borchert's damaging model [60] to a bilinear bond-slip law, where the stiffness of the ascending branch was reduced with time, as it is shown in Figure 2.18.
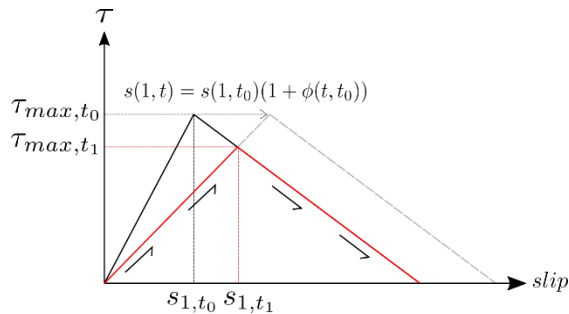
Figure 2.18: Evolution of the bond-slip law proposed in Emara *et al.* [73].

The authors calculated the creep coefficient with time from the evolution of tensile strain in the adhesive, which was used to reduce the stiffness of the ascending branch [80]. A good agreement between the numerical and the experimental results in terms of evolution of slip at the loaded end with time was obtained.

2.5.2 Service temperature effect

Temperature effect on CFRP strips

The viscoelastic polymer used as a matrix in CFRP are strongly affected by temperature [83]. However, the *fib* Bulletin 90 suggested that the service temperature should be lower than the T_g of the CFRP. Commercial FRP elements are composed by matrix with a T_g ranging between 130 and 140 ˚C, therefore service temperatures have a negligible effect on the mechanical properties of FRP materials.

Cao *et al.* [89] and Nardone *et al.* [90] investigated the effect of temperature on CFRP strips through tensile tests under different moistures and temperatures, concluding that CFRP laminates experienced a decrease of 30% on the tensile strength when the temperature was 70 °C, however, no significant change on the stiffness was observed. This study also concluded that specimens submitted to temperature cycles from -15˚C to 36˚C showed slight decreases on the tensile strength and elastic modulus.

Temperature effect on the adhesive

Adhesives are very sensitive to environmental conditions. Their performance and mechanical properties drop when the ambient temperature increases [87]. Through adhesive single-lap shear tests under different temperatures, Galvez *et al.* [91] observed that temperatures until 72 ˚C can cause a post-curing effect on the adhesives, increasing their cross-links and, consequently, enhancing their mechanical properties, however, after long exposures, the elastic modulus and the tensile strength decreased.

The effect of the exposure to different environmental conditions has been also investigated by Silva *et al.* [92], where adhesive dog-bone specimens were left under different environmental conditions for 480 days and tested afterwards until failure. From this study, it was concluded that the T_g decreased after exposure of the specimens to chlorides and freeze-thaw cycles (between -18 and +20˚C) and increased after the exposure to thermal cycles (between -15 and +60˚C). Additionally, an increase in the mechanical properties was observed after the temperature cycles due to the post-curing effect.

Ferrier *et al.* [93] suggested that the service temperature should be around 15 °C lower than the glass transition temperature of the adhesive to avoid high creep effects on the structural epoxy.

Regarding the study of the combined effect of temperature and sustained loading on the adhesive behaviour, studies such as Costa *et al.* [94–96] and Emara *et al.* [87] observed that the

higher the sustained load level and ambient temperatures, the higher the decrease on the mechanical properties and the increase of strain with time were obtained. Furthermore, Silva *et al.* [97] observed that the sustained loading response was highly dependent on the curing time, being greater the strain evolution when the curing time decreased.

Temperature effect on the FRP-concrete joints

Several experimental studies have been carried out in order to understand the effect of temperature conditions on the time-dependent behaviour of the bonded joint. Dai *et al.* [98] compared the experimental results presented in [99–103] finding that when the ambient temperature is close to the T_g of the adhesive, the interfacial fracture energy decreases significantly. Moreover, for temperatures lower than T_g, the relationship between the fracture energy and the temperature is still not clear, as can be seen in Figure 2.19.
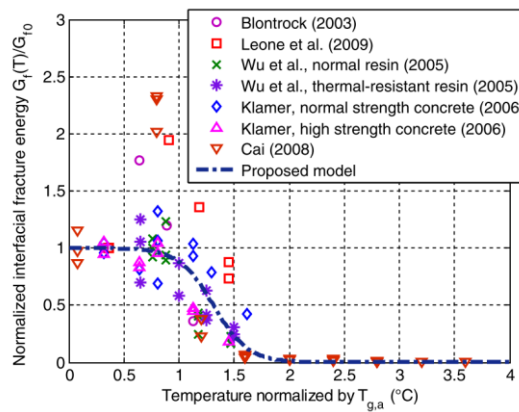
Figure 2.19: Effect of the temperature on the interfacial energy [98].

The effect of temperature conditions has been also studied in Ferrier *et al.* [93,104] for double-shear bond specimens strengthened with EBR FRP a under sustained loading and temperatures ranging from 20 to 60°C, finding that temperature was highly affecting the ultimate capacity of the bonded joint, and for sustained load levels up to 40% of the ultimate load the creep was linear viscoelastic.

Gullapalli *et al.* [88] focused their study on the effect of service conditions on the bond performance of concrete elements strengthened with EBR. Specimens were submitted under 40°C and loaded at 80% their ultimate load for 87 hours. Another example of experimental study was carried out by Jeong *et al.* [105–107] where concrete elements strengthened with EBR CFRP laminates were loaded under a sustained load level of 45% of the carrying capacity and service temperatures (21 °C and 30 °C). Both studies stated that the combination of sustained loading

and service temperature had an increasing effect on the activated length and the ultimate load of the bonded joint.

Borchert *et al.* [60] and Emara *et al.* [108] studied the long-term response of the NSM strengthening systems under service temperatures. Both authors observed an increasing evolution on the slip and strain in the CFRP strip with time caused by creep, being higher as the temperature and sustained load level increased. Borchert *et al.* [60] concluded that for long curing time of the resin, the load capacity of the NSM CFRP-concrete joint increased as well.

Emara *et al.* [108] concluded that ambient temperature was affecting more to the bonded joint response in comparison with the humidity, and that the combination of a relative humidity of 90%, an ambient temperature of 40˚C and a sustained load level of 50% of the ultimate load, caused the failure of the bonded joint.

With the aim of studying the effect of day-night cycles, some authors carried out long-term tests under cyclic environmental conditions [109–112]. Fernandes *et al.* [109] submitted NSM CFRP-concrete specimens to different ambient conditions and exposure times. An increase of 8% on the ultimate load was observed for specimens under thermal cycles ranging between 20˚C and 80˚C, which was explained because of a possible post-curing effect of the bonded joint during the exposure time.

On the other hand, Gamage *et al.* [110–112] studied the response of specimens submitted to cyclic temperatures ranging between 20-50˚C, 90% of RH and sustained loading levels of 25% and 35% of the ultimate load. These studies concluded that the major effect on the carrying capacity of the bonded joint was during the initial 2000 hours (around 22% of reduction on the ultimate load) and beyond this point, a negligible reduction was observed. Furthermore, it was observed that specimens under a high number of thermal cycles experienced a concrete cover failure, while specimens under low number of thermal cycles, failure was attained in the concrete-adhesive interface.

3 Methodology

The aim of this chapter is to present the methodology carried out to achieve the proposed objectives of the thesis. The chapter is structured into three main sections: material characterisation, instantaneous monotonic behaviour and sustained loading behaviour.

3.1 Material characterization

All materials involved in the bonded joint (CFRP, adhesive and concrete) were mechanically evaluated, in terms of elastic modulus and strength, following the corresponding standards [113–118], along the different experimental series. Additionally, the curing degree and the glass transition temperature of the adhesive were also characterized.

3.1.1 CFRP laminate

The CFRP strips used in this thesis were Sika CarboDur S NSM 1030, provided by the company SIKA AG. The strips were composed by unidirectional carbon fibres with an epoxy matrix, having a cross-section of 10 mm × 3 mm. The CFRP strips were provided at the beginning of the thesis in one single batch. From this batch, six CFRP specimens of 350 mm length were characterized according to ISO 527-5 standard [114]. Tests were carried out in a servo-hydraulic testing machine Servosis MUE-60T under displacement control at a rate of 2 mm/min. The instrumentation consisted of two strain gauges bonded at each side of the laminate and a load cell of 100 kN capacity to register the applied load.

Figure 3.1a shows a typical image of the failure of the CFRP specimens obtained in the tensile tests, while Figure 3.1b shows the stress-strain curve obtained for all the tested CFRP strips. A tensile strength of 3.2 GPa (with Standard Deviation, SD = 68.3 MPa) and an elastic modulus of 169.3 GPa (SD = 13.1 MPa) were obtained.
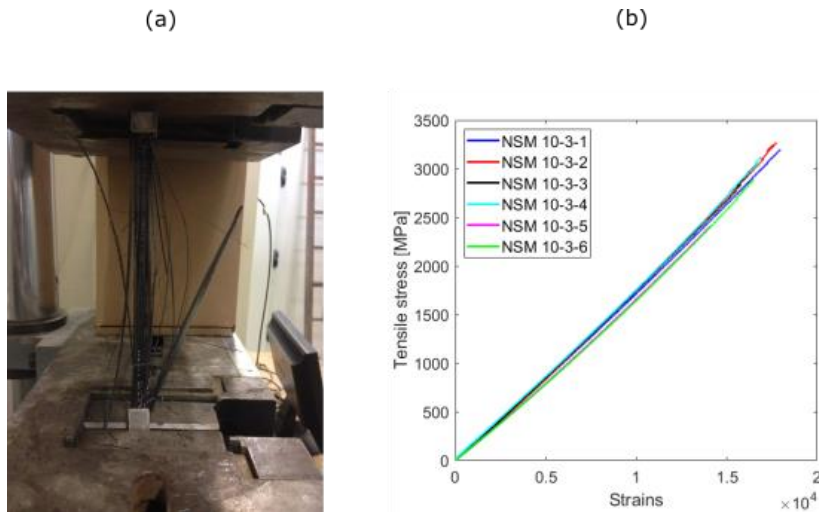
Figure 3.1: (a) Failure of the CFRP strip in the tensile test and (b) stress-strain curve obtained from the instantaneous characterization.

In this thesis, the long-term properties of the CFRP strips were not studied due to their good resistance to creep under long-term loading [50].

3.1.2 Adhesive

The adhesive used in this thesis was the bi-component thixotropic epoxy resin Sika-30 provided by the company SIKA AG. In all cases, the epoxy components were mixed with a resin-hardener ratio of 3:1 at ambient temperature and were cured for 12 days.

Instantaneous and sustained loading tensile tests were performed to evaluate the mechanical properties of the adhesive, while Dynamic Mechanical Analysis (DMA) and Differential Scanning Calorimetry (DSC) tests were carried out to investigate its thermophysical properties.

Instantaneous mechanical characterization

The instantaneous mechanical behaviour of the adhesive was investigated through tensile tests until failure according to ISO 527-2 [113]. Six dog-bone resin specimens with a cross-section of 10 mm × 5 mm were cast and cured for 12 days at 20 °C. Tensile tests were performed in an MTS Insight 5 kN testing machine at a displacement rate of 1 mm/min. The instrumentation consisted of one extensometer and two strain gauges placed at both sides of the middle section

of the specimen. The test setup and instrumentation are shown in Figure 3.2a, and the stress-strain curves obtained from the instantaneous tests are shown in Figure 3.2b.

(a)   (b)
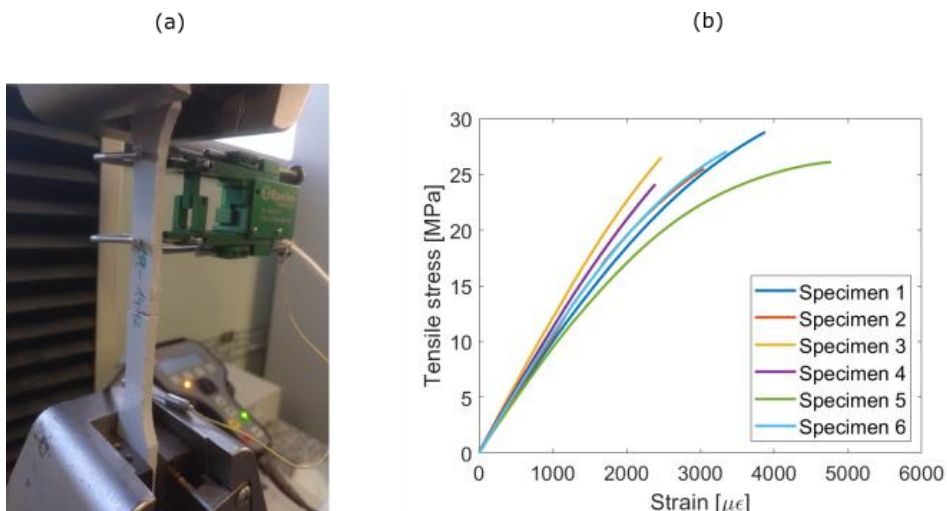
Figure 3.2: Tensile instantaneous test of the adhesive.

From the instantaneous characterization, an average tensile strength and maximum strain of 27.2 MPa (SD = 4.5 MPa) and 2770 µε (SD = 711 µε) were obtained, respectively. The average elastic modulus obtained was 10.7 GPa (SD = 471.4 MPa).

Thermophysical characterization

The thermophysical properties of the adhesive were studied through DSC and DMA tests after 12 days of curing at 20 °C [118].

The DSC method applies an increase of temperature to the specimen and measures the physical and chemical changes in the material through the enthalpy of reaction so as to obtain T_g [78,79]. Figure 3.3 shows the results obtained from the seven DSC tests performed during the curing process. At the curing stage, the specimen releases energy in an exothermal process, causing a decrease in the enthalpy of reaction, calculated as the area between the baseline and the peak in Figure 3.3.
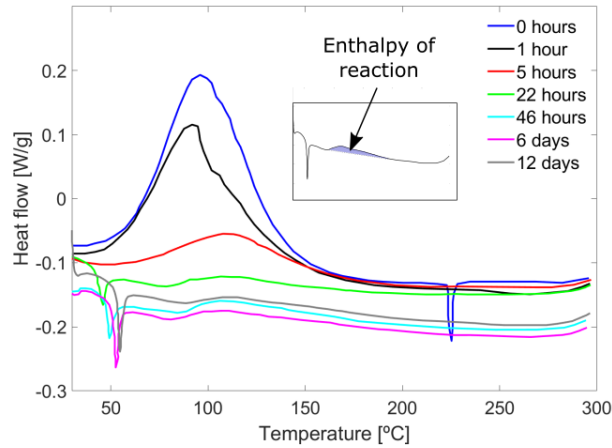
Figure 3.3: DSC carried out during the curing time.

On the other hand, in the DMA test a cyclic non-destructive stress with a constant frequency is applied to the adhesive specimen while the temperature increases with time. Three different methods to measure the T_g can be used from this test: the storage modulus (E'), the loss modulus (E'') and the loss factor ($tan(\delta)$). The storage modulus (E') is the material's capacity to store energy and is defined as the elastic part of the viscoelastic behaviour of the material. The loss modulus (E'') represents the loss of energy during one loading cycle and is defined as the viscous part of the viscoelastic behaviour of the material. The loss factor ($tan(\delta)$) is obtained from the ratio E''/E' [80]. The temperatures applied during the DMA test ranged between 20°C and 100°C with an increasing rate of 2°C/min. In this thesis, the non-destructive stress applied to the adhesive specimen was a cyclic displacement of 10 μm at a frequency of 1 Hz [80]. From the DSC tests, a T_g of 53.1°C and a curing degree α of 96.3% were obtained, while from the DMA a T_g ranging between 50.8°C and 57.5°C was obtained. Further details regarding the thermophysical characterization of the material are presented in Chapter 6 (Paper C).

3.1.3 Concrete

Instantaneous mechanical characterization

The concrete used to cast the blocks was provided by the company Àrids Bofill SA. The concrete blocks used for the instantaneous characterization of the NSM CFRP-concrete specimens were cast from the first batch, and those devoted to the sustained loading campaigns were cast from the second batch. In both cases, the concrete had a maximum aggregate size of 12 mm, the consistency was fluid, and the expected compressive strength was 30 MPa. The

47

mechanical properties of concrete were tested though compressive and indirect tensile tests on six concrete cylinders of 300 mm × 150 mm, in accordance with the ASTM C469 / C469M-10 [115] and UNE 12390-3 [116]. The results obtained from the mechanical instantaneous characterization are presented in Table 3.1.

Table 3.1: Mechanical properties of the concrete casted during the thesis.

Nº of Batch	Compressive strength [MPa]	Tensile strength [MPa]	Elastic modulus [GPa]	Poisson ratio
1	36.86 (SD = 2.50 MPa)	5.72 (SD = 0.44 MPa)	46.86 (SD = 5.30 GPa)	0.11 (SD = 0.005)
2	33.80 (SD = 1.86 MPa)	4.84 (SD = 0.19 MPa)	33.14 (SD = 1.6 GPa)	0.11 (SD = 0.010)

Figure 3.4a shows the typical failure mode obtained from the compressive test and Figure 3.4b presents the stress-strain curves obtained from the cylindrical specimens tested under compression.

(a)   (b)
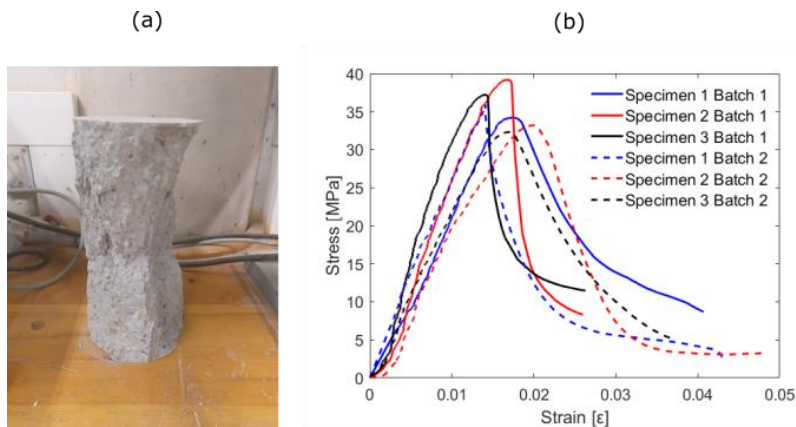
Figure 3.4: (a) Concrete specimen tested under compression test and (b) results from the compression tests.

Mechanical characterization under sustained loading

To study the creep behaviour of concrete under sustained loading, two 300 mm × 150 mm cylinders from the first batch were submitted to a sustained compressive load of 40% the compressive strength, according to ASTM C 512/C 512M [117]. The strain caused by creep after

1000 hours of testing was around 187 με (in compression). Therefore, in this thesis it was assumed that sustained loading does not have an effect on the concrete.

The shrinkage of concrete was measured through two strain gauges placed inside two concrete blocks (one of 200 mm × 200 mm × 300 mm and one of 200 mm × 200 mm × 370 mm) and were kept under laboratory conditions for 1900 hours. It could be observed that de increase of strain due to the shrinkage was around 30 με at the end of the test. Therefore, from this test it could be concluded that shrinkage is not causing any important effect on the concrete block.

3.1.4   NSM CFRP-concrete specimen preparation

In this thesis, the preparation of the NSM CFRP-concrete specimens was carried out according to the following steps:

1. Concrete blocks of 200 mm × 200 mm × 300 mm and 200 mm × 200 mm × 370 mm were cast and cured for 28 days. During the curing process, specimens were covered with blankets and periodically watered. Moulds were removed after one week from casting and specimens were kept under laboratory conditions until testing.

2. NSM grooves were cut with an electric saw after 15 days of curing. The grooves' depth was 15 mm in all the specimens, while groove thicknesses of 7.5 mm and 10 mm were cut to study the effect of the adhesive layer thickness. The thickness of 7.5 mm was set to satisfy the *fib* 90 [11], where the groove dimensions must be between 1.5 and 2 times the FRP size, and the second was set to satisfy the ACI 440.2R [48] requirement which stablishes that the groove thickness must be at least 3 times the laminate thickness.

3. CFRP strips were cut from a continuous roll provided by SIKA company. To study the effect of the bonded length, three values were tested, 150 mm, 225 mm and 300 mm. Unbonded lengths of 20 mm and 50 mm were left at the loaded end and the free end, respectively. Figure 3.5 depicts the positioning of the CFRP strip in the concrete element groove.
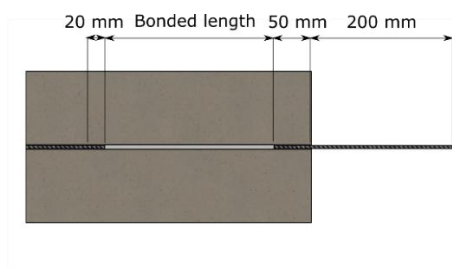
Figure 3.5: Positioning of the CFRP strip in the bonded joint.

4. The next step is to mix adhesive in a resin-hardener ratio of 3:1 by weight and mixed for 5 minutes.

5. The bonded length is limited in the groove with cardboard pieces wrapped with Teflon tape in order to avoid the adhesive to spread along the joint. Once the adhesive is prepared, it is poured into the groove.

6. Finally, the CFRP strip is carefully inserted into the groove and the depth position is measured at the loaded and free ends to ensure that the strip is aligned with the concrete specimen.

7. To cure the adhesive of the bonded joint, specimens were left for 12 days under laboratory conditions.

3.2   Instantaneous bond behaviour of the NSM FRP-concrete joint

In order to experimentally investigate the bond behaviour of different NSM CFRP-concrete joints' configurations, three bonded lengths (150 mm, 225 mm and 300 mm) and two groove thicknesses (7.5 mm and 10 mm) were used. Four specimens were tested for each specimen configuration, giving a total of 16 specimens tested under pull-out single shear test.

A numerical methodology based on a finite differences model was designed to predict the instantaneous load-slip curve for each bonded joint configuration. Furthermore, from the numerical methodology, the distribution of slip, strain, and bond shear stress along the FRP were obtained. This study is developed and further detailed in Chapter 4 (Paper A).

In the following sections, the setup and the instrumentation of the monotonic tests are presented. Furthermore, the numerical methodology developed in this thesis to calculate the instantaneous bond behaviour of NSM CFRP-specimens is explained.

3.2.1   NSM CFRP-concrete monotonic setup

In this thesis, single-shear will be adopted as instantaneous set-up, because of its simplicity and reliability. In order to obtain more similar conditions to a real application, the concrete block will be partially confined [15,72,119,120]. As a consequence, a slight rotation of the block is allowed.

Monotonic tests until failure were carried out in a servo-hydraulic Servosis MUE-60T testing machine under displacement control at a rate of 0.2 mm/min. The set-up used consisted of a 60 mm wide rigid steel plate vertically fixing the top surface of the concrete block and a second 50

mm wide steel plate horizontally fixing the concrete bock to avoid the rotation of the specimen. The set-up was designed to admit different specimen configurations in terms of concrete block length and bonded lengths, allowing also to test other strengthening techniques such as the EBR. Figure 3.6a shows the set-up used for the instantaneous test, while Figure 3.6b shows a lateral view of the set-up, and Figure 3.6c a detailed view of the FRP position on the concrete groove.
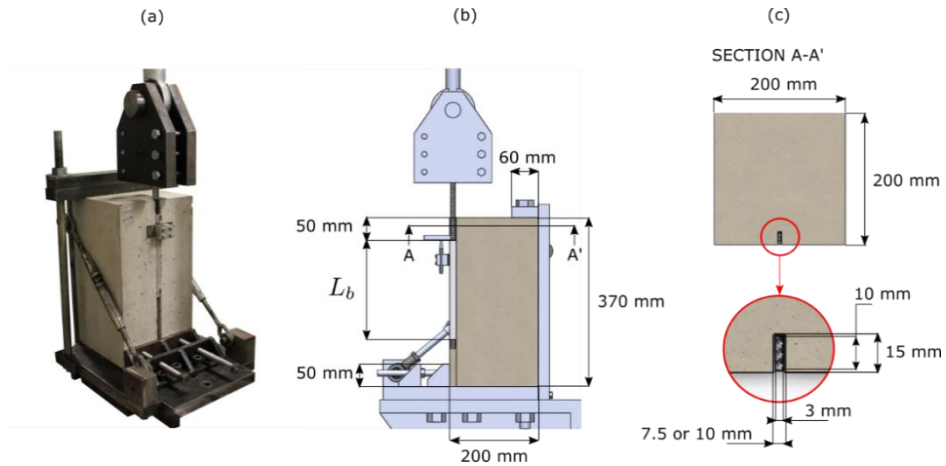
Figure 3.6: (a) Set-up used for the instantaneous test of the NSM CFRP-concrete specimens, (b) lateral view of the instantaneous test set-up and (c) detailed view of the groove and FRP dimensions.

A steel clamp made of S220 steel (with a yield strength of 300 MPa and an ultimate strength of 400 MPa) was designed to grip the strip. This clamp admitted laminate thicknesses until 100 mm and it was designed to resist a maximum load of 130 kN to not surpass the yield strength of the steel. To grip the CFRP strip, 6 steel bolts of quality 8.6 were tightened at 110 N·m of torque and the gripping plates were made of knurled steel. To avoid unexpected failures, a safety factor of 2.0 was applied, therefore, instantaneous tests would not be allowed to surpass loads higher than 65 kN. To avoid damaging the CFRP strip during the test, aluminium tabs of 2 mm x 10 mm x 100 mm were bonded onto the CFRP surface. Figure 3.7 presents a scheme of the steel clamp.
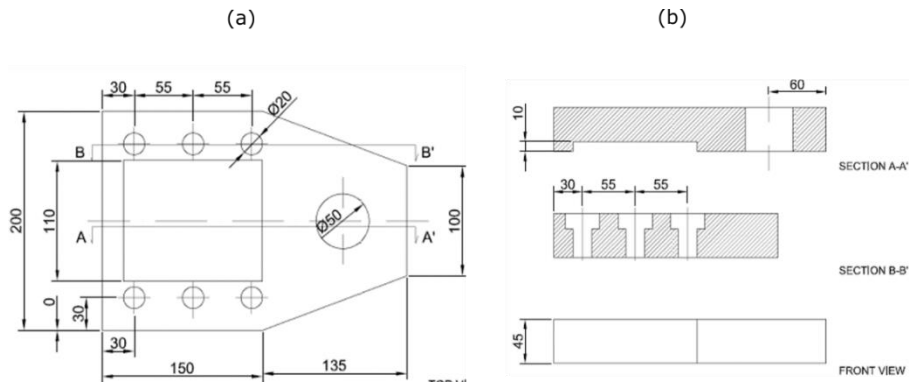
Figure 3.7: (a) Dimensions of the steel clamp and (b) sections of the clamp.

3.2.2 Instrumentation of the monotonic tests

The instrumentation used in the tests consisted of one load cell of 100 kN to register the load applied to the specimen and one LVDTs was placed at the loaded end to measure the slip.

Additionally, the Digital Image Correlation (DIC) technique was used to study the redistribution of strain in the front surface of the specimen during the test. The DIC system has been proved to be an effective tool for measuring displacements and strains in concrete elements [121–123], and consists of applying a speckle pattern to the area of interest (AOI) and taking pictures along the tests. Afterwards, using a correlating software, all the speckles in the surface are tracked to obtain the movement of each point of the AOI. The frequency of image acquisition used during the test was of 1 image/second. The camera used a diaphragm aperture of f/5.6, a resolution of 2452 × 2056 pixels, a focal length of 23 mm and the closing of the diaphragm was set at 1.000 μsec. One 2D system, consisting of one camera placed perpendicular to the area of interest to capture the in-plane displacements, and one 3D system, consisting of two cameras placed at 125 mm distance one from each other and focusing to the same AOI, were installed. The distance between the cameras and the front surface of the specimen was 840 mm in both cases (2D and 3D). Figure 3.8 shows the location of the cameras used in the instantaneous tests.

Figure 3.8: DIC system installed in the instantaneous test.

To assess the quality of the speckle pattern, and therefore the accuracy of the DIC system, the well-known Mean Intensity Gradient (MIG) parameter, proposed by Pan *et al.* [124], was calculated. The MIG calculates the difference of grey-scale colour between two consecutive pixels of the AOI, quantifying the level of gradient of the images. The higher the MIG value is, the higher contrast has the image, and therefore, more accuracy will be found in the correlation. The MIG value is calculated using Eq. 3.1,

$$MIG = \frac{\sum_{i=1}^{W}\sum_{j=1}^{H}\left|\Delta f\left(x_{ij}\right)\right|}{W \times H} \tag{3.1}$$

where *W* and *H* are the width and height in pixels, respectively, and *Δf(xij)* is the gradient of colour between two consecutive pixels. To correlate the images recorded during the instantaneous tests, the correlation softwares VIC 2D and VIC 3D were used to calculate the displacements and strain fields of the AOI. Table 3.2 presents the parameters used in the correlation for the 2D and 3D systems in terms of subset size, stepsize, correlation criteria, the ratio mm/pixels and the MIG value.

Table 3.2: Correlation parameters of the 2D and 3D systems.

System	Subset [pixels]	Stepsize [pixels]	Correlation criteria	mm/pixel	MIG
2D	21	5	ZNCC[*1]	0.114	33.04
3D	29	7	ZNCC[*1]	[*2]	32.09 (left) and 25.18 (right)

[*1] ZNCC = Zero-Normalized Cross-Correlation.

[*2] the relationship mm/pixel cannot be determined because the value varies in the AOI.

To compare the results of both systems, the strains in the vertical direction calculated are shown in Figure 3.9 for a specimen with a bonded length of 225 mm and a groove thickness of 10 mm.
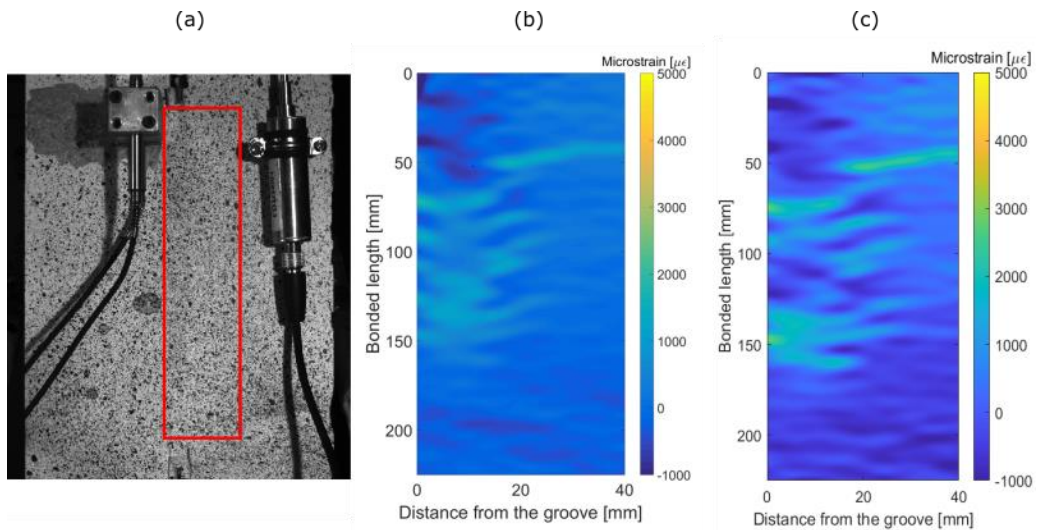
Figure 3.9: (a) Area of interest (AOI) of the NSM CFRP-concrete specimens and the comparison of the strain fields obtained with the (b) 2D and (c) 3D systems.

The 3D system allowed to calculate the out of the plane displacements, but in terms of in-plane displacements very similar results were obtained in comparison with the 2D system. From Figure 3.9 it can be seen that the strain values measured by both systems were around 4500 µε. Furthermore, both systems measured correctly the compressive struts generated in the specimen surface. Even though the use of a 3D system allows to register out of the plane

displacements, a higher computational capacity and calculation time is needed to correlate the AOI points. For these reasons, only results obtained from the 2D system were presented in Chapter 5.

3.2.3   Numerical prediction of the instantaneous behaviour

A numerical procedure was developed to predict the instantaneous response of the bonded joint until failure. This numerical process was developed using the software Matlab and was based on solving the differential equation governing the bonded joint through an iterative procedure based on a finite differences model. This model was conceived to be very adaptable to different bond-slip laws.

This model was calibrated with the experimental results and allowed to obtain the load-slip curve, strain, stress and slip distributions along the bonded length. The main steps followed in the numerical methodology were:

1. Initially, a slip at the loaded end is defined.
2. The load profile along the FRP is calculated using the bond-slip law.
3. From the load distribution, the strain in the FRP and the concrete can be calculated.
4. The strain in the free end is compared to a threshold (close to zero), if it's higher, another iteration increasing the load at the loaded end is performed, if it's lower, the present iteration finishes and the slip at the loaded end is increased to obtain a new combination of values load-slip.
5. The numerical procedure is repeated until the slip at the loaded end is higher than the value of slip defined by the user.

Figure 3.10 shows the steps followed in the numerical methodology to calculate the instantaneous response of the bonded joint.
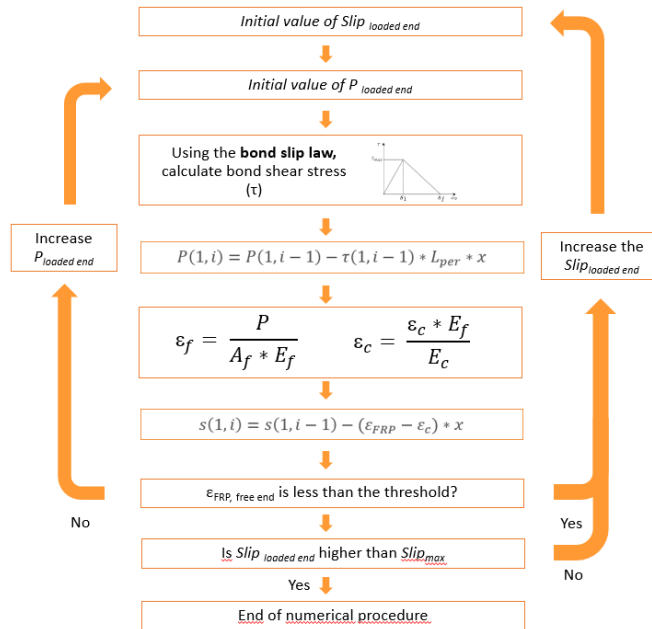
Figure 3.10: Scheme of the numerical methodology to calculate the instantaneous behaviour of the bonded joint.

The numerical model is further detailed and compared with the experimental data in Chapter 4 (Paper A).

3.3 Sustained-loading bond behaviour of the NSM FRP-concrete joint

Finally, the third part of the methodology, carried out in Chapters 5, 6 and 7 (papers B, C and D, respectively), consisted of studying the response of the adhesive and NSM CFRP-concrete joints under the combination of sustained loading and different high service temperatures from an experimental and numerical point of view.

In total, five experimental series were carried out along the thesis, studying the effect of different high service temperatures. Each experimental series consisted of nine adhesive specimens (under 15%, 30% and 50% of the tensile strength) and eight NSM CFRP-concrete specimens (under 15% and 30% of the ultimate load) under the same environmental conditions. Experimental series 1 (20 °C) and 2 (40 °C) aimed to investigate the effect of steady temperature conditions on the specimens' behaviour, while the objective of series 3A (18-38 °C), 3B (22-

43 °C) and 4 (20-40 °C) was to study the effect of thermal cycles of the global behaviour. In addition, to study the effect of the preconditioning on the specimens' bond response, no preconditioning stage was applied to series 4. Even though the experimental series for the adhesive and the pull-out specimens were the same, in paper C, the experimental series were labelled as "C + number of series", and in paper D, were labelled as "S + number of series". Table 3.3 presents the list of experimental series carried out during the thesis.

Table 3.3: Experimental series carried out in the thesis.

Series	Temperature function [24 h]	Preconditioning	Objective T°C [°C]	Test duration [hours]
S1/C1	Steady	Yes	20.0	1000
S2/C2	Steady	Yes	40.0	1000
S3-A/ C3-A	Cycles 24 h	Yes	18.0 – 38.0	600
S3-B/ C3-B	Cycles 24 h	Yes	22.0 – 43.0	1000
S4/C4	Cycles 24 h	No	20.0 – 40.0	1000

Note: the nomenclature SX is used for adhesive specimens and CX for NSM CFRP-concrete specimens.

3.3.1 Sustained loading tests of adhesive specimens

To study the creep behaviour of the adhesive used to bond the strengthening system to the concrete element, adhesive specimens were submitted to sustained tensile loading tests for 1000 hours. Following the ISO 527-2 [113], dog-bone adhesive specimens with a cross-section of 5 mm × 10 mm were cast and cured for 12 days at 20 °C.

The set-up used in the sustained loading tests is presented in Figure 3.11. A lever arm with a magnification factor of 4.0 applied the gravity load onto the specimen.
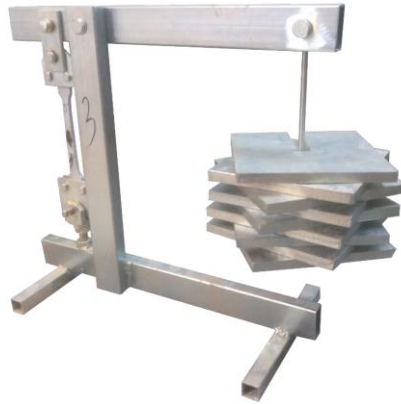
Figure 3.11: Tensile sustained-loading test set-up for adhesive specimens.

The instrumentation consisted of two strain gauges bonded at each side of the mid-section of the specimen. In addition, to measure the temperature on the specimens' surface, a temperature strain gauge was bonded to one specimen that was kept inside the climatic chamber without any sustained load.

In series C1, C3 (A and B) and C4, three sustained loading levels corresponding to the 15%, 30% and 50% the tensile strength, previously obtained from the instantaneous characterisation, were studied. For each sustained loading level, three specimens were tested to validate the obtained results while one specimen was left unloaded. In series C2, to study the dependence of the creep and the sustained load level, additional sustained loads of 5%, 10%, 15%, 20%, 30%, 40% and 50% the tensile strength were tested for 1000 hours. The sustained load levels represent the range of values of sustained loading that bonded joints are submitted under service conditions. In total, 52 adhesive specimens were tested in all the experimental series, 10 specimens in each series C1, C3 (A and B) and S4, and 22 specimens in series C2.

Chapter 6 (Paper C) shows further details of the experimental configuration and presents the results obtained from the tests carried out.

3.3.2   Sustained loading tests of NSM CFRP-concrete specimens

The effect of sustained loading and service temperature on the bonded joint behaviour was studied through single shear tests under a constant gravity load for 1000 hours. In each experimental series, eight NSM CFRP-concrete specimens combining two bonded lengths (150 mm and 225 mm), two groove thicknesses (7.5 mm and 10 mm) and two sustained load levels

(15% and 30% the ultimate load of the specimen) were tested. These sustained load levels represent load range that the CFRP-concrete joint can undergo in a flexural configuration under service conditions. In total, 32 NSM CFRP-concrete specimens were tested under sustained loading in five experimental series under steady and cyclic temperatures (detailed in Table 3.3).

The setup of the experimental tests was based on the instantaneous test setup, previously described in chapter 3.2.1, which was adapted to a level arm with a magnifying factor of 8.3. Since the sustained load applied to the specimens was much lower than in the instantaneous tests, steel clamps were designed based on the instantaneous clamp, but scaled to the level of load used for the sustained loading test. Figure 3.12a presents the experimental set-up used in the sustained loading tests and Figure 3.12b depicts a schematic lateral view of the set-up.

(a)   (b)
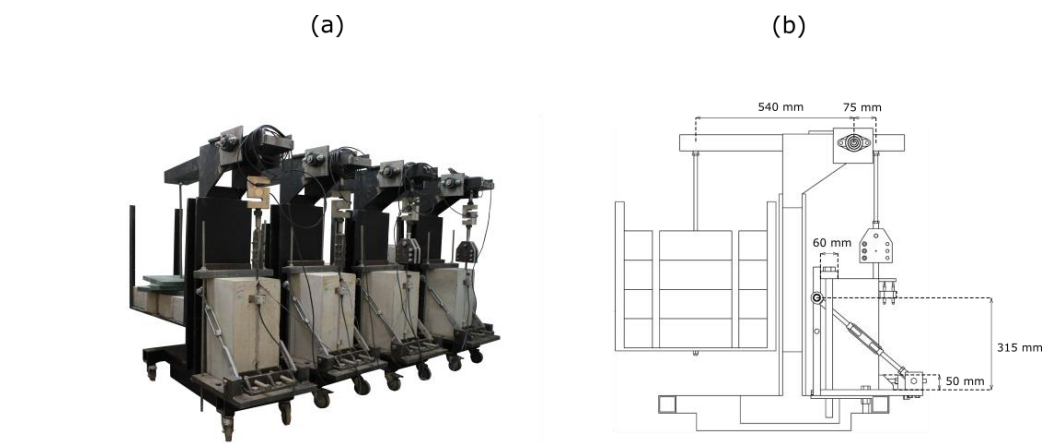
Figure 3.12: (a) Set-up used for the sustained loading tests and (b) schematic lateral view of the set-up.

The instrumentation used in this test consisted of one Linear Variable Differential Transformer (LVDT) placed at the loaded end to register the relative displacement between the CFRP strip and the concrete element, and a load cell to obtain the load applied to the specimen. Moreover, to measure the temperature inside the bonded joint, a temperature strain gauge was bonded onto the CFRP strip of one spare specimen without sustained loading. The rotation of the lever arm caused by the sustained load was controlled through a strain was bonded onto the CFRP strip that registered the evolution of axial strain with time. Figure 3.13 presents the

variation of load in % for each block tested under sustained load in the experimental series S1. The rest of experimental series presented similar results.
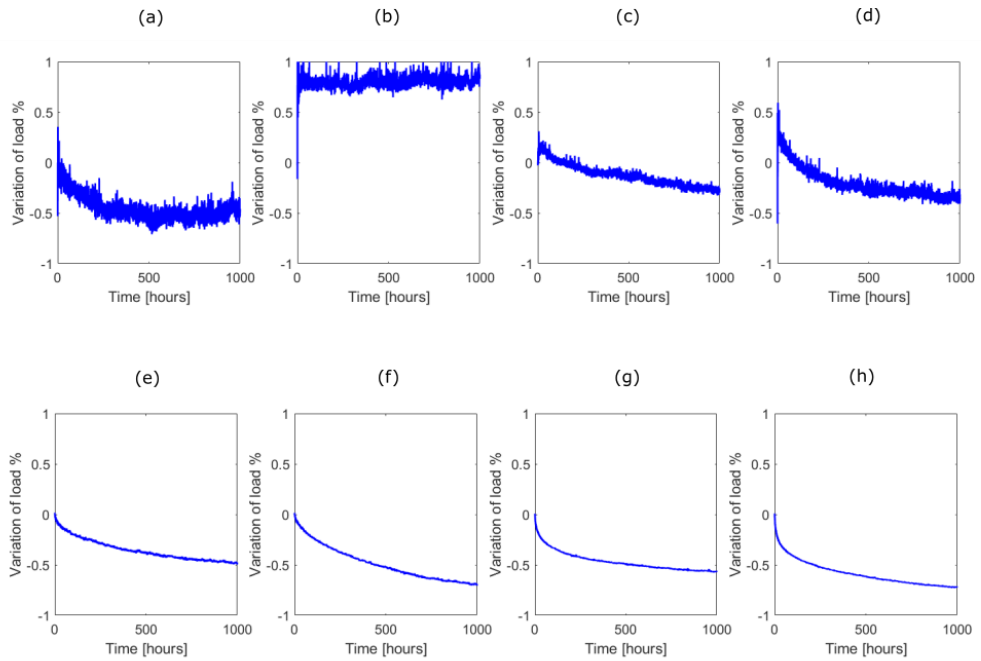
Figure 3.13: Variation obtained from the strain gauges in specimens (a) NSM-150-10-15, (a) NSM-150-7.5-15, (a) NSM-150-10-30, (a) NSM-150-7.5-30, (a) NSM-225-10-15, (a) NSM-225-7.5-15, (a) NSM-225-10-30 and (a) NSM-225-7.5-30 from series S1.

It can be observed that in all the cases, the sustained load measured by the strain gauge slightly reduces with time, probably caused by creep of the set-up. However, the percentage of decrease in load with time after 1000 hours was lower than 0.9 %.

The acquisition system was programmed for two stages: (i) during the initial two hours, all measurements were recorded at an acquisition frequency of 5 Hz; (ii) afterwards, measurements were recorded every 5 minutes for 10 seconds at a frequency of 5 Hz.

The study of the experimental behaviour of the NSM CFRP-concrete specimens under the combination of sustained loading and high service temperatures is presented in Chapters 5 and 7 (Papers B and D).

3.3.3 Numerical prediction of the sustained loading response

The numerical procedure developed in Chapter 4 to predict the instantaneous response was adapted to calculate the response of the NSM CFRP-concrete specimens under sustained loading. The creep effect caused by the sustained loading was considered damaging the bond-slip law in terms of decreasing the stiffness and the bond shear strength. Figure 3.14 shows the evolution of the bond-slip law adopted for specimens which are under sustained loading.
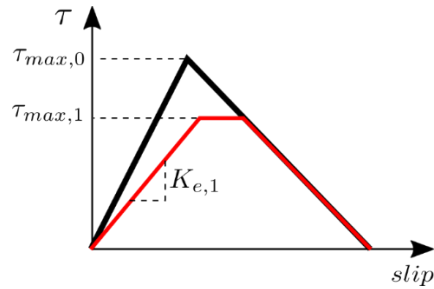
Figure 3.14: Evolution of the bond-slip law under sustained loading.

The proposed numerical methodology is presented as an extension of the one presented for the instantaneous behaviour, but this time, the value of the load is constant through the test. Once the governing equations are solved for a time t, the numerical method degrades a bond-slip law to redistribute the bond shear stress along the bonded joint, then, a new iteration step starts for a new time t. Figure 3.15 shows the sequence of steps followed to calculate the bonded joint response under sustained loading.

Set the sustained load $P_{loaded\ end}$ and set time $t = 0$.

Initial value of Slip $_{loaded\ end}$

Using the **bond slip law,** calculate bond shear stress (τ)

$$P(1,i) = P(1,i-1) - \tau(1,i-1) * L_{per} * x$$

Increase $Slip_{loaded\ end}$

$$\varepsilon_f = \frac{P}{A_f * E_f} \qquad \varepsilon_c = \frac{\varepsilon_c * E_f}{E_c}$$

$$s(1,i) = s(1,i-1) - (\varepsilon_{FRP} - \varepsilon_c) * x$$

$\varepsilon_{FRP,\ free\ end}$ is less than the threshold?

No   **Yes**

Next time t

End of test?

Yes   **No**

End of the numerical procedure
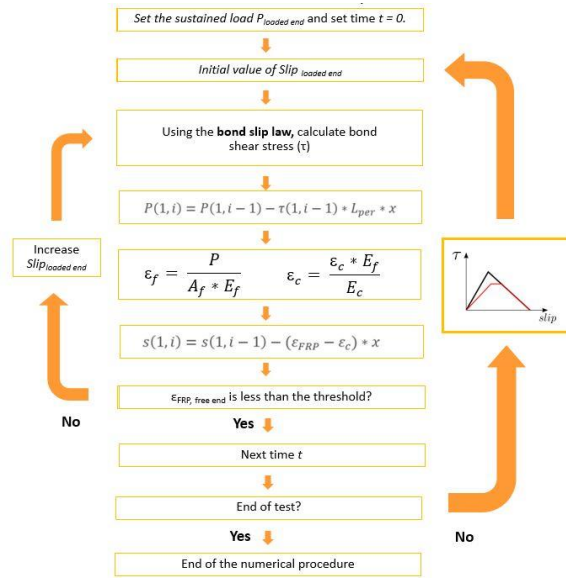
Figure 3.15: Flowchart of the steps followed in the numerical procedure for specimens under sustained loading.

The degradation of the bond-slip stiffness is calibrated with the experimental creep results of adhesive specimens, and the reduction of the bond shear strength (τ_{max}) is experimentally adjusted to the NSM CFRP-concrete specimens tested in series S1.

The proposed model is extensively detailed in Chapter 5 (Paper B), where the calibration of the degradation of the bond-slip law is further explained and the numerical results are compared with the experimental results.

PART III: Publications and discussion

4 Paper A: Characterization and Simulation of the Bond Response of NSM FRP Reinforcement in Concrete

Javier Gómez *[1], Lluís Torres[1] and Cristina Barris[1]

[1]AMADE, Polytechnic School, University of Girona, 17003, Girona, Spain

*Corresponding author

Characterization and Simulation of the Bond Response of NSM FRP Reinforcement in Concrete

Javier Gómez * , **Lluís Torres** and **Cristina Barris**

AMADE, Polytechnic School, University of Girona, 17003 Girona, Spain; lluis.torres@udg.edu (L.T.);
cristina.barris@udg.edu (C.B.)

* Correspondence: javier.gomez@udg.edu; Tel.: +34-972-418-817

check for
updates

Abstract: The near-surface mounted (NSM) technique with fiber reinforced polymer (FRP) reinforcement as strengthening system for concrete structures has been broadly studied during the last years. The efficiency of the NSM FRP-to-concrete joint highly depends on the bond between both materials, which is characterized by a local bond–slip law. This paper studies the effect of the shape of the local bond–slip law and its parameters on the global response of the NSM FRP joint in terms of load capacity, effective bond length, slip, shear stress, and strain distribution along the bonded length, which are essential parameters on the strengthening design. A numerical procedure based on the finite difference method to solve the governing equations of the FRP-to-concrete joint is developed. Pull-out single shear specimens are tested in order to experimentally validate the numerical results. Finally, a parametric study is performed. The effect of the bond–shear strength slip at the bond strength, maximum slip, and friction branch on the parameters previously described is presented and discussed.

4.1 Introduction

The use of fibre reinforced polymer (FRP) materials for strengthening existing concrete structures has been widely studied during the last years because of the potential advantages of these materials compared to the conventional ones [4]. The most commonly used techniques for strengthening reinforced concrete (RC) structures with FRPs are the so-called externally bonded reinforcement (EBR) and near-surface mounted (NSM) reinforcement. While in the EBR methodology the FRP reinforcement is bonded on the exterior face of the structural element, in the NSM system the FRP is installed into groves cut in the concrete cover where it is bonded with the appropriate adhesive. The NSM technique has attracted the attention of researchers and industry in recent years due to several potential advantages compared to the EBR system,

such as no need of specific surface preparation except grooving, better anchorage capacity, better protection in front of external agents like fire or vandalism, and no relevant change in the aesthetics of the structural element [19].

A number of research works have been carried out in order to obtain analytical solutions of the differential equations governing the bond performance of the FRP-to-concrete joint. This differential equation is based on the local bond–slip behaviour, relating the bond and slip at every point along the bonded length. For the EBR technique, for instance, Yuan *et al.* proposed an analytical solution based on a local bilinear bond–slip law in [67] and a trilinear bond–slip one with an exponential descending branch in [54]. In a later work, Ali *et al.* [68] adapted Yuan's analytical solution to the NSM strengthening system. Even though these authors proposed closed form equations to calculate the global bond behaviour, these are not always easy to implement and are only suitable for specific local bond–slip laws.

In recent years, experimental and numerical studies have provided solutions to the global bond behaviour of the EBR strengthening technique [23,44,87–91], although less attention has been paid to the NSM strengthening systems [28,55]. Focusing specifically on the characterization of the local bond behaviour of NSM FRP-to-concrete joints, several bond–slip laws have been proposed in the literature, with different shapes and stages. Some examples are the models proposed by Sena *et al.* [28], Borchert *et al.* [55], Zhang *et al.* [22]**,** and Seracino *et al.* [36]. The effect of their differences on the structural bond response and design implications is not always straightforward, thus, development of numerical tools that allow obtaining and comparing the response for different models is of main interest.

The aim of this paper is to study the effect of the shape of the local bond–slip law on the global bond behaviour of NSM FRP strengthening systems. For this purpose, a numerical procedure based on finite difference method is proposed to solve in a general way the differential equation that characterizes the bond behaviour of the FRP-to-concrete joint, which can be applied independently of the specific local bond–slip law. The numerical results are then verified by comparison between numerical and experimental results. Finally, a parametric study to evaluate the effects of the parameters defining the local behaviour of the NSM FRP strengthened bonded joint is carried out.

4.2 Bond Mechanisms in NSM FRP Strengthening Systems

In the NSM FRP strengthening system, the forces are transferred from the FRP material to the internal faces of the concrete groove through its perimeter in contact with the adhesive. This way, there are two main issues improving the transfer of stresses with respect to the EBR reinforcement: the higher ratio of the area of the perimeter in contact with the adhesive to the FRP area, and the transmission to the concrete material through a confined zone in the interior of the slot in the concrete cover.

The global bond stress-slip response for NSM strips subjected to a pull-out force is generally characterized by an initial, relatively stiff, linear behaviour, followed by a nonlinear curve up to the maximum value of the bond stress (bond strength), after which the originated damage causes a softening branch. Moreover, in NSM strengthening systems, it has been observed the activation of a friction component for relatively large slips as an extension of the softening branch [4,55,92–94]. The presence of a friction branch has been also reported in the bond behaviour of other strengthening materials as fibre reinforced cementitious matrix composites (FRCM) [95,96].

The bond mechanisms generated in the NSM FRP technique can lead to several types of failure modes, which are mainly influenced by the bonded length, FRP surface and shape, groove configuration, materials mechanical properties and adhesive properties [15,97]. In general, the failure modes can be grouped into three main categories: failure at the FRP-adhesive interface, failure at the epoxy–concrete interface, and adhesive cover splitting [4].

The global bond stress-slip performance of an NSM FRP strip bonded to a concrete block is the result of the local bond–slip behaviour at every point along the bonded length, which can be considered the constitutive model characterizing the bond behaviour of the NSM FRP element. Different models and shapes can be found in the literature for these local laws, and the assessment of their results is the main objective of this paper.

4.3 Assessment of the Bond–Slip Response of NSM FRP

4.3.1 Governing Equation and Global Response

In the pull-out single shear test (pull-push test), the load is transferred from the FRP to the concrete through the adhesive. Figure 4.1a shows the stress equilibrium of an infinitesimal

element of FRP NSM concrete element of length *dx*. Figure 4.1b shows the stress equilibrium of the FRP-adhesive interface in an infinitesimal element of length *dx*.

a)   b)
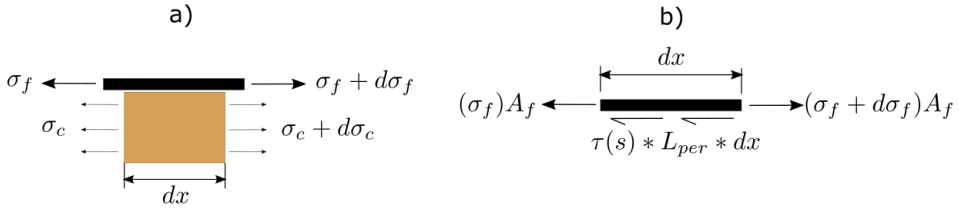
Figure 4.1: Stress equilibrium (a) in the FRP-concrete joint, and (b) in the FRP-adhesive interface.

From stress equilibrium between FRP and concrete, and the FRP-adhesive interface, Eq. 4.1 and Eq. 4.2 can be obtained,

$$A_f d\sigma_f + A_c d\sigma_c = 0, \tag{4.1}$$

$$\frac{d\sigma_f}{dx} - \frac{\tau(s) * L_{per}}{A_f} = 0, \tag{4.2}$$

where σ_f is the stress in the FRP, A_f is the FRP area, calculated as the product of the FRP thickness (t_f) by the FRP width (w_f), σ_c is the stress in the concrete, A_c is the area of concrete, $\tau(s)$ is the bond–slip law of the joint, and L_{per} is the is the intermediate perimeter in the adhesive.

The slip of the bonded joint can be defined as the relative displacement between the FRP and the concrete element.

$$s = u_f - u_c, \tag{4.3}$$

where *s* is the slip, u_f is the FRP displacement and u_c is the concrete displacement. Using the constitutive equations of the FRP and the concrete, Eq. 4.4 and Eq. 4.5 are obtained,

$$\frac{ds}{dx} = \varepsilon_f - \varepsilon_c = \frac{\sigma_f}{E_f} - \frac{\sigma_c}{E_c}, \tag{4.4}$$

$$\frac{d^2s}{dx^2} = \frac{1}{E_f}\frac{d\sigma_f}{dx} - \frac{1}{E_c}\frac{d\sigma_c}{dx}, \tag{4.5}$$

where E_f is the elastic modulus of the FRP, ε_f is the strain in the FRP, E_c is the elastic modulus of the concrete, and ε_c is the strain in the concrete.

Finally, by substituting Eq. 4.1 and Eq. 4.2 into Eq. 4.5, the differential equation governing the bond–slip behaviour of a NSM FRP-to–concrete bonded joint is:

$$\frac{d^2s(x)}{dx^2} - \tau(s) * L_{per}\left(\frac{1}{E_f * A_f} - \frac{1}{E_c * A_c}\right) = 0, \tag{4.6}$$

It is worth mentioning that usually the second term in the parenthesis corresponding to the concrete properties is much lower than the first and can be neglected (Ko *et al.* [125]).

Eq. 4.6 can be solved analytically using the boundary conditions

$$\varepsilon_f = 0 \text{ at } x = 0, \tag{4.7}$$

$$s = s(L_b) \text{ at } x = L_b, \tag{4.8}$$

where ε_f is the strain in the FRP at the free end, L_b is the bonded length, and $s(L_b)$ is the applied slip at the loaded end.

This differential equation can be solved for specific shapes of the local bond-stress slip law [74]. In the rest of cases a numerical procedure is required.

The numerical model implemented in this work is based on the finite difference method and aims to solve the governing equation of the bonded joint for any type of local bond–slip law. Following this methodology, the bonded length (L_b) is discretized into n uniform small increments of length $\Delta x = L_b/n$. The increments are delimited by $n+1$ points, which position is defined by $x_i = i \cdot \Delta x$ ($i = 0,1, …n$) (Figure 4.2). The procedure is based on an incremental slip methodology that pretends to simulate a usual experimental test under monotonic increase of the loaded end slip (this way, possible snap-back effect after maximum load is not reproduced in the simulations, Zou *et al.* [126]). Starting from the loaded end and moving towards the free end, the procedure calculates, for every studied point, the slip and the load transmitted between two adjacent sections. For a certain value of slip at the loaded end, an iterative process is carried out in which $P(j,1)$ is a lower bound value of the initial load at the loaded end at iteration j. $P(j,1)$ is used to calculate the corresponding strain in the FRP (ε_{FRP}), the strain in the concrete (ε_c), and the bond–shear stress (τ) using the bond–slip law at the loaded point. Still, at iteration j, the load at every point i, $P(j,i)$, is calculated using Eq. 4.9 along the FRP and towards the free end, by:

$$P(j,i) = P(j,i-1) - \tau(j,i-1) * L_{per} * \Delta x, \tag{4.9}$$
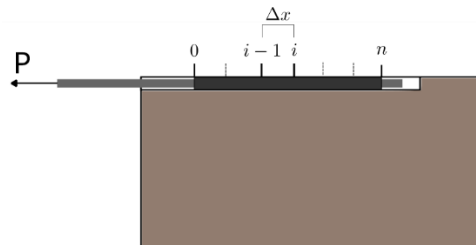
Figure 4.2: Scheme of the discretization along the FRP.

From the load profile obtained using Eq. 4.9, the strain distribution in the concrete and the FRP can be obtained, and, subsequently, the slip profile along the FRP is calculated as

$$s(j,i) = s(j,i-1) - (\varepsilon_f - \varepsilon_c) * \Delta x, \tag{4.10}$$

Increments of P at the loaded end are applied until convergence is attained, which happens when the ε_f at the free end is less than a prescribed tolerance, set to be a value close to zero. Once convergence is achieved, the corresponding load is registered and the process is repeated for a new value of slip at the loaded end, defined as *s(j+1,1)*. At this point, the iterative procedure is again repeated. The procedure finishes when all the points of the load–slip curve are calculated. Figure 4.3 shows the flowchart of the numerical procedure.
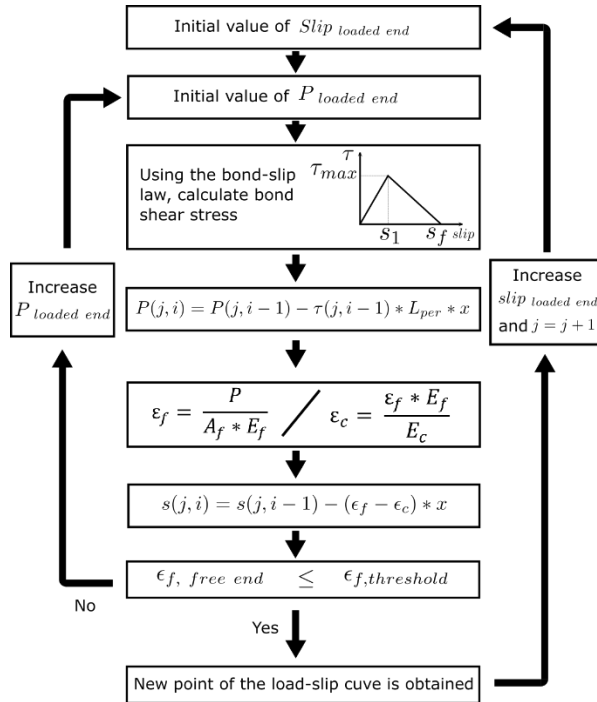
Figure 4.3: Scheme of the discretization along the FRP.

4.3.2   Comparison of the Numerical Results with Existing Analytical Solutions

In order to verify the numerical procedure developed, a comparison with analytical solutions available for some specific laws is presented in this section. For the sake of simplicity, only the analytical solution for the bilinear bond–slip law proposed by Yuan *et al.* [74] is taken as a reference, considering a bond–shear strength (τ_{max}) of 15 MPa, a slip at the bond–shear strength (s_1) of 0.1 mm and a maximum slip (s_f) of 1.13 mm. These values have been chosen according to

experimental results available in the literature. Four different situations are simulated by modifying the bonded length (L_b = 200 and 400 mm) and the FRP area (A_f = 14 and 30 mm^2). The results, presented in Figure 4.4, show good agreement between the analytical and the numerical solutions, and therefore the suitability of the developed procedure.
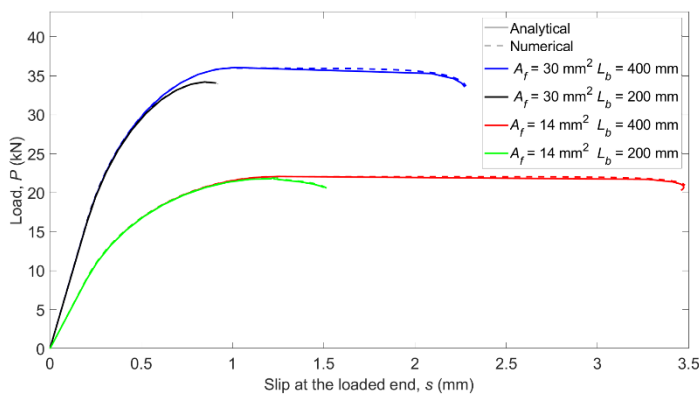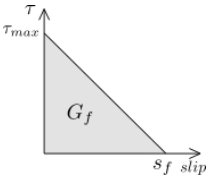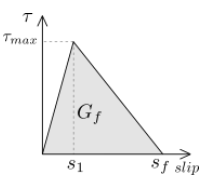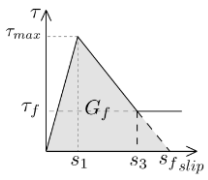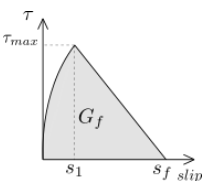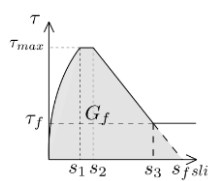
Figure 4.4: Comparison between the analytical and the numerical models.

4.4   Bond–Slip Behaviour at a Local Level

In this work, six different models (Table 4.1) based on two of the most widely accepted constitutive laws for bond characterization of NSM FRP systems (the Bilinear law [57] and Borchert law [60]) are considered. The study focuses on the effect of the combination of their parameters on the structural global response of the bonded joint. From the bilinear law, four combinations are studied: i) a bilinear (BL) model; ii) a linear descending (LD) model, which does not consider the initial elastic branch; iii) a two stage bond–slip law with a non-linear ascending branch (TSANL) model, with the aim to study the effect of the shape of the ascending branch; and iv) a bilinear plus friction (BLF) model, with the purpose to obtain the effect of friction in a bilinear bond–slip law. On the other hand, from Borchert law (BO), one additional modification is proposed, consisting in suppressing the original bond–shear strength plateau (BONP).

Table 4.1: Equations of the bond–slip models used in the parametric study.

Bond–slip model	Equation

Linear Descending (LD)

$$\tau(s) = \begin{cases} \tau_{max} * \dfrac{(s_f - s)}{s_f}, & s > 0 \text{ and } s \leq s_f \\ 0, & s \geq s_f \end{cases}$$

Bilinear (BL)

$$\tau(s) = \begin{cases} \tau_{max} * \dfrac{s}{s_1}, & s < s_1 \\ \tau_{max} * \dfrac{(s_f - s)}{(s_f - s_1)}, & s > s_1 \text{ and } s \leq s_f \\ 0, & s \geq s_f \end{cases}$$

Bilinear-friction (BLF)

$$\tau(s) = \begin{cases} \tau_{max} * \dfrac{s}{s_1}, & s < s_1 \\ \tau_{max} * \dfrac{(s_f - s)}{(s_f - s_1)}, & s > s_1 \text{ and } s \leq s_3 \\ \tau_f, & s \geq s_3 \end{cases}$$

Two-stage ascending non-linear (TSANL)

$$\tau(s) = \begin{cases} \tau_{max} * \left(\dfrac{s}{s_1}\right)^{\propto}, & s < s_1 \\ \tau_{max} * \dfrac{(s_f - s)}{(s_f - s_1)}, & s > s_1 \text{ and } s \leq s_f \\ 0, & s \geq s_f \end{cases}$$

Borchert (BO)

$$\tau(s) = \begin{cases} \tau_{max} * \left(\dfrac{s}{s_1}\right)^{\propto}, & s < s_1 \\ \tau_{max}, & s \geq s_1 \text{ and } s \leq s_2 \\ \tau_{max} - \dfrac{(\tau_{max} - \tau_f)}{(s_f - s_1)} * (s - s_1), & s > s_2 \text{ and } s \leq s_3 \\ \tau_f, & s \geq s_3 \end{cases}$$

Borchert no plateau ($s_1 = s_2$) (BONP)
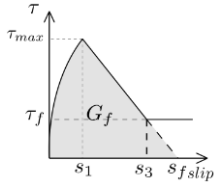
$$\tau(s) = \begin{cases} \tau_{max} * \left(\dfrac{s}{s_1}\right)^{\propto}, & s < s_1 \\[2ex] \tau_{max} - \dfrac{(\tau_{max} - \tau_f)}{(s_f - s_1)} * (s - s_1), & s > s_1 \ and \ s \leq s_3 \\[2ex] \tau_f, & s \geq s_3 \end{cases}$$

Note: τ = bond–shear stress; s = slip; τ_{max} = bond–shear strength; s_1 = slip when the bond–shear strength is achieved; s_2 = final slip of the plateau; s_3 = initial slip of the friction plateau; s_f = maximum slip of the bonded joint; τ_f = friction bond–shear stress; α = experimental parameter that control the shape of the bond–slip law.

4.5 Global Bond–Slip Response for Different Local Bond–Slip Laws

The main objective of this section is to evaluate the influence of the local bond law on the global behaviour of the FRP laminates bonded to concrete as NSM strengthening system, when subject to a pull-out force, using the numerical model described in Section 3, and the bond–slip laws introduced in Section 4.2.

4.5.1 Parameters Used

The values of the parameters that define the different local bond–slip laws, as well as the properties of materials and characteristics of specimens have been chosen according to previous experimental campaigns found in the literature [24,31,41,57,60,127], with the aim to simulate conditions as realistically as possible.

The elastic modulus of the laminate and concrete are 150 GPa and 33 GPa, respectively. The concrete block cross-section is 200 × 200 mm and the groove thickness and width are 5 mm and 15 mm, respectively. The bonded length (L_b) has been set as 200 mm, and the laminate section is 1.4 × 10 mm.

Regarding the bond–slip parameters, bond–shear strength has been set as 15 MPa, and the corresponding slip as 0.1 mm. In bond–slip models that have a friction branch, τ_f has been defined as the 35% of τ_{max}. The initial point of the plateau of BO model is $s_1 = 0.8 \cdot s_2$, and the experimental parameter α is 0.31 [60].

Another parameter that is crucial for the simulations is the fracture energy (G_f), typically defined as the area under the bond–slip law [25]. In those bond–slip laws with a friction branch, G_f is calculated according to Haskett *et al.* [76], as the area under the ascending and descending

stages of the bond–slip law, without taking into account the friction stage, as illustrated in Figure 4.5. A value of 8.5 N/mm has been set for G_f in all the models [41,57,127].
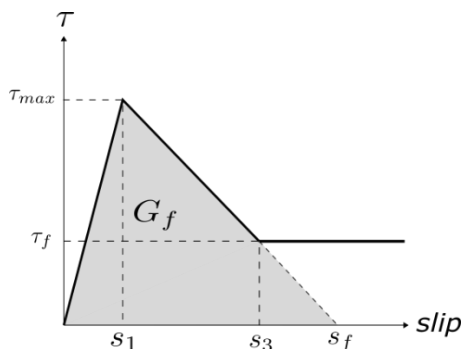
Figure 4.5: Fracture energy obtained from the bond–slip law.

The comparison between the studied bond–slip laws is shown in Figure 4.6. As indicated before, it can be observed that the bond–shear strength (τ_{max}) is 15 MPa, and the corresponding slip (s_1) is 0.1 mm, except for the LD model, which does not consider s_1.
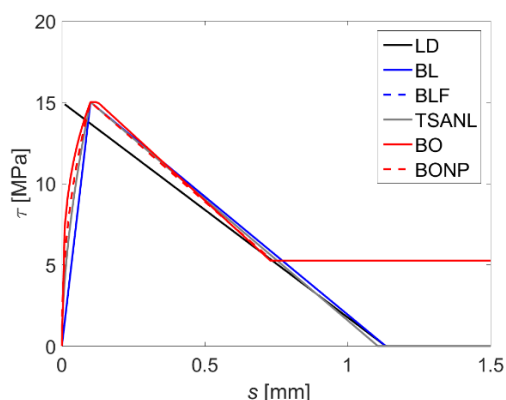
Figure 4.6: Comparison of the bond–slip models.

4.5.2 Load–Slip Response

The comparison of the load–slip curves obtained from each bond–slip law is shown in Figure 4.7. Overall, two main tendencies can be observed. The first one (Figure 4.7a), followed by LD, BL and TSANL models, achieve a maximum load, which remains constant as the slip in the loaded end increases until failure. This plateau is obtained because the maximum activated length is attained when the slip in the loaded point is equal to s_f, meaning that this point does not carry load anymore (debonding). Therefore, the load capacity will remain constant and the slip will keep increasing until failure. In the second trend (Figure 4.7b), followed by BLF, BO, and BONP

models, the load increases up to the maximum carrying capacity, where a sudden decrease takes place followed by a residual (friction) bond force. The difference between these two trends falls to the effect of the friction branch of the local bond–slip law after the loaded point reaches debonding.

Focusing on the initial part of the load–slip curve (interior plot in Figure 4.7) it can be seen that the LD model shows the highest stiffness, because the ascending branch of the bond–slip law has an infinite stiffness. Besides, it can be observed that bond–slip models with a non-linear ascending branch (TSANL, BO, and BONP) exhibit a stiffer branch of the load–slip curve than BL and BLF models caused by the fact that for a fixed value of s_1 the area under the ascending branch is greater in those cases with non-linear tendency.
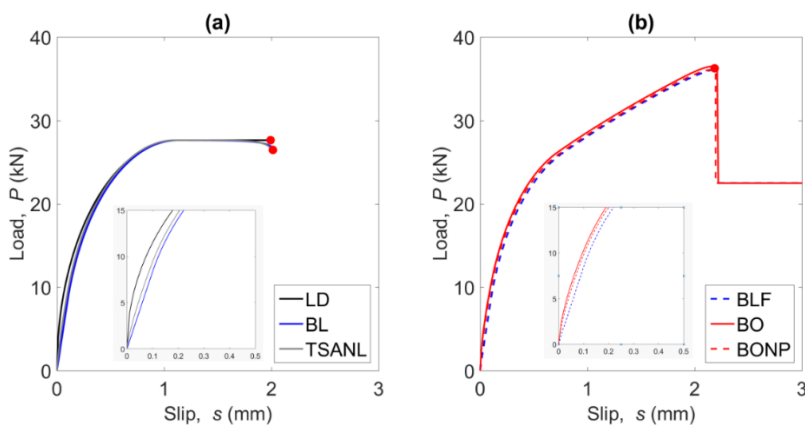
Figure 4.7: Comparison of the load–slip curves, (a) shows LD, BL and TSANL models, and (b) shows BLF, BO, and BONP models.

4.5.3 FRP Strain, Bond–Shear Stress and Slip along the Bonded Length

Following the numerical procedure, the FRP strain, bond–shear stress and slip can also be obtained. Figure 4.8 shows the response along the bonded length for the different laws (loaded end at $x = 0$ mm, free end at $x = 200$ mm) evaluated at the situation of imminent failure (marked with a red dot in Figure 4.7). For 7.5 mm grooved specimens, the failure point was defined as the point before the load drops to 0, and for 10 mm grooved specimens, the failure was defined as the maximum load point.
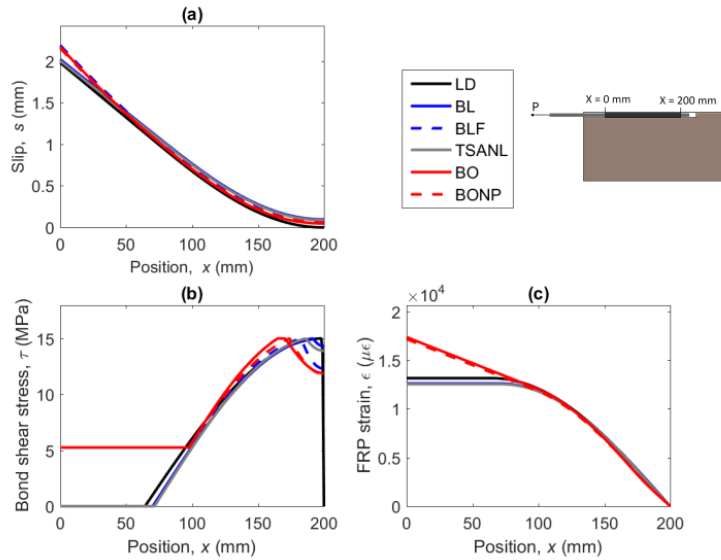
Figure 4.8: (a) FRP slip, (b) bond–shear stress, and (c) FRP strains along the bonded length for the different bond–slip models.

From Figure 4.8a it can be observed that the shape of the bond–slip law has a small effect on the slip profile along the FRP. It can also be seen that BLF, BO and BONP exhibit slightly higher values for the slip at the loaded end. Furthermore, the slip at the free end equals to 0 for the LD model, contrarily to the rest of models, which show a small value of slip.

An evident difference between the models with and without friction can be observed in the bond stress distribution along the bonded length (Figure 4.8b). Models that include friction still transmit bond–shear stress after the softening stage, whilst the other models exhibit a completely damaged zone, where no load is transmitted. Hence, for friction bond–slip models, the increase of the area under the bond–shear stress profile allows the joint to carry more load even though the zone near the loaded end is damaged.

Figure 4.8c shows the FRP strain distribution. In models without friction, the strain profile stabilizes when the maximum load is attained. On the other hand, strain values in the FRP do not stabilize for BLF, BO, and BONP models, because of the load keeps increasing after the loaded end surpasses the softening stage.

4.6 Experimental Program

In this section, an experimental program is presented and the results, in terms of load–slip curves are discussed. Then, a relatively simple methodology to obtain the bond–slip law from the experimental load–slip curve is presented. Finally, the theoretical results obtained from the numerical procedure are compared to experimental values.

4.6.1 Material Properties

The concrete used in the experimental campaign has been characterized according to the UNE 12390-3 [116] and the ASTM C469 / C469M-10 standard [115]. From the characterization tests on 150 × 300 mm cylindrical specimens, a compressive strength of 36.9 MPa and an elastic modulus of 46.8 GPa were obtained.

Carbon-FRP (CFRP) strips with 3 × 10 mm cross-section were used in the experimental campaign. Their mechanical properties were tested according to ISO 527-5 [114], obtaining an elastic modulus of 169.3 GPa and a tensile strength of 3205.9 MPa.

The bi-component epoxy resin used in this program was tested according to the ISO 527-2 standard [113] after 12 days of curing under 20ºC and 55%RH, obtaining an elastic modulus of 10.7 GPa and a tensile strength of 27.9 MPa.

4.6.2 Experimental Details

4.6.2.1 Parameters of the Study

Four different NSM configurations were tested, combining two different groove thicknesses (7.5 mm and 10 mm) and two different bonded lengths (150 mm and 225 mm). Four specimens were tested per each configuration, giving a total of 16 specimens tested in a pull-out single shear test.

The fib Bulletin 90 [11] limits the deepness of the groove in order to avoid epoxy cover splitting. ACI 440.2R [69], in turn, suggests that the groove thickness should be, at least, 3 times the laminate thickness. In order to study the effect of the resin layer thickness, two groove thicknesses were defined in this study: 10 mm and 7.5 mm. The first one was set according to the ACI 440.2R requirement, whilst the second groove thickness was chosen to satisfy the fib [50] condition that establishes that the minimum groove dimensions must be 1.5 or 2 times the laminate size.

Regarding the effect of the bonded length, Seracino *et al.* [23] used bonded lengths between 100 mm and 350 mm and concluded that the minimum L_b to achieve the maximum carrying capacity was 200 mm. Furthermore, Zhang *et al.* [46] tested NSM strengthened concrete elements with bonded lengths between 25 and 350 mm. From their study, it was observed that the experimental effective bonded lengths for the different specimens were between 150 and 175 mm.

The bonded lengths used in this experimental campaign were chosen to be above and below the values suggested in [23] and [46], in order to validate if the finite differences model is able to predict the response for short and long bonded lengths.

4.6.2.2   Test Setup

In order to study the effect of the bonded length and the groove thickness, four pull-out single shear configurations were designed. Four specimens were tested for each configuration defined in Table 4.2.

Table 4.2: Characteristics of the specimens.

Specimen ID	Bonded length (mm)	Groove thickness (mm)	Maximum load (kN)	Failure mode
NSM – 150 – 10	150	10	43.85	F-A
NSM – 225 – 10	225	10	54.74	F-A
NSM – 150 – 7.5	150	7.5	47.14	C
NSM – 225 – 7.5	225	7.5	57.71	C
Note: F-A = FRP-adhesive interface, C = cohesive failure in the concrete.				

The specimens were identified as NSM – L_b – t_g, where L_b stands for the bonded length and t_g for the groove thickness. The tests were carried out under a single shear test configuration, as shown in Figure 4.9. The specimen was rigidly fixed with a 60 mm wide plate to avoid translation in the vertical direction and also perpendicularly in the opposite side with a 50 mm plate to avoid rotation. At the top of the specimen a length of 50 mm was left unbonded to avoid stress concentrations in that zone [26]. The concrete block dimensions used on the short-bonded length specimens were 200 × 200 × 300 mm, and for the long-bonded length specimens 200 × 200 × 370 mm. A servo-hydraulic Servosis MUE-60T testing machine was used to apply the load. The test was performed under displacement control with a speed of 0.2 mm/min. One

LVDT was placed in the loaded end to measure the relative displacement between the CFRP strip and the concrete.
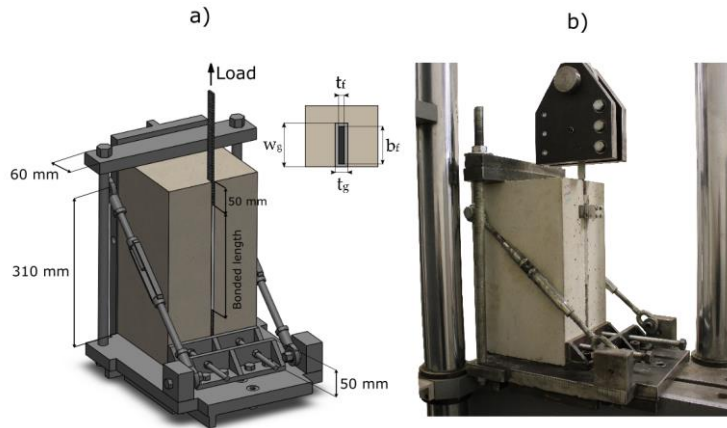
Figure 4.9: (a) scheme of the set-up for the pull-out single shear test, and (b) picture of the tests.

4.6.3   Experimental Results

The results obtained from the experimental tests are shown in Figure 4.10, where the average load–slip curves for the four tested configurations are presented.
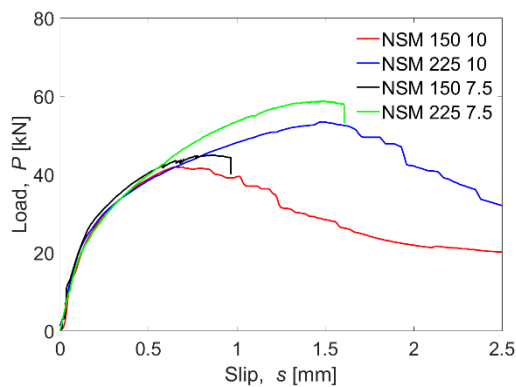
Figure 4.10: Experimental results from the single shear tests.

Failure loads for the narrowest groove specimens were slightly higher than for those with the widest grooves: the failure load of NSM-150-7.5 was 7.1% higher than NSM-150-10, and NSM-225-7.5 failure load was 10.0% higher than in the NSM-225-10 case. Besides, differences in the failure load can be observed: 10 mm grove thickness specimens failed in the FRP-adhesive interface while 7.5 mm grove thickness specimens failed in the resin–concrete interface.

As can be observed, in specimens with 10 mm groove thickness, after reaching the maximum load, the slip continued increasing although the load decreased, which could be interpreted as all the bonded length being activated and damaged, as well as friction effect taking place. On the other hand, failure of the specimens with 7.5 mm groove was sudden and instantaneous: after reaching the maximum load, the load capacity dropped abruptly with no friction effects. For this reason, in this study, two different bond–slip laws have been defined: a bilineal law for the case of 7.5 mm groove specimens and a bilineal plus friction law for the case of 10 mm groove specimens. Finally, it should be noticed that the slip at the end of the elastic stage and at the maximum load was similar both for specimens with 10 mm and 7.5 mm groove thickness.

Regarding the effect of the bonded length, it can be seen that the initial tendency of the load–slip curves was the same for both bonded lengths. On the other hand, as the bonded length increased, the maximum load carrying capacity increased as well. Increasing the bonded length 50% caused a load increase of 24.8% and a 22.4% for specimens with 10 mm and 7.5 mm groove thickness, respectively.

4.6.4   Bond–Slip Law Adjusted to the Experimental Results

From the experimental tests results, a bilinear bond–slip law could be obtained from the load–slip curves [108] for specimens with 7.5 mm groove and 10 mm groove. For the case of specimens with 7.5 mm groove thickness, the slip at the bond strength (s_1) was obtained at the end of the linear branch of the load–slip, whilst the maximum slip (s_f) could be estimated from the slip where the maximum load was achieved (Figure 4.11). Once s_1 and s_f were estimated, the value of the bond–shear strength (τ_{max}) was obtained from a least-squares approach that estimated the optimum value of τ_{max} to obtain the experimental load until P_{max}.
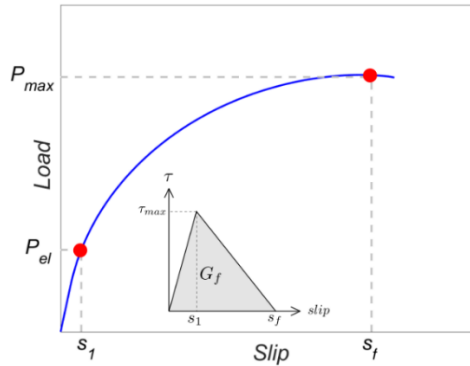
Figure 4.11: Bond–slip law parameters obtained from the load–slip curve for 7.5 mm grooved specimens.

For specimens with 10 mm groove thickness, which present a frictional stage after the maximum load is achieved, a trilinear bond–slip model with a friction branch has been adopted. In this model, s_1 and s_f are assumed equal to the values obtained for the 7.5 mm grooved specimens. Once the values of s_1 and s_f are defined, the methodology to calculate τ_{max} is the same as that defined for 7.5 mm grooved specimens. The friction bond–shear strength (τ_f) was defined as 35% of τ_{max}, following the reccomendations in [60].

Figure 4.12 shows the two adjusted bond–slip laws, for 7.5 mm and for 10 mm groove specimens, with their corresponding parameters.
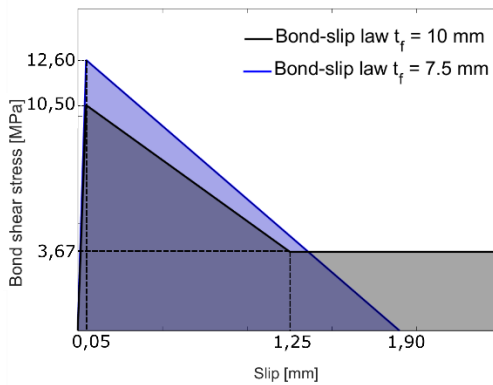
Figure 4.12: Experimental bond–slip laws for the NSM with 7.5 mm and 10 mm thickness grooves.

It can be observed that for the specimens with 7.5 mm groove thickness, τ_{max} is higher than for specimens with 10 mm groove thickness, implying higher fracture energy and justifies the higher maximum load experimentally obtained.

4.6.5   Comparison between Experimental and Numerical Results

By introducing the previously obtained bond–slip laws and the materials' mechanical properties in the finite differences model, the theoretical load–slip curves of the bonded joints are obtained. The comparison between the theoretical and experimental behaviour is shown in Figure 4.13.
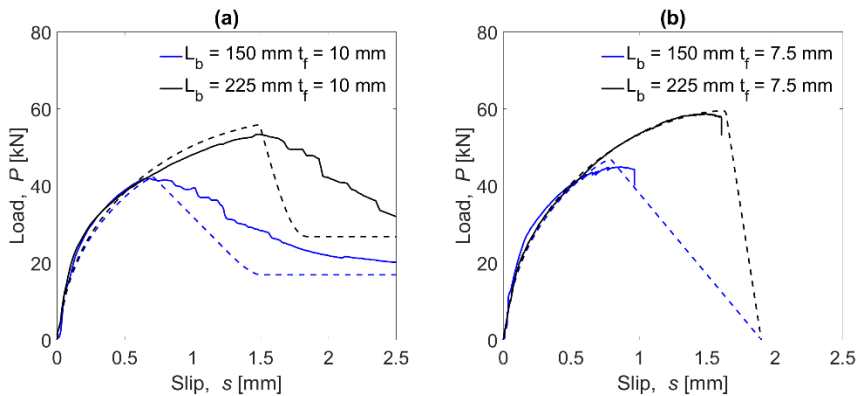
Figure 4.13: Comparison between the experimental (continuous lines) and the theoretical (dashed lines) values for the NSM with (a) 10 mm and (b) 7.5 mm groove thickness.

As expected, a close agreement between the predicted response and the experimental values is observed. Focusing on Figure 4.13a (10 mm groove thickness), it can be seen that the ascending stages of the load–slip curves and the maximum loads are correctly predicted, although the experimental results show a smoother decrease of the load once the maximum load is attained than the evolution predicted by the theoretical model. In the case of Figure 4.13b (7.5 mm groove thickness), the ascending branch and the maximum load are also correctly predicted.

4.7   Parametric Study

In the previous section, the bilinear and bilinear + friction bond–slip laws were implemented in the finite differences model. In this section, a parametric study is performed using the six different bond–slip models defined in Section 4.2 (Table 4.1) to better investigate the influence of other modifications of the bond–slip law.

The effect of four bond–slip law parameters on the maximum load (P_{max}) and on the effective bonded length (L_{eff}) are studied. The studied parameters are: i) the bond–shear strength (τ_{max}), ii) the slip at the bond–shear strength (s_1), iii) the maximum slip (s_f) and iv) the friction bond–shear strength (τ_f). L_{eff} is defined here as the bonded length needed to withstand the maximum stabilized load, therefore, it is only applicable to bond–slip models without friction branch. Computationally, the calculation of L_{eff} is measured from the first point that achieves s_f until the point that has less than 3% of the maximum FRP strain [75].

4.7.1   Effect of the Bond–Shear Strength (τ_{max})

Using the numerical model, the load–slip curve, and the slip, bond–shear stress and FRP strain profile along the bonded length are obtained. For the sake of brevity, only the response of the BL model is shown in Figure 4.14, however, the trends observed for the BL model can be extrapolated to the other bond–slip models. A range of τ_{max} between 10 MPa and 20 MPa has been considered taking $\tau_{max,0}$ = 10 MPa as a reference for normalization of results and, being s_f = 1.13 mm, s_1 = 0.1 mm, s_2 = 0.12 mm, and τ_f = 5.25 MPa.

In Figure 4.14, the curves are represented for the situation where the slip at the loaded end arrives at s_f. It is clearly seen that P_{max} increases with τ_{max} (Figure 4.14a). This is because an increase of τ_{max} implies an increase of G_f, thus, a higher load is needed to damage the bonded joint. In Figure 4.14b, where the slip profile is shown, it can be observed that as the τ_{max} increases, the activated bonded length decreases. At x = 200 mm the slip in the free end when τ_{max} is 10 MPa, is equal to 0.0091 mm, but when τ_{max} is 20 MPa, the slip in the free end is negligible, meaning that the activated length decreases with the increase of τ_{max}.

In Figure 4.14c the bond stress profile is represented. In that case, it can be seen that as τ_{max} increases, the bond–shear profile becomes narrower because every segment along the bonded length is able to transfer a larger bond–shear force. Finally, as the bond–shear strength (τ_{max}) increases, the strain in the loaded end increases as well (Figure 4.14d). It is worth noticing that as the bond–shear strength capacity increases, the activated bonded length decreases.
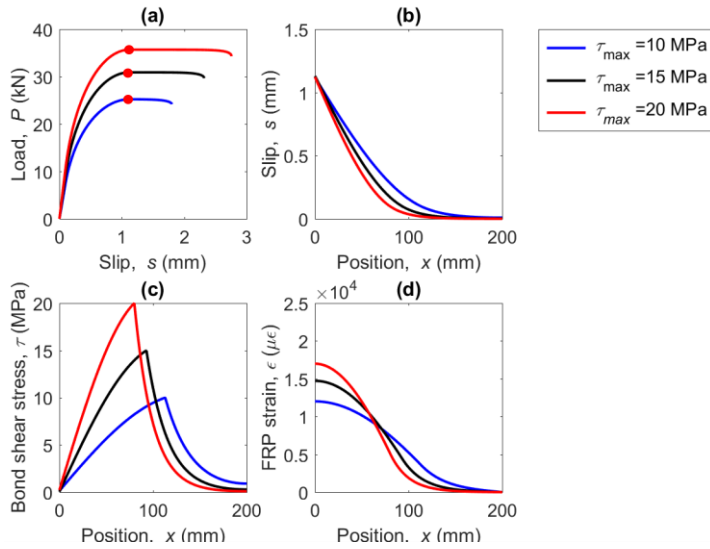
Figure 4.14: (a) Load–slip curve, (b) slip along the FRP, (c) bond–shear stress along the FRP, and (d) strains along the FRP for three values of bond–shear strength and a bilinear bond–slip law.

In Figure 4.15, the increase of the maximum load is depicted in function of the increase of the τ_{max}, previously normalized with respect to $\tau_{max,0}$ = 10 MPa. In general terms, a practically linear increase of the maximum load with the bond–shear strength can be observed for all the models. This is due to the fact that increasing τ_{max} without changing the value of s_f causes a linear increase of the fracture energy (G_f), leading to a situation where a higher load is needed to damage the bonded joint.

Moreover, it can be seen that LD, BL, and TSANL models show very similar results, meaning that these models are analogously affected by the increase of the bond–shear strength. These models show an increase of P_{max} of 41% when τ_{max} is 20 MPa. Finally, BLF, BO, and BONP, show lesser effect on the maximum load than the other models, because of the friction branch, which remains constant for all the cases. Although these models increase their G_f, the increase of the area under the bond–slip curve is smaller than in the non-friction cases. The increase of P_{max} in these models arrives to 30% when τ_{max} is 20 MPa. Finally, the BLF model is slightly less affected than BO and BONP models, because of the non-linear ascending branch of Borchert models, which experience a higher increase of G_f when τ_{max} increases.
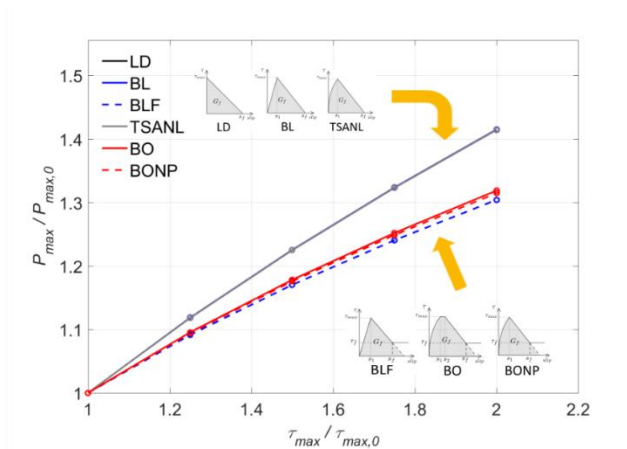
Figure 4.15: Variation of P_{max} versus τ_{max}.

The influence of τ_{max} on the effective length, L_{eff}, is shown in Figure 4.16 for models without friction. In general, a decrease of its value is observed as τ_{max} increases, as expected: if the bond–shear strength increases, every finite element of the bonded length can transfer a larger shear force, hence, less bonded length is needed to transfer the total load. It is worth noticing that the three models behave in a very similar way, indicating that assuming either the one stage model, the bilinear model or the model with a non-linear ascending stage, does not provide a difference on the effective bonded length for different bond strengths.
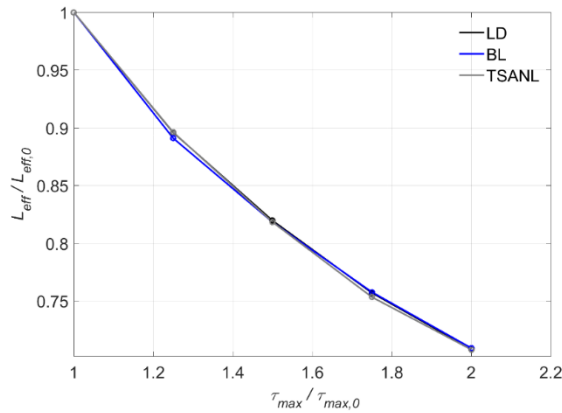
Figure 4.16: Variation of L_{eff} versus τ_{max}.

4.7.2 Effect of the slip at the bond–shear strength (s_1)

A range for s_1 between 0.1 mm and 0.5 mm has been considered, taking $s_{1,0}$ = 0.1 mm for normalization of results, and keeping τ_{max} = 15 MPa. The value of the G_f when $s_{1,0}$ = 0.1 mm is equal to 8.5 N/mm. In order to meet the new value of s_1, G_f varies between 8.5 N/mm and 10.9

N/mm, depending on the model considered. In BO model, the difference between s_1 and s_2 has been kept constant for all cases. The linear descending (LD) model is not included because the slip at the bond–shear strength is 0, and if this point is shifted horizontally, it would become a bilinear (BL) model.

The results are plotted in Figure 4.17 in terms of increment of the maximum load with respect to the increment of s_1. As observed, in all models the load increment is considerably small (with a maximum variation of 8.9%). For the BL model, no effect on the maximum load is obtained for a substantial increment of s_1, because τ_{max} and s_f are constant, and therefore, the fracture energy (G_f) remains the same.
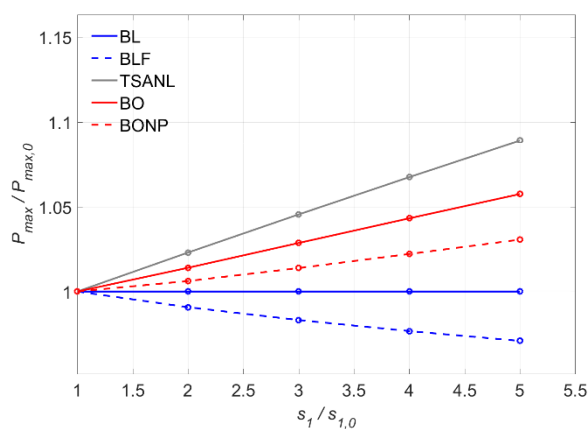
Figure 4.17: Variation of P_{max} versus s_1.

In the case of the BLF model, the maximum load decreases as the s_1 increases. Even though the fracture energy (G_f) remains constant for all the s_1 values, as can be seen in Table 4.3, the area under the total bond shear–slip curve, considering the three stages (elastic, softening and friction) sligthly decreases with the increment of s_1. It should be noticed, however, that the maximum load decrease only arrives up to 3% of the initial load.

It is also seen that bond–slip models that have a non-linear ascending branch (TSANL, BO, and BONP models) exhibit an some increase on the maximum load (P_{max}), caused by the increase of area under the elastic stage curve from the shifting of s_1. This effect can be observed in Table 4.3 through an increment of the fracture energy (G_f) with the increase of s_1. It should be noticed that the variation of the fracture energy for TSANL and BONP models is the same, therefore, in Table 4.3, only BONP model is showed. In BO and BONP cases, the increase of the fracture energy is mitigated by the decreasing of friction area between s_3 and s_f (Table 4.1): since the

value of s_f is kept constant and s_1 increases, the value of s_3 shifts horizontally, causing a reduction of area between s_3 and s_f.

Table 4.3: Variation of fracture energy for the BONP, BO and BLF models.

s_1 [mm]	$\dfrac{s_1}{s_{1,0}}$	BONP $\left(\dfrac{G_f - G_{f,0}}{G_{f,0}}\right) * 100$	BO $\left(\dfrac{G_f - G_{f,0}}{G_{f,0}}\right) * 100$	BLF $\left(\dfrac{G_f - G_{f,0}}{G_{f,0}}\right) * 100$
0.10	1	0 %	0 %	0 %
0.20	2	4.64 %	6.85 %	0 %
0.30	3	9.29 %	13.71 %	0 %
0.40	4	13.94 %	20.56 %	0 %
0.50	5	18.59 %	27.42 %	0 %

The TSANL model is more affected by the modification of s_1 than the other models, since it does not have a friction branch and the total area under the bond–slip law will not decrease with the shifting of s_1, and the increase of the fracture energy will not be mitigated. The increase of G_f in the TSANL model is the same as in the BONP model, since the definition of G_f has been considered as in Figure 4.5.

Figure 4.18 shows the variation of the effective bonded length with s_1 for TSANL and BL models. The effective bonded length (L_{eff}) increases as s_1 increases. Since higher slips are obtained in the elastic stage, a longer bonded length will be activated and L_{eff} will increase.

Moreover, the BL model is more sensitive to the variation of s_1 than the TSANL model, because the change in the non-linear ascending branch of the TSANL model slightly increases the area under the elastic branch, improving the resistance of the joint under in this stage. This way, the increase of slip caused by the s_1 shifting is mitigated by this increase of resistance.
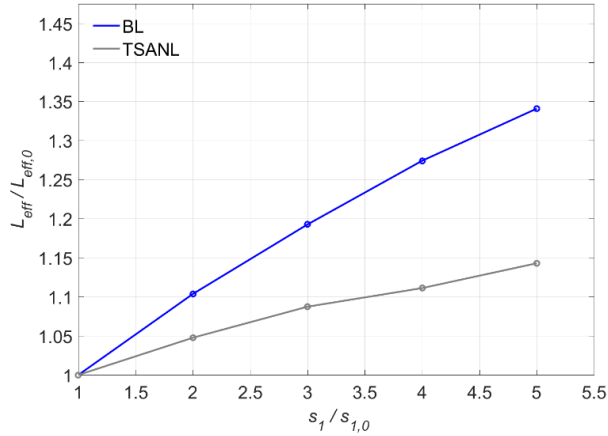
Figure 4.18: Variation of L_{eff} versus s_1.

4.7.3 Effect of the maximum slip (s_f)

Fixing the values of the bond–shear strength (τ_{max}) and the slip at the bond shear strength (s_1) to 15 MPa and 0.1 mm, respectively, and setting the fracture energy (G_f) to the values obtained in Section 4.7.1 (ranging between 8.5 N/mm and 11.33 N/mm) for each model, the values of the initial maximum slip ($s_{f,0}$) are between 0.70 mm and 0.75 mm. Because the bond–slip models have different shapes, and therefore, different values of G_f, the maximum slip, which satisfies the conditions of τ_{max} and s_1, will be different for each bond–slip law, as seen in Figure 4.19.
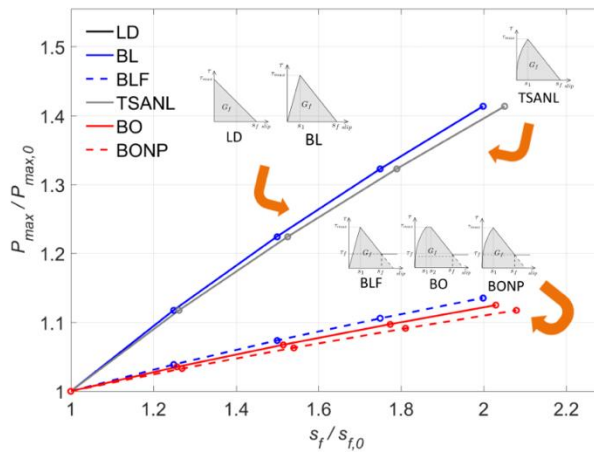
Figure 4.19: Variation of P_{max} versus s_f.

Overall, in Figure 4.19 it can be seen that all the models show an increasing tendency of P_{max} with s_f, because as s_f increases, G_f increases as well. The LD model presents exactly the same curve as the BL, since in both cases G_f is the same. Moreover, as indicated in previous subsections, models without friction branch—such as LD, BL, and TSANL—are more sensitive to the increase of s_f because the shifting of the slip affects directly to G_f, P_{max} increases up to 41% when s_f is the highest value. It is worth noticing that the TSANL is slightly less sensitive because the area under the elastic branch is higher than in LD and BL models, causing that the increment of s_f affects proportionally less to G_f and P_{max}, around 13% when s_f is the maximum value. As for the models with friction branch—BLF, BO, and BONP—increase the P_{max} caused by the shifting of s_f is diminished by the effect of the friction branch in the total area as indicated in previous subsections.

Figure 4.20 shows that L_{eff} increases with the increase of s_f for all models. A higher s_f allows the bonded joint to have higher slips while transferring load, and consequently, more bonded length is activated. LD model exhibits the highest influence of s_f and BL model is the less affected model.
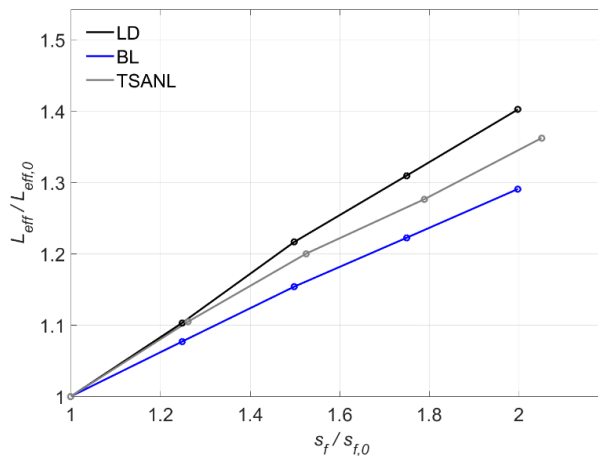
Figure 4.20: Variation of L_{eff} versus s_f.

4.7.4 Effect of the friction branch (τ_f)

Only BLF, BO, and BONP (with friction branch) models are included in this section. The bond–slip law parameters are set to τ_{max} = 15 MPa, s_1 = 0.1 mm, and G_f = 8.5 N/mm. The bond–shear stress of the friction branch ranges between 10% and 40% of τ_{max}, therefore τ_f will vary between 1.5 MPa ($\tau_{f,0}$) and 6 MPa.

Figure 4.21 shows the variation of P_{max} with the increase of τ_f. It can be seen that all models present the same almost linear rising tendency, as expected. For example, for an increase of 2.5 times $\tau_{f,0}$ (i.e. τ_f = 3 MPa), the increase of P_{max} is around 17%, while for 4 times $\tau_{f,0}$ (τ_f = 6 MPa), P_{max} increases around 35%.
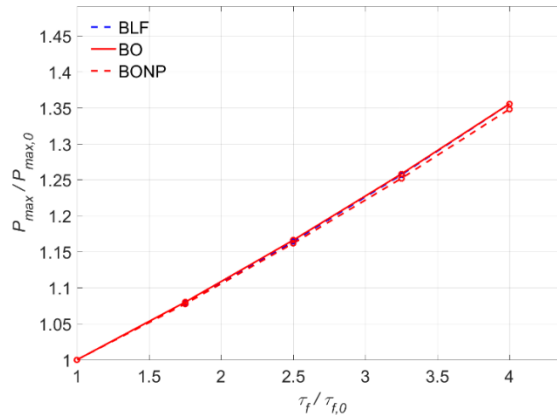
Figure 4.21: Variation of P_{max} versus τ_f.

4.8 Conclusions

A study on the effect of the local bond–slip law characterizing the material bond behaviour and its parameters on the global structural bond response of NSM FRP strengthened RC elements has been presented. A numerical method has been developed in order to being able to solve the governing equations of the bonded joint for any type of bond–slip law.

From the comparison between the results of the different bond–slip laws, the following conclusions are obtained:

- In models not including a friction branch after softening, a maximum value of load is attained, which stabilizes for a certain value of the bonded length. In contrast, in models with friction component, the load continuously increases up to a certain slip beyond which only the friction component remains. Furthermore, models with non-linear ascending branch show a stiffener initial load–slip response.

- The non-linear ascending branch effect on the maximum load is practically negligible. Small differences of P_{max} are observed between BL and TSANL models, and BLF and BONP models, respectively.

- The shape of the bond–slip law has a small effect on the slip profile along the FRP. However, the bond stress and slip distribution at maximum state along the bonded length is strongly affected by the friction branch.

From the comparison between numerical and experimental results, it can be concluded that:
- A close agreement between the finite differences model and the experimental results is obtained. The comparison between the load–slip curves obtained experimentally and numerically showed that the ascending part is correctly predicted until failure.
- A somewhat larger maximum load of around 7–10% was obtained for specimens with 7.5 mm groove thickness compared to those with 10 mm. As the groove thickness decreased, the maximum load of the bonded joint increased.
- Specimens with 10 mm groove thickness showed a behaviour indicating the existence of a friction branch in their local bond law and the failure was in the FRP-adhesive interface. Conversely, the behaviour of 7.5 mm groove thickness specimens was properly described using a bilinear function, while the failure was in the resin–concrete interface.

From the parametric study carried out, the following conclusions can be drawn:
- As the bond–shear strength increases, the maximum load grows, and conversely, the effective bonded length decreases.
- The slip at the bond shear strength, s_1, has a small effect on the maximum load and an increasing effect on the effective bonded length.
- The maximum load and the effective bonded length increase with the maximum slip. Moreover, bond–slip laws without friction branch are much more sensitive to the shifting of the maximum slip.
- The presence of a friction stage in the local bond behaviour causes an increase on the maximum load. As the bond–shear strength on the friction branch increases, the maximum load increases as well.

5 Paper B: Experimental study and numerical prediction of the bond response of NSM CFRP laminates in RC elements under sustained loading

Javier Gómez[1*], Cristina Barris[1], Younes Jahani[1], Marta Baena[1] and Lluís Torres[1]

[1]AMADE, Polytechnic School, University of Girona, 17003, Girona, Spain

[*]Corresponding author

ELSEVIER

Experimental study and numerical prediction of the bond response of NSM CFRP laminates in RC elements under sustained loading

Javier Gómez *, Cristina Barris, Younes Jahani, Marta Baena, Lluís Torres

AMADE, Polytechnic School, University of Girona, 17003 Girona, Spain

HIGHLIGHTS

- In monotonic pull-out tests, higher strain was observed in specimens with narrower grooves.
- Creep behaviour of adhesive did not depend on the load until 30% of the ultimate load.
- In sustained loading tests, higher slip was obtained as sustained loading increased.
- A time-dependent model was proposed to predict the behaviour of the bonded joint.

ABSTRACT

This paper presents a study into bond behaviour under sustained loading of Near-Surface Mounted (NSM) Carbon-Fibre Reinforced Polymers (CFRP) concrete joints, through an experimental programme and a numerical analysis. The experimental programme consisted of eight NSM CFRP-concrete pull-out specimens tested under sustained loading and laboratory conditions (20 °C and 55%HR) inside a climatic chamber. Previously, the instantaneous bond behaviour of the NSM CFRP-concrete joint was studied using 18 specimens tested until failure. Furthermore, the tensile behaviour of the adhesive under instantaneous and sustained loading was studied at different loading levels under the same environmental conditions. Finally, a numerical procedure was proposed to predict the bonded joint response under sustained loading. A creep coefficient and a strength reduction factor were applied to the instantaneous bond-slip law to simulate the degrading effect the sustained loading had on the behaviour of the bonded joint. Good agreement between the experimental and numerical results was obtained for the tested parameters, however, further research needs to be carried out in order to extrapolate this methodology to other cases.

5.1 Introduction

The durability of Reinforced Concrete (RC) structures can be effectively enhanced by employing strengthening techniques such as Externally Bonded Reinforcement (EBR) or Near-Surface Mounted (NSM) reinforcement using Fibre Reinforced Polymer (FRP) strips and bars. Recently, the NSM FRP technique has drawn scientific and industry attention thanks to several advantages it exhibits compared to the EBR FRP technique such as better anchorage capacity and not needing any surface preparation except for grooving [21,128]. Despite this, the main concern when designing NSM FRP strengthened RC structures is to avoid their premature debonding failure.

93

Although the short-term bond behaviour of the NSM FRP-concrete joint has been widely studied [22,29,41,75,127,129], less attention has been paid to its long-term performance. However, this is an important area as damaging effects caused by long-term external actions can affect and modify the mechanical performance of the NSM FRP-concrete bonded joint.

In recent years, some authors have experimentally studied the bond behaviour of EBR FRP-concrete joints under sustained loading conditions (Mazzoti *et al.* [130], Ferrier *et al.* [93], Jeong *et al.* [106] and Dash *et al.* [131]). These studies observed that environmental conditions and sustained loading over time had an important effect on the strengthening system's performance. For instance, decreases in the thermomechanical material properties of the bonded joint and strain redistribution along the FRP were observed when elevated temperatures and high sustained loads were applied to EBR FRP-concrete specimens.

On the other hand, only a few studies into the response of NSM FRP concrete elements under different sustained load levels have been carried out. In one such study, Borchert *et al.* [60] analysed NSM FRP-concrete joints under sustained load and different temperatures and proposed a local bond-slip law for the bonded joint that included a friction branch; adopted from the bond-slip law of deformed reinforcing steel bars [132]. Moreover, they proposed a time-dependent bond-slip law (Figure 5.1) where, to consider the long-term effects, the stiffness of the ascending branch, the bond shear strength (τ_{max}) and the residual strength (τ_f) were reduced with time.

Emara *et al.* [73,108], in turn, carried out an experimental study on NSM FRP-concrete elements under sustained loads and different ambient conditions. Their results showed that the combination of high service temperature and high humidity significantly affected the bond behaviour of the joint and so they proposed a damage model for a bilinear bond-slip law, where the stiffness of the ascending branch was reduced with time.

Both models proposed that the softening branch did not vary with time in order to avoid unrealistic increases of fracture energy. Figure 5.1 shows the initial bond-slip laws (black curves) and the time-dependent bond-slip laws (red curves) proposed in Borchert *et al.* [60] (Figure 5.1a) and Emara *et al.* [73] (Figure 5.1b).
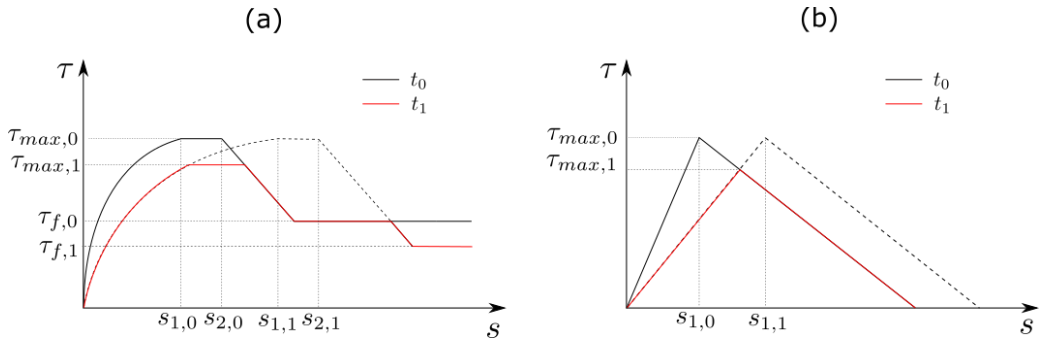
Figure 5.1: Time-dependent bond-slip laws proposed in (a) Borchert *et al.* [60] and (b) Emara *et al.* [73].

It has been widely accepted that the long-term deformations observed in NSM CFRP-concrete joints take place mainly due to the creep performance of the adhesive [73]. Therefore, several studies focussing solely on the creep behaviour of the adhesive under sustained loading and different ambient temperatures can be found in the literature (Costa *et al.* [94–96], Majda *et al.* [85], Meshgin *et al.* [86] and Emara *et al.* [87]). These studies presented the experimental results of tensile tests of resin specimens under sustained loading and concluded that high sustained load levels, together with the ambient conditions and curing times, have an important effect on the thermomechanical properties of the resin. Jeong *et al.* [105,106] and Emara *et al.* [73,87] used the creep coefficient obtained from the long-term adhesive tensile tests to predict the behaviour of FRP-concrete bonded joints under sustained loading. From these studies, higher creep coefficients and strains were observed for specimens under high sustained loading levels and high temperatures and humidity. Moreover, Emara *et al.* [87] observed a linear viscoelastic behaviour of the adhesive up to 60% of the tensile strength under laboratory conditions. On the other hand, Borchert *et al.* [60,133] obtained a creep coefficient from an experimental programme on resin specimens under single shear tests. Results showed a high increase in the resin strain after 1000 hours at 20ºC for specimens under 40% of the maximum load.

From this literature review, it can be concluded that even though the long-term behaviour of adhesives under sustained loading has received considerable attention, there is still a lack of knowledge on the overall behaviour of the NSM CFRP-concrete joints under sustained loading and, therefore, more research work needs to be developed in this field.

This paper aims to contribute to the study of the bond behaviour of Carbon-FRP (CFRP) strips bonded to concrete elements under sustained loading. For this purpose, an experimental

programme consisting of eight NSM CFRP-concrete elements and nine resin specimens under sustained loading and laboratory conditions (20ºC and 55% RH) has been carried out inside a climatic chamber. A previous experimental programme to evaluate the instantaneous behaviour of the bonded joint and the adhesive behaviour is performed through pull-out and tensile tests, respectively. A numerical methodology has been proposed to analytically predict the bond behaviour of the NSM CFRP-concrete joint under sustained loading. The presented methodology proposes a time-dependent bond-slip law that has been calibrated with the experimental results obtained from the NSM CFRP-concrete and resin tests. Finally, the numerical results obtained from the methodology presented here are shown and conclusions are drawn.

5.2 Experimental behaviour of the adhesive

In this section, the tensile behaviour of the adhesive used in the NSM CFRP-concrete joint (Sika 30) is characterized through an instantaneous experimental campaign to obtain the corresponding tensile strength and elastic modulus, and a sustained-loading experimental programme designed to study the adhesive's behaviour under service conditions.

5.2.1 Instantaneous behaviour

To characterize the instantaneous behaviour of the adhesive, six dog-bone resin specimens were cast and cured in accordance with ISO 527-2 [113]. Tensile tests were performed in an MTS Insight 5 kN testing machine at a test speed of 1 mm/min. The instrumentation consisted of one extensometer and two strain gauges placed at both sides of the middle section of the specimen. The test setup and instrumentation are shown in Figure 5.2.
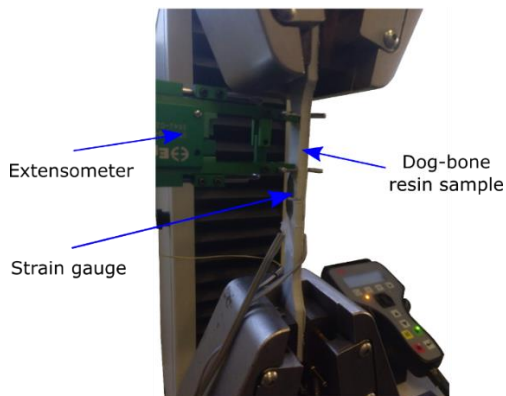
Figure 5.2: Test setup and instrumentation of adhesive tensile tests.

The average tensile strength obtained from the instantaneous tests was 27.2 MPa (with a Standard Deviation, SD = 4.5 MPa) and the average maximum strain was 2770 με (SD = 711 με). The average elastic modulus obtained was 10.7 GPa (SD = 471.4 MPa). The average and enveloping stress-strain curves are presented in Figure 5.3.
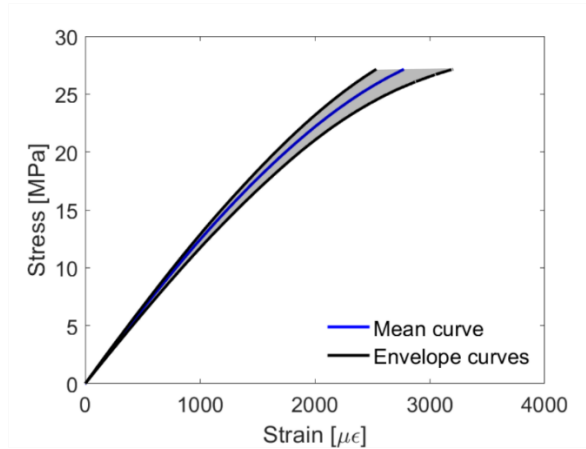
Figure 5.3: Stress-strain curve of the instantaneous adhesive tensile test.

5.2.2 Sustained loading response

5.2.2.1 Test setup

To characterize the behaviour of the adhesive under sustained loading, nine dog-bone resin specimens were cast and cured following ISO 527-2 [113]. Three sustained loading levels were applied: 15%, 30% and 50% of the tensile strength previously obtained in the instantaneous tests. Three specimens were tested for each load level. Tests were performed inside a climatic chamber under 55% RH and 20ºC for 1000 hours.

The experimental setup for the adhesive sustained-loading test is shown in Figure 5.4. The loads were applied using a lever arm with a magnifying factor of 4. Two strain gauges were bonded at each side of the mid-section.

Figure 5.4: Experimental test set-up of the adhesive characterization under sustained loading.

5.2.2.2 Experimental results

Figure 5.5 shows the evolution of the axial strain during time for the three levels of sustained loading. Continuous curves represent the average trends from three different samples, while dashed curves correspond to the maximum and minimum enveloping values.
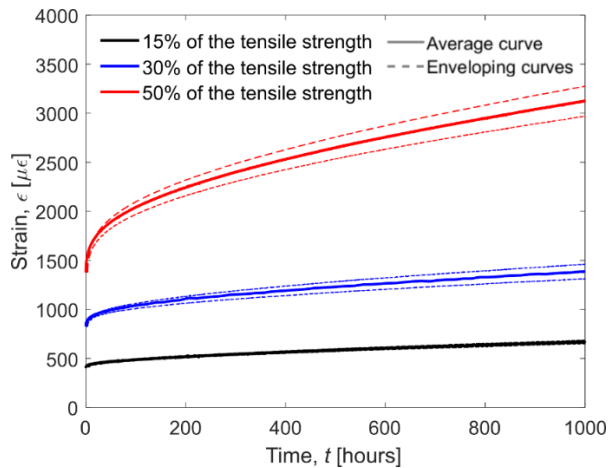
Figure 5.5: Evolution of strain in the resin along time.

Creep behaviour is defined as a continuous increase of strain under a sustained loading and is usually divided into three stages. The first, also called primary stage, is characterized by a high non-linear increase of strains at a decreasing rate. During the second stage, a linear increase of strain is observed. Finally, the third stage is recognised by an increase of strain at a growing rate until failure [84]. In Figure 5.5, two main stages can be identified: the primary stage, where an early high increase of strain can be observed after loading, and the secondary stage, where the

increase of strain follows a more linear trend. As expected, as the sustained loading level increases, the strain in the adhesive becomes greater and increases at a higher rate. Furthermore, the final strain results of specimens loaded at 50% of their tensile strength (3124 $\mu\varepsilon$) are even higher than the ultimate strain obtained from the instantaneous characterization. This phenomenon was also observed by Costa *et al.* [94], who attributed this effect to the fact that during the sustained-loading tensile tests the resin specimens reorganize their internal structure and thus withstanding the load without failing.

The creep compliance $J_c(t)$, defined as the strain caused by a unit of sustained load, determines whether a viscoelastic material behaves in a linear or non-linear manner with respect to the applied stress. It is calculated as:

$$J_C(t) = \frac{\varepsilon(t)}{\sigma_0} \tag{5.1}$$

where $\varepsilon(t)$ is the tensile strain during time and σ_0 is the applied stress. The creep compliance for the different sustained loading levels is presented in Figure 5.6. Specimens under 15% and 30% of the tensile strength show similar curves, meaning that the strain can be considered proportional to the applied load and that the resin specimens presented a linear viscoelastic behaviour for sustained loading levels up to 30%.

On the other hand, the creep compliance curve for specimens under 50% of the tensile strength is higher than that of the other two load levels. This indicates that the behaviour of specimens under a sustained load of 50% is not in the linear viscoelastic stage.

5.2.2.3 Adjustment of a creep function

Figure 5.6 depicts the increment with time of the strain under sustained loading due to creep.
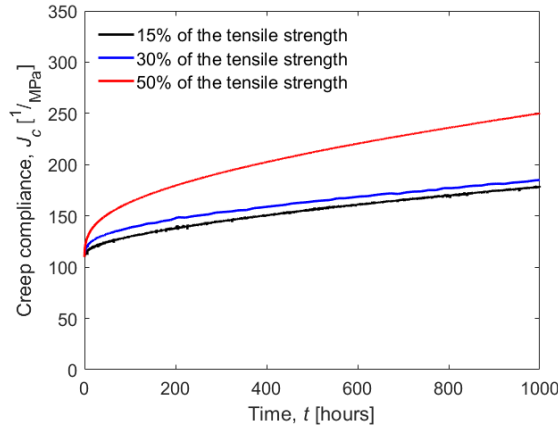
Figure 5.6: Experimental creep compliance curves of the adhesive at 15%, 30% and 50% of the tensile strength.

The creep coefficient was calculated according to Eq. (5.2) for the different load levels,

$$\Phi(t) = \frac{\varepsilon(t) - \varepsilon(t_0)}{\varepsilon(t_0)} \tag{5.2}$$

where $\varepsilon(t)$ is the strain along time and $\varepsilon(t_0)$ is the strain at the loading moment. Since the adhesive behaved in a linear viscoelastic stage for a sustained load up to 30% of the tensile strength, the creep coefficient was calculated from the average values obtained from the specimens loaded at 15% and 30% depending on the time. Its values are presented in Table 5.1.

Table 5.1: Creep coefficient obtained from the sustained loading resin tests.

Time [hours]	1	10	100	1000
$\Phi(t)$	0.04	0.1	0.3	0.7

A power function was adjusted to the experimental creep coefficient values, and has been defined as:

$$\Phi(t) = 0.046 * t^{0.40} \tag{5.3}$$

where t is the elapsed time in hours. This function was adjusted until t = 1000 hours, which was the duration of the test.

5.3 Bond behaviour of NSM CFRP-concrete joint under sustained loading

This section aims to study the NSM CFRP-concrete bonded joint response under sustained loading. First, the instantaneous behaviour of the bonded joint under a monotonic load until failure is characterised through pull-out tests. The maximum load and failure mode are obtained for each bonded joint configuration.

Next, an experimental study of the bonded joint response for 1000 hours at 20ºC and 55% RH is presented. Two different load levels, 15% and 30% of the maximum load, two different groove sizes, 7.5 and 10 mm, and two bonded lengths, 150 and 225 mm, are evaluated.

All specimens were loaded under a pull-out single shear test configuration. The increase of slip, defined as the relative displacement between the CFRP laminate and the concrete block, is presented and discussed. The concrete blocks sizes were 200 mm × 200 mm × 300 mm for the short-bonded lengths (L_b = 150 mm) and 200 mm × 200 mm × 370 mm for the long-bonded lengths (L_b = 225 mm and 300 mm).

5.3.1 Material properties

All specimens were cast from the same concrete batch. Concrete compressive strength and elastic modulus were characterized following ASTM C469 / C469M-10 [115] and UNE 12390-3 [116] standards, obtaining a result of 33.0 MPa (3 specimens, SD = 1.8 MPa) and 33.1 GPa (3 specimens, SD = 1.6 GPa) respectively.

CFRP Sika CarboDur S NSM 1030 strips of 10 mm × 3 mm were used. Six CFRP specimens were characterized according the ISO 527-5 standard [114], obtaining a tensile strength of 3.2 GPa (SD = 68.3 MPa) and an elastic modulus of 169.3 GPa (SD = 13.1 MPa).

The Sika 30 bi-component epoxy resin (previously characterized in Section 5.2) was used as the adhesive in this experimental campaign.

5.3.2 Instantaneous bond behaviour of the NSM CFRP-concrete joint

5.3.2.1 Experimental parameters

To study the short-term behaviour of NSM CFRP-concrete joints, specimens combining two bonded lengths (L_b), 150 mm and 225 mm, and two groove thicknesses (t_g), 7.5 mm and 10 mm, were tested until failure. This section presents an extension of the experimental campaign

presented in Gómez *et al.* [134]. Four specimens were tested for each pull-out configuration. To further study the effect of the bonded length, two additional NSM CFRP-concrete specimens with L_b = 300 mm and t_g = 10 mm were also tested. As such, a total of 18 specimens were tested under monotonic loading. Each specimen was labelled ST-L_b-t_g, where ST stands for Short-Term test, L_b for bonded length in mm, and t_g the groove thickness in mm.

The ACI 440.2R [48] proposes that groove thickness should be equal to or greater than three times the laminate thickness. That said, *fib* Bulletin 90 [50] establishes a minimum groove dimension of 1.5 or 2 times the laminate size to avoid epoxy cover splitting. To study the effect the thickness of the adhesive, two groove thicknesses were used in the experimental programme: 7.5 mm and 10 mm. Taking into account that the laminate thickness is 3.0 mm, the 7.5 mm groove thickness was set to satisfy the requirement of the *fib*, whilst the 10 mm groove thickness was selected to meet the ACI 440.2R requirements. Therefore, two adhesive thicknesses were studied: 3.5 mm for the 10 mm grooved specimens, and 2.25 mm for the 7.5 mm grooved specimens. The groove height was set to 15 mm for all cases to comply with the ACI 440.2R and *fib* requirements of 1.5 times the height of the NSM strip.

Several experimental studies examining the effect of the bonded length and the laminate size [23,35,46,67] have been carried out and concluded that the minimum bonded length to achieve the maximum capacity of the bonded joint for laminate sizes similar to those used in this experimental programme ranges between 150 mm and 250 mm. Therefore, the bonded lengths used in the experimental campaign were chosen to be lower and upper bond values of those suggested in the literature.

5.3.2.2   Test setup

Tests were carried out under a pull-out single shear configuration. The short-term setup used in the monotonic tests and a schematic drawing of the setup are shown in Figure 5.7a and Figure 5.7b, respectively.
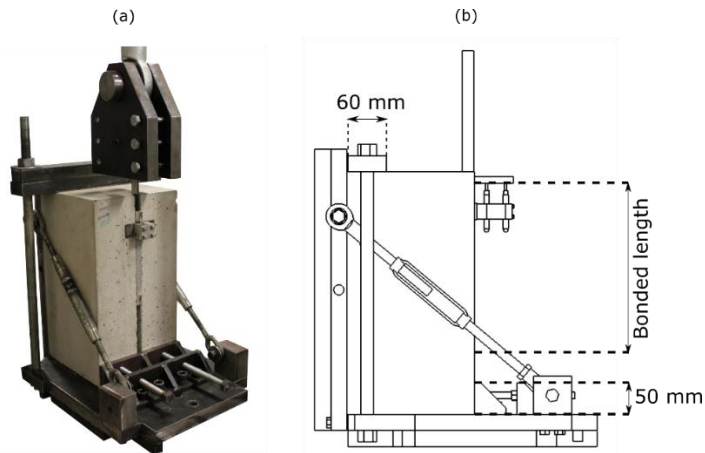
Figure 5.7: (a) Set-up of the pull-out single shear test and (b) scheme of the set-up.

The top surface of the concrete block was clamped with a 60 mm-wide steel reaction element [26]. To avoid premature failure, the concrete blocks were internally reinforced with four 10 mm in diameter steel bars.

5.3.2.3   Instrumentation

The instrumentation used in the monotonic pull-out tests consisted of one LVDT placed at the loaded end to capture the relative displacement between the CFRP strip and the concrete element.

Additionally, a Digital Image Correlation (DIC) system was installed to register the displacement and strain field of the front surface of the bonded joint during the test. The DIC system has been proven to be an effective tool for measuring displacements and strains in concrete elements [121,123,135]. A 2D system, consisting of a single camera, was placed perpendicular to the surface of interest to capture the in-plane displacements. Speckle patterns were applied to the samples' front surfaces. Correlation software was used to track all points of the defined surface to obtain the corresponding displacement and strain field. The camera used had a diaphragm aperture of f/5.6, and the closing of the diaphragm was 1.000 μsec. The image acquisition frequency used in the test was 1 image/second and the camera's recording resolution was 2452 × 2056 pixels and focal length 23 mm, thus obtaining a conversion factor of 0.114 mm/pixel in the area of interest. A subset of 21 pixels, a step size of 5 pixels, and a Zero-Normalized Cross-Correlation (ZNCC) criteria were used for correlating the images.

5.3.2.4   Experimental results

The load-slip curves obtained from the short-term tests are shown in Figure 5.8, and the average maximum load and failure mode obtained for each NSM CFRP-concrete specimen configuration are presented in Table 5.2.
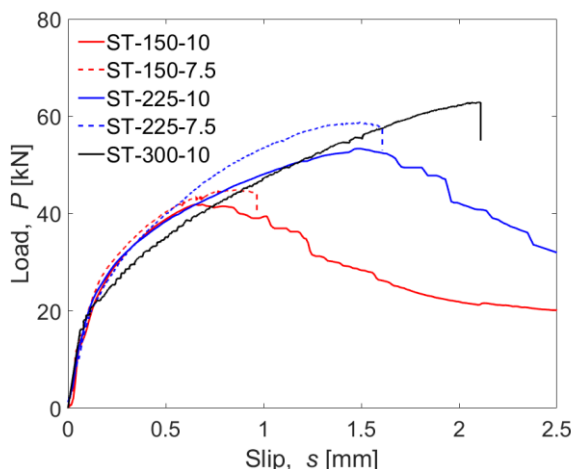
Figure 5.8: Experimental average load-slip curves for the short-term pull-out tests.

Table 5.2: Experimental results of the short-term pull-out tests.

Nomenclature	L_b [mm]	t_g [mm]	Maximum load [kN]	Failure mode
ST-150-10	150	10	41.9	F-A
ST-150-7.5	150	7.5	45.1	C
ST-225-10	225	10	53.3	F-A
ST-225-7.5	225	7.5	58.6	C
ST-300-10	300	10	62.8	F-A

Note: F-A = FRP-adhesive interface, C = cohesive failure in the concrete.

It can be observed that for relatively low load levels, while all the specimens followed the same initial trend, differences in the maximum load were obtained. The maximum load increased with the bonded length. It is worth noting that for the 10 mm grooved specimens, the increase in maximum load between specimens with L_b = 150 and 225 mm (ST-150-10 and ST-225-10, respectively) was 27.3%, while the increase between specimens with L_b = 225 and 300 mm (ST-225-10 and ST-300-10, respectively) was 17.7%, indicating that, even though the

maximum load increases with the bonded length, this increment is not proportional to the bonded length.

On the other hand, for the same bonded length, specimens with a groove thickness of 10 mm generally achieved a lower maximum load than the 7.5 mm grooved specimens. Additionally, the failure mode was different: 10 mm grooved specimens showed a failure in the FRP-adhesive interface (Figure 5.9a), while 7.5 mm grooved specimens presented a cohesive failure in the concrete (Figure 5.9b).
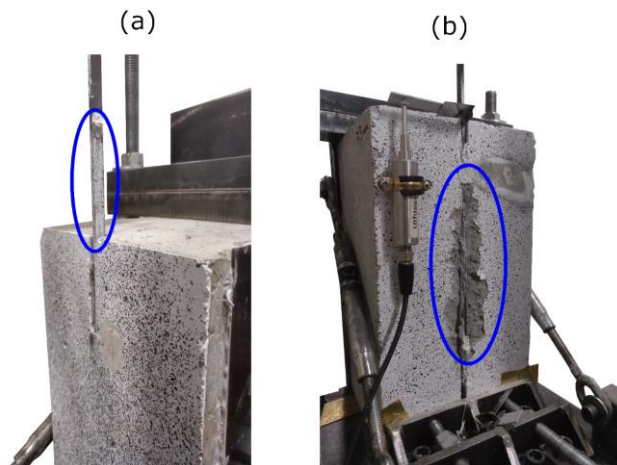
Figure 5.9: (a) Failure in the FRP-adhesive interface and (b) cohesive failure in the concrete.

This behaviour could be attributed to the different shear stiffness ($G_a \times t_a$, where G_a is the shear modulus of the adhesive and t_a is the adhesive thickness) of the adhesive, which would be higher for the 10 mm grooved specimens and therefore the strain transmitted to the concrete would be lower than in 7.5 mm grooved specimens.

To better understand the differences between the failure modes of the 10 mm and 7.5 mm grooved specimens, Figure 5.10a and Figure 5.10b present the strain fields in the vertical direction at the maximum load obtained with the DIC 2D system, for an ST-225-10 specimen and an ST-225-7.5 specimen, respectively. In Figure 5.10, red lines represent the groove position, and positive values of strain refer to compressive stresses, while negative values indicate tensile stresses.
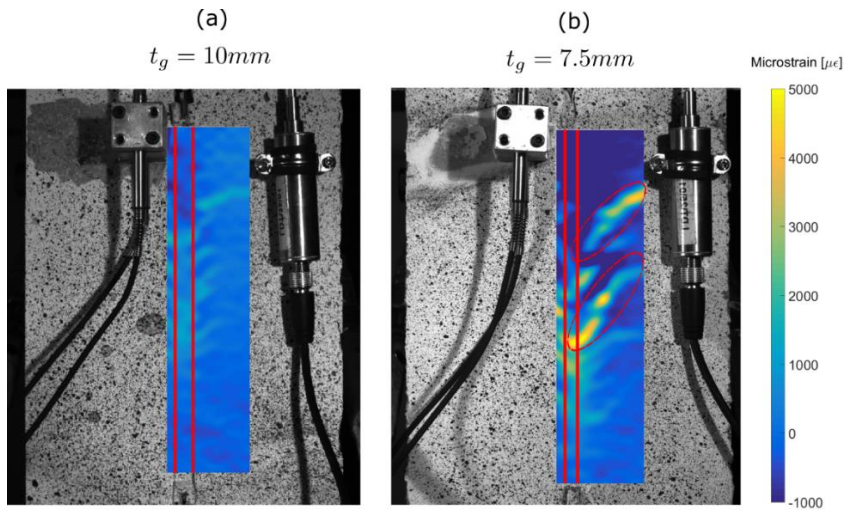
Figure 5.10: Strain field in the vertical direction measured by the DIC 2D system for (a) a 10 mm grooved specimen and (b) a 7.5 mm grooved specimen.

It can be observed that a maximum strain value of 2000 $\mu\varepsilon$ and 4500 $\mu\varepsilon$ was obtained in the concrete surface for the 10 mm and 7.5 mm grooved specimens, respectively. This indicates that, probably, the 7.5 mm grooved specimens achieved their maximum concrete compressive capacity, whilst in the 10 mm grooved samples, the maximum compressive strain of concrete was not achieved.

After the maximum load was achieved, in the 10 mm grooved specimens, because of the residual friction between the FRP and the adhesive, the bonded joint withstood a residual load that smoothly decreased as the slip between the FRP and the concrete increased. This behaviour was not observed in the 7.5 mm grooved specimens, which failed suddenly. Specimens with L_b = 300 mm and t_g = 10 mm also failed by the FRP-adhesive interface, but this time small cracks started to appear in the concrete surrounding the groove, indicating that the compressive stress carried out by the concrete was probably close to the compressive strength.

5.3.3 Sustained loading response of NSM CFRP-concrete specimens

Eight specimens were tested under a pull-out single shear test configuration, in laboratory conditions and under sustained loading for 1000 hours. NSM CFRP-concrete specimens combined two bonded lengths, 150 mm and 225 mm, two groove thicknesses, 7.5 mm and 10

mm and two levels of sustained load, 15% and 30% of the maximum load obtained from the short-term tests.

5.3.3.1 Test setup and instrumentation

Figure 5.11a shows the setup used in the sustained-loading tests while Figure 5.11b shows a schematic drawing of the setup. The setup used was an adaptation of the short-term setup, with a lever arm with a multiplying factor of 8.3.

(a)   (b)
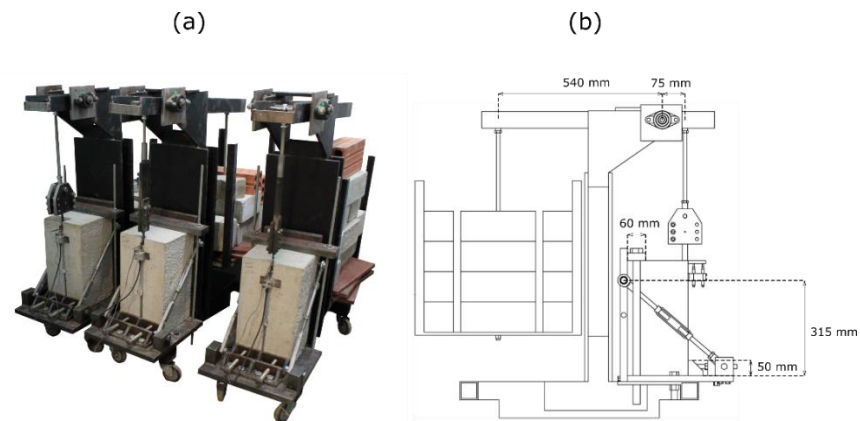
Figure 5.11: (a) Image of the set-up for the sustained-loading pull-out test and (b) scheme of the set-up.

The instrumentation for each specimen consisted of one LVDT placed at the loaded end to capture the slip between the FRP and the concrete and one strain gauge placed at the unbonded loaded end of the laminate to measure the FRP strain either during the loading process or along the testing period.

5.3.3.2 Experimental parameters

Table 5.3 summarizes the characteristics and loads for the specimens. Each specimen was labelled LT-L_b-t_g-%P_u, where LT stands for Long-Term and the rest of parameters are the same as those previously defined in Section 5.3.2.1.

Table 5.3: NSM CFRP-concrete specimens tested under sustained loading.

Nomenclature	L_b [mm]	t_g [mm]	Applied load [kN]	% P_u experimental
LT-150-10-15	150	10	6.4	14.6
LT-150-7.5-15	150	7.5	6.5	13.8
LT-150-10-30	150	10	12.8	29.3
LT-150-7.5-30	150	7.5	14.1	30.0
LT-225-10-15	225	10	8.2	14.9
LT-225-7.5-15	225	7.5	8.9	15.5
LT-225-10-30	225	10	15.2	27.8
LT-225-7.5-30	225	7.5	17.5	30.3

It is worth noting that, even though the load levels applied to the specimens were the same for the 7.5 mm and 10 mm grooved specimens, the maximum load (P_u) for both groove thicknesses was different. Therefore, the load corresponding to 15% or 30% of P_u was different for specimens with different groove thicknesses.

5.3.3.3   Experimental results

Figure 5.12a presents the evolution of slip and Figure 5.12b the increase of slip with time for all the NSM CFRP-concrete specimens. Continuous curves represent the 10 mm grooved specimens, and dashed lines the 7.5 mm grooved specimens.
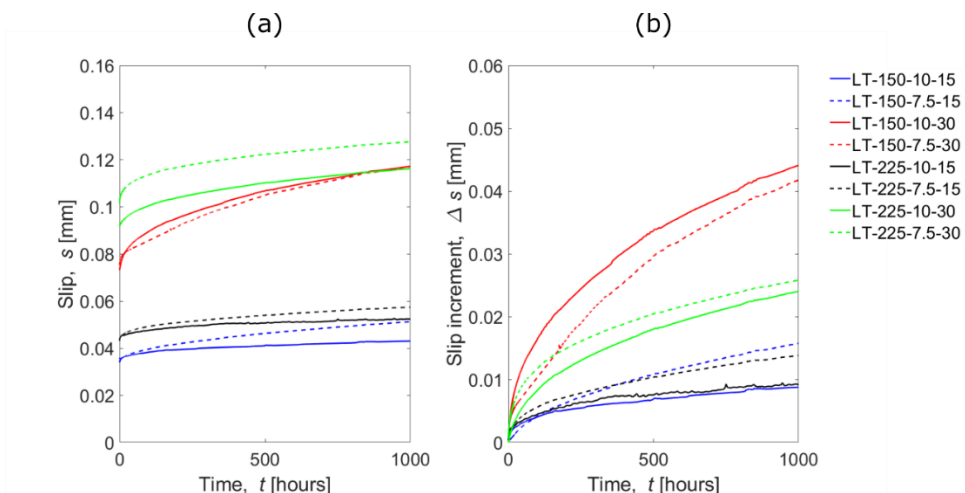
Figure 5.12: (a) Total slip at the loaded end and (b) increment of slip with time.

Overall, two main stages in the behaviour of the bonded joints can be identified; a first stage with a high increase of slip with time, and a second stage where the increase of slip becomes more linear [73]. As expected, the specimens loaded at 30% of P_u experienced higher slips than those loaded at 15% of P_u.

Focusing on Figure 5.12b, short-bonded length specimens under 30% P_u (red curves) experienced a higher increase of slip with time than their long-bonded length counterparts (green curves) despite being subjected to similar load levels (%P_u). This high increase of slip could be attributed to the fact that the short-bonded length specimens developed a higher average bond shear stress along the FRP, causing more damage to the bonded joint. On the other hand, it can be observed that for a sustained loading level of 15% P_u, the specimens present very similar increases of slip regardless of their bonded length.

Regarding the effect of the groove thickness, similar increases of slip at the loaded end were obtained for specimens with equal bonded lengths and sustained load levels. In general, the 7.5 mm grooved specimens experienced a higher increase of slip, caused by the fact that they were loaded at higher loads, than their 10 mm counterparts. However, the LT-150-10-30 specimen obtained a higher increment of slip than LT-150-7.5-30, showing a change in the previous tendency for wider adhesive layers in combination with shorter bonded lengths.

5.4 Numerical methodology to calculate the NSM CFRP-concrete joint response under sustained loading

5.4.1 Instantaneous bond behaviour of the NSM CFRP-concrete specimens

Based on the short-term bond-slip response, the parameters of idealized typical bilinear bond-slip laws were adjusted using the experimental bond-slip response results [134]. The resulting laws are reproduced in Figure 5.13.
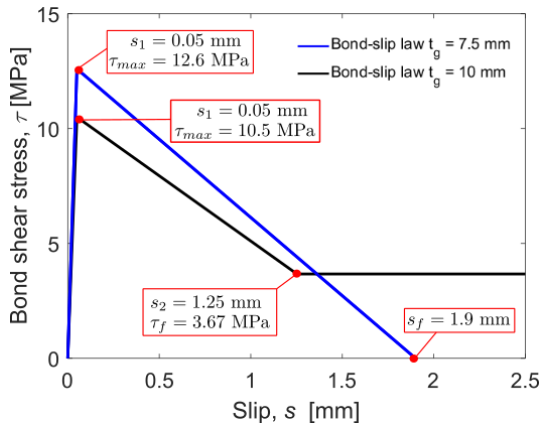
Figure 5.13: Bond-slip laws obtained from the experimental monotonic tests.

For the 7.5 mm grooved specimens (with an adhesive layer of 2.25 mm), a bilinear bond-slip law was considered, since a rather sudden failure was obtained once the maximum load was attained. However, for the 10 mm grooved specimens (with an adhesive layer of 3.5 mm), a bilinear bond-slip law including a friction stage was considered to take into account the residual load stage observed during the failure.

As observed in Figure 5.13, in comparison with 10 mm grooved specimens, the adjusted bond shear strength (τ_{max}) was higher for specimens with 7.5 mm groove thickness and which is justified by the higher maximum load experimentally obtained.

Figure 5.14 presents the theoretical load-slip curves (dashed lines) obtained from a numerical integration procedure, (considering the local bond-slip laws presented in Figure 5.13), in comparison with the experimental results (continuous lines) obtained from the pull-out short-term tests. A general good agreement between the numerical and experimental data can be observed.
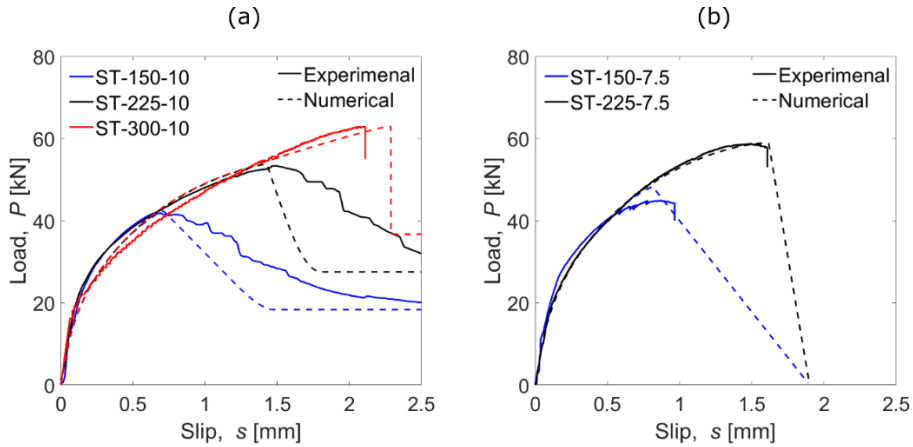
Figure 5.14: Comparison of experimental and numerical results for (a) 10 mm grooved specimens and (b) 7.5 mm grooved specimens.

5.4.2 Numerical prediction of the bond behaviour under sustained loading

5.4.2.1 Numerical procedure

The proposed numerical procedure is based on a Finite Differences Model (FDM) and departs from the numerical methodology previously developed for instantaneous bond-slip behaviour.

The methodology divides the bonded length of the FRP-concrete joint into small increments of length, Δx, so as the position, x, of all points at which the equilibrium equations will be assessed is defined. Starting from the loaded end and moving towards the free end, the procedure calculates, for each studied point and for a certain load level, the slip and the load transmitted by Δx taking into account the degradation of the bond-slip law with time (see Section 5.4.2.2 for further details).

The differential equation governing the bond–slip behaviour of an NSM FRP-to-concrete bonded joint is [74,75]:

$$\frac{d^2 s(x)}{dx^2} - \frac{\tau(s) * L_{per}}{E_f * A_f} = 0 \qquad (5.4)$$

where E_f is the FRP modulus of elasticity, A_f is the FRP cross-section, $\tau(s)$ is the local bond-slip law of the joint and L_{per} is the intermediate perimeter of the adhesive layer [73], calculated using Eq. 5.5,

$$L_{per} = 2 * (b_f + t_a) + (t_f + t_a) \qquad (5.5)$$

where b_f is the strip width, t_f is the strip thickness and t_a is the adhesive thickness.

111

Initially the process defines a load and a slip at the loaded end, which is then used to calculate the strain in the FRP (ε_f), the strain in the concrete (ε_c) and the bond shear stress (τ) using the bond-slip law. The load P at every section along the FRP can be calculated as:

$$P(j,i) = P(j,i-1) - \tau(j,i-1) * L_{per} * \Delta x \qquad (5.6)$$

In Eq. 5.6, the subscript "i" indicates the current point being studied, and the subscript "i-1" refers to the previous studied point, towards the loaded end. Subscript "j" indicates the iteration for a time t. $P(j,1)$ is the sustained load applied to the bonded joint. From the load profile obtained, the strain distribution in the concrete and the FRP can be calculated. Then, the slip profile is calculated as:

$$s(j,i) = s(j,i-1) - (\varepsilon_f - \varepsilon_c) * \Delta x \qquad (5.7)$$

The convergence condition is that ε_f at the free end must be less than a minimum tolerance, set to be a value close to zero. Otherwise, a new iteration is needed; an increment of slip at the loaded end is added and the process is repeated until the convergence criterion is achieved. Once the equilibrium at time t_i is achieved, the next time step is analysed and the time-dependent bond-slip law is modified. As the numerical procedure is designed for a sustained-load test, the load in the loaded end is kept the same as in the previous step.

The numerical procedure is illustrated in Figure 5.15. The red dashed rectangular area indicates the procedure for the instantaneous behaviour, while the steps outside this area refer to the time-dependent degradation of the bond-slip response.
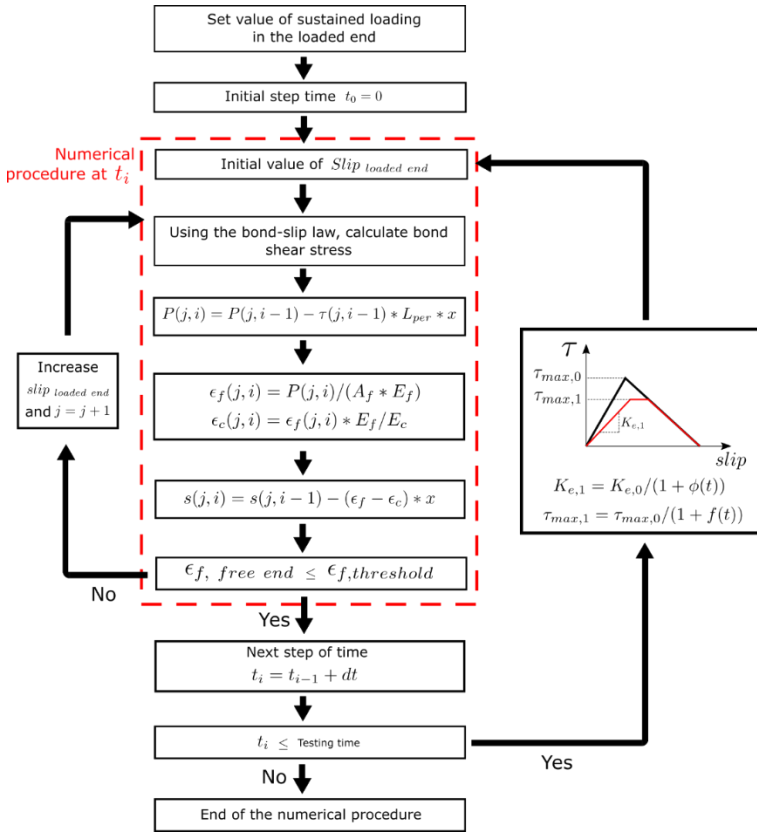
Figure 5.15: Flowchart of the numerical procedure.

5.4.2.2   Proposed time-dependent bond-slip law

As observed in the experimental results, the NSM CFRP-concrete joint experiences an increment of slip with time under sustained loading. In this work, this effect is attributed to a reduction in time-dependent effective stiffness ($K_e(t)$) and bond shear strength ($\tau_{max}(t)$), which are defined similarly as in [60,73]. To avoid an unrealistic increase of fracture energy, the softening branch of the proposed time-dependent bond-slip law is maintained as the softening branch at t_0 [136]. Figure 5.16 shows the approximate shapes for the resultant time-dependent bilinear (Figure 5.16a) and bilinear plus friction (Figure 5.16b) bond-slip laws, where $s_{1,0}$ is the initial slip at the bond shear strength τ_{max}, and $s_{1,1}$ is the slip at the bond shear stress at t_1. Black and red curves represent the bond-slip laws at t_0 and t_1, respectively.
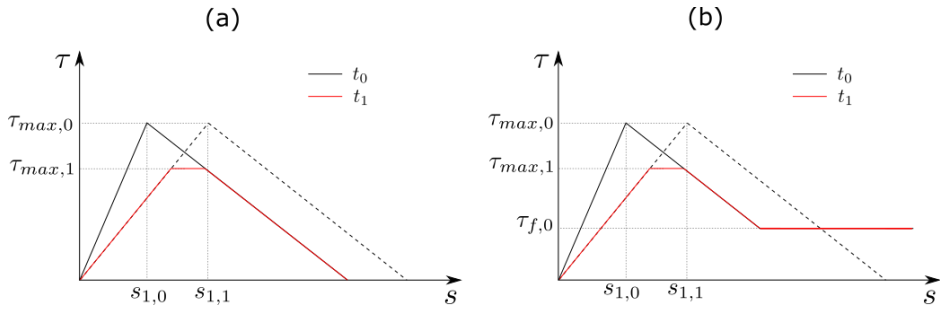
Figure 5.16: Time-dependent bond-slip models: (a) a bilinear model and (b) a bilinear plus friction model.

The proposed model is governed by two parameters: a creep coefficient $\Phi(t)$ that reduces the effective stiffness, and a strength reduction coefficient ($f(t)$) that reduces the bond shear strength.

The reduction of the stiffness of the ascending branch of the bond-slip law is carried out by using the Effective Modulus Method (EMM), as follows:

$$K_e(t) = \frac{K_{e,0}}{(1 + \Phi(t))}$$

(5.8)

where $K_e(t)$ is the time-dependent stiffness at time t and $K_{e,0}$ is the initial stiffness. As the stiffness of the bond-slip law is mainly dependent on the adhesive creep behaviour, the creep coefficient $\Phi(t)$ has been determined from the resin tests under sustained loading.

On the other hand, the bond shear strength $\tau_{max}(t)$ is reduced with time as:

$$\tau_{max}(t) = \tau_{max,0} \cdot a(t)$$

(5.9)

where $\tau_{max,0}$ is the initial bond strength at loading, and $a(t)$ is defined as:

$$a(t) = \frac{1}{1 + f(t)}$$

(5.10)

with $f(t)$ being a strength reduction coefficient. The coefficient $f(t)$ is obtained from the experimental results and it is shown in Figure 5.17 for specimens under 30% of P_u.
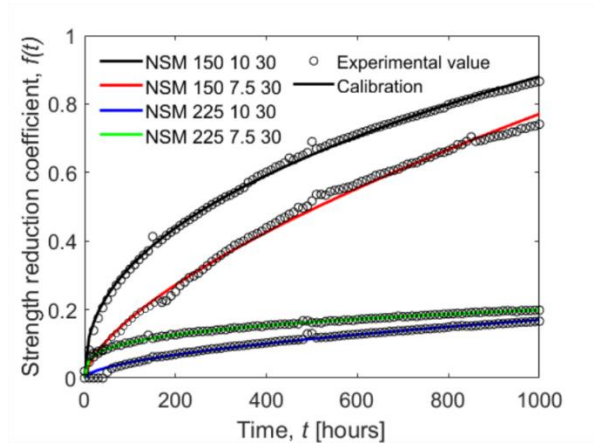
Figure 5.17: Strength reduction coefficient evolution with time for each specimen.

The shape of these curves can be described by a power function as follows:

$$f(t) = \alpha \cdot t^{\beta} \tag{5.11}$$

where t is the elapsed time in the sustained loading test in hours, α is a scaling factor and β is a parameter that controls the rate of growth of the function.

5.4.2.3 Calibration of the strength reduction factor parameters α and β

The calibration of parameters α and β has been performed by means of the least-square differences method and the obtained $f(t)$ coefficient is shown in Figure 5.17 in continuous lines. The resultant time-dependent bond-slip law is presented in Figure 5.18 for specimens LT-150-7.5 loaded at 30% (Figure 5.18a) and 15% (Figure 5.18b) at different time steps (0, 250, 500, 750 and 1000 hours).
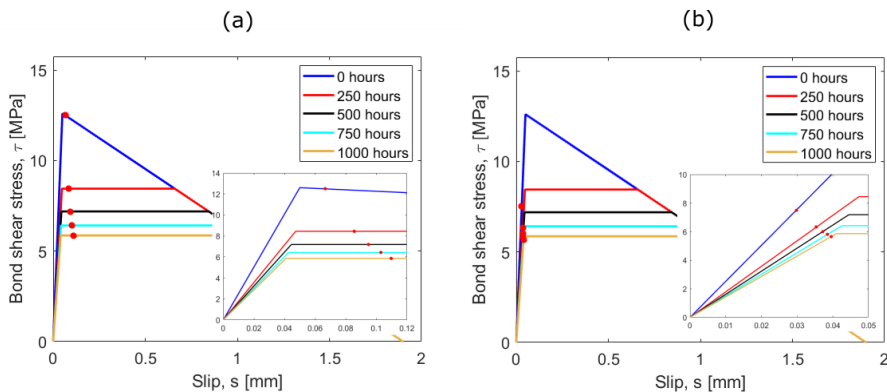
Figure 5.18: Evolution of the local bond-slip law with time for (a) LT-150-7.5-30 and (b) LT-150-7.5-15 specimens.

A red dot indicates the stress-slip situation of the loaded end. For specimens under 30% of P_u, the loaded end has already surpassed the point of τ_{max} at $t = 0$ h (Figure 5.18a). However, for specimens loaded at 15% of P_u, the strength reduction does not affect the overall time-dependent behaviour because the loaded end did not reach the maximum bond shear strength τ_{max}, as is observed in Figure 5.18b. This effect was noticed in all specimens loaded at 15% P_u. Since the values obtained for β ranged between 0.35 and 0.55, for the sake of simplicity an average value of 0.45 is adopted. With this simplification, a comparison between the numerical and experimental values of the slip at the loaded end is shown in Figure 5.19. Continuous and dashed lines represent the experimental and numerical values, respectively. A general good agreement can be observed between the experimental data and the numerical predictions.
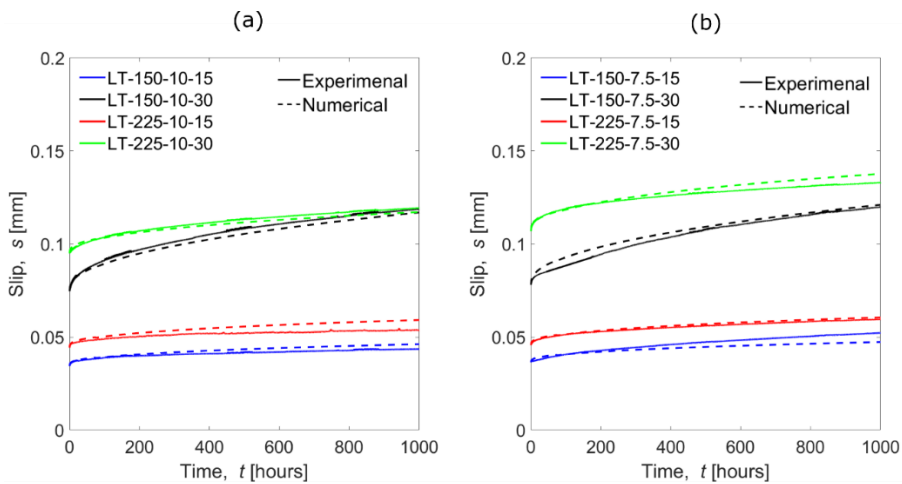
Figure 5.19: Comparison of the experimental and numerical slip at the loaded end (a) for 10 mm grooved specimens and (b) for 7.5 mm grooved specimens obtained in the present study.

5.4.2.4 Application of the numerical methodology to other experimental studies

In this section, the proposed methodology is extended to predicting the experimental results presented in [73], which was focused on the effect groove thickness, bonded length and sustained loading level have on the behaviour of NSM CFRP concrete specimens under sustained loading and room conditions. In that study, a different epoxy adhesive type (E_a = 6600 MPa, f_{ta} = 20 MPa), CFRP material (E_f = 160 GPa, f_{fe} = 2400 MPa) with a different section (10 mm × 1.4 mm), groove thicknesses (5 mm and 10 mm), bonded lengths (60 mm, 90 mm and 120 mm) and

sustained load levels (25% and 50% of P_u), were used. Specimens were labelled L-S-G, where L stands for the bonded length, S the sustained load level and G the groove thickness.

Values of the parameter α are obtained (as indicated in the previous section) considering $\beta = 0.45$, and the resultant theoretical evolution of slip with time is shown in Figure 5.20, together with the experimental values.
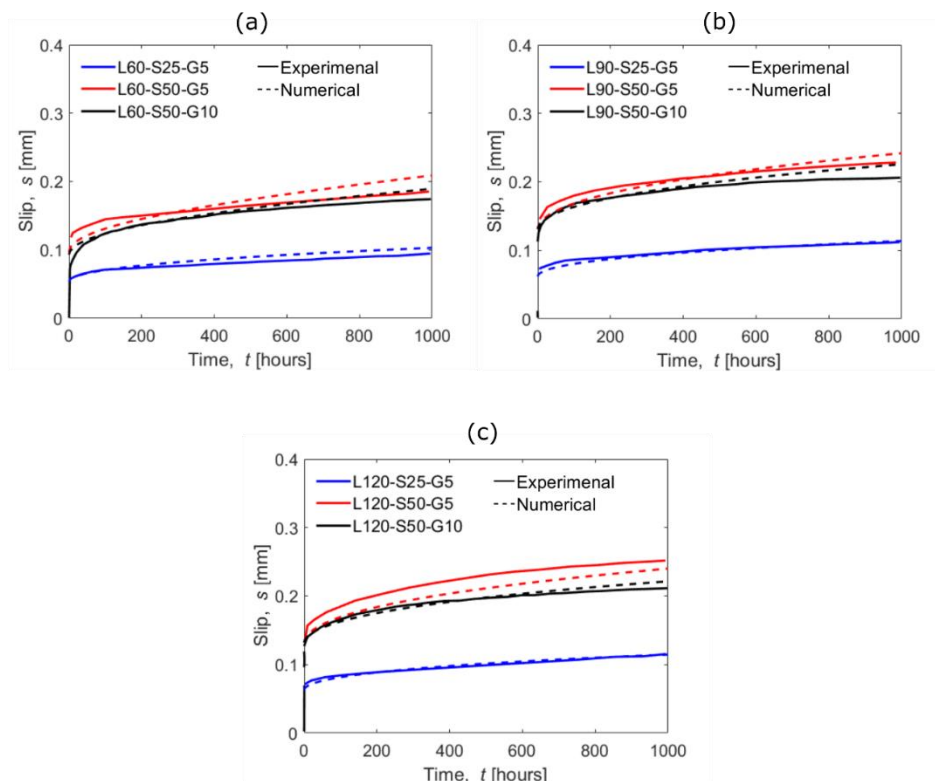
Figure 5.20: Comparison between the numerical and experimental values for specimens with (a) $L_b = 60$ mm, (b) $L_b = 90$ mm and (c) $L_b = 120$ mm obtained in [73].

Since the strength reduction coefficient is dependent on the applied load, the average bond shear stress (τ_{avg}) is taken as a reference variable:

$$\tau_{avg} = \frac{P}{L_b \cdot L_{per}}$$
(5.12)

and compared to the previously obtained parameter α (Table 5.4). As expected, a general increasing trend of α with the increase of τ_{avg} is observed, although two ranges of τ_{avg} can be identified, each one for the two different experimental campaigns.

Table 5.4: Values of α and τ_{avg} obtained considering $\beta = 0.45$.

Specimen	$\alpha \times 100$	τ_{avg} [MPa]
LT-L150-t10-P30	3.9	2.7
LT-L150-t7.5-P30	3.2	3.2
LT-L225-t10-P30	0.7	2.3
LT-L225-t7.5-P30	0.9	2.5
L60-S50-G5	6.0	6.5
L60-S50-G10	5.5	6.0
L90-S50-G5	4.0	5.4
L90-S50-G10	3.0	5.0
L120-S50-G5	4.0	4.1
L120-S50-G10	2.5	3.7

In order to propose a model suitable to be extrapolated to other results, a non-dimensional parameter τ_{avg}/τ_{max} is defined. In Figure 5.21, the relationship between α and τ_{avg}/τ_{max} is shown.
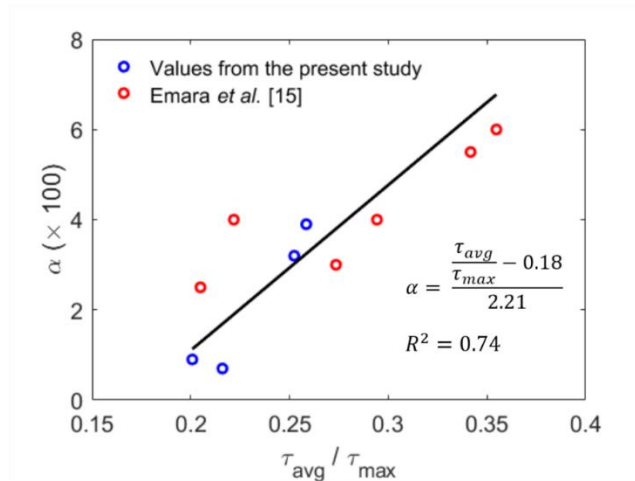
Figure 5.21: Relationship between α - τ_{avg}/τ_{max}.

Regardless of the scatter of the data, an ascending tendency can be observed, meaning that as the average shear stress in the bonded joint increases α, and consequently the strength reduction coefficient, increase as well, causing a higher reduction on the time-dependent bond strength. Even though a relationship between α and τ_{avg}/τ_{max} has been observed in this study, as it was based on a limited number of specimens, more experimental tests should be carried out to further assess this relationship. Finally, it should be mentioned that due to the nature of

118

the pull-out single shear configuration test, the possible effect of cracking is not directly included in the tests. Cracking in beams is a phenomenon taking place at relatively low loads and crack spacing tends to decrease as the load increases. For considering cracking effect, new series of tests with different bonded lengths should be carried out to compare the influence on the response.

5.5 Conclusions

This work aimed to study the behaviour of NSM CFRP-concrete bonded joints under sustained loading and laboratory conditions. Pull-out and dog-bone adhesive specimens were subjected to sustained loading for 1000 hours. A numerical procedure based on FDM to predict the bond behaviour under sustained loading based on a time-dependent local bond-slip was proposed and validated. Based on the analysis of the experimental results and corresponding range of parameters presented in this work the following conclusions are drawn.

From the adhesive specimens tested under tensile sustained loading, it can be concluded that:

- Adhesive specimens loaded up to 30% of P_u were under a linear creep stage, meaning that the creep behaviour did not depend on the applied load.
- A creep coefficient was adjusted with a power function from specimens loaded at 15% and 30% of P_u.

From the sustained loading tests of the NSM CFRP-concrete specimens, the following conclusions can be drawn:

- As expected, specimens under 30% of P_u experienced a higher increase of slip in comparison to specimens under 15% of P_u.
- Short-bonded length specimens under 30% of P_u experienced a higher increase of slip than long-bonded length specimens. However, no effect of the bonded length was observed in specimens under 15% of P_u.

From the proposed numerical procedure with which to model the NSM CFRP-concrete joint bond response under sustained loading, it can be concluded that:

- A time-dependent bond slip law based on a strength reduction factor and a creep coefficient is proposed to predict the behaviour of the bonded joint.
- The strength reduction factor was adjusted through a power function defined by two parameters: α and β. While parameter β could be experimentally adjusted to a mean

value of 0.45, an increasing relationship between the average bond stress normalized with the bond shear strength, τ_{avg}/τ_{max}, and parameter α was able to be identified.

- Specimens under 15% of P_u were not affected by the strength reduction factor. In these cases, the time-dependent behaviour was only governed by the creep coefficient.

- Further experimental tests at service loading levels are needed to better explore the relationship between τ_{avg}/τ_{max} and α.

The experimental series carried out and the corresponding selected range of parameters allowed the conclusions above to be reached. However, further research is needed to expand the number of tests and parameters.

6 Paper C: The effect of steady and cyclic environmental conditions on the tensile behaviour of a structural adhesive under sustained loading

Javier Gómez[1], Cristina Barris[1]*, Younes Jahani[1], Marta Baena[1] and Lluís Torres[1]

[1]AMADE, Polytechnic School, University of Girona, 17003, Girona, Spain

*Corresponding author

The effect of steady and cyclic environmental conditions on the tensile behaviour of a structural adhesive under sustained loading

Javier Gómez[1], Cristina Barris[1,*], Younes Jahani.[1], Marta Baena[1] and Lluís Torres[1]

[1] AMADE, Polytechnic School, University of Girona, 17003 Girona, Spain

[*] Corresponding author, cristina.barris@udg.edu

Abstract

Structural adhesives are commonly used to bond Fibre Reinforced Polymer (FRP) materials to Reinforced Concrete (RC) structures so they can withstand service conditions. This paper presents an experimental study on the combined effect of sustained loading and service steady and cyclic temperatures on the thermophysical and mechanical properties of an epoxy adhesive.

Four experimental series consisting of nine adhesive tensile dog-bone specimens were tested under sustained loading and temperatures ranging between 18°C and 43°C for a duration of 1000 hours. Moreover, the residual properties of the adhesive have been evaluated through instantaneous tensile tests and Differential Scanning Calorimetry (DSC) after sustained loading tests.

Results showed a significant increase in strain with time, a reduction in the mechanical properties, and an increase in the glass transition temperature and curing degree of the adhesive after the exposure at service conditions and sustained loading.

From this work it could be concluded that the combination of sustained loading and service temperatures have a significant effect on the creep behaviour of the adhesive, and cyclic temperatures have a greater effect on the adhesive even though the average temperature is below the steady temperature.

Keywords: Epoxy adhesive, Creep behaviour, High-temperature properties, Thermal analysis, Mechanical testing.

6.1 Introduction

The use of adhesives in civil structures is an excellent solution to bond Fibre Reinforced-Polymers (FRP) to concrete elements [17,137–139]. Externally Bonded Reinforcement (EBR) [25,44,70,74] and Near Surface-Mounted (NSM) [21–23,76] have become the most prevalent strengthening techniques in this field. In both cases, cold-curing adhesives are the most widely used bonding agents thanks to their ease of use and good mechanical properties after a short curing time. Because the role that structural adhesives play is essential for the adequacy and durability of a concrete-FRP joint, their mechanical properties and effect on the behaviour of bonded joints has been widely studied [30,93,140–143]. These studies concluded that the properties of an adhesive directly affect the load carrying capacity and failure mode of the bonded joint.

In real service conditions, along with sustained loading, structural adhesives can be subjected to harmful environmental conditions, which can change their mechanical properties and the durability of the concrete-FRP joint. Therefore, it is extremely important to study how these external actions change the behaviour of structural adhesives. To investigate the mechanical behaviour of a structural adhesive under different environmental conditions, Emara *et al.* [87] performed an experimental programme combining service temperatures, degrees of humidity and sustained loading levels. Their study concluded that the combination of high service temperature and sustained loading had an important effect on the tensile creep behaviour of the adhesive, whereas relative humidity had a lower effect on the adhesive's performance. Ferrier *et al.* [93], in turn, found that the service temperature of the adhesive should be around 15°C lower than the glass transition temperature (T_g) in order to avoid significant creep effects. Other studies have focussed on the mechanical and physical properties of structural adhesives after exposure to different environmental conditions. Hence, Silva *et al.* [92,97] carried out an experimental programme on dog-bone tensile tests of adhesive specimens after exposing them to different environmental conditions during 120, 240 and 480 days. Their study concluded that specimens exposed to water with chlorides and freeze-thaw cycles experienced a decrease in the T_g, while specimens under thermal cycles experienced an increase in the tensile strength, elastic modulus and T_g, caused by the post-curing effect of the resin. The post-curing effect on structural adhesives due to environmental conditions was also investigated by Moussa *et al.* [144,145]. In their studies, dog-bone adhesive specimens were submitted to cyclic temperatures ranging from 30°C to 60°C during an exposure time of 14 hours that resulted in

123

an increase in the mechanical properties due to post-curing effect on the adhesive. According to [144], the more thermal energy transmitted to the adhesive due to the increment of temperature, the greater the number of molecular links, therefore causing an increase in the adhesive's strength, curing degree (α) and T_g .

The mechanical behaviour of structural adhesives under sustained loading has also been studied from analytical and numerical points of view [85,86,94,143,146]. The evolution of the mechanical properties of adhesives is defined by analytical expressions that are based on rheological models and adjusted from experimental results.

Most of the previous studies focussed on constant service conditions. However, less attention has been paid to the study of cycles of temperature, which may be more representative of real-life conditions, where civil structures are subjected to cyclic temperature conditions due to the day-night cycle. In particular, the combined effect of sustained loading and cyclic thermal conditions has been studied for CFRP-steel joints [147–149] and FRP-concrete joints [88,105,107,110,112,131,150–152], but there is still a lack of knowledge on how cyclic environmental conditions specifically affect the mechanical behaviour of the adhesive with time.

The present study aims to contribute to the understanding of the effect of cyclic service temperature conditions on epoxy adhesives for structural strengthening of RC structures through sustained loading tensile tests. Four experimental series studying two steady service temperatures and three cyclic temperatures were carried out, giving a total of 52 specimens. After the tensile sustained loading tests, instantaneous tensile tests were carried out to obtain the residual strength and elastic modulus of the studied adhesive. Finally, Differential Scanning Calorimetry (DSC) analyses were performed to study the influence of steady and cyclic service conditions on the adhesive thermophysical properties.

6.2   Instantaneous characterization of the adhesive

The adhesive used was the bi-component thixotropic epoxy resin Sika 30. The components were mixed with a resin-hardener ratio of 3:1 at ambient temperature and cured for 12 days. Since this adhesive is commonly used to bond FRP laminates or steel plates to concrete, it is composed of (approximately) 55% silica quartz filler, which provides a high elastic modulus in comparison with other epoxy resins. According to the manufacturer, for a curing time of 7 days

under +15°C, the tensile strength and elastic modulus of the epoxy resin are 26 MPa and 11.2 GPa, respectively.

6.2.1 Mechanical characterization

The tensile strength and the elastic modulus were obtained from the instantaneous tests of six dog-bone specimens following ISO 527-2 specifications [113]. The tests were performed in an MTS Insight 5 kN testing machine at a test speed of 1 mm/min (Figure 6.1). The instrumentation consisted of two strain gauges bonded at each side of the mid-section of the specimen and one extensometer to measure the evolution of strain during the test.

Figure 6.1: Set-up for the instantaneous tensile test of adhesive specimens.

A tensile strength (f_{ta}) of 26.1 MPa (with a Standard Deviation, SD, of 4.5 MPa), an elastic modulus (E_a) of 10.7 GPa (with an SD of 471.4 MPa) and a maximum strain of 2770 $\mu\varepsilon$ (with an SD of 711 $\mu\varepsilon$) were obtained.

6.2.2 Thermophysical characterization

DSC and Dynamic Mechanical Analysis (DMA) tests were performed after 12 days of curing at 20°C [118]. The DSC method is used to measure the physical and chemical changes in the material when an increase of temperature is applied to the specimen. During the curing process, the specimen releases energy in an exothermal process, causing a decrease in the enthalpy of reaction. The enthalpy of reaction is measured by integrating the area between the peak corresponding to the curing and a baseline, as is shown in Figure 6.2a. The curing degree α is defined as:

$$\alpha = \frac{H_{r,t=0} - H_r}{H_{r,t=0}} \tag{6.1}$$

where H_r is the enthalpy of reaction in J/g and $H_{r,t=0}$ is the residual enthalpy at curing time $t = 0$ hours. Moreover, from the DSC test, the T_g can be obtained according to [118,153].

On the other hand, the DMA test consists of applying a cyclic non-destructive stress to the adhesive specimen at a constant frequency and an increasing temperature with time. This test measures the T_g through three different methods: the storage modulus (E'), the loss modulus (E'') and the loss factor ($tan(\delta)$). The storage modulus is defined as the elastic part of the viscoelastic behaviour of the material and is the material's capacity to store energy. The loss modulus is defined as the viscous part of the viscoelastic behaviour of the material and represents the loss of energy during one loading cycle. The loss factor, or damping, is calculated as the ratio between E'' and E' [154]. The temperatures tested in the DMA ranged between 20°C and 100°C with a heating rate of 2°C/min. A cyclic displacement of 10 µm at a frequency of 1 Hz was applied to the specimen [154].

Figure 6.2a and Figure 6.2b show the results obtained from the DSC and the DMA, respectively.
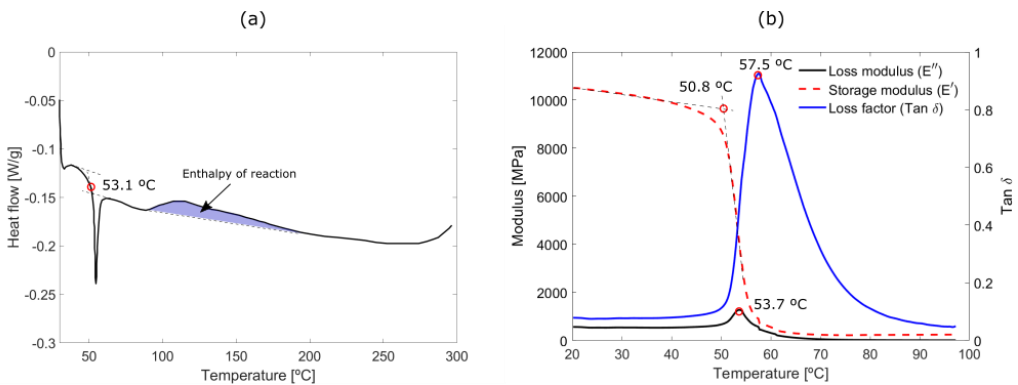
Figure 6.2: Results from the (a) DSC test and the (b) DMA test.

From the DSC tests, T_g was 53.1°C, the enthalpy of reaction at $t = 0$ hours was $H_{r,t=0} = 88.76$ J/g, and the enthalpy at $t = 12$ days was $H_r = 3.29$ J/g, giving $\alpha = 96.3\%$. From the DMA test, the T_g calculated from the onset of the storage modulus curve drop, the loss modulus peak and loss factor peak ($tan(\delta)$) was 53.7°C, 50.8°C and 57.5°C, respectively.

6.3 Experimental time-dependent behaviour of the adhesive

An experimental programme consisting of four experimental series was performed under sustained loading and different temperature conditions and a relative humidity of 55% inside a climatic chamber. Sustained loading was applied through a gravity loading system with a lever arm with a magnification factor of 4 (Figure 6.3). The instrumentation consisted of two strain gauges, each one bonded at one side of the mid-section.

Figure 6.3: Set-up of the sustained loading test.

Adhesive specimens were named C-%f_{ta}, where C stands for the experimental series and %f_{ta} indicates the percentage of tensile strength (f_{ta}) applied as sustained loading (Table 6.1).

For each of the four series, three sustained loading levels were tested, corresponding to 15%, 30% and 50% of f_{ta}. Additionally, in one of the experimental series, supplementary levels of 5%, 10%, 20% and 40% of f_{ta} were tested. At each load level, three specimens were tested and one reference specimen (R) was left unloaded, giving a total of 52 adhesive specimens.

Series C1 and C2 were performed at steady temperatures of 20°C and 40°C, respectively, while series C3-A, C3-B and C4 were executed in different temperature cycles, as detailed in Table 6.1. The maximum average service temperature was set to be around 15°C lower than T_g for all series [93].

In all series except for C4, a seven-day preconditioning stage coincident with the temperature function of the sustained loading test was applied in order to acclimatize the specimens. In series C4, specimens were loaded at the same time as the initiation of the temperature cycles in order to study the effect of preconditioning. Moreover, in C4 the temperature function was triangular, meaning that the objective temperature was steadily increasing or decreasing (see Figure 6.4), without any horizontal plateau.

For series C3, two different phases were applied. In phase A (C3-A), a range of temperatures very similar to those of C4 (18-38°C, compared to 20-40°C in C4), but with a trapezoidal temperature cycle were applied (see Figure 6.4). This phase was finalised at 600 hours because the amplitude of strain caused by the thermal cycle stabilized. After that, to study the behaviour of the specimens under a change on the climatic conditions, the specimens were subjected to the phase B (C3-B) conditions, where the objective trapezoidal cyclic temperature was increased from 22°C to 43°C.

Table 6.1: Experimental series.

Series	Load level [% of P_u] (nº of specimens)	Temperature function [24 h]	Precond -itioning	Phase	Specimens' surface temperature [°C]	Average temperature of the specimen' surface [°C]	Test duratio n [hours]
C1	15 (3)/30 (3)/50 (3) / R (1)	Steady	Yes	-	20	20	1000
C2	5 (3)/10 (3)/15 (3)/20 (3)/30 (3)/40 (3)/50 (3) / R (1)	Steady	Yes	-	40	40	1000
C3	15 (3)/30 (3)/50 (3) / R (1)	Trapezoidal	Yes	A	18 - 37	26.9	600
				B	23 - 43	33.7	1000
C4	15 (3)/30 (3)/50 (3) / R (1)	Triangular	No	-	20 - 40	30.0	1000

128

Figure 6.4 shows the comparison between the temperature measured on the specimens' surface (black curve) and the objective temperature (red curve) of every experimental series under cyclic temperature.
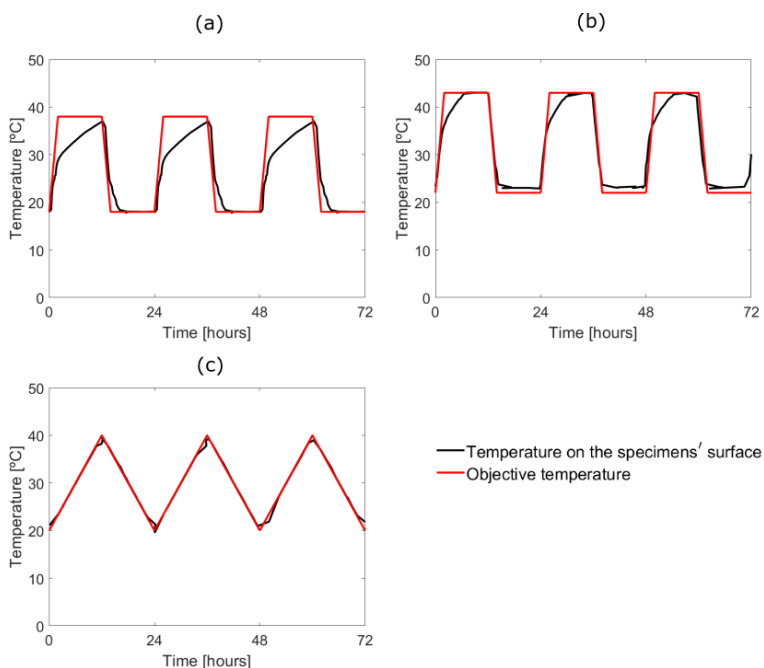
Figure 6.4: Temperature cycles applied in the experimental series (a) C3-A, (b) C3-B and (c) C4.

In the C3 series, some differences can be observed between the objective ascending temperature (red line) and the surface temperature of the specimen (black line). This could be attributed to a combined effect between the programmed rate of variation and the thermal inertia of additional materials in the chamber during the test. The softer slope of the ascending branch (in °C/min) in the cycles of series C4 compared to C3 allowed the specimens to more precisely follow objective cycle.

6.3.1 Evolution of strain with time

Figure 6.5 presents the evolution of axial strain in the adhesive specimens at the different sustained loading stages (detailed in Table 6.1) for each series. Each curve was obtained as the average of the three specimens tested at the given sustained loading level. In Figure 6.5c, the dashed grey line indicates the end of the test, while black crosses in Figure 6.5b, Figure 6.5d and Figure 6.5e indicate the failure of the specimens.
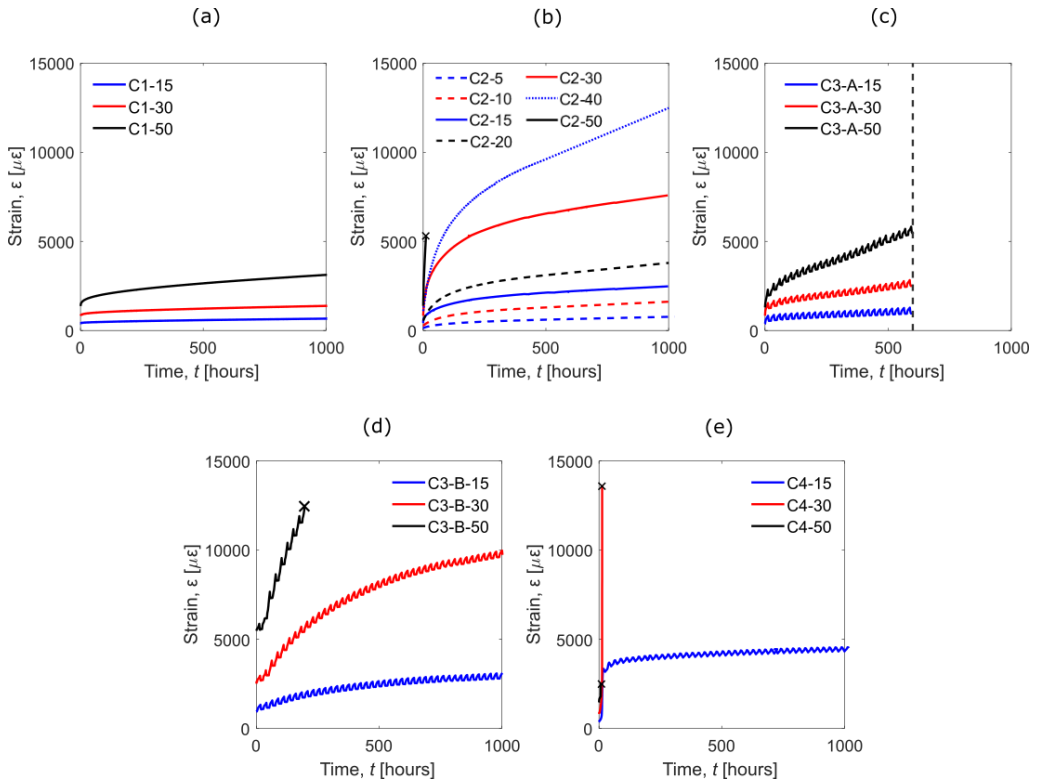
Figure 6.5: Evolution of strain obtained in experimental series (a) C1, (b) C2, (c) C3-A, (d) C3-B and (e) C4.

Regardless of the temperature conditioning (steady or cyclic temperature), an initial stage with a high increase of strain and a second stage where the increase of strain tends to be lower and more constant can be observed. Some specimens eventually experienced a high increase of strain that led to failure. In the following sub-sections, the effect of sustained loading, high service temperature, preconditioning and thermal cycles is further analysed and discussed.

6.3.1.1 Effect of sustained loading

The increase in sustained loading causes a general increment of the time-dependent strain, as expected. Furthermore, specimens under 15% of f_{ta} did not fail during the test, even though specimens C4-15 developed a significant increment of strain during the first temperature cycle due to the lack of preconditioning. For sustained loading levels of 30% of f_{ta}, only specimens C4-30, failed after a few hours of loading. Finally, for specimens loaded at 50% of f_{ta}, only C1 and C3-A specimens endured until the end of the test, developing a final strain of 3120 $\mu\varepsilon$ and 5345

$\mu\varepsilon$ for C1 and C3-A, respectively. In contrast, C2, C3-B and C4 specimens under 50% of f_{ta} failed after 11 hours, 197 hours and 7 hours, respectively.

In some specimens, the time-dependent strain was higher than the instantaneous ultimate strain. This effect was also observed in [87]. Costa *et al.* [94] attributed this phenomenon to a continuous reorganization of the internal structure of the adhesive, allowing it to withstand higher deformations than the ultimate strain under instantaneous load.

6.3.1.2   Effect of high service temperature

The strain level increased with the increase in temperature (C2 series in Figure 6.5b compared to C1 series in Figure 6.5a). Furthermore, specimens under 40°C experienced the highest strain with time of all the experimental series, which is because the average temperature during the test was also the highest [60,87]. In this series, no failure was obtained in specimens under sustained loading levels up to 40% of f_{ta}.

6.3.1.3   Effect of the preconditioning period

A preconditioning stage of seven days was applied to all the experimental series except series C4, where significantly higher strains were observed in their first thermal cycle in comparison with the others. Furthermore, C4 specimens failed after 12 hours (when the first peak temperature of 40°C was achieved), and 7 hours (when the temperature was 22.7°C) for loading levels of 30% and 50% of f_{ta}, respectively.

6.3.1.4   Effect of thermal cycles on the overall time-dependent behaviour

The effect of temperature cycles on the evolution of the tensile strain can be identified in series C3 and C4 (Figure 6.5c, Figure 6.5d and Figure 6.5e) through relatively small oscillations of strain at every cycle. The amplitude of strain related to temperature cycles, caused by the thermal expansion and contraction of the adhesive, was observed not to be significant compared to the mean value of the time-dependent strain, especially in the stage where creep tends to a constant slope. However, to better identify the effect of thermal cycles on the time-dependent strain behaviour, Figure 6.6 represents the increment of adhesive strain with time occurring after instantaneous deformation ($\Delta\varepsilon$) for experimental series C1, C2, C3-A and C3-B, at the loading levels of 15 and 30% of f_{ta}.
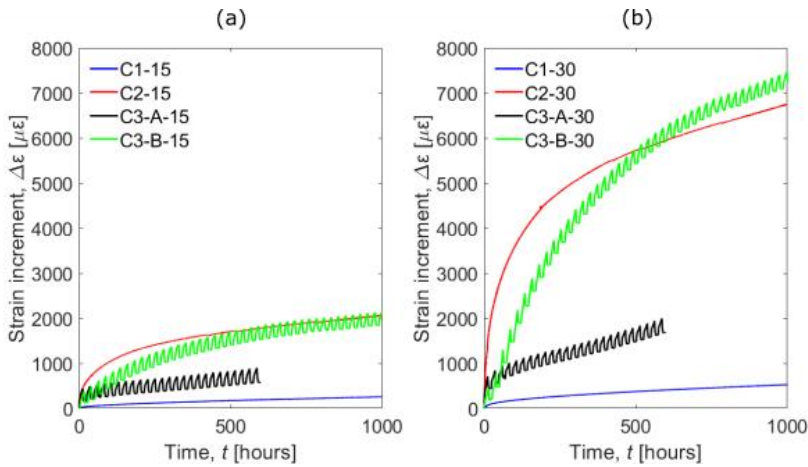
Figure 6.6: Increment of strain with time for specimens under (a) 15% of f_{ta} and (b) 30% of f_{ta}.

It is observed that the strain response of series C3-A (cyclic temperature between 18°C and 37°C with average value of 26.9°C) lies between that of the C1 and C2 series (steady temperature conditions, at 20°C and 40°C, respectively), as was to be expected.

However, for the case of C3-B (cyclic temperature between 23°C and 43°C with an average value of 33.7°C), the mean time-dependent strain clearly surpassed the trend indicated by the C2 series in specimens under 30% of f_{ta} (C3-B-30) at t = 540 hours and at around 1000 hours the C3-B-15 specimens reached the C2 trend. Even though the average temperature in C3-B was lower than the steady temperature in C2, the fact that the maximum temperature of the C3-B series was higher than 40°C, might have caused more molecular motion which degraded the secondary bonds of the adhesive thus increasing the strain in the specimen [144] and, consequently, increasing the creep behaviour of the adhesive. Furthermore, it should be remembered that the C3-B series was previously loaded under C3-A thermal condition for 600 hours, hence, the initial stage with high creep deformation due to loading had already taken place during the C3-A thermal period. The fact that during the stage with a rather constant slope the C3-B specimens showed higher value of $\Delta\varepsilon$, might indicate that the temperature cycles caused greater damage to the specimens (measured as strain increment in this work).

6.3.1.5   Effect of the thermal cycles on the strain amplitude

To further study the effects of sustained loading on strain oscillations caused by the thermal cycles, the evolution of ascending amplitude of strain ($A_{\varepsilon,a}$) and the descending amplitude of strain ($A_{\varepsilon,d}$) at each cycle was measured. $A_{\varepsilon,a}$ and $A_{\varepsilon,d}$ were calculated as the strain difference

132

between the lower and upper temperatures at each thermal cycle (valley to peak for the ascending amplitude and peak to valley for the descending one). Results are presented in Figure 6.7 for experimental series C3-A, C3-B and C4.
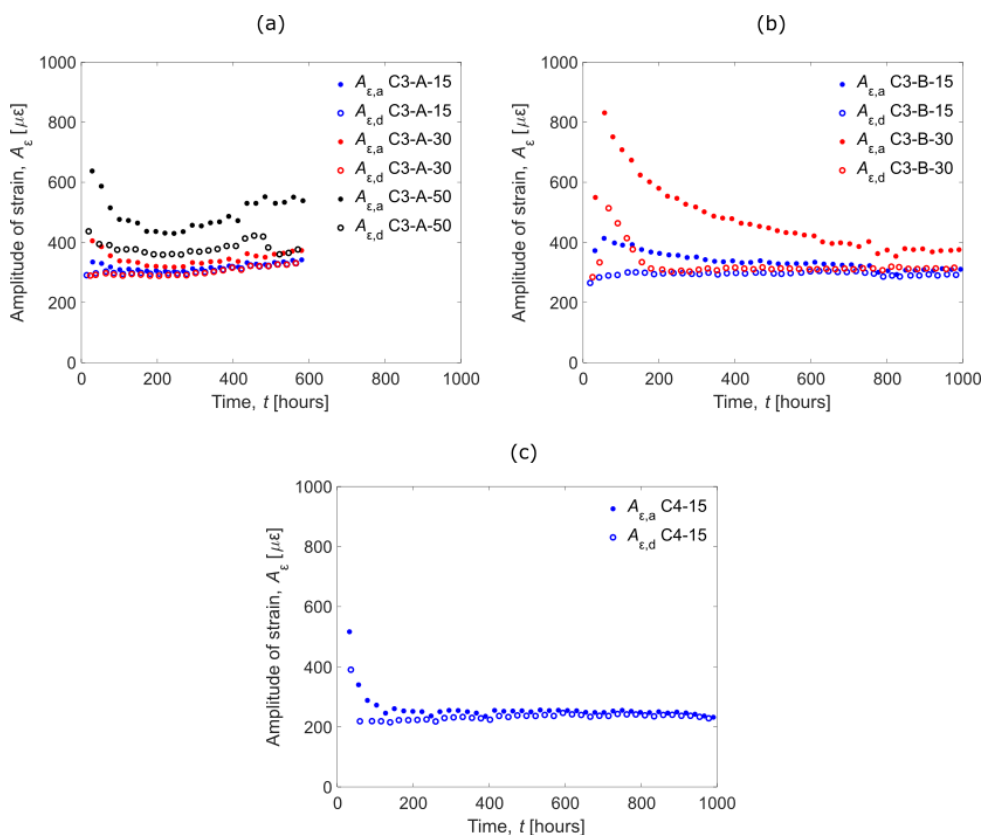
Figure 6.7: Evolution of the strain amplitude obtained in the adhesive specimens in experimental series (a) C3-A, (b) C3-B and (c) C4.

In general, for sustained loadings of 30% and 50% of f_{ta}, the ascending amplitude is higher than the descending one, due to the effect of creep on the adhesive. This effect cannot be noticed in specimens loaded at 15% of f_{ta}, probably because, in this case, the effect of creep is not so relevant.

Furthermore, the difference between $A_{\varepsilon,a}$ and $A_{\varepsilon,d}$ decreases with time which might be attributed to the stabilizations of the creep effect in its secondary stage. However, for the case of specimens C3-A-50, loaded at 50% of f_{ta}, the difference between $A_{\varepsilon,a}$ and $A_{\varepsilon,d}$ is maintained until the end of the test, showing that for higher load levels, creep effects play an important role on the strain behaviour.

Regarding the effect of preconditioning (Figure 6.7c), as was previously observed in Figure 6.5e, high oscillations of strain were obtained during the initial thermal cycles. In particular, C4-15 specimens experienced an $A_{\varepsilon,a}$ = 2890 $\mu\varepsilon$. This value has not been included in Figure 6.7c for scaling reasons. Beyond the second thermal cycle, the specimens were better conditioned and the amplitude of strain decreased, obtaining a lower amplitude of strain in comparison to C3-A and C3-B.

6.3.2 Evolution of creep compliance with time

Creep compliance, *J(t)*, provides information about the linearity of the viscoelastic behaviour of adhesive with respect to the load applied. *J(t)* was obtained by dividing the adhesive tensile strain $\varepsilon(t)$ by the applied stress σ_0 [155]:

$$J_C(t) = \frac{\varepsilon(t)}{\sigma_0} \tag{6.2}$$

Figure 6.8 presents the creep compliance curves for each experimental series. Continuous blue, red and black curves stand for specimens under 15%, 30% and 50% of f_{ta}, respectively. Additionally, for the C2 series, dashed blue, red, and black curves represent specimens under 5%, 10% and 20% of f_t and the dotted blue line represent specimens under 40% of f_{ta}.

In the C1 series, similar creep compliance values were obtained for specimens under 15% and 30% of f_t, while it was slightly higher for the C1-50 specimens, indicating a linear viscoelastic behaviour for specimens at room temperature conditions until sustained loading levels up to 30% of f_t.

As the service temperature increased, higher values of creep compliance were obtained. For example, in the C2 series, specimens under 30% of f_{ta} showed a J_c (t = 1000 hours) value of 1047 MPa^{-1}, compared to 184.5 MPa^{-1}, obtained in C1. Furthermore, it was also observed that for the C2 series similar curves were obtained for sustained loading levels ranging between 5% and 15% of f_{ta}. For higher sustained loading levels, higher creep compliance curves were obtained, meaning that the linear viscoelastic behaviour can be assumed for sustained loading levels up to 15% of f_{ta}. By comparing the C2 series with C1, it can be seen that the maximum loading level that can be included in the viscoelastic behaviour decreases as service temperatures increases.

In the experimental series C3-A, where cyclic temperature conditions were applied, slightly different creep compliance curves were obtained for all load levels. Although small but some difference is appreciated between specimens loaded at loaded at 15% and 30% when compared to C1. Moreover, from comparison between C3-A and C3-B series, it can be seen that as the

average service temperature increased, higher values of creep compliance were obtained, as expected.

In the non-preconditioned series C4, the increase in temperature during the first cycles caused high values of strain to develop in the adhesive and, consequently, high values of creep compliance were obtained.
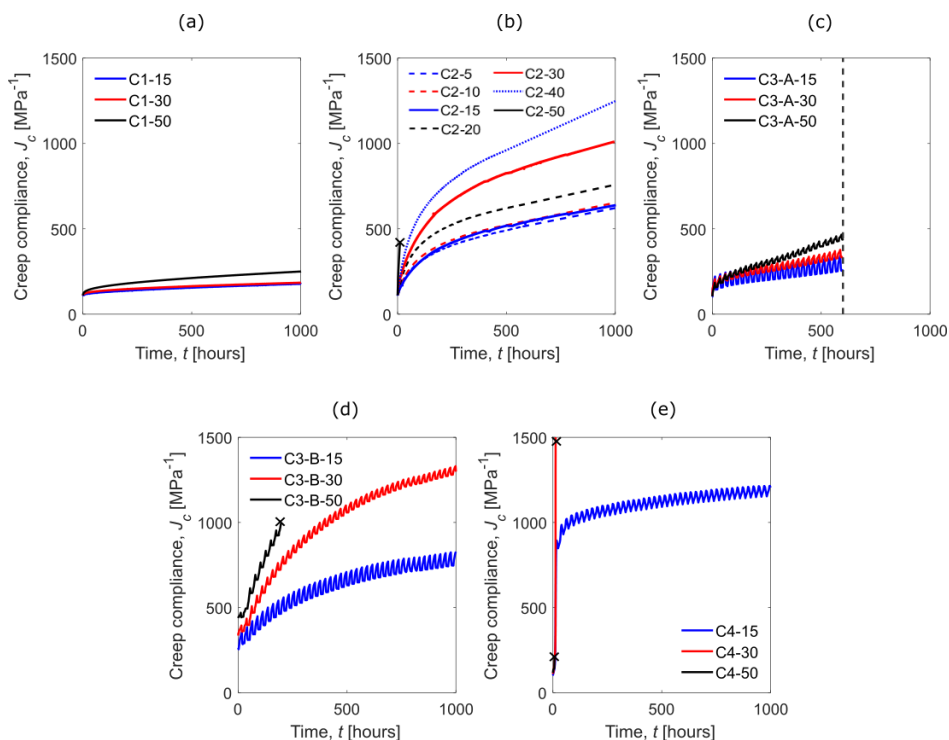
Figure 6.8: Creep compliance curves obtained in experimental series (a) C1, (b) C2, (c) C3-A, (d) C3-B and (e) C4.

6.4 Post-long-term mechanical and thermophysical behaviour of the adhesive specimens

To study the effect of high service temperatures and sustained loading on the mechanical and thermophysical properties, tensile tests and DSC tests were performed in each experimental series after the sustained loading tests.

For the experimental series C3-A, before C3-B series started, one adhesive specimen under 15% f_{ta} was maintained at room conditions (20°C +/- 1°C) to study the post-long-term behaviour. Moreover, to study the effects of the temperature cycles on the adhesive's response, one

specimen was kept inside the climatic chamber without sustained loading during the experimental series C3-A and C3-B.

6.4.1   Results from the mechanical characterization

Tensile tests until failure were performed for all specimens that did not fail during the sustained loading tests to study the effect of sustained loading and service conditions on the load carrying capacity of adhesive.

Table 6.2 shows the mechanical properties obtained from the post-sustained instantaneous loading tests ($E_{a,LT}$ and $f_{ta,LT}$), and the ratio with the instantaneous values previously obtained in Section 6.2.1(E_a and f_{ta}).

Table 6.2: Tensile strength and stiffness of adhesive specimens after long-term tests.

Series	Specimen	$f_{ta,LT}$ [MPa]	$\dfrac{f_{ta,LT}}{f_{ta}}$	$E_{a,LT}$ [MPa]	$\dfrac{E_{a,LT}}{E_a}$
C1	C1-R-PLT-15	21.8 (SD = 1.89)	0.83	9147.5 (SD = 561.3)	0.85
	C1-R-PLT-30	22.5 (SD = 1.55)	0.86	9030.0 (SD = 302.6)	0.84
	C1- R-PLT-50	22.0 (SD = 2.60)	0.84	8815.5 (SD = 344.8)	0.82
C2	C2-R-PLT-15	24.2 (SD = 0.4)	0.92	8907.1 (SD = 555.2)	0.83
	C2-R-PLT-30	22.5 (SD = 1.8)	0.86	7573.0 (SD = 677.1)	0.71
	C2- R-PLT-50	-	-	-	-
C3-A	C3-A-R-PLT-15	23.2	0.88	8984.0	0.84
	C3-A-R-PLT-30	*	*	*	*
	C3-A- R-PLT-50	*	*	*	*
C3-B	C3-B-R-PLT-15	24.1 (SD = 2.65)	0.92	9284.4 (SD = 2106.2)	0.87
	C3-B-R-PLT-30	23.3 (SD = 2.96)	0.89	8521.8 (SD = 1154.3)	0.79
	C3-B-R-PLT-50	-	-	-	-
	C3-B- R-PLT-NL	26.85	1.03	10294.3	0.96
C4	C4-R-PLT-15	20.1 (SD = 1.1)	0.77	7928.9 (SD = 497.7)	0.74
	C4-R-PLT-30	-	-	-	-
	C4- R-PLT-50	-	-	-	-

Note: "-" indicates that the specimen failed during the sustained loading test and "*" indicates that the specimen was not tested post-long-term because it was used in series C3-B.

Overall, all specimens subjected to sustained loading experienced a decrease in the mechanical properties of the adhesive, both in the tensile strength and the elastic modulus. In general, when increasing the level of sustained loading, the mechanical properties decreased. The specimen subjected to thermal conditions but unloaded (C3-B-R-PLT-NL) did not suffer any reduction in their tensile strength that should be taken into account, and kept almost the same elastic modulus (ratios of 1.03 and 0.96 were obtained for E_a and f_{ta}, respectively).

Taking series C1 as a reference, it can be generally observed that specimens from series C2 presented slightly higher $f_{ta,LT}$ and lower $E_{a,LT}$. The increase in $f_{ta,LT}$ could be explained because of a post-curing effect taking place at high temperatures (always below the T_g), while the reduction of $E_{a,LT}$ could be explained because these specimens underwent longer time-dependent strains once the specimen was unloaded which induced a less stiff response.

Results from the specimens in the C3-A series (cyclic temperature between 18°C and 37°C with average value of 26.9°C) fell between those of the C1 and C2 series. Specimens from series C3-B obtained similar $f_{ta,LT}$ as the specimens in C2. Even though the average temperature in series C3-B was lower than temperature in series C2, the maximum temperature of the thermal cycle in C3-B caused a post-curing effect which resulted in a similar value of $f_{ta,LT}$.

From the experimental series C4, only specimens under 15% of f_{ta} could be tested. In this case, a substantial decrease in the mechanical properties was observed in the post-long-term tests, which could be attributed to the lack of preconditioning of these specimens.

6.4.2 Results from thermophysical characterization

Table 6.3 shows H_r, α and T_g calculated from the DSC tests performed after each experimental series and at the reference time of 12 days (R), previously shown in Section 6.2.2.

Table 6.3: Enthalpy of reaction (H_r), curing degree (α) and glass transition temperature (T_g) obtained from the DSC test after each experimental series.

	Series					
	R	C1	C2	C3-A	C3-B	C4
H_r [J/g]	3.3	3.1	1.7	1.9	0	2.6
α [%]	96.3	96.6	98.0	97.9	100	97.1
T_g [°C]	53.1	53.1	56.7	59.7	65.4	58.9

The curing degree α obtained in the C1 series after the sustained loading test was slightly higher than the value obtained in the instantaneous characterization, while no difference in T_g was observed. In the rest of the experimental series, where specimens were subjected to higher temperatures than in C1, the curing degree was higher, indicating some post-curing effect. This increasing effect was also observed in T_g, which increased with the service temperature (C2 compared to C1). Hence, it can be stated that relatively high service temperatures might cause more cross-links to develop between the molecules of the adhesive specimen, thus increasing the glass transition temperature [92,142,144,145]. Regarding the effect of the temperature cycles, it can be seen that higher T_g values were obtained in comparison with the C2 series, as was observed in Silva *et al.* [92]. From comparisons between the C3-A and C3-B series, it can be seen that the higher increase of T_g was obtained as higher temperature cycles were applied (C3-B compared to C3-A).

6.5   Conclusions

The present work aimed to study the behaviour of a structural adhesive under sustained loading and different steady and cyclic temperature service conditions. For that purpose, four experimental series of sustained loading tensile tests were carried out. In each series, nine specimens were subjected to different levels of sustained loading (15%, 30% and 50% of the tensile strength) for 1000 hours inside a climatic chamber. The service temperature conditions were modified for each series in order to observe their influence on the tensile response of the adhesive. From the sustained loading tests, the following conclusions can be drawn:

-   The tensile strain in the adhesive increased with the service temperature and sustained loading, as would be expected.

- Only specimens from the experimental series C1 (steady temperature at 20°C) and C3-A (cyclic temperature between 18°C and 38°C) were able to withstand a load level of 50% of f_{ta} until the end of the test (1000 hours and 600 hours, respectively).
- The lack of a preconditioning stage caused high values of strain in the C4 series, leading to premature failure in specimens under 30% and 50% of f_t.
- Higher strains were obtained in comparison with the ultimate instantaneous strain due to the reorganization of the internal structure of the adhesive specimens with time.
- In the experimental C1 series, a linear creep stage could be assumed for sustained loading levels up to 30% of the tensile strength, while in the experimental C2 series (steady temperature at 40°C), a linear viscoelastic behaviour was observed for specimens under sustained loading levels between 5% and 15% of f_{ta}.
- Thermal cycles in C3-B caused a higher increase of strain than expected, considering the average temperature of the cycles. Additionally, temperature cycles caused oscillations of strain in the specimens. That said, however, these strain variations were not significant in comparison with the evolution of strain with time.
- The strain amplitude observed in the specimens decreased with time, becoming higher as the sustained load level increased.

Additionally, tensile and DSC tests were performed to study the mechanical and thermophysical properties of the adhesive before and after service conditions. From this, the following conclusions can be stated:

- A general decrease of the mechanical properties was observed in the tensile tests after the sustained loading.
- A general increase in T_g and α was observed after the sustained loading tests. A higher increase in T_g was observed in specimens that were subjected to cyclic temperature (C3-A, C3-B, C4) compared to the series held under steady temperatures (C1 and C2).
- As the average temperature in the experimental series increased, the value of T_g increased as well.

7 Paper D: Sustained loading bond response and post-sustained loading behaviour of NSM CFRP-concrete elements at different service temperatures

Javier Gómez[1], Cristina Barris[1*], Marta Baena[1] Ricardo Perera[2] and Lluís Torres[1]

[1]AMADE, Polytechnic School, University of Girona, 17003, Girona, Spain

[2]Department of Mechanical Engineering, Technical University of Madrid, 28040, Madrid, Spain

[*]Corresponding author

Sustained loading bond response and post-sustained loading behaviour of NSM CFRP-concrete elements under different service temperatures

Javier Gómez[1], Cristina Barris[1*], Marta Baena[1], Ricardo Perera[2] and Lluís Torres[1]

[1] AMADE, Polytechnic School, University of Girona, 17003 Girona, Spain

[2] Department of Mechanical Engineering, Technical University of Madrid, Spain

[*] Corresponding author, cristina.barris@udg.edu

Abstract

Nowadays, one of the foremost procedures for strengthening concrete structures is the Near-Surface Mounted (NSM) technique. This paper presents an experimental study on the effect sustained loading and different service temperatures (steady and cyclic) have on NSM Carbon Fibre-Reinforced Polymer (CFRP)-concrete bonded joints and their post-sustained loading load-slip behaviour. Four experimental campaigns using eight NSM CFRP-concrete specimens were performed by employing two different service load levels (15% and 30% of the ultimate load) and combining two groove thicknesses (7.5 and 10 mm) and two bonded lengths (150 and 225 mm). Two steady state temperatures (20 and 40 °C) and two cyclic service temperatures (ranging between 20 and 40 °C) were programmed. The slip obtained was proportional to the sustained load level. Furthermore, higher slips were registered for specimens under higher mean temperatures in the cycle. After 1000 hours of sustained load testing, the specimens were tested under monotonic loading until failure (post-sustained loading tests). In general, the ratio between the post-sustained loading ultimate load and the instantaneous ultimate load was close to the unity, although some differences were perceived in series S2 (steady 37.7 °C) with a mean increase of 6.3 %, and series S3-B (cyclic temperature ranging between 24.6 and 39.2°C) with a mean reduction of 9%.

Keywords: CFRP; NSM; Bond; Sustained Loading; Temperature.

7.1 Introduction

The use of Fibre-Reinforced Polymers (FRP) to strengthen concrete structures has been steadily gaining popularity over the last decades. Externally Bonded Reinforcement (EBR) and Near-Surface Mounted (NSM) techniques are currently the most well-known methodologies employed to enhance the load-carrying capacity of civil structures. Standards and guidelines such as the fib Bulletin 90 [11], the ACI 440.2R-17 [69], and the CNR-DT 200 R1/2013 [51] have already approved the design of FRP strengthening systems for concrete structures.

Even though the short-term bond behaviour of EBR and NSM methodologies has been extensively studied over the past decades, less attention has been paid to their behaviour under service conditions. External circumstances, such as sustained loading or environmental temperature conditions, can cause significant damage, either to the concrete [156–158] itself or to the strengthening system during its service life, which can then lead to a reduction of the load-carrying capacity, resulting in premature bond failures [88,109,159]. It is extremely important, therefore, to investigate the behaviour of FRP strengthening systems under real service environmental conditions.

The effect of sustained loading in NSM CFRP strengthening systems was experimentally evaluated in Emara *et al.* [73] and Gómez *et al.* [160] for room conditions. In both studies, sustained loading caused a substantial increase in the relative slip between the CFRP and concrete, although the load applied was much lower than the ultimate load of the bonded joint. From these investigations, numerical models based on the degradation of the bond-slip law of the bonded joint were proposed to predict their sustained loading behaviour.

On the other hand, high service temperatures have been proved to significantly affect the performance of FRP strengthening systems. In general, dramatic decreases in the bond strength and stiffness of the joint have been observed when temperatures are close to the glass transition temperature (T_g) [100,159,161–166], along with an increase in the bonded length needed to carry the maximum load [162,164], a redistribution in the FRP strain [100,162,165], and a change in the failure mode [100,166].

Furthermore, because service temperatures do not remain constant with time in real applications but rather oscillate during the day-night cycle and during the different seasonal weather conditions, it is crucial that the effects such cyclic temperatures might have on the structural response of the bonded joint are investigated. Fernandes *et al.* [109] performed durability tests of NSM CFRP-concrete specimens under cyclic temperature (20 to 80 °C)

conditions for six months and obtained a significant variation in the stiffness and a similar value of the ultimate load in comparison with the instantaneous values. On the contrary, when Lee *et al.* [88,167] studied the effect cyclic temperature conditions have on concrete elements strengthened with NSM CFRP rods using temperature cycles ranging from -15 to 55 °C they detected a decrease in the ultimate load of the bonded joint as the temperature cycles being applied were increased.

Several other experimental studies focused their investigations on the effects of the combination of sustained loading performance and high service temperatures, evaluating their impact on the activated length, the residual strength, and the stiffness of the bonded joint. Some contributions [105,131] have concluded that the combination of high service temperature with sustained loading caused an increase in the overall strength of the EBR bonded joint, while others [88,110,112] observed a reduction in the EBR joint strength.

In the field of NSM strengthening, only a few investigations on the subject of the combination of sustained loading and high service temperatures are to be found in the literature. For instance, Borchert *et al.* [60] observed a loss of the load carrying capacity which was attributed to the creep effect caused by the combination of both factors, while Emara *et al.* [108] concluded that service conditions greatly affected the bonded joint performance, causing a significant increase in the slip with time between the CFRP and the concrete element. Nevertheless, less attention has been paid to the effect of cyclic environmental conditions, such as day-night cycles, and these may prove crucial for a better understanding of the bond behaviour of FRP strengthening systems.

This paper aims to contribute to the understanding on how steady and cyclic service temperature conditions affect the sustained loading bond response of NSM CFRP-concrete elements through an experimental programme using sustained loading single-shear tests. The effects the service load level, temperature, groove thickness and preconditioning have are presented and discussed. Furthermore, following the sustained loading tests, monotonic tests have been carried out to investigate the residual strength, stiffness and failure mode of the bonded joints.

7.2 Experimental programme

Four experimental series (S1 to S4) - each consisting of eight specimens - were performed under sustained loading (ST) and different service temperatures at 55% relative humidity (RH). Two different service loads were applied (15% and 30% of the ultimate load of the NSM CFRP-concrete joint) which represent the range of load values that the CFRP-concrete joint can undergo in a flexural configuration under service conditions. Furthermore, two steady-state and two cyclic service temperatures were programmed. Their bond response was studied by analysing the slip between the CFRP and concrete with time.

The instantaneous bond behaviour of the NSM specimens was experimentally investigated and presented previously by Gómez *et al.* [134]. The ultimate loads (P_u), stiffnesses (K_e) and failure modes that were obtained have been summarised in Table 7.1. Specimens are labelled as I-L_b-t_g, where I stands for instantaneous test, and L_b and t_g are the bonded length and groove thickness, respectively.

Table 7.1: Experimental results of the instantaneous pull-out tests.

Nomenclature	Bonded length, L_b [mm]	Groove thickness, t_g [mm]	Ultimate load, P_u [kN]	Stiffness, K_e [kN/m]	Failure mode
I-150-10	150	10	43.9	172.8	F-A
I-150-7.5	150	7.5	47.1	183.5	C
I-225-10	225	10	54.7	175.4	F-A
I-225-7.5	225	7.5	57.7	181.7	C

Note: F-A = failure in the FRP-adhesive interface; C = cohesive failure in the concrete.

All the specimens that did not fail during the sustained loading (SL) were tested using a monotonic pull-out configuration to investigate the residual mechanical characteristics of the bonded joints and were called post-sustained loading (PSL) specimens.

7.2.1 Specimen characteristics

In each experimental series eight NSM CFRP-concrete specimens combining two groove thicknesses (7.5 and 10.0 mm) and two bonded lengths (150 and 225 mm) were loaded under two sustained load levels (15% and 30% of the instantaneous ultimate load, P_u). Concrete blocks measuring 200 mm × 200 mm × 300 mm and 200 mm × 200 mm × 370 mm were used for short and long bonded length specimens, respectively. Figure 7.1a shows a lateral view of the setup for the single shear test and Figure 7.1b presents a detailed view of the groove dimensions and the CFRP strip into the groove.

(a)   (b)
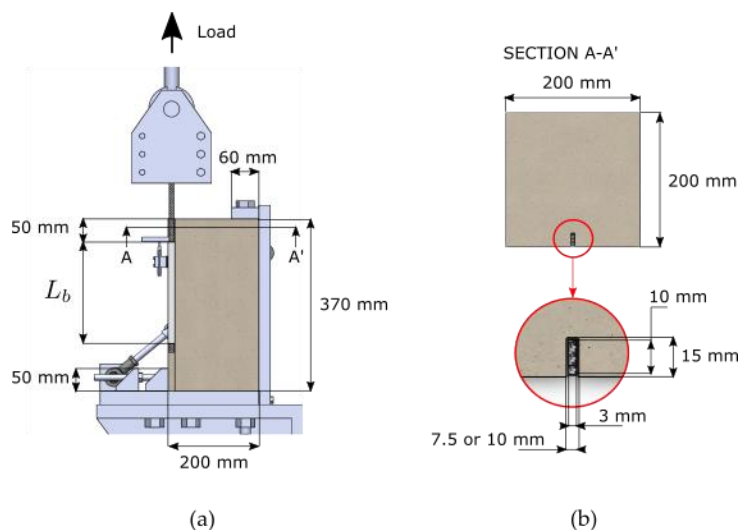
Figure 7.1: (a) lateral view of the setup and (b) detailed view of the groove dimensions and CFRP strip position.

For each experimental series, the concrete blocks were cast with a standard ready-mix concrete supplied by a local company and cured for 28 days under laboratory conditions. Once the concrete had cured, 15 mm deep grooves were then cut and cleaned. The adhesive was prepared by mixing a 3:1 ratio of resin and hardener, as indicated by the manufacturer. Next, CFRP strips were carefully introduced into the grooves and then the NSM CFRP-concrete specimens were subsequently cured for 12 days under laboratory conditions before testing.

The specimens under sustained loading were called S-SL-L_b-t_g-%P_u, where S stands for the series number, SL for Sustained-load, L_b and t_g are the bonded length and groove thickness, respectively, and %P_u the percentage of ultimate load applied as sustained load.

The residual response of the NSM CFRP-concrete joint after SL was evaluated for all the specimens by employing an instantaneous pull-out test until failure at room temperature (20 °C and 55% RH). Each specimen was then called S-PSL-L_b-t_g-%P_u, where PSL stands for post-sustained-loading and the rest of the parameters representing the same as those previously defined above. It should be noted that the specimens from series S3-B were those from the S3-A series, therefore, only the S3-B series specimens' PSL behaviour following the sustained-loading (SL) tests could be studied.

7.2.2   Material properties

All the concrete blocks were cast from the same concrete batch. Following the ASTM S3-A69 / S3-A69M-10 [115] and UNE 12390-3 [116] standards, a concrete compressive strength of 33.0 MPa (with Standard Deviation, SD = 1.8 MPa) and an elastic modulus of 33.1 GPa (SD = 1.6 GPa) were obtained.

CFRP Sika CarboDur S NSM 1030 strips of 10 mm × 3 mm were used. A tensile strength of 3.2 GPa (SD = 68.3 MPa) and an elastic modulus of 169.3 GPa (SD = 13.1 GPa) were obtained following the ISO 527-5 standard [114]. To measure the thermophysical properties of the adhesive, Differential Scanning Calorimetry (DSC) tests were performed after 12 days of curing at 20°C [118]. A T_g of 53.1 °C and a curing degree (α) of 96.3% were obtained.

The adhesive used in the experimental campaigns was Sika 30 bi-component epoxy resin, which had been previously characterized according to the ISO 527-2 standard [113]. The tensile strength and elastic modulus were, respectively, 26.1 MPa (SD = 4.5 MPa) and 10.7 GPa (SD = 471.4 MPa).

7.2.3   Test set-up and instrumentation

All tests were performed using a direct pull-out shear configuration. The test set-up for the sustained loading tests consisted of adapting the set-up applied in the instantaneous characterization of the NSM CFRP-concrete joint [160] by using a steel lever arm with a magnifying factor of 8.3 (Figure 7.2a). For the PSL tests, the instantaneous characterization set-up was used (Figure 7.2b).

Figure 7.2: Set-up used for (a) SL tests; (b) PSL tests.

For the SL tests, the instrumentation consisted of one LVDT (Linear Variable Differential Transformer) placed at the loaded end to measure the relative displacement between the CFRP and the concrete, and one strain gauge bonded at the loaded end to register the load applied to the bonded joint. To measure the internal temperature of the bonded joint, a temperature strain gauge was bonded onto the CFRP surface, inside the NSM groove, of a dummy specimen, which was also kept inside the climatic chamber during the tests, in each of the series. Another temperature strain gauge was bonded onto the NSM groove surface of the same dummy specimen to measure the temperature on the specimen's surface. In the case of the post-sustained loading monotonic tests, the instrumentation consisted of one LVDT placed at the loaded end.

7.2.4 SL experimental series

The details of each experimental series are listed in Table 7.2, i.e., where the cycle function (steady for constant objective temperature and cyclic for 24h-periodical temperature cycles), whether the specimens were preconditioned (or not) before loading, the objective temperature in the climate chamber, the temperature measured on the specimen's surface, the temperature measured inside the NSM groove (attached to the CFRP) and the duration of the test are presented.

Table 7.2. Details of experimental series.

Series	Temperature function [24 h]	Preconditioning	Objective T°C [°C]	T°C on the specimen's surface [°C]	T°C in the NSM [°C]	Test duration [hours]
S1	Steady	Yes	20.0	19.9	18.7	1000
S2	Steady	Yes	40.0	40.1	37.7	1000
S3-A	Cycles 24 h	Yes	18.0 – 38.0 (28.0) [1]	18.0 – 36.9 (26.9) [1]	17.8 – 33.9 (25.6) [1]	600
S3-B	Cycles 24 h	Yes[2]	22.0 – 43.0 (32.5) [1]	23.0 – 43.0 (33.7) [1]	24.6 - 39.2 (31.3) [1]	1000
S4	Cycles 24 h	No	20.0 – 40.0 (30.0) [1]	19.6 – 39.5 (30.1) [1]	21.9 – 31.9 (26.8) [1]	1000

[1] Mean temperature indicated in brackets; [2] Preconditioning consisted of the temperature regime of the previous experimental series (S3-A).

In the experimental series S1 (previously presented in Gómez *et al.* [160]) and S2, specimens were tested under steady temperatures, while in series S3 and S4, trapezoidal and triangular 24-hour temperature cycles, respectively, were applied (Figure 7.3). Experimental series S3 was split into two different steps. First, specimens were subjected to an objective temperature cycle ranging between 18.0 and 38.0 °C (S3-A) and then, after 600 hours of testing and without any unloading, the same specimens were subjected to a new objective temperature cycle ranging between 22.0 and 43.0 °C (S3-B). Series S1-S3 were subjected to a thermal preconditioning before loading which consisted of acclimatizing the specimens to the objective temperature for seven days. In series S4, the specimens were loaded without undergoing any previous preconditioning stage.

Figure 7.3 shows the details of the objective temperature (red curve), the temperature on the specimen's surface (blue curve) and the temperature inside the NSM groove (black curve) for all series. As observed, the temperature on the specimen's surface was generally lower than the objective temperature for both steady and cyclic temperature series, basically due to thermal inertia effects. Furthermore, in the cyclic temperature series, the mean temperature measured inside the NSM groove was between 1.3 and 3.3 °C lower than on the specimen's

surface, while in the steady temperature cycles this difference did not occur. Finally, in the S3 series, with a trapezoidal shape for the objective temperature, the temperature inside the NSM groove reached higher values than in the S4 series where a triangular shape was programmed as the objective temperature.
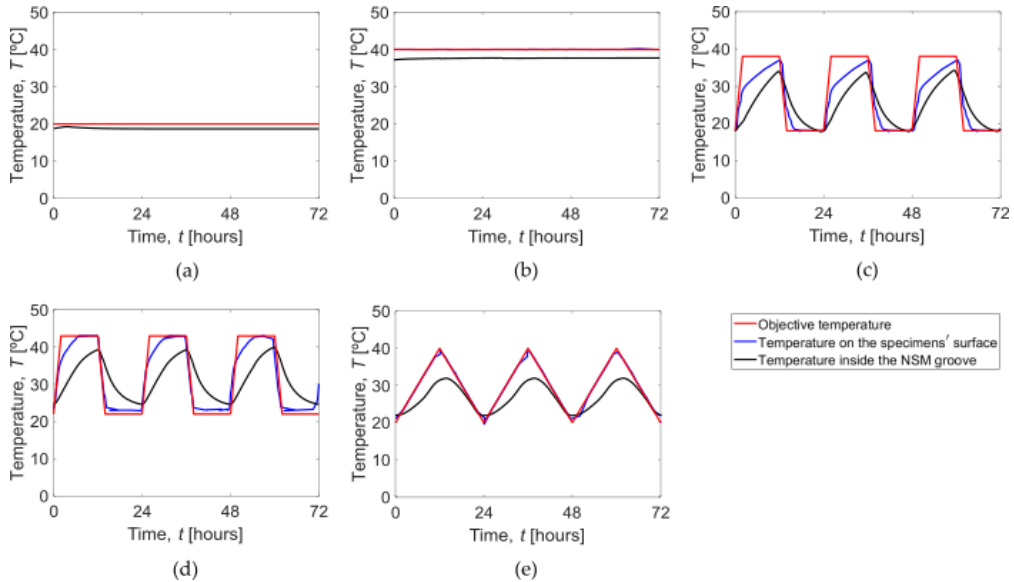
Figure 7.3. Temperature in the experimental series: (a) S1; (b) S2; (c) S3-A; (d) S3-B; (e) S4.

7.3   SL bond behaviour of NSM CFRP-concrete specimens

The evolution of slip with time was obtained from the sustained loading tests in all series, as seen in Figure 7.4.
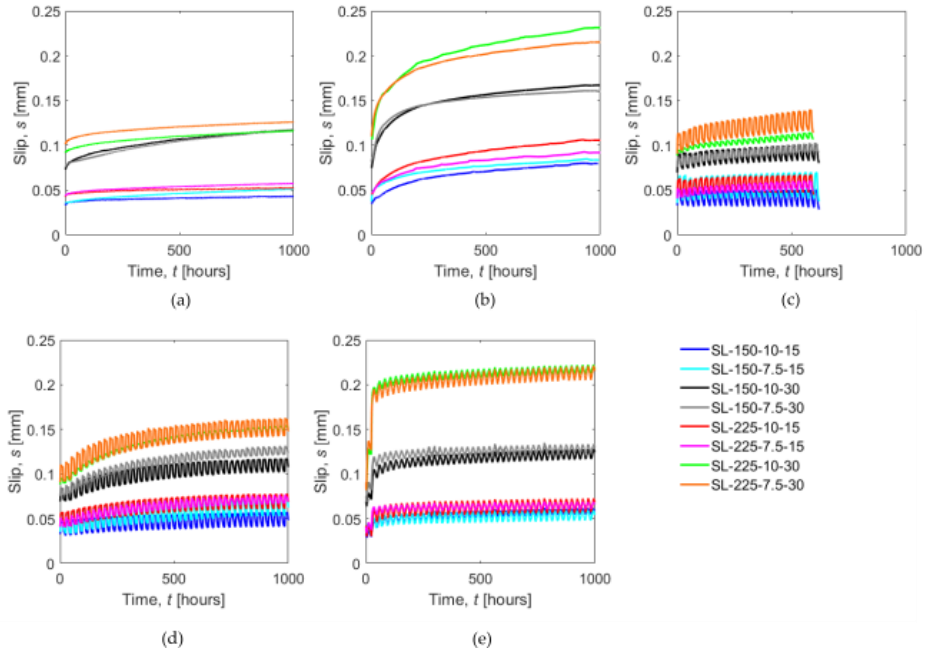
Figure 7.4: Slip at the loaded end obtained in series (a) S1; (b) S2; (c) S3-A; (d) S3-B; (e) S4.

Overall, two different stages were identified in the slip evolution with time for all experimental series: an initial stage with a high non-linear increase in slip and a second stage where the slip evolution tended to increase at a lower and constant rate with time. In the following subsections, the effects of the sustained load level, thermal effects, preconditioning and groove size are discussed.

7.3.1 Effect of sustained load levels

The effect of sustained load levels can be clearly observed in Figure 7.4 for all the experimental series, i.e., as expected, the higher the sustained load, the higher the slip and increment of slip. This effect was observed regardless of the temperature conditioning, bonded length or groove size. Moreover, the specimens under 30% P_u experienced approximately double the slip than the under 15% P_u specimens. This linearity in the slip with respect to load was also observed in Emara *et al.* [108].

7.3.2 Thermal effects

7.3.2.1 Effect of steady temperatures

The effect of different steady temperatures on the slip behaviour can be observed by comparing series S1 (with a steady 18.7 °C inside the NSM groove, Figure 7.4a) and S2 (37.7 °C, Figure 7.4b). As expected, higher slips were obtained in the S2 series which could be attributed to the effect temperature has on the creep behaviour of the adhesive [108]. Furthermore, of all the experimental series it was the S2 specimens that showed the highest increments of slip; albeit with the only exception being the S4 specimens which experienced a significant increase in the slip in the first cycles which is attributed to the lack of preconditioning (see Section 3.2.3). In contrast, series S1, with the lowest temperature, experienced the smallest effect on the creep behaviour of the bonded joint. This behaviour was likewise observed in Emara *et al.* [108], where the highest increases of slip were obtained in specimens subjected to the highest temperatures.

7.3.2.2 Effect of cyclic temperatures

The temperature cycles in series S3-A, S3-B and S4 caused important fluctuations in the evolution of slip as a result of the thermal effects on the materials. These slip oscillations were relatively high in comparison with the increase in slip due to the sustained loading effect, especially in those cases under 15% P_u where the evolution of slip was small.

In Figure 7.5, the comparison of the slip evolution between the S1 (with a steady temperature in the NSM groove of 18.7 °C) and S3-A (with a cyclic temperature of 17.8-33.9 °C) series is presented.
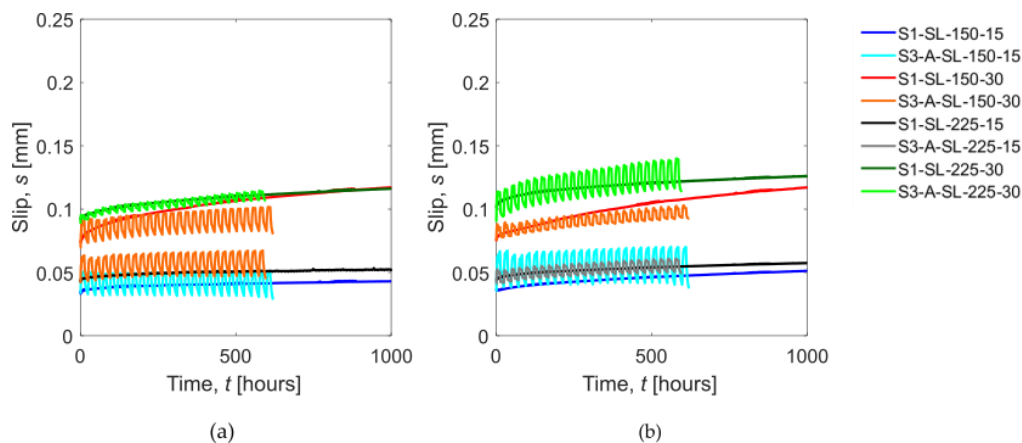
Figure 7.5. Comparison of the slip evolution with time obtained in series S1 and S3-A for groove thicknesses of: (a) 7.5 mm; (b) 10 mm.

It can be observed that, in general, similar mean evolutions of slip were obtained in both series despite the temperature cycles applied in S3-A. This could be explained by the fact that in series S3-A, the average temperature measured in the NSM groove (25.6 °C) was relatively far away from the T_g of the adhesive (53.1 °C), thus leading to a small influence in comparison with the effect of sustained loading.

On the other hand, Figure 7.6 depicts a comparison between the evolution of slip in the S3-A series with its trapezoidal cyclic temperature between 17.8 and 33.9 °C and a mean temperature of 25.6 °C , and the S3-B with the same shape for the temperature cycles but ranging between 24.6 and 39.2 °C and with a mean value of 31.3 °C.
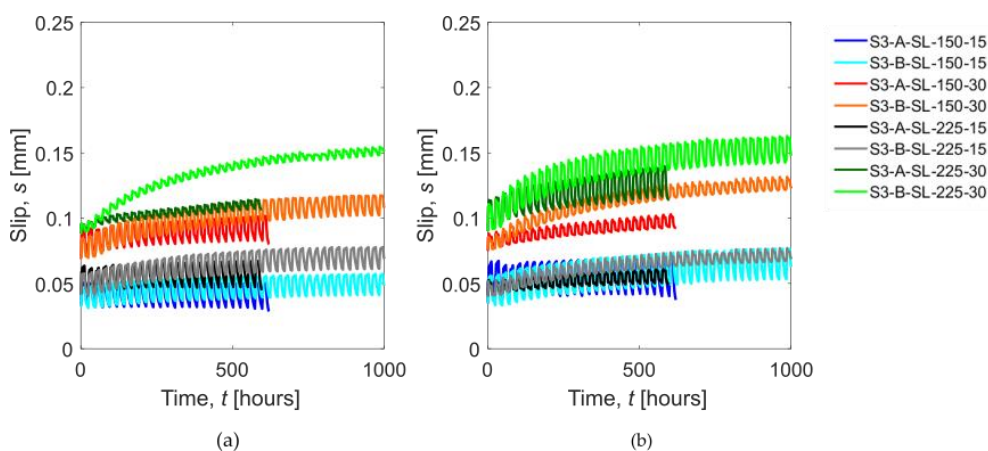
Figure 7.6. Comparison of the slip evolution with time obtained in series S3-A and S3-B for groove thicknesses of: (a) 7.5 mm; (b) 10 mm.

Comparison between these series seems to indicate a somewhat greater influence of temperature in the S3-B series, mainly in those cases loaded at 30% P_u, which could be attributed to the higher mean and maximum temperatures in the S3-B series and being closer to the T_g of the adhesive.

Finally, Figure 7.7 depicts the comparison of the slip evolution with time between S2, (with a steady temperature of 37.7 °C) and S3-B (with a trapezoidal cyclic temperature between 24.6 and 39.2 °C and a mean temperature of 31.3 °C).
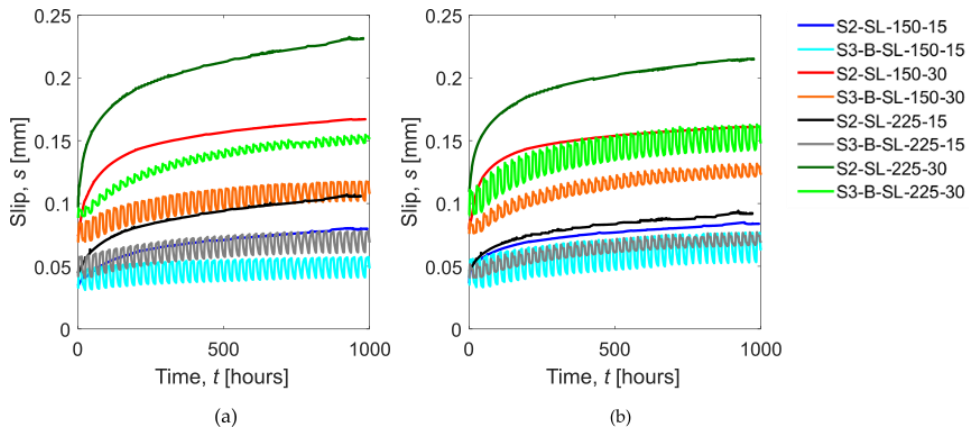
Figure 7.7. Comparison of the slip evolution with time obtained in series S2 and S3-B for groove thicknesses of: (a) 7.5 mm; (b) 10 mm.

The lower values of slip obtained in the S3-B series could be attributed to the fact that the mean temperature in S3-B was 6.4 °C lower than that of the S2 series, even though the peak temperature of the cycle was slightly higher than the steady temperature in S2 (see Table 7.2).

To sum up, in general terms the effect the temperature exerted on the sustained loading behaviour became more significant as the average temperature in the NSM CFRP-concrete joint moved closer to the T_g of the adhesive.

7.3.2.3   Effect of preconditioning

As shown in Figure 7.4, results from series S4 indicate that the thermal preconditioning of the specimens had a significant effect - particularly important in the first temperature cycles - on the bonded joint response. This behaviour was also observed in [60] where a very high increase in FRP strain was observed in specimens under a sustained load of 40% P_u, when the temperature was raised from 20 to 50 °C. However, after around three cycles, the slip evolution stabilized and similar increases of slip with time were obtained among the S1, S3-A and S4 series, probably because the average temperatures inside the NSM groove were relatively low (18.7 °C for series S1, 25.6°C for S3-A and 26.8 °C for S4).

7.3.3 Effect of groove thickness

While in the previous sections the comparisons were made among different series, in this section the effect of the groove thickness is analysed. Since the instantaneous slip caused by the percentage of sustained load is different for 7.5 and 10 mm groove thicknesses, to better compare its effect, the evolution of the slip increase, defined as the slip occurring after the instantaneous slip (Δs), is presented in Figure 7.8 for the different series. For series S4 (Figure 7.8d), the instantaneous slip was taken three first cycles after the test started to avoid the effect of the preconditioning.
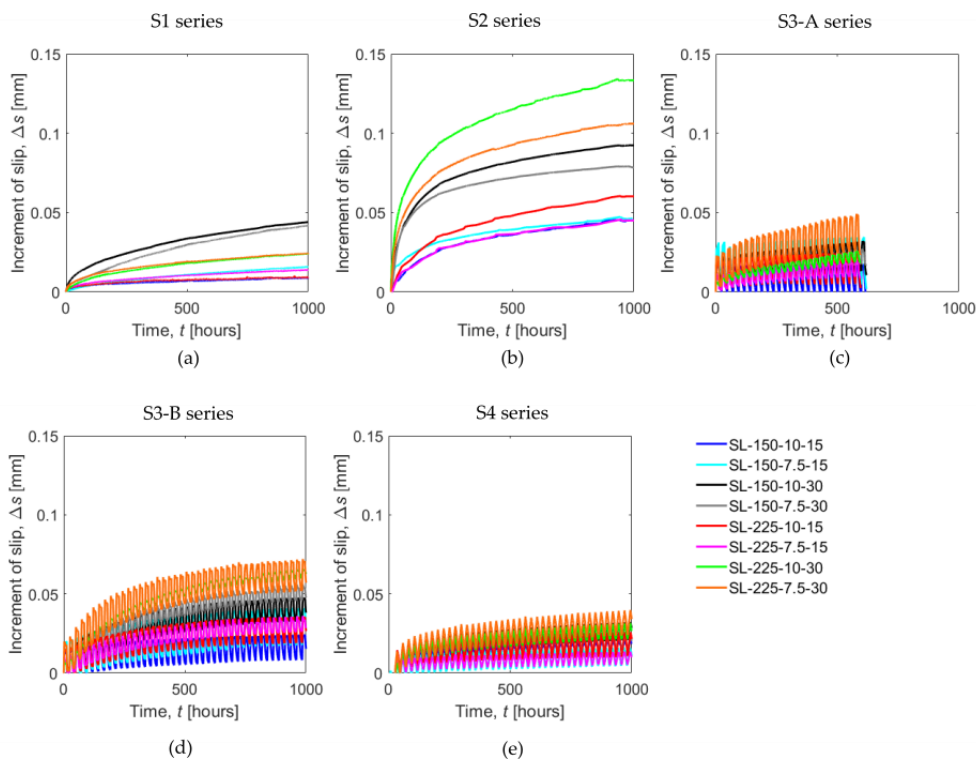
Figure 7.8: Increment of slip at the loaded end obtained in (a) S1 series; (b) S2 series; (c) S3-A series; (d) S3-B series; (e) S4 series.

In general, the effect of the groove thickness was small in comparison with other parameters such as the sustained load level. At $t = 1000$h, the maximum difference in slip evolution between the specimens with different groove thicknesses was found in S2 series for specimens loaded at 30% P_u and with a bonded length of 225 mm. This was equal to 0.016 mm.

In series S1, slightly higher increases of slip were obtained in specimens with narrower grooves, probably because more sustained loads were applied to the 7.5 mm specimens

compared to the 10 mm ones [160]. However, in the S2 and S3-B series, where temperature had a more significant effect, as the average temperature increased, the 10 mm specimens experienced higher slips than the 7.5 mm specimens did, especially those under 30% P_u. This might be attributed to more of the adhesive surface being in contact with the ambient temperature, thus causing greater damage to the bonded joint.

7.4 PSL bond behaviour of NSM CFRP-concrete specimens

The residual bond response of the NSM CFRP-concrete specimens after sustained loading, in terms of ultimate load ($P_{u,PSL}$), stiffness ($K_{e,PSL}$) and post-sustained loading (PSL) failure mode, was studied using instantaneous pull-out tests until failure. Table 7.3 presents the ratio of $P_{u,PSL}$, obtained from the PSL tests, with respect to the value of the instantaneous P_u for each experimental series. Due to gripping/un-gripping operations during long-term and subsequent pull-out tests, four specimens experienced a premature FRP failure in the zone of the gripping system (S1-PSL-225-10-15, S1-PSL-225-10-30, S1-PSL-225-7.5-30, S2-PSL-150-7.5-15). While the results from these specimens have been considered non-representative and consequently removed from the analysis of ultimate load, they were, however, retained for the stiffness comparisons (since the initial part of the curve could be used).

Table 7.3. PSL results.

Series	Specimen	$\dfrac{P_{u,PSL}}{P_u}$	$\dfrac{K_{e,PSL}}{K_e}$
	S1-PLT-150-10-15	1.05	0.95
	S1-PLT-150-7.5-15	0.95	0.94
	S1-PLT-150-10-30	1.03	0.84
S1	S1-PLT-150-7.5-30	0.99	0.90
	S1-PLT-225-10-15	*	1,11
	S1-PLT-225-7.5-15	0.95	0.78
	S1-PLT-225-10-30	*	0,93
	S1-PLT-225-7.5-30	*	0,81
S2	S2-PLT-150-10-15	1.08	1.02
	S2-PLT-150-7.5-15	*	1.02

	S2-PLT-150-10-30	1.10	0.85
	S2-PLT-150-7.5-30	1.03	0.65
	S2-PLT-225-10-15	1.06	0.79
	S2-PLT-225-7.5-15	1.07	0.92
	S2-PLT-225-10-30	1.12	0.67
	S2-PLT-225-7.5-30	0.98	0.57
	S3-B-PLT-150-10-15	1.07	1.05
	S3-B-PLT-150-7.5-15	0.93	0.95
	S3-B-PLT-150-10-30	0.89	0.90
	S3-B-PLT-150-7.5-30	0.86	0.77
S3-B	S3-B-PLT-225-10-15	0.88	0.89
	S3-B-PLT-225-7.5-15	0.97	0.96
	S3-B-PLT-225-10-30	0.96	0.61
	S3-B-PLT-225-7.5-30	0.80	0.71
	S4-PLT-150-10-15	0.91	0.94
	S4-PLT-150-7.5-15	0.97	1.10
	S4-PLT-150-10-30	0.99	0.82
	S4-PLT-150-7.5-30	0.99	0.88
S4	S4-PLT-225-10-15	1.01	0.99
	S4-PLT-225-7.5-15	1.04	0.89
	S4-PLT-225-10-30	0.92	0.73
	S4-PLT-225-7.5-30	1.06	0.60

7.4.1 Effect on the ultimate load and failure mode

Overall, no significant differences were obtained in the PSL ultimate load compared to the instantaneous characterization values (the mean ratio of all specimens being equal to 0.99). Likewise, ratios close to the unity were observed when analysing the global results of groups of specimens under either 15% or 30% P_u.

Some aspects should be highlighted when analysing the different series. For instance, series S1 does not present any significant effects from the sustained loading conditions, despite

presenting a mean global reduction of $P_{u,PSL}$ lower than 1%, and no relevant differences being observed either for load values or bonded length and groove thickness. Some differences, however, can be identified in series S2 and S3-B. For example, series S2 presents a mean global increment of 6.3% (probably due to the post-curing effect on the adhesive) with similar values for the two load levels, and a slightly more pronounced increment for the 10 mm groove thickness (9%) than for the 7.5 mm thickness (3%). Meanwhile, for S3-B in terms of temperature cycles, an 8% global reduction can be seen. This influence is greater in the specimens loaded at 30% P_u (12% reduction) than in those loaded at 15% P_u (4% reduction), which might indicate that there the temperature cycles exert some influence, albeit mainly for the higher sustained load value. On the other hand, with a final global mean value of the ratio close to the unity, no clear tendencies are observed in series S4 with temperature cycles but without preconditioning. The results presented are in accordance with the observations made in Fernandes *et al.* [109], where small decreases of the ultimate load were observed in specimens subjected to outdoor environmental conditions (around 12%).

As for the failure mode of the NSM CFRP-concrete joint, no differences were generally obtained in comparison with the instantaneous characterization, with the main failure mode being the cohesive failure in the concrete for specimens with a 7.5 mm groove thickness and failure in the FRP-adhesive interface for specimens with a 10 mm groove thickness. However, specimens S3B-PSL-150-10-30 and S3B-PSL-225-10-30 experienced a failure in the adhesive-concrete (A-C) interface, which indicates a decrease in the bond at the interface. Figure 7.9 shows two examples of failure modes obtained from PSL tests: a failure in the A-C interface obtained in specimen S3-B-PSL-225-10-30 (Figure 7.9a), and a cohesive concrete failure obtained in specimen S3-B-PSL-225-7.5-30 (Figure 7.9b).

Figure 7.9. (a) S3-B-PSL-225-10-30 failure in the A-C interface; (b) S3-B-PSL-225-7.5-30 cohesive failure in the concrete.

7.4.2 Effect on the stiffness

The PSL load-slip load is illustrated in Figure 7.10 (black curve) together with the load-slip curves obtained in the instantaneous characterization (blue curve) for specimens PSL-225-10-30 from each series (S1, S2, S3-B and S4). Note that in Figure 7.10a, the specimen experienced a premature failure in the CFRP strip (marked with an X in Figure 7.10). A reduction in the initial stiffness was observed in all specimens, but there was an overall recovery as the load in the instantaneous test surpassed the value of the sustained loading. This effect is attributed to the unloading-loading path as a combination of damage and creep effects. During the sustained loading tests, the activated length was lower than the total bonded length (L_b) and, consequently, the effects of sustained loading affected only part of L_b. Subsequently, as the load was increased in the monotonic PSL test, as the load increased, the activated length increased and moved towards the free end and joint stiffness was recovered because this zone had not been activated during the sustained loading test.
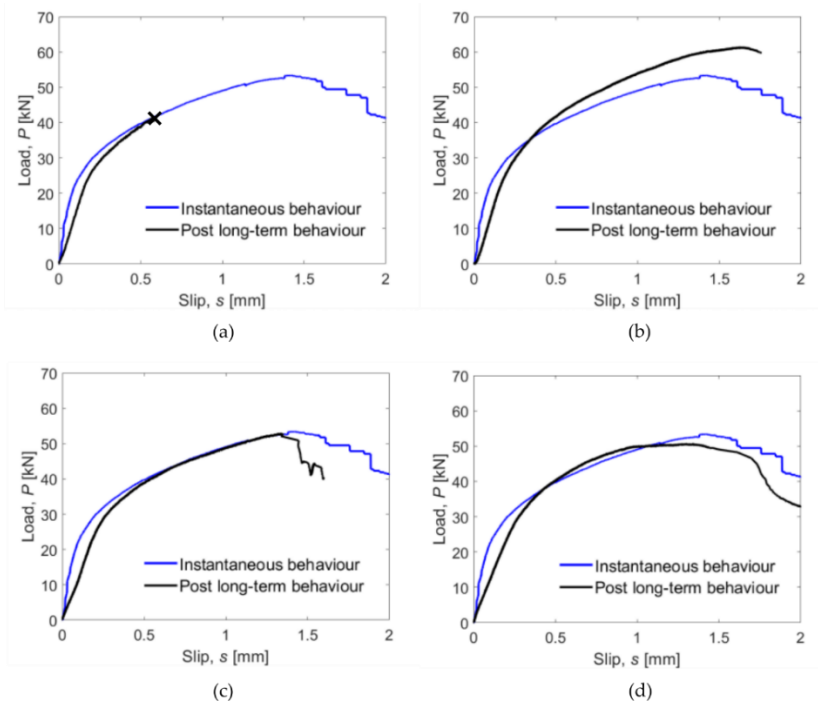
Figure 7.10: Comparison between the instantaneous behaviour and the post-SL behaviour
of the specimen PSL-225-10-30 in (a) S1, (b) S2, (c) S3-B and (d) S4.

When the observed values of all the specimens are considered, the global overall reduction of the stiffness was about 14% (see Table 7.3). This reduction was more noticeable for specimens loaded under 30% of the initial ultimate load, and, in particular, those from series S2, thus showing that the higher the sustained load level and average temperature are, the greater the decrease in stiffness is. These observations agree with the results presented in Fernandes *et al.* [109], where a significant decrease in the stiffness of the bonded joint was observed in specimens under cyclic environmental conditions.

7.5 Conclusions

The present work experimentally studied the bond behaviour of an NSM CFRP-concrete joint under sustained loading and different service temperature conditions. Four experimental campaigns consisting of eight NSM CFRP-concrete pull-out single shear tests (SL tests) were performed under sustained loading for 1000 hours inside a climatic chamber at different temperature conditions, combining steady and cyclic objective temperatures. After that, post-

sustained loading tests (PSL tests), where the specimens were tested under monotonic loading until failure, were carried out.

From the SL tests the following conclusions can be drawn:
- Overall, the slip values obtained in specimens under 15% and 30% P_u were proportional to the applied load;
- Similar slips were obtained in specimens with short and long bonded lengths under a sustained loading level of 15% P_u;
- Higher slips were obtained in the 10 mm grooved specimens in comparison with the 7.5 mm grooved specimens under high steady temperatures;
- Significant slip oscillations, caused by the thermal expansion of the materials, were observed in series with temperature cycles;
- As the mean temperature of the thermal cycle increased, so too did the slip at the loaded end;
- Specimens under temperature cycles (S3-A, S3-B and S4) experienced increases of slip that ranged between S1 and S2 slips, since the temperatures in the NSM groove fell between 20 and 40 °C;
- The decisive effect of the preconditioning cycles was observed during the initial loading days as the specimens that had been submitted to preconditioning temperature cycles experienced lower increases in slip during the first temperature cycles.

From the PSL tests the following conclusions can be drawn:
- The ratio of the PSL ultimate load with respect to the initial instantaneous ultimate load was globally close to unity. However, some differences were observed in series S2 with its global increment of 6.3% and in series S3-B with a global reduction of 8%;
- Overall, no change in the failure modes were observed in the instantaneous post-sustained loading tests;
- A global reduction in the initial stiffness in the load-slip curve was observed, followed by its recovery at higher loads as the load of the PSL test surpassed the value of the sustained loading.

During their service life, civil structures are submitted to a combination of sustained loading and cyclic environmental conditions. This study has helped to appreciate and understand the effect thermal cycles have in constantly loaded CFRP-concrete joints. The bonded joints have been shown to be affected by creep and have their mechanical properties reduced. Therefore, it can be concluded that environmental conditions must be taken into account when designing of CFRP strengthened civil structures.

While this study limited the sustained loading tests to 1000 hours, further studies would need to extend this further, especially for higher average temperatures where the high increases of slip were observed in this work.

8 Discussion

This chapter presents the discussion of the results obtained through the different parts of the thesis. The discussion is divided into four parts that correspond to the four articles presented in this thesis.

8.1 Bond behaviour of NSM CFRP-concrete specimens under monotonic instantaneous loading

The instantaneous bond behaviour of NSM CFRP-concrete specimens is highly affected by the geometrical and mechanical parameters of the bonded joint. Moreover, the definition of the local bond-slip law can derive in a different global load-slip response. Paper A was focused on studying, from a numerical point of view, the effect of the main parameters of several bond-slip laws (the bond-shear strength and its corresponding slip, the maximum slip, and the friction branch) on the global response of the bonded joint, in terms of ultimate load, effective bonded length, slip, strain and bond shear stress distributions, and load-slip curves. Additionally, experimental instantaneous single shear tests of NSM CFRP-concrete specimens were carried out combining two bonded lengths and two groove thicknesses.

A numerical procedure based on a finite differences model was proposed to solve the differential equation of the NSM CFRP-concrete joint bond response. Using this numerical methodology, a parametric study on the effect of the bond-slip law on the global behaviour of the bonded joint was performed. Six bond-slip laws taken from the literature were implemented and compared in terms of load-slip response and slip, bond shear stress and strain profiles along the bonded length, shown in Figure 8.1.
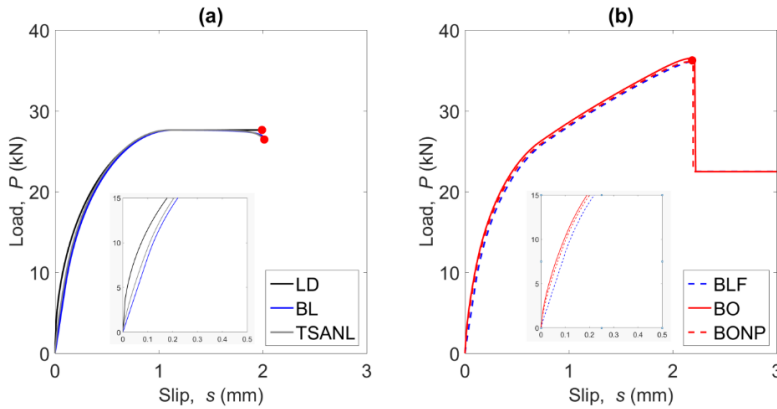
Figure 8.1: Comparison of the load-slip curves obtained using (a) bond-slip laws not including a friction stage and (b) bond-slips including a friction stage.

It was observed that significant differences were obtained in models including a friction branch, where the ultimate load did not stabilize with the increase of the bonded length, contrarily to the specimens not including a friction stage, where a stabilization of the ultimate load was observed. This was caused by the fact that when the bonded joint started to debond, the unbonded length was still transmitting force, increasing the carrying capacity of the bonded joint until failure. Furthermore, from Figure 8.1 it can be seen that bond-slip laws with the steeper ascending elastic branches (LD, BO and BONP), showed the highest stiffness on the load-slip curve.

Furthermore, from the numerical procedure, the slip, the strain in the FRP and the bond shear stress distribution along the bonded joint were calculated at the situation of imminent failure using each of the bond-slip laws, presented in Figure 8.2.
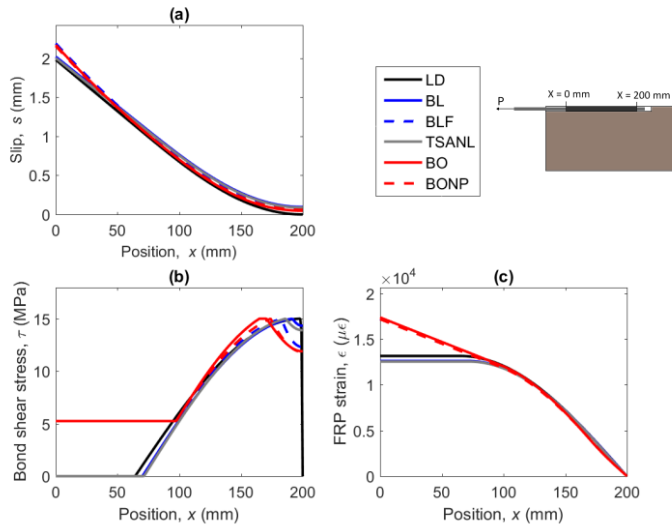
Figure 8.2: (a) Slip, (b) bond shear stress and (c) FRP strain distributions obtained using the different bond-slip laws.

As observed in Figure 8.2a, the shape of the bond-slip law had a small effect on the slip profile along the FRP. Furthermore, an evident difference between the models with and without friction can be observed in the bond stress and the strain distributions along the bonded length (Figure 8.2b and Figure 8.2c, respectively).

The shape of the bond-slip law had a negligible effect on the slip distribution along the FRP and very small differences were observed in the load-slip curves. However, a continuous increase on the FRP strain and a plateau on the bond shear stress after the initiation of the debonding were observed for bond-slip laws including a friction stage.

In order to validate the numerical procedure, four pull-out single shear test configurations were tested instantaneously compared to the numerical results. From the experimental results, it was observed that specimens with a groove thickness of 7.5 mm obtained a maximum load around 7-10% higher compared to the specimens with a groove thickness of 10 mm. This was attributed to the fact that the shear stiffness of the 10 mm grooved specimens was higher than 7.5 mm grooved specimens therefore the strain transmitted to the concrete was lower. Furthermore, an increasing effect on the ultimate load was observed as the bonded length increased: specimens with a bonded length of 225 mm obtained an average increase on the ultimate load of 29.2% in comparison to specimens with a bonded length of 150 mm.

Regarding the failure mode, specimens with a groove thickness of 7.5 mm obtained a cohesive failure within the concrete, causing a sudden drop of the load, while specimens with a groove thickness of 10 mm faced a failure in the FRP-adhesive interface which derived in a constant decrease of load as the slip increased. The difference on the failure mode was attributed to the fact that the cross-section of the 7.5 mm groove was lower in comparison with the 10 mm groove, which means that higher strain was transmitted to the concrete, which lead to the cohesive failure. For specimens with a 10 mm groove thickness, which presented a frictional stage after achieving the ultimate load, a bilinear bond-slip law with a friction stage is assumed.

From the experimental observations, a local bilinear bond-slip law was adjusted to the bond behaviour of specimens with a groove thickness of 7.5 mm. For specimens with a groove thickness of 10 mm, a bilinear plus friction bond-slip law was considered to take into account the effect of a frictional stage at the debonding phase. Implementing the calibrated bond-slip laws in the finite differences model, the resultant load-slip curves were obtained for each specimen configuration. Figure 8.3 shows the comparison between numerical and experimental load-slip curves for each NSM CFRP-concrete configuration.
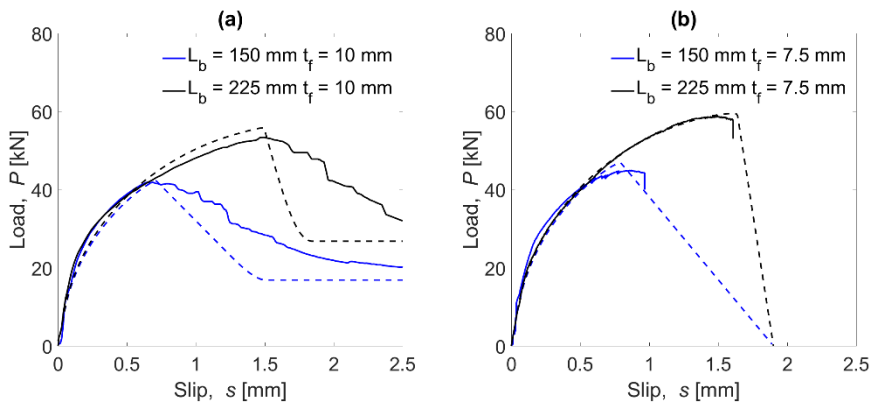
Figure 8.3: Comparison between the numerical and experimental load-slip curves for (a) specimens with a 10 mm groove thickness and (b) specimens with a 7.5 mm groove thickness.

From Figure 8.3, it can be seen that the numerical results presented a close agreement with the experimental results in terms of stiffness and ultimate load.

The parametric study performed on this investigation combined six bond-slip laws and studied the effect of the bond shear strength (τ_{max}) and its corresponding slip (s_1), the maximum slip (s_f) and the friction bond shear strength (τ_f). A range of values was provided for each study

165

variable and the ultimate load and the effective bonded length were evaluated for each case. Figure 8.4 shows the parameters studied in the parametric study.
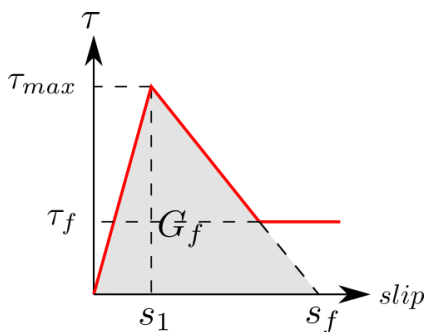
Figure 8.4: Main parameters of the BL and BLF models.

The bond shear strength (τ_{max}) had an increasing effect on the fracture energy, with the consequent increase on the ultimate load of the bonded joint. On the other hand, the effective bonded length decreased as expected, as higher local bond shear strength, less bonded length is needed to carry the total load.

The corresponding slip at the bond shear strength (s_1) had a small effect on the ultimate load since the shifting of this point caused very small variations of the fracture energy. On the other hand, a slight increase on the effective bonded length could be observed because higher slips are obtained in the elastic stage.

An increase in the maximum slip (s_f) also implied an increase in the fracture energy. As a consequence, s_f had an increasing effect on the ultimate load and the effective bonded length. Bond-slip laws including a friction stage were less affected by the increase of s_f, since the total area under the bond-slip law experienced a lower decrease.

The friction bond-shear stress (τ_f) had a clear increasing effect on the ultimate load because the points of the bonded joint that were debonded could still transfer some shear load to the bonded joint. Furthermore, it was observed that the increase in the bond shear strength caused an increase on the area under the bond-slip law (fracture energy, G_f) which led to an increase on the ultimate load of the bonded joint.

This article demonstrated the importance of the correct calibration of the local behaviour of the bonded joint. The shape and parameters (bond shear strength and its corresponding slip, the maximum slip and the friction stage) of the bond-slip law has an enormous effect on the load-slip curve and the strain, stress and slip profiles of the bonded joint. This study also showed that by implementing a numerical model based on a finite differences model, it is possible to

accurately predict the instantaneous response of NSM CFRP-concrete specimens independently on the bond-slip law shape.

8.2 Effect of sustained loading on NSM CFRP-concrete specimens

Service conditions such as sustained loading have been proved to have an important effect on the bonded joint performance. Paper B aimed to study the bond behaviour of NSM CFRP-concrete joints and the tensile behaviour of an epoxy adhesive under a service sustained load levels (15% and 30% the ultimate load for NSM CFRP-concrete specimens, and 15%, 30% and 50% the tensile strength for the adhesive specimens) for 1000 hours under 20 ˚C and 55% RH from experimental and numerical points of view.

To study the instantaneous experimental behaviour of NSM CFRP-concrete specimens, the experimental campaign presented in paper A was extended and specimens with a groove thickness of 10 mm and a bonded length of 300 mm were tested. For specimens with a groove thickness of 10 mm, it was observed that the ultimate load did not stabilize with the increase of the bonded length, meaning that friction was increasing the total load transmitted by the bonded joint.

The adhesive was initially characterized by using instantaneous tensile tests, obtaining a tensile strength of 27.2 MPa and an elastic modulus of 10.7 GPa. In the sustained loading tensile tests of the adhesive, the evolution of strain, creep compliance and creep coefficient were obtained. In general terms, the higher sustained load was, the higher evolution of strain was observed. The final strain obtained in the sustained loading test was higher than that obtained in the instantaneous test, probably due to an internal structural reorganization that allowed to withstand the load without failure. Figure 8.5 presents the creep compliance curves obtained for the three sustained loading levels.
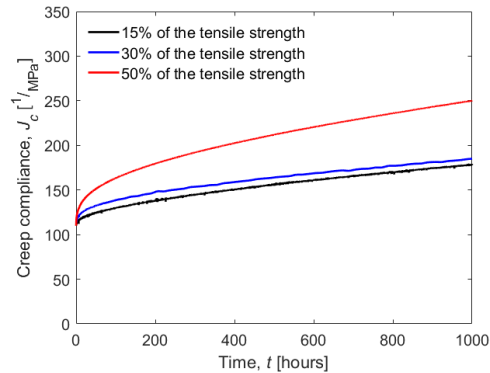
Figure 8.5: Creep compliance curves obtained from epoxy specimens under 15%, 30% and 50%the ultimate tensile strength.

The creep compliance curves of specimens under 15% and 30% were coincident, while the curve of specimens under 50% was clearly higher, indicating that the adhesive presented a linear viscoelastic behaviour until sustained load levels of 30% the tensile strength. Therefore, a power function to represent the increase of the creep coefficient with time could be adjusted for adhesive specimens under sustained loading levels up to 30% the tensile strength.

Regarding the pull-out single shear test results, it could be observed that as the bonded length increased, the ultimate load increased as well. However, it is worth noticing that the increase of ultimate load between specimens with L_b = 150 mm and L_b = 225 mm, the increase of load was 27.3%, while the increase between specimens with L_b = 225 mm and L_b = 300 mm, the increase of load was 17.8%

in Figure 8.7 it can be seen that the NSM CFRP-concrete specimens under sustained loading also present an initial stage with a high non-linear increase of slip, followed by a second stage where the evolution of slip became more linear. Furthermore, it was observed that specimens under 30% the ultimate load, obtained higher evolutions of slip in comparison with specimens under 15% P_u, as expected. Regarding the effect of the groove thickness, specimens with a groove thickness of 7.5 mm obtained slightly higher evolution of slips than 10 mm grooved specimens. This was attributed to the fact that specimens with narrower grooves were loaded under a higher sustained load, because the ultimate instantaneous load was higher in comparison with wider grooved specimens. From the comparison of specimens with different bonded lengths, specimens under 30% the ultimate load and a short bonded length (150 mm) experienced higher increases of slip with time. This effect was explained because shorter bonded joints are exposed to a higher average bond shear stress, which can cause more damage

168

on the bonded joint with time. On the other hand, no effect of the bonded length of the joint was observed in specimens under 15% the ultimate load.

Using the numerical methodology developed in paper A, a degradation model of the bond-slip law was proposed and implemented to take into account the creep behaviour of the bonded joint. The damage model was based on the concept of a degradation of the ascending stiffness due to creep and a strength reduction factor. The creep coefficient ($\phi(t)$) was previously adjusted from the experimental results of the adhesive specimens under sustained load. On the other hand, the strength reduction coefficient was proposed as a power function ($\alpha \cdot t^\beta$) that was calibrated from the NSM CFRP-concrete specimens under sustained loading. The strength reduction coefficient did not affect specimens under 15% the ultimate load because in these cases the bond shear stress at the loaded end did not reach the bond shear strength. Figure 8.6 presents the degradation model of the bond-slip law assumed in paper B, together with the equations of the evolution of stiffness (K_e) and bond shear strength (τ_{max}) with time (t).

$$\tau_{max}(t) = \frac{\tau_{max,0}}{1 + \alpha \cdot t^\beta}$$

$$K_e(t) = \frac{K_{e,0}}{(1 + \Phi(t))}$$
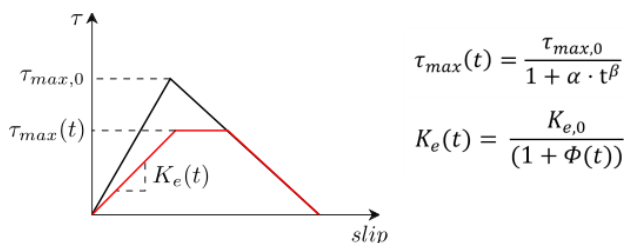
Figure 8.6: Degradation of the bond-slip law under sustained loading with time.

The parameter β is a coefficient affecting the bond strength. In this paper, it was experimentally adjusted to a mean value of 0.45. On the other hand, an increasing relationship between the parameter α and the average bond stress normalized with the bond shear strength was defined and calibrated to experimental results in each situation. Numerical and experimental results were compared in terms of evolution of slip at the loaded end with time. Figure 8.7 shows the comparison of the evolution of slip numerically and experimentally obtained.
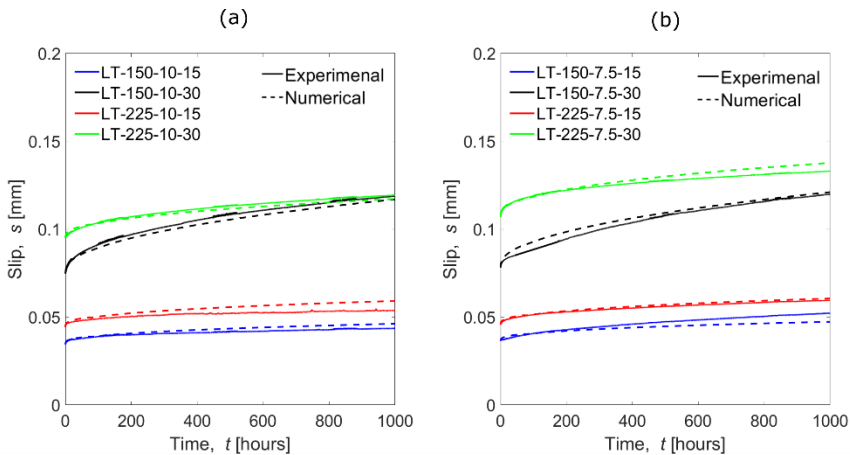
Figure 8.7: Comparison of the experimental and numerical evolutions of slip for (a) specimens with 10 mm groove thickness and (b) specimens with 7.5 mm groove thickness.

A close agreement between the numerical and experimental results was observed. However, the numerical model was adjusted for the selected range of parameters, therefore, there is a need to expand the number of test and study variables to further investigate this topic.

To sum up, this paper presented a numerical methodology that can predict the NSM CFRP-concrete response under sustained loading and room conditions. This methodology is its highly adaptable to many test configurations and environmental conditions. Furthermore, an experimental programme on sustained loading tensile tests and pull-out single-shear specimens at room temperature has been presented. From this study it has been seen that the sustained tensile tests of adhesive specimens provide a good prediction on the reduction of the stiffness of the bond-slip law of the FRP-concrete joint with time.

8.3 Adhesive specimens under the combination of sustained loading and service temperatures

It is well-known that the adhesive is the most sensitive material of the bonded joint to service conditions. The combination of sustained loading and service temperatures near the glass transition temperature of the adhesive can cause a dramatic decrease on the thermomechanical properties of the material, which can directly affect the carrying capacity of the structure.

Paper C aimed to experimentally study the effect of steady and cyclic service temperatures on the evolution of the axial strain of adhesive dog-bone specimens. In total, five experimental series consisting of sustained tensile loading tests were performed under three load levels (15%,

170

30% and 50% the tensile strength) for 1000 hours in a climatic chamber. The first experimental series was previously presented in paper B, and in this paper the results are compared with the other experimental series. Furthermore, to study the effect of service conditions on the residual behaviour of adhesive specimens, Differential Scanning Calorimetry (DSC) and monotonic tensile tests until failure were carried out after sustained loading tests.

In series C1 and C2, specimens were submitted under steady service temperatures of 20 ˚C and 40 ˚C, while in series C3-A, C3-B and C4, temperature cycles of 18-38 ˚C, 22-43 ˚C and 20-40 ˚C were applied to the specimens, respectively.

Figure 8.8 presents the evolution of strain with time for all the experimental series. From the strain evolution, a primary stage with a high non-linear increase of strain and a second stage with a more linear evolution of strain were observed. As expected, as the sustained load level increased, the time-dependent strain increased as well.
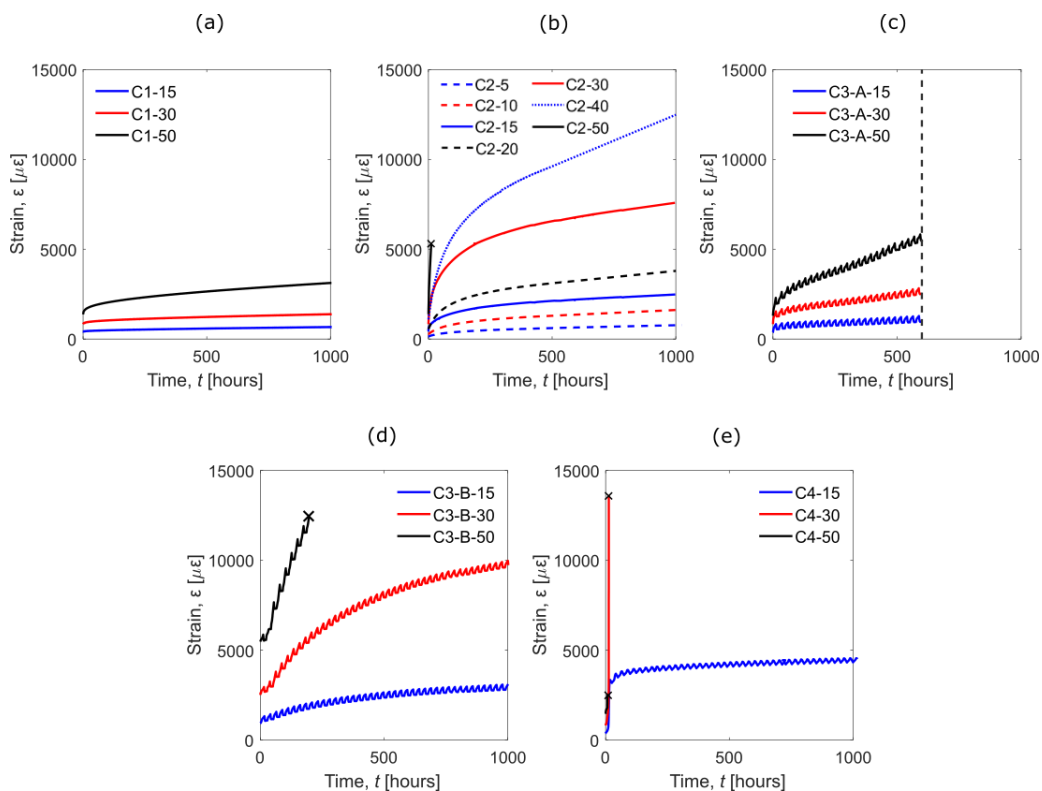
Figure 8.8: Increase of strain with time in series (a) C1, (b) C2, (c) C3-A, (d) C3-B and (e) C4.

Service temperature had a noticeable effect on the evolution of axial strain with time: the higher average temperature was, the higher the time-dependent strain was obtained. Moreover, only specimens from series with lower service temperatures (series C1 and C3-A

171

under 20 ˚C and 18-38 ˚C, respectively) were able to withstand 50% the tensile strength, while in the other series, with temperatures closer to the T_g, specimens at this sustained load level failed after some hours of loading. This was probably because the combination of sustained loading and high service temperatures caused a high increase of time-dependent strain which could not be withstood by the adhesive.

From the creep compliance curves showed in paper B, it was observed that in series C1 (20 ˚C) specimens presented a linear viscoelastic stage under sustained loading levels up to 30% the tensile strength. In the experimental series C2, it was observed that the linear viscoelastic behaviour could be assumed for sustained loading levels between 5% and 15% the tensile strength. Therefore, it was concluded that as the temperature in the epoxy increased, the upper limit of the linear viscoelastic behaviour decreased.

Focussing on the study of temperature cycles, it was observed that the adhesive specimens experienced strain oscillations with the thermal cycles. However, the amplitude of these oscillations was not significant in comparison with the total evolution of strain with time. These strain oscillations were higher as the sustained load level was higher, and a general decrease of the amplitude of strain was observed with time.

The time-dependent strain obtained in specimens from C3-B series (under temperature cycles) was higher than expected, considering that the average temperature of the thermal cycle was lower in comparison with temperature from series C2. The fact that the maximum temperature in series C3-B (43 ˚C) was higher than the temperature un series C2 (40 ˚C) might have caused more molecular motions in the specimens which damaged more the specimen.

Specimens without preconditioning (C4 series) presented a very high increase of strain during the first thermal cycles. Moreover, the lack of preconditioning caused the failure of all specimens under 30% and 50% the tensile strength after few hours of loading.

After the sustained loading tests, epoxy specimens that did not fail were tested under monotonic tensile tests, and a DSC tests were performed to study their residual mechanical and thermophysical properties, respectively.

From the tensile tests, a decrease on the tensile strength and elastic modulus were generally observed with respect to the instantaneous characterization before sustained loading. Furthermore, it was observed that as the sustained load level increased, the mechanical properties reduced.

In comparison with series C1, specimens from series C2 obtained slightly higher tensile strengths attributed to the post-curing effect that took place at high service temperature.

Regarding the series with temperature cycles, specimens from series C3-A obtained a tensile strength and elastic modulus that ranged between that of series C1 and C2, probably because the average temperature of the thermal cycle also ranged between the temperatures in C1 and C2. On the other hand, specimens from C3-B obtained similar results as the specimens in C2 even though the average temperature of the thermal cycle was lower than the temperature in C2. The maximum temperature of the thermal cycle caused a post-curing effect on the adhesive specimens, increasing their tensile strength. Finally, from the comparison of specimens from C4, a substantial decrease on the mechanical properties due to the lack of preconditioning was observed.

From the DSC tests carried out after sustained loading tests, the curing degree (α) and the T_g were obtained for each specimen tested. The values of T_g and α increased after sustained loading tests, indicating a post-curing effect developed during loading. Specimens that were subjected to thermal cycles obtained higher increases of T_g than specimens under steady temperatures. As the average temperature increased, T_g increased as well, which was attributed to a higher post-curing creating more cross-links between the molecules of the adhesive.

This study has shown that the creep response of this epoxy adhesive specimens is strongly affected by environmental conditions and sustained loading. The higher the sustained load levels and average temperatures are applied to the adhesive specimens, the higher the strain with time is obtained. Moreover, this study has highlighted the importance of the preconditioning period before loading.

Finally, this investigation has proved that the thermomechanical properties of the adhesive are highly affected by service conditions, which is especially important to correctly design FRP strengthening systems.

8.4   NSM CFRP-concrete bond response under the combination of sustained loading and service temperatures.

The mechanical properties of epoxy adhesives dramatically decrease once the temperature approaches the T_g of the material. For exposure temperatures lower than T_g, the decrease of the adhesive's mechanical properties can be really significant (investigated in Paper C) and it results necessary to investigate how is this affecting the global behaviour of the NSM CFRP-concrete joint.

The objective of Paper D was to investigate the bond response of the NSM CFRP-concrete joint under service sustained load levels (15% and 30% the ultimate load) and different service temperatures below the T_g (steady and cyclic temperatures) for 1000 hours from an experimental point of view. Moreover, instantaneous Post-Sustained-Loading tests (PSL) were carried out after each series to evaluate the change on the instantaneous response. The first experimental series under sustained loading was previously presented and discussed in paper B, in this paper, the comparison with other experimental series will be performed.

Since the experimental programme of NSM CFRP-concrete specimens under sustained loading was performed simultaneously with the sustained tensile tests of adhesive specimens, five experimental series were carried out in total. Figure 8.9 shows the objective temperature (red curves), the temperature on the specimens' surface (blue curves) and temperature inside the groove (black curves) for each experimental series.
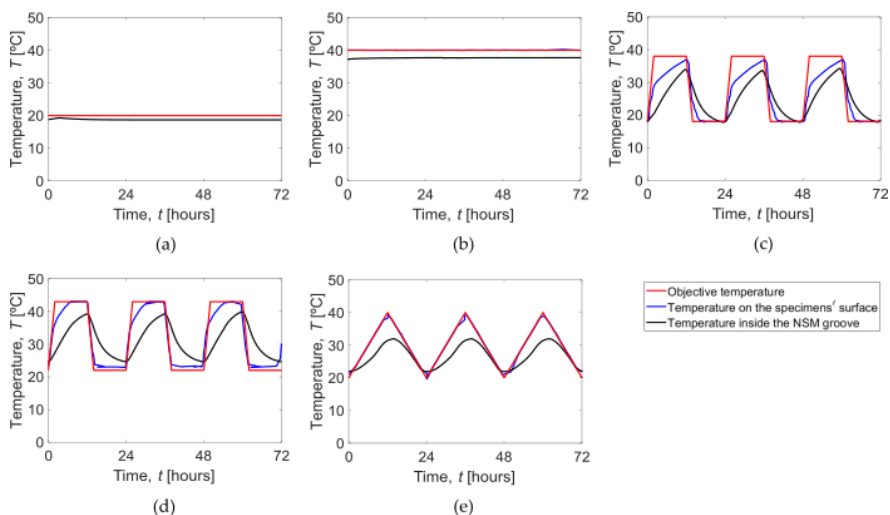
Figure 8.9: Temperature in the experimental series (a) S1, (b) S2, (c) S3-A, (d) S3-B and (e) S4.

The temperature on the specimens' surface was slightly lower than the objective temperature due to thermal inertia effects. Furthermore, in the series with thermal cycles, the temperature inside the NSM was lower than the surface's temperature, but in series under steady temperatures, this difference of temperature was not significant.

Figure 8.10 depicts, for each experimental series, the evolution of slip at the loaded end for all the specimen's configurations.
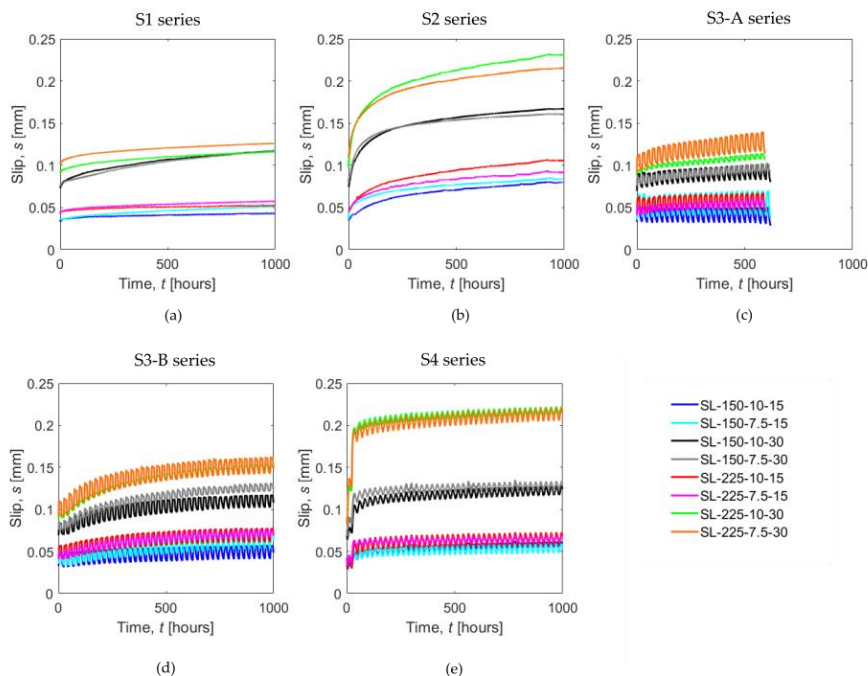
Figure 8.10: Slip at the loaded end obtained in series (a) S1, (b) S2, (c) S3-A, (d) S3-B and (e) S4.

As a general trend, NSM CFRP-concrete joints at the higher environmental temperatures obtained the higher slips at the loaded. NSM CFRP-concrete specimens under cyclic temperatures experienced slip oscillations with time caused by the thermal expansion of the materials. These slip oscillations were relatively high in comparison with the increase of slip with time, as observed in the tensile sustained loading tests of adhesive specimens (paper C).

From the comparison of specimens loaded at 15% and 30% the ultimate load in series S1, it could be seen that the slip was proportional to the load applied, indicating that the creep behaviour did not depend on the sustained load level, therefore, they presented a linear viscoelastic behaviour.

In all the experimental series, specimens with different bonded lengths and a sustained loading level of 15% ultimate load obtained similar slips. This could be caused because specimens at this load level experienced a linear viscoelastic behaviour. From the creep compliance curves of obtained from the tensile sustained loading tests of adhesive specimens (paper C), it was observed that in experimental series S2 (or C2 in paper C) the linear viscoelastic behaviour could be considered until a sustained load level of 15% ultimate load.

Overall, specimens with different groove thickness obtained a similar slip evolution, however, in series S2, specimens with a groove thickness of 10 mm obtained higher slips those with a groove thickness of 7.5 mm. Furthermore, the slip differences were higher as the sustained load level increased as well. Therefore, as the load level and the ambient temperature increased, higher differences of slip were observed and temperature had more effect on specimens with thicker layers of adhesive.

Experimental series under cyclic temperatures (S3-A, S3-B and S4) obtained increases of slip ranging between the results obtained in experimental series S1 and S2. This was attributed to the fact that the average temperature in the temperature cycles laid between 20 °C and 40 °C.

The effect of the preconditioning stage was studied through the experimental series S4. In this experimental series, a very high increase of slip was observed when the sustained load was applied and thermal cycles were applied. On the other hand, experimental series which were submitted under a preconditioning stage obtained a much lower increase of slip with time.

With the objective to study the residual behaviour of the NSM CFRP-concrete joint, monotonic instantaneous tests until failure were carried out under pull-out single shear configuration after 1000 hours of sustained loading. Figure 8.11 shows the load-slip curves obtained from the Post-Sustained-Loading (PSL) test for the specimen PSL-225-10-30 in each experimental series.
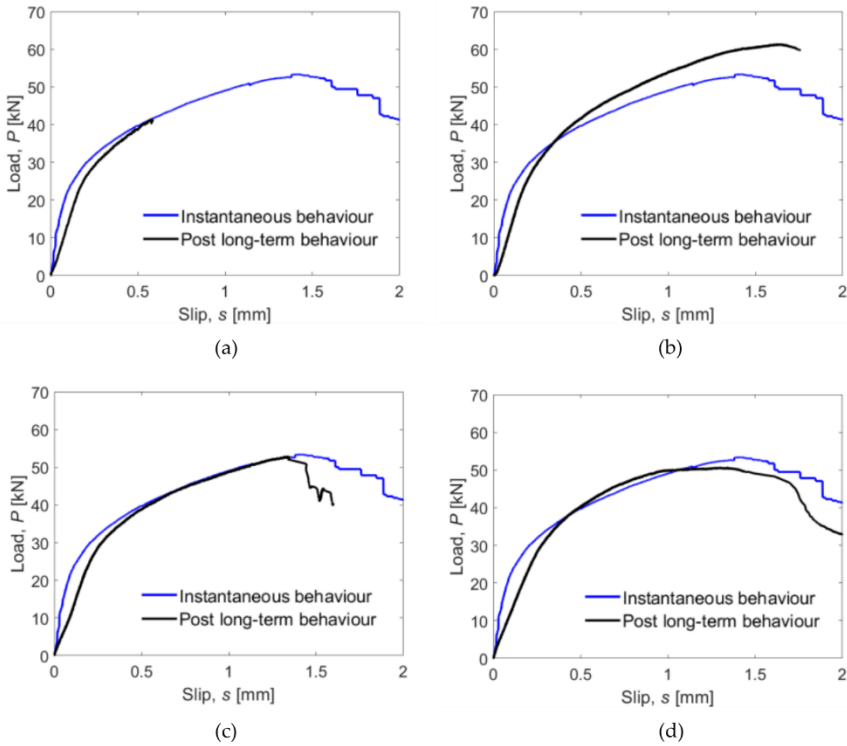
Figure 8.11: Comparison between the instantaneous behaviour and the post-SL behaviour of the specimen PSL-225-10-30 in series (a) S1, (b) S2, (c) S3-B and (d) S4.

Comparing the load-slip curves obtained in the PSL tests and the curves obtained from the instantaneous characterization, a significant decrease on the stiffness could be observed in the linear ascending stage. As both the average service temperature and the sustained load increased, the reduction of stiffness increased as well, as expected. Moreover, it was observed that when the load in the PSL test surpassed the sustained load level, the stiffness recovered because this part of the bonded joint was not damaged during the sustained loading test.

In the PSL tests of series C1 and C4, similar ultimate loads to the instantaneous characterization values were obtained. This was attributed to the fact that the average temperature of the cycle (25.6 ˚C) was similar to the temperature in C1 (20 ˚C). On the other hand, specimens from series C2 and C3-B experienced an average decrease on the ultimate load of 6.3% and 8.0%, respectively. This indicates that the damage induced by the combination of sustained loading and high service temperature lead to a small decrease on the ultimate capacity of the bonded joint.

Regarding the failure mode, no change was observed in the PSL tests in comparison with the instantaneous characterization. Specimens with a groove with of 7.5 mm obtained a cohesive failure in the concrete, while specimens with a groove thickness of 10 mm obtained the failure in the FRP-adhesive interface.

This paper has proved the importance of the study of the creep behaviour of NSM CFRP-concrete joints. It has been proved that sustained loading has an important effect on the service response of the bonded joint in terms of increase of slip with time.

Furthermore, this study evidenced the effect of service conditions on the instantaneous response of NSM CFRP-concrete specimens. From the PSL tests, it could be observed that the monotonic behaviour is significantly affected, especially in terms of stiffness, being higher as higher temperatures and sustained load levels were applied.

8.5   Concluding remarks

In this sub-section, the main contributions from the previous four sections are presented and further compared.

The instantaneous behaviour of the NSM CFRP-concrete bonded joint can be adequately predicted by the numerical methodology presented in Chapter 4. This methodology was extended to the time-dependent behaviour of the joint through a degradation model of the bond-slip law (Chapter 5). The creep behaviour of the adhesive was considered the main agent of the damaging model. Results between numerical and experimental data showed good agreement, although the model should be further calibrated with more experimental results, so as to validate the proposed equation.

Comparing the experimental results of the combination of sustained loading and environmental conditions (Chapter 4.3 and Chapter 4.4), similarities in the shape of the strain evolution (epoxy specimens) and slip evolution (NSM specimens) could be observed: a primary stage with a high non-linear increase of slip or strain was observed, followed by a secondary stage where the increase became more linear. However, it might seem that adhesives were slightly more affected by environmental conditions than bonded joints. For instance, in the experimental series S4/C4, adhesive specimens loaded at 30% tensile strength failed after some ours of loading, while the NSM CFRP-concrete specimens did not fail after 1000 hours of loading.

This could be probably attributed to a more aggressive exposure to thermal conditions in the case of the adhesive rather than in the NSM joint.

The application of temperature cycles has been proved to have a noticeable effect on the response of adhesive and NSM CFRP-concrete specimens. Significant strain and slip oscillations were observed with time in adhesive and NSM CFRP-concrete specimens, respectively. In both cases, for temperature cycles with an average temperature of 26.9 ˚C, the slip and strain evolutions obtained from the experimental series under thermal cycles laid between the cases from the experimental series under steady temperatures (20 ˚C and 40 ˚C). However, for cyclic temperatures with a higher average temperature (32.5 ˚C), the strain evolution in the adhesive specimens was similar to the specimens under 40 ˚C, while NSM CFRP-concrete specimens experienced an increase of slip between the experimental series under steady temperatures.

Finally, regarding the residual capacity of the specimens after the exposure to high service temperatures and sustained loading, adhesive and NSM CFRP-concrete specimens experienced an overall decrease on the mechanical properties (tensile strength and elastic modulus for the adhesive, and ultimate load and stiffness for the NSM CFRP-concrete specimen). This means that there is a direct relationship between the adhesive strength and the carrying capacity of the bonded joint, therefore, the study of the effect of service conditions on adhesive and NSM CFRP-concrete specimens is complementary.

PART IV: Concluding remarks and future works

9 Conclusions

During the last decades, NSM strengthening systems using FRP materials have emerged as an excellent solution to strengthen RC structures and enhance their structural capacity. In comparison with other strengthening techniques, NSM technique presents some advantages such as a better anchorage capacity and better protection against environmental conditions. A number of studies have been focused on the analysis of the instantaneous capacity of the NSM FRP-concrete bonded joints, however, these joints need to be designed for long-term conditions considering, in addition to sustained loading, environmental conditions such as temperature (steady increments/decrements of temperature and/or thermal cycles).

The main objective of the thesis was to study the time-dependent bond behaviour of concrete elements strengthened with CFRP using the NSM technique, under different environmental conditions (steady and cyclic temperatures), from an experimental and numerical point of view.

Instantaneous bond tests were performed to evaluate the effects of several parameters on the load-slip behaviour and mode of failure. The main studying parameters were the bonded length and groove thickness. From the obtained experimental results, a numerical model was implemented to reproduce the bond behaviour of the NSM CFRP-concrete joint, which is an essential requirement to consider in design methods.

To study the time-dependent behaviour of the adhesive and NSM CFRP-concrete specimens, sustained loading tests at different service temperatures were performed. Five experimental series were performed at different steady and cyclic temperatures combining two service sustained load levels. These tests were carried out inside a climatic chamber for 1000 hours, and afterwards, an instantaneous test was performed to study the residual capacity of the specimens.

Finally, the numerical methodology developed to calculate the instantaneous behaviour of NSM CFRP-concrete joints was used to implement a degradation model of the bond-slip law. In this way, the time-dependent behaviour of the bonded joints could be predicted with time and compared with the experimental data.

9.1 Numerical model and experimental validation of the instantaneous bond behaviour of NSM CFRP-concrete joints

The instantaneous behaviour of the NSM CFRP-concrete joints was studied from a numerical and experimental point of view in paper A. From comparison between the results of different local bond-slip models, it was concluded that:

- Models not including a friction stage achieved a maximum load in the load-slip curve, while models including a friction stage did not attain a stabilization of the maximum load.
- Models with non-linear ascending branch showed a stiffener initial load-slip response, although the effect on the maximum load was negligible.

From comparison with experimental results, it was observed that:

- A close agreement between the numerical and the experimental results in terms of load-slip curves were obtained for all the specimens' configurations.
- The groove thickness could determine whether the failure will be in the FRP-adhesive interface, with the presence of a friction stage (10 mm groove thickness specimens), or in the concrete layer, in a sudden manner (7.5 mm groove thickness specimens).

From the parametric study, it was observed that that as the bond shear strength increases, the ultimate load of the bonded joint increases as well, and the effective bonded length decreases.

9.2 Experimental time-dependent behaviour of the adhesive

The response of NSM CFRP-concrete joints under the combination of sustained loading and environmental conditions was experimentally studied in papers B and D. The main conclusions are presented below:

- Service conditions, especially ambient temperature, have been proved to have damaging effect on the performance of NSM CFRP-concrete bonded joints with time.
- Adhesives under a sustained loading level up to 30% and at room conditions, experiment a linear viscoelastic behaviour, while specimens at 40 ˚C, only specimens until 15% experiment a linear viscoelastic behaviour.
- Even though the studied range of temperatures are below the glass transition temperature of the adhesive, noticeable increases of strain are measured with time.
- Significant strain oscillations are observed in specimens under cyclic temperatures.

- Specimens under the highest thermal cycles are more affected than specimens at 40 ˚C, even though the average temperature of the thermal cycle is lower.
- The preconditioning of the adhesive specimens to the environmental conditions before loading is crucial. The lack of it will cause major increases of strain during the initial hours after loading, and in some cases, leading to creep failure.
- An increase on the T_g and the α, and a reduction of the tensile strength and the elastic modulus are observed after sustained loading tests.

9.3 Experimental time-dependent behaviour of NSM CFRP-concrete joints

The response of NSM CFRP-concrete joints under the combination of sustained loading and environmental conditions was experimentally studied in papers B and D. The main conclusions are presented below:

- As expected, as the sustained load level and the temperature increased, the evolution of slip increased as well.
- For the temperature range and load levels considered in this study, the creep behaviour of the bonded joint was more affected by the temperature than the sustained loading level.
- Similar evolutions of slips at the loaded end were observed for all specimens under 15% of P_u, regardless of the bonded length.
- Slightly higher slips were obtained in specimens with narrower grooves at 20 ˚C, although at 40 ˚C, specimens with wider grooves experience the highest slips, which might be caused by the fact that more adhesive was in contact with the ambient temperature.
- Cyclic temperatures highly affected the creep response of the bonded joint. The level of effect was mainly determined by the average temperature of the thermal cycle.
- The lack of a preconditioning stage caused high increases of slip during the initial hours.
- After sustained loading, NSM CFRP-concrete specimens experienced a decrease on the stiffness of the monotonic load-slip, being higher as the sustained load level and the temperature were higher. On the other hand, they seemed not to be affected in terms of carrying capacity and failure mode.

9.4 Numerical prediction of time-dependent behaviour of NSM CFRP-concrete response

The numerical procedure developed in this thesis was proved to give accurate predictions on the time-dependent performance of NSM CFRP-concrete specimens. The main conclusions were presented in paper B, and they can be summarized as follows:

- The numerical procedure correctly predicted the evolution of slip measured in the experimental series carried out in this thesis. Additionally, the model was validated with existing results in the literature, providing accurate results in all the cases.

- The calibration of the creep coefficient with the tensile sustained loading tests of adhesive specimens seemed to give a good prediction on the damage model of the bond-slip law with time.

- The strength reduction factor could be adjusted using a power function and calibrated with the experimental results of the NSM CFRP-concrete specimens under sustained loading and room conditions.

- This numerical methodology can be a good strategy to easily predict the behaviour of NSM CFRP-concrete joints due to the ease of implementation and the adaptability to any test configuration and bond-slip law.

10 Future works

Based on the findings of this work, several suggestions for future investigations are drawn.

- To study the effect of the combination of cyclic temperature in combination with different humidity levels (inside a climatic chamber and outdoor exposition) and to develop further studies under real-life environmental conditions.

- To further investigate the tensile behaviour of the adhesive under different environmental conditions to understand how temperature and humidity can modify the limits of its linear viscoelastic behaviour. Furthermore, this work could be expanded to different types of adhesives (e.g. cementitious adhesives), test configurations and test durations.

- To investigate the effects of the environmental conditions and sustained loading in NSM strengthening systems using other FRP materials (such as GFRP), other shapes (squared or round), and other types of adhesives (with other mechanical and physical properties).

- To study the applicability of the numerical procedure developed in this thesis to take into account the effects of steady and cyclic temperature.

- The numerical methodology could also be adapted to calculate the response of NSM CFRP-concrete specimens under a non-linear viscoelastic behaviour. This would allow to extrapolate the applicability of the numerical model to predict the bond behaviour under many other testing conditions, such as high temperatures, humidity levels and water immersion.

11 References

[1] Comité Europeen de Normalisation. Eurocode 2: Design of concrete structures: Part 1-1: 437 General rules and rules for buildings 2004.

[2] GangaRao HVS, Taly N, Vijay P V. Reinforced Concrete Design with FRP Composites. CRC Press; 2006.

[3] Hensher D. Fiber-Reinforced-Plastic (FRP) Reinforcement for Concrete Structures. Elsevier Science; 1993.

[4] Ahmad J. Machining of Polymer Composites. Springer; 2009. doi:10.1007/978-0-387-68619-6.

[5] Bisby L a. ISIS Educational Module 2: An Introduction to FRP Composites for Construction. ISIS Canada Educ Modul 2006:1–54.

[6] Carolin A. Carbon fibre reinforced polymers for strengthening of structural elements. Luleå University of Technology, 2003.

[7] Balaguru P, Nanni A, Giancaspro J. FRP composites for reinforced and prestressed concrete structures. New York: Taylor & Francis; 2009.

[8] Jassal M, Ghosh S. Aramid fibres - An overview. Indian J Fibre Text Res 2002;27:290–306. doi:10.1007/s11096-016-0312-7.

[9] Mallick P. Fiber-Reinforced Composites. CRC Press 2007.

[10] Szabó ZK. Bond characteristics of NSM reinforcements based on advanced test methods. Budapest University of Technology and Economics, 2013.

[11] fib bulletin 90. Externally applied FRP reinforcement for concrete structures. International Federation for Structural Concrete; 2019.

[12] Baena M, Torres L, Turon A, Barris C. Experimental study of bond behaviour between concrete and FRP bars using a pull-out test. Compos Part B Eng 2009;40:784–97. doi:10.1016/j.compositesb.2009.07.003.

[13] Sonnenschein R, Gajdosova K, Holly I. FRP Composites and their Using in the Construction of Bridges. Procedia Eng 2016;161:477–82. doi:10.1016/j.proeng.2016.08.665.

[14] FIB bulletin 14. Externally bonded FRP reinforcement for RC structures. vol. 14. International Federation for Structural Concrete; 2001. doi:10.1016/0262-5075(85)90032-6.

[15]   Yao J, Teng JG, Chen JF. Experimental study on FRP-to-concrete bonded joints. Compos Part B Eng 2005;36:99–113. doi:10.1016/j.compositesb.2004.06.001.

[16]   Konrad Zilch KB. A general bond stress slip relationship for NSM FRP strips. Proc. of FRPRCS-8, Patras (Greece): 2007.

[17]   Tumialan JG, Vatovec M, Kelley PL. Case study: strengthening of parking garage decks with near-surface-mounted CFRP bars. J Compos Constr 2007;11:523–30. doi:10.1061/(ASCE)1090-0268(2007)11:5(523).

[18]   Sharaky IA, Torres L, Baena M, Miàs C. An experimental study of different factors affecting the bond of NSM FRP bars in concrete. Compos Struct 2013;99:350–65. doi:10.1016/j.compstruct.2012.12.014.

[19]   Sharaky IA, Torres L, Baena M, Vilanova I. Effect of different material and construction details on the bond behaviour of NSM FRP bars in concrete. Constr Build Mater 2013;38:890–902. doi:10.1016/j.conbuildmat.2012.09.015.

[20]   Jos CP. Design Procedures for the Use of Composites in Strengthening of Reinforced Concrete Structures. vol. 19. Springer; 2016. doi:10.1007/978-94-017-7336-2.

[21]   De Lorenzis L, Teng JG. Near-surface mounted FRP reinforcement: An emerging technique for strengthening structures. Compos Part B Eng 2007;38:119–43. doi:10.1016/j.compositesb.2006.08.003.

[22]   Sena Cruz JM, Barros JAO, Gettu R, Azevedo ÁFM. Bond Behavior of Near-Surface Mounted CFRP Laminate Strips under Monotonic and Cyclic Loading. J Compos Constr 2006;10:295–303. doi:10.1061/(ASCE)1090-0268(2006)10:4(295).

[23]   Seracino R, Jones NM, Ali MS, Page MW, Oehlers DJ. Bond Strength of Near-Surface Mounted FRP Strip-to-Concrete Joints. J Compos Constr 2007;11:401–9. doi:10.1061/(ASCE)1090-0268(2007)11:4(401).

[24]   Zhang SS, Teng JG, Yu T. Bond-Slip Model for Interfaces between Near-Surface Mounted CFRP Strips and Concrete. FRPRCS 2013:1–7.

[25]   Chen JF, Teng JG. Anchorage Strength Models for FRP and Steel Plates. J Struct Eng 2001;127:784–91.

[26]   Savoia M, Mazzotti C, Ferracuti B. A new single-shear set-up for stable debonding of FRP-concrete joints. Constr Build Mater 2009;23:1529–37. doi:10.1016/j.conbuildmat.2008.04.003.

[27]   Ferrier E, Rabinovitch O, Michel L. Mechanical behavior of concrete–resin/adhesive–FRP

structural assemblies under low and high temperatures. Constr Build Mater 2016;127:1017–28. doi:10.1016/j.conbuildmat.2015.12.127.

[28]   Yao J, Teng JG. Plate end debonding in FRP-plated RC beams-I: Experiments. Eng Struct 2007;29:2457–71. doi:10.1016/j.engstruct.2006.11.022.

[29]   De Lorenzis L, Rizzo A, La Tegola A. A modified pull-out test for bond of near-surface mounted FRP rods in concrete. Compos Part B Eng 2002;33:589–603. doi:10.1016/S1359-8368(02)00052-5.

[30]   Choi KK, Meshgin P, Reda Taha MM. Shear creep of epoxy at the concrete-FRP interfaces. Compos Part B Eng 2007;38:772–80. doi:10.1016/j.compositesb.2006.10.003.

[31]   Sena-Cruz J, Barros JAO. Bond between Near-surface mounted carbon-fiber-reinforced polymer laminate strips and concrete. J Compos Constr 2004;8:519–27. doi:10.1061/(ASCE)1090-0268(2004)8.

[32]   Coelho MRF, Sena-Cruz JM, Neves LAC. A review on the bond behavior of FRP NSM systems in concrete. Constr Build Mater 2015;93:1157–69. doi:10.1016/j.conbuildmat.2015.05.010.

[33]   Zhang SS, Yu T, Chen GM. Reinforced concrete beams strengthened in flexure with near-surface mounted (NSM) CFRP strips: Current status and research needs. Compos Part B Eng 2017;131:30–42. doi:10.1016/j.compositesb.2017.07.072.

[34]   Fernandes P, Silva P, Cruz JS. Bond and flexural behaviour of a NSM CFRP strengthening system under fatigue loading. 7th Int Conf FRP Compos Civ Eng 2014:1–6.

[35]   Bilotta A, Ceroni F, Di Ludovico M, Nigro E, Pecce M, Manfredi G. Bond Efficiency of EBR and NSM FRP Systems for Strengthening Concrete Members. J Compos Constr 2011;15:757–72. doi:10.1061/(ASCE)CC.1943-5614.0000204.

[36]   Iovinella I, Prota A, Mazzotti C. Influence of surface roughness on the bond of FRP laminates to concrete. Constr Build Mater 2013;40:533–42. doi:10.1016/j.conbuildmat.2012.09.112.

[37]   Rao GA, Prasad BKR. Influence of the roughness of aggregate surface on the interface bond strength. Cem Concr Res 2002;32:253–7. doi:10.1016/S0008-8846(01)00668-8.

[38]   BLASCHKO M. Bond Behavior of CFRP Strips Glued into Slits. Fibre-Reinforced Polym. Reinf. Concr. Struct., World Scientific Publishing Company; 2003, p. 205–14. doi:doi:10.1142/9789812704863_0017.

[39]   Lee D, Cheng L, Hui JY-G. Bond Characteristics of Various NSM FRP Reinforcements in Concrete. J Compos Constr 2013;17:117–29. doi:10.1061/(ASCE)CC .1943-5614.0000318.

[40]   Oehlers DJ, Rashid R, Seracino R. IC debonding resistance of groups of FRP NSM strips in reinforced concrete beams. Constr Build Mater 2008;22:1574–82. doi:10.1016/j.conbuildmat.2007.03.021.

[41]   Ceroni F, Pecce M, Bilotta A, Nigro E. Bond behavior of FRP NSM systems in concrete elements. Compos Part B Eng 2012;43:99–109. doi:10.1016/j.compositesb.2011.10.017.

[42]   Hassan T, Rizkalla S. Investigation of Bond in Concrete Structures Strengthened with Near Surface Mounted Carbon Fiber Reinforced Polymer Strips. J Compos Constr 2003;7:248–57. doi:10.1061/(ASCE)1090-0268(2003)7:3(248).

[43]   Maeda T, Asano Y, Sato Y, Ueda T, Kakuta Y. A study on bond mechanism of carbon fibre sheet. Non-metallic (FRP) reinforcement for concrete structures. Proc. 3rd Int. Symp. Sapporo, Japan, 1997, p. 279–86.

[44]   Lu XZ, Teng JG, Ye LP, Jiang JJ. Bond-slip models for FRP sheets/plates bonded to concrete. Eng Struct 2005;27:920–37. doi:10.1016/j.engstruct.2005.01.014.

[45]   Camli US, Binici B. Strength of carbon fiber reinforced polymers bonded to concrete and masonry. Constr Build Mater 2007;21:1431–46. doi:https://doi.org/10.1016/j.conbuildmat.2006.07.003.

[46]   Zhang SS, Teng JG, Yu T. Bond Strength Model for CFRP Strips Near-Surface Mounted to Concrete. J Compos Constr 2014;18. doi:10.1061/(ASCE)CC.1943-5614.0000402.

[47]   Neubauer, U., Rostasy FS. Bond behaviour of CFRP-laminates for the strengthening of concrete members. Proc IABSE Conf Compos Constr - Conv Innov Innsbruck, 1997 1998:717–22.

[48]   ACI 440.2R-08. Guide for the design and construction of externally bonded FRP systems for strengthening existing structures. American Concrete Institute; 2008.

[49]   CNR – Advisory Committee on Technical Recommendations for Construction. CNR DT 215/2018: Guide for the design and construction of externally bonded FRP systems for strengthening existing structures. Rome, Italy: 2018.

[50]   fib bulletin 90. Externally applied FRP reinforcement for concrete structures. Lausanne, Switzerland: International Federation for Structural Concrete; 2019.

[51]   CNR. Guidelines for the Design and Construction of Externally Bonded FRP Systems for Strengthening Existing Structures - Timber structures, CNR-DT 200 R1/2013. Rome, Italy: Advisory committee on technical recommendations for construction; 2013. doi:10.1111/j.1538-7836.2010.03753.x.

[52]   Australia S. Design Handbook for RC Structures Retrofitted with FRP and Metal Plates: Beams and Slabs, Standards Australia. Sydney, Australia: Standards Australia GPO Box 476; 2008.

[53]   Dai J, Ueda T, Sato Y. Development of the Nonlinear Bond Stress–Slip Model of Fiber Reinforced Plastics Sheet–Concrete Interfaces with a Simple Method. J Compos Constr 2005;9:52–62. doi:10.1061/(ASCE)1090-0268(2005)9:1(52).

[54]   (JCI) JCI. Technical report of technical committee on retrofit technology. Proc. Int. Symp. latest Achiev. Technol. Res. Retrofit. Concr. Struct., 2003.

[55]   Bilotta A, Faella C, Martinelli E, Nigro E. Design by testing procedure for intermediate debonding in EBR FRP strengthened RC beams. Eng Struct 2013;46:147–54. doi:10.1016/j.engstruct.2012.06.031.

[56]   ACI 440.2R-08. Guide for the design and construction of externally bonded FRP systems for strengthening concrete structures. 2008.

[57]   Seracino R, Raizal Saifulnaz MR, Oehlers DJ. Generic Debonding Resistance of EB and NSM Plate-to-Concrete Joints. J Compos Constr 2007;11:62–70. doi:10.1061/(ASCE)1090-0268(2007)11:1(62).

[58]   Zhishen Wu, Hong Yuan, Niu H. Stress Transfer and Fracture Propagation in Different Kinds of Adhesive Joints. J Eng Mech 2002;128:562–573. doi:10.1061/(ASCE)0733-9399(2002)128.

[59]   Yuan H, Lu X, Hui D, Feo L. Studies on FRP-concrete interface with hardening and softening bond-slip law. Compos Struct 2012;94:3781–92. doi:10.1016/j.compstruct.2012.06.009.

[60]   Borchert K, Zilch K. Bond behaviour of NSM FRP strips in service. Struct Concr 2008;9:127–42. doi:10.1680/stco.2007.00015.

[61]   Brosens K. DVG. Plate end and shear design for external CFRP laminates. Proc. Fract. Mech. Concr. Struct. Fram., Gifu, Japan: 1998, p. 1793–804.

[62]   Brosens K. Anchorage of externally bonded steel plates and CFRP laminates for the strengthening of concrete elements. KATHOLIEKE UNIVERSITEIT LEUVEN, 2001.

[63]   Monti G, Renzelli M, Luciani P. FRP adhesion in uncracked and cracked concrete zones. Fibre-Reinforced Polym. Reinf. Concr. Struct., n.d., p. 183–92. doi:10.1142/9789812704863_0015.

[64]   Nakaba K, Kanakubo T, Furuta T, Yoshizawa H. Bond Behavior between Fiber-Reinforced Polymer Laminates and Concrete. ACI Struct J 2001;98:359–67.

[65]   Savoia M. Non-linear bond-slip law for FRP-concrete interface. Proc 6th Int Symp FRP Reinf Concr Struct 2003:163–72.

[66]   Cruz JS, Barros J. Modeling of bond between near-surface mounted CFRP laminate strips and concrete. Comput Struct 2004;82:1513–21. doi:10.1016/j.compstruc.2004.03.047.

[67]   Ceroni F, Barros JAO, Pecce M, Ianniciello M. Assessment of nonlinear bond laws for near-surface-mounted systems in concrete elements. Compos Part B Eng 2013;45:666–81. doi:10.1016/j.compositesb.2012.07.006.

[68]   Zhang SS, Teng JG, Yu T. Bond-slip model for CFRP strips near-surface mounted to concrete. Eng Struct 2013;56:945–53. doi:10.1016/j.engstruct.2013.05.032.

[69]   ACI 440.2R-17. Guide for the design and construction of externally bonded FRP systems for strengthening existing structures. Farmington Hills, Michigan, USA: American Concrete Institute; 2017.

[70]   Ferracuti B, Savoia M, Mazzotti C. Interface law for FRP-concrete delamination. Compos Struct 2007;80:523–31. doi:10.1016/j.compstruct.2006.07.001.

[71]   Zhang W. Experimental study on fatigue behaviour of CFRP plates externally bonded to concrete substrate. Struct Concr 2016;17:235–44. doi:10.1002/suco.201500044.

[72]   Mazzotti C, Savoia M, Ferracuti B. An experimental study on delamination of FRP plates bonded to concrete. Constr Build Mater 2008;22:1409–21. doi:10.1016/j.conbuildmat.2007.04.009.

[73]   Emara M, Barris C, Baena M, Torres L, Barros J. Bond behavior of NSM CFRP laminates in concrete under sustained loading. Constr Build Mater 2018;177:237–246. doi:10.1016/j.conbuildmat.2018.05.050.

[74]   Yuan H, Teng JG, Seracino R, Wu ZS, Yao J. Full-range behavior of FRP-to-concrete bonded joints. Eng Struct 2004;26:553–65. doi:10.1016/j.engstruct.2003.11.006.

[75]   Ali MSM, Oehlers DJ, Griffith MC, Seracino R. Interfacial stress transfer of near surface-mounted FRP-to-concrete joints. Eng Struct 2008;30:1861–8. doi:10.1016/j.engstruct.2007.12.006.

[76]   Haskett M, Oehlers DJ, Ali MSM. Local and global bond characteristics of steel reinforcing bars. Eng Struct 2008;30:376–83. doi:10.1016/j.engstruct.2007.04.007.

[77]   Japan Society of Civil Engineers (JSCE). Recommendations for upgrading of concrete structures with use of continuous fiber sheets. Japan Society of Civil Engineers; 1997.

[78]   Goertzen WK, Kessler MR. Creep behavior of carbon fiber/epoxy matrix composites. Mater Sci Eng A 2006;421:217–25. doi:10.1016/j.msea.2006.01.063.

[79]   Ascione F, Berardi VP, Feo L, Giordano A. An experimental study on the long-term behavior of CFRP pultruded laminates suitable to concrete structures rehabilitation. Compos Part B Eng 2008;39:1147–50. doi:10.1016/j.compositesb.2008.03.008.

[80]   Mazzotti C, Savoia M. Stress redistribution along the interface between concrete and FRP subject to long-term loading. Adv Struct Eng 2009;12:651–62. doi:10.1260/136943309789867926.

[81]   Yamaguchi T, Kato Y, Nishimura T, Uomoto T. Creep Rupture of FRP Rods Made of Aramid, Carbon and Glass Fibers. Non-metallic Reinf. Concr. Struct., Sapporo (Japan): Japan Concrete Institute; 1997, p. 179–86.

[82]   Malvar L. Durability of Composites in Reinforced Concrete. Proc. First Int. Conf. Durab. Compos. Constr., Canada: n.d., p. 361–72.

[83]   CEB-FIP Bulletin 90. Externally applied FRP reinforcement for concrete structures. fédération internationale du béton; 2019.

[84]   Findley WN, Lai JS, Onaran K, Christensen RM. Creep and Relaxation of Nonlinear Viscoelastic Materials With an Introduction to Linear Viscoelasticity. vol. 18. New York: Dover Publications; 1979. doi:10.1115/1.3424077.

[85]   Majda P, Skrodzewicz J. A modified creep model of epoxy adhesive at ambient temperature. Int J Adhes Adhes 2009;29:396–404. doi:10.1016/j.ijadhadh.2008.07.010.

[86]   Meshgin P, Choi KK, Reda Taha MM. Experimental and analytical investigations of creep of epoxy adhesive at the concrete-FRP interfaces. Int J Adhes Adhes 2009;29:56–66. doi:10.1016/j.ijadhadh.2008.01.003.

[87]   Emara M, Torres L, Baena M, Barris C, Moawad M. Effect of sustained loading and environmental conditions on the creep behavior of an epoxy adhesive for concrete structures strengthened with CFRP laminates. Compos Part B Eng 2017;129:88–96. doi:10.1016/j.compositesb.2017.07.026.

[88]   Gullapalli A, Lee JH, Lopez MM, Bakis CE. Sustained Loading and Temperature Response

of Fiber-Reinforced Polymer-Concrete Bond. Transp Res Rec J Transp Res Board 2010;2131:155–62. doi:10.3141/2131-15.

[89]   Cao S, Wu Z, Wang X. Tensile Properties of CFRP and Hybrid FRP Composites at Elevated Temperatures. J Compos Mater 2009;43:315–30. doi:10.1177/0021998308099224.

[90]   Nardone F, Di Ludovico M, De Caso Y Basalo FJ, Prota A, Nanni A. Tensile behavior of epoxy based FRP composites under extreme service conditions. Compos Part B Eng 2012;43:1468–74. doi:10.1016/j.compositesb.2011.08.042.

[91]   Galvez P, Lopez de Armentia S, Abenojar J, Martinez MA. Effect of moisture and temperature on thermal and mechanical properties of structural polyurethane adhesive joints. Compos Struct 2020;247:112443. doi:10.1016/j.compstruct.2020.112443.

[92]   Silva P, Fernandes P, Sena-Cruz J, Xavier J, Castro F, Soares D, et al. Effects of different environmental conditions on the mechanical characteristics of a structural epoxy. Compos Part B Eng 2016;88:55–63. doi:10.1016/j.compositesb.2015.10.036.

[93]   Ferrier E, Michel L, Jurkiewiez B, Hamelin P. Creep behavior of adhesives used for external FRP strengthening of RC structures. Constr Build Mater 2011;25:461–7. doi:10.1016/j.conbuildmat.2010.01.002.

[94]   Costa I, Barros J. Tensile creep of a structural epoxy adhesive: Experimental and analytical characterization. Int J Adhes Adhes 2015;59:115–24. doi:10.1016/j.ijadhadh.2015.02.006.

[95]   Costa I, Barros J. Creep of structural adhesives: an overview. Proc. 6th Int. Conf. FRP Compos. Civ. Eng. CICE 2012, 2012, p. 1–8.

[96]   Costa IG, Barros JAO. Assessment of the long term behaviour of structural adhesives in the context of NSM flexural strengthening technique with prestressed CFRP laminates. In: Sena-Cruz JB& J, editor. Proc. 11th Int. Symp. Fiber Reinf. Polym. Reinf. Concr. Struct. - FRPRCS-11, Guimarães: 2013, p. 1–10.

[97]   Silva P, Valente T, Azenha M, Sena-Cruz J, Barros J. Viscoelastic response of an epoxy adhesive for construction since its early ages: Experiments and modelling. Compos Part B Eng 2017;116:266–77. doi:10.1016/j.compositesb.2016.10.047.

[98]   Dai J-G, Gao WY, Teng JG. Bond-Slip Model for FRP Laminates Externally Bonded to Concrete at Elevated Temperature. J Compos Constr 2013;17:217–28. doi:10.1061/(ASCE)CC.1943-5614.0000337.

[99]   Blontrock H. Analysis and modeling of the fire resistance of concrete elements with

externally bonded FRP reinforcement. Ghent University, Ghent, Belgium, 2003.

[100]   Leone M, Matthys S, Aiello MA. Effect of elevated service temperature on bond between FRP EBR systems and concrete. Compos Part B Eng 2009;40:85–93. doi:10.1016/j.compositesb.2008.06.004.

[101]   Klamer EL, Hordijk DA, Janssen HJM. The influence of temperature on the debonding of externally bonded CFRP. Proc 7th Int Symp Fiber Reinf Polym Reinf Concr Struct 2005:1551–70.

[102]   Cai ZH. Research on bond property of FRP-to-concrete interface under elevated temperatures. Tongji Univ., Shanghai, China, 2008.

[103]   Z. W. Temperature Effect on Bonding and Debonding Behavior between FRP Sheets and Concrete. J Soc Mat Sci, Japan 2005;54:474–80.

[104]   Ferrier E, Hamelin P. Durability of External Carbon Epoxy Reinforcement of Concrete 1998.

[105]   Jeong Y, Lopez MM, Bakis CE. Effects of temperature and sustained loading on the mechanical response of CFRP bonded to concrete. Constr Build Mater 2016;124:442–52. doi:10.1016/j.conbuildmat.2016.07.123.

[106]   Jeong Y, Lee J, Kim WS. Modeling and measurement of sustained loading and temperature-dependent deformation of carbon fiber-reinforced polymer bonded to concrete. Materials (Basel) 2015;8:435–50. doi:10.3390/ma8020435.

[107]   Jeong Y, Lopez MM, Bakis CE. Effects of Sustained Loading and Temperature on a Concrete-Epoxy Bonded Interface. J Mater Civ Eng 2020;32:1–13. doi:10.1061/(ASCE)MT.1943-5533.0003051.

[108]   Emara M, Torres L, Baena M, Barris C, Cahís X. Bond response of NSM CFRP strips in concrete under sustained loading and different temperature and humidity conditions. Compos Struct 2018;192:1–7. doi:10.1016/j.compstruct.2018.02.048.

[109]   Fernandes P, Sena-Cruz J, Xavier J, Silva P, Pereira E, Cruz J. Durability of bond in NSM CFRP-concrete systems under different environmental conditions. Compos Part B Eng 2018;138:19–34. doi:10.1016/j.compositesb.2017.11.022.

[110]   Gamage JCPH, Al-Mahaidi R, Wong MB. Integrity of CFRP-concrete bond subjected to long-term cyclic temperature and mechanical stress. Compos Struct 2016;149:423–33. doi:10.1016/j.compstruct.2016.04.040.

[111]   Gamage JCPH, Al-Mahaidi R, Wong MB. Durability of CFRP-Strengthened Concrete

Members Under Extreme Temperature and Humidity. Aust J Struct Eng 2017;9:111–8. doi:10.1080/13287982.2009.11465014.

[112]   Gamage JCPH, Al-Mahaidi R, Wong B, Ariyachandra MREF. Bond characteristics of CFRP-strengthened concrete members subjected to cyclic temperature and mechanical stress at low humidity. Compos Struct 2017;160:1051–9. doi:10.1016/j.compstruct.2016.10.131.

[113]   ISO 527-2:2012. Determination of tensile properties-Part 2: Test conditions for moulding and extrusion plastics. Geneva, Switzerland: 2012.

[114]   ISO 527-5:2009. Determination of tensile properties - Part 5: Test conditions for unidirectional fibre-reinforced plastic composites. vol. 1. Geneva, Switzerland: 2009.

[115]   ASTM C469 / C469M-10. Standard Test Method for Static Modulus of Elasticity and Poisson's Ratio of Concrete in Compression. West Conshohocken, PA: 2010.

[116]   UNE 12390-3. Testing hardened concrete. Part 3: Compressive strength of test specimens. Madrid: AENOR; 2003.

[117]   ASTM C 512/C 512M. Standard Test Method for Creep of Concrete in Compression. ASTM Int 2010;87:1–5. doi:10.1520/C0512_C0512M-15.

[118]   ASTM International. ASTM D3418-99: Standard Test Method for Transition Temperatures of Polymers By Differential Scanning Calorimetry. West Conshohocken, United States: 1999.

[119]   Savoia M, Mazzotti C, Ferracuti B. Mode II fracture energy and interface law for FRP - Concrete bonding with different concrete surface preparations. Fract Mech Concr Concr Struct Vols 1-3 2007;1–3:1249-1257\n1886.

[120]   Carrara P, Ferretti D, Freddi F, Rosati G. Shear tests of carbon fiber plates bonded to concrete with control of snap-back. Eng Fract Mech 2011;78:2663–78. doi:10.1016/j.engfracmech.2011.07.003.

[121]   Bendetti M Di, Gómez J, Cholostiakow S, Fergani H, Barris C, Guadagnini M. Reliability of DIC measurements for the structural monitoring of FRP RC elements. 9th Int. Conf. Fibre-Reinforced Polym. Civ. Eng. (CICE 2018), PARIS 17-19 JULY 2018, 2018.

[122]   Benedetti M Di, Colom JG, Barris C, Guadagnini M, Torres L. Effect of DIC setup and analysis parameters on the measurement of deformation in load tested FRP RC beams. COST Action TU1207 Next Gener. Des. Guidel. Compos. Constr. Eff., 2017, p. 4–9.

[123]   Barris C, Torres L, Vilanova I, Miàs C, Llorens M. Experimental study on crack width and

crack spacing for Glass-FRP reinforced concrete beams. Eng Struct 2017;131:231–42. doi:10.1016/j.engstruct.2016.11.007.

[124]   Pan B, Lu Z, Xie H. Mean intensity gradient: An effective global parameter for quality assessment of the speckle patterns used in digital image correlation. Opt Lasers Eng 2010;48:469–77. doi:10.1016/j.optlaseng.2009.08.010.

[125]   Ko H, Matthys S, Palmieri A, Sato Y. Development of a simplified bond stress-slip model for bonded FRP-concrete interfaces. Constr Build Mater 2014;68:142–57. doi:10.1016/j.conbuildmat.2014.06.037.

[126]   Zou X, Sneed LH, D'Antino T. Full-range behavior of fiber reinforced cementitious matrix (FRCM)-concrete joints using a trilinear bond-slip relationship. Compos Struct 2020;239:112024. doi:10.1016/J.COMPSTRUCT.2020.112024.

[127]   Bilotta A, Ceroni F, Barros JAO, Costa I, Palmieri A, Szabó ZK, et al. Bond of NSM FRP-Strengthened Concrete: Round Robin Test Initiative. J Compos Constr 2015;20:04015026. doi:10.1061/(asce)cc.1943-5614.0000579.

[128]   Dalfré GM, Barros JAO. NSM technique to increase the load carrying capacity of continuous RC slabs. Eng Struct 2013;56:137–53. doi:10.1016/j.engstruct.2013.04.021.

[129]   Novidis D, Pantazopoulou SJ, Tentolouris E. Experimental study of bond of NSM-FRP reinforcement. Constr Build Mater 2007;21:1760–70. doi:10.1016/j.conbuildmat.2006.05.054.

[130]   Mazzotti C, Savoia M. Long Term Properties of Bond Between Concrete and Frp. Concrete 2005;1–3:531–8.

[131]   Dash S, Jeong Y, Lopez MM, Bakis CE. Experimental Characterization of Moisture , Temperature and Sustained Loading on Concrete-FRP Bond Performance. Proc 11th Int Symp Fiber Reinf Polym Reinf Concr Struct - FRPRCS-11 2013:1–7.

[132]   Eligehausen R, Popov EP, Bertero V V. Local Bond Stress-Slip Relationships of Deformed Bars Under Generalized Excitations. Earthq Eng Res Cent 1982;4:69–80.

[133]   Borchert K, Zilch K. Time Depending Thermo Mechanical Bond Behavior of Epoxy Bonded Pre-Stressed FRP-Reinforcement. Proc 7th Int Symp Fiber Reinf Polym Reinf Concr Struct - FRPRCS-7 2005:671–683.

[134]   Gómez J, Torres L, Barris C. Characterization and Simulation of the Bond Response of NSM FRP Reinforcement in Concrete. Materials (Basel) 2020;13. doi:10.3390/ma13071770.

[135] Di Benedetti M, Guadagnini M, Gómez J, Barris C, Torres L. Experimental study on the DIC setup for the analysis of FRP RC members. Adv. Compos. Constr. ACIC 2017 - Proc. 8th Bienn. Conf. Adv. Compos. Constr., 2017.

[136] Comité Euro-International du Betón. CEB-1997. Serviceability Models - Behaviour and modelling in serviceability limit states including repeated and sustained load sustained loads. CEB, Bulletin d'information No. 235. Lausanne, Switzerland: 1997.

[137] Blaschko M, Zilch K. Rehabilitation of concrete structures with CFRP strips glued into slits. Mater Struct 1999;26:185–9. doi:10.1007/BF02472937.

[138] Meier U. Carbon Fiber-Reinforced Polymers : Modern Materials in Bridge Engineering. Struct Eng Int 1992;2:7–12. doi:https://doi.org/10.2749/101686692780617020.

[139] Buyukozturk BO, Bakhoum MM, Member S, Beattie SM. Shear behaviour of joints in precast concrete segmental bridges 1991;116:3380–401.

[140] Benyoucef S, Tounsi A, Adda Bedia EA, Meftah SA. Creep and shrinkage effect on adhesive stresses in RC beams strengthened with composite laminates. Compos Sci Technol 2007;67:933–42. doi:10.1016/j.compscitech.2006.07.007.

[141] Torres L, Sharaky IA, Barris C, Baena M. Experimental study of the influence of adhesive properties and bond length on the bond behaviour of NSM FRP bars in concrete. J Civ Eng Manag 2016;22:808–17. doi:10.3846/13923730.2014.914097.

[142] Benedetti A, Fernandes P, Granja JL, Sena-Cruz J, Azenha M. Influence of temperature on the curing of an epoxy adhesive and its influence on bond behaviour of NSM-CFRP systems. Compos Part B Eng 2016;89:219–29. doi:10.1016/j.compositesb.2015.11.034.

[143] Ferrier E, Hamelin P. Long-time concrete-composite interface characterization for reliability prediction of RC beam strengthened with FRP. Mater Struct Constr 2002;35:564–72. doi:10.1617/13691.

[144] Moussa O, Vassilopoulos AP, De Castro J, Keller T. Time-temperature dependence of thermomechanical recovery of cold-curing structural adhesives. Int J Adhes Adhes 2012;35:94–101. doi:10.1016/j.ijadhadh.2012.02.005.

[145] Moussa O, Vassilopoulos AP, Castro J De, Keller T. Long-term development of thermophysical and mechanical properties of cold-curing structural adhesives due to post-curing. J Appl Polym Sci 2013;127:2490–6. doi:10.1002/app.37965.

[146] Feng CW, Keong CW, Hsueh YP, Wang YY, Sue HJ. Modeling of long-term creep behavior of structural epoxy adhesives. Int J Adhes Adhes 2005;25:427–36.

doi:10.1016/j.ijadhadh.2004.11.009.

[147]   Agarwal A, Ng TS, Foster S, Hamed E. Durability of steel-CFRP adhesive joints under sustained loading and wet thermal-cycles. ICCM Int Conf Compos Mater 2013;2013-July:2317–25.

[148]   Agarwal A, Foster SJ, Hamed E. Testing of new adhesive and CFRP laminate for steel-CFRP joints under sustained loading and temperature cycles. Compos Part B Eng 2016;99:235–47. doi:10.1016/j.compositesb.2016.06.039.

[149]   Agarwal A, Foster SJ, Hamed E. Wet thermo-mechanical behavior of steel-CFRP joints - An experimental study. Compos Part B Eng 2015;83:284–96. doi:10.1016/j.compositesb.2015.08.025.

[150]   Liang H, Li S, Lu Y, Yang T. The combined effects of wet–dry cycles and sustained load on the bond behavior of FRP–concrete interface. Polym Compos 2019;40:1006–17. doi:10.1002/pc.24785.

[151]   Shi J, Zhu H, Wu Z, Seracino R, Wu G. Bond Behavior between Basalt Fiber–Reinforced Polymer Sheet and Concrete Substrate under the Coupled Effects of Freeze-Thaw Cycling and Sustained Load. J Compos Constr 2013;17:530–42. doi:10.1061/(asce)cc.1943-5614.0000349.

[152]   Hartanto D, Hamed E, Agarwal A, Foster SJ. Behaviour of steel-CFRP lap joints under hygrothermal cycles and sustained loadings. Compos Struct 2018;203:740–9. doi:10.1016/j.compstruct.2018.07.032.

[153]   ISO-11357-2. Plastics - differential scanning Calorimetry - Part 2: determi- nation of glass transition temperature. Genève, Switzerland: ISO International Organization for Standardization; 1999.

[154]   Menard; KP, Menard N. Dynamic Mechanical Analysis: a practical introduction. Taylor & Francis; 2002. doi:10.1002/9780470027318.a2007.pub3.

[155]   ISO International Organization for Standardization. ISO-899-1. Plastics - determination of creep behaviour - Part 1: tensile creep. Geneva, Switzerland: 2003.

[156]   Farzampour A. Temperature and humidity effects on behavior of grouts. Adv Concr Constr 2017;5:659–69. doi:10.12989/acc.2017.5.6.659.

[157]   Farzampour A. Compressive Behavior of Concrete under Environmental Effects. In: Pavel Krivenko, editor. Compressive Strength Concr., IntechOpen; 2020. doi:10.5772/intechopen.85675.

[158] Mansouri I, Shahheidari FS, Hashemi SMA, Farzampour A. Investigation of steel fiber effects on concrete abrasion resistance. Adv Concr Constr 2020;9:367–74. doi:10.12989/acc.2020.9.4.367.

[159] Aydin H, Gravina RJ, Visintin P. Durability of Adhesively Bonded FRP-to-Concrete Joints. J Compos Constr 2016;20:04016016. doi:10.1061/(asce)cc.1943-5614.0000657.

[160] Gómez J, Barris C, Jahani Y, Baena M, Torres L. Experimental study and numerical prediction of the bond response of NSM CFRP laminates in RC elements under sustained loading. Constr Build Mater 2021;288. doi:10.1016/j.conbuildmat.2021.123082.

[161] Pan Y, Xian G, Li H. Effects of Freeze-Thaw Cycles on the Behavior of the Bond between CFRP Plates and Concrete Substrates. J Compos Constr 2018;22:1–14. doi:10.1061/(ASCE)CC.1943-5614.0000846.

[162] Yun Y, Wu YF. Durability of CFRP-concrete joints under freeze-thaw cycling. Cold Reg Sci Technol 2011;65:401–12. doi:10.1016/j.coldregions.2010.11.008.

[163] Silva MAG, Biscaia H, Chastre C. Influence of temperature cycles on bond between glass fiber-reinforced polymer and concrete. ACI Struct J 2013;110:977–87. doi:10.14359/51686153.

[164] Silva MAG, Biscaia HC, Marreiros R. Bond-slip on CFRP/GFRP-to-concrete joints subjected to moisture, salt fog and temperature cycles. Compos Part B Eng 2013;55:374–85. doi:10.1016/j.compositesb.2013.06.015.

[165] Biscaia HC, Ribeiro P. A temperature-dependent bond-slip model for CFRP-to-steel joints. Compos Struct 2019;217:186–205. doi:10.1016/j.compstruct.2019.03.019.

[166] Borosnyói A. Influence of service temperature and strain rate on the bond performance of CFRP reinforcement in concrete. Compos Struct 2015;127:18–27. doi:10.1016/j.compstruct.2015.02.076.

[167] Lee H, Jung WT, Chung W. Bond behavior of near surface mounted CFRP rods under temperature cycling. Eng Struct 2017;137:67–75. doi:10.1016/j.engstruct.2017.01.057.